7th International Symposium on **Focused Ultrasound** 2020

A Virtual Event, November 9-13, 2020

Abstract Book

Part 2 – Poster Abstracts

Focused Ultrasound Foundation

Sponsor Acknowledgements

Diamond Sponsor

INSIGHTEC

Gold Sponsors

E& Pure Power

PI PIEZO TECHNOLOGY

Silver Sponsors

BRACCO LIFE FROM INSIDE

DAXSONICS ultrasound

UFFC IEEE Ultrasonics, Ferroelectrics, and Frequency Control Society

光 新光人壽 慈善基金會 Shin Kong Life Foundation

SNO 25th Anniversary Society for NeuroOncology

SONIC CONCEPTS

Verasonics® The leader in Research Ultrasound™

Poster Abstracts

The following abstracts were withdrawn by the authors:

P-BBB-5	P-BTU-1	P-IMM-1	P-TEC-5
P-BRT-11	P-DRD-5	P-MIS-5	P-TEC-14
P-BRT-20	P-DRD-7	P-STR-2	P-WOM-4

P-BBB-1

Topic: Blood-Brain Barrier Opening

Presentation Type: Poster

The feasibility of blood-nerve barrier disruption using focused ultrasound and microbubbles in a rodent model

Daniel Umansky, Chenchen Bing, Tak Ho Chu, Amine Benaceur, Chris Krasnichuk, Samuel Pichardo, Rajiv Midha

University of Calgary, Calgary, AB, Canada

Background: In peripheral nervous system (PNS), the endoneurial microvessels within the nerve fascicle and the investing perineurium which directly contact the circulating blood form the blood nerve barrier (BNB). BNB protects the endoneurial microenvironment, but also limits the effective delivery of therapeutic agents into the injured site for treatment. Focused ultrasound (FUS) combined with microbubbles (MB) have been proved to successfully achieve the blood-brain barrier disruption. However, the effect of this combined treatment on the PNS and BNB, to our knowledge, have not been investigated. This study aims to evaluate the feasibility of using FUS and MB to achieve BNB disruption in a rodent model for localized delivery of therapeutic agents into the PNS.

Materials and Methods: Four Female rats (Sprague Dawley, 250-350 g) were used in this study. All procedures were approved by the Animal Care and Use Committee in University of Calgary. The animal was anesthetized using 1 – 2 L/min of 100% oxygen mixed with 2-3% isoflurane. Upon shaving, the sciatic nerve was surgically exposed on both legs. After preparation, the animal was transferred and stabilized on the benchtop FUS system (RK50, FUS Instruments) for target localization. Prior to FUS sonication, Evans blue dye was injected via tail vein, and 5 minutes were allowed for adequate circulation. A bolus injection of MB (n = 3 for 20 µl/kg, n = 1 for 40 µl/kg, Definity, Lantheus) was administered via tail vein, followed by 0.2ml saline flush. Two dosages were used to investigate the effective dosage threshold. Pulsed FUS exposures were delivered immediately after the MB injection with a fundamental frequency of 476.5 kHz. The pulse width was 10 ms with 1 Hz repetition frequency and the total exposure duration was 120 sec. The peak negative pressure at the focus was 0.3 MPa. Acoustic emissions during the exposures were collected via a passive cavitation detector. The treated nerve was harvested afterwards, and histology analysis was performed to compare to a well-established rodent crush-injury model developed in our group to evaluate the BNB disruption effect.

Figure 1. Blood-nerve barrier disruption effect and acoustic emissions during FUS exposures.

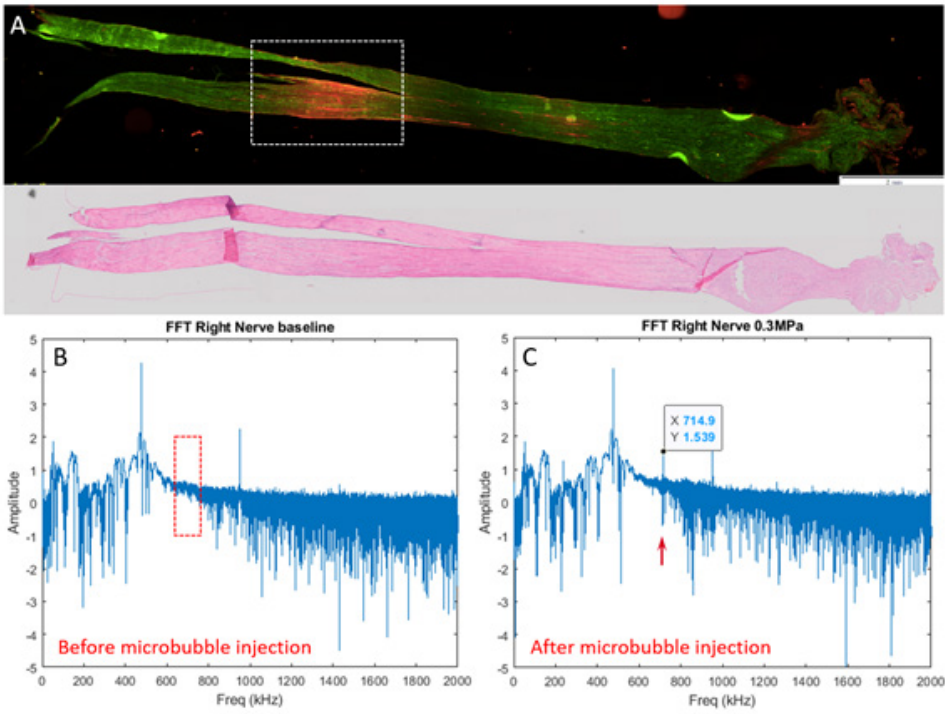

Results: Evans blue dye leakage was confirmed at the target region in histology evaluation (red, Figure 1A) in the nerve administered with 40 µl/kg MB, and two of three nerves administered with 20 µl/kg MB, indicating a higher dosage might be required to achieve effective BNB disruption. Prior to MB injection, no ultra-harmonic emission was detected via the passive acoustic detector (Figure 1B), which was detected after bubble injection (Figure 1C, indicated by arrow).

Conclusions: Disruption of BNB in the PNS was achieved using focused ultrasound and microbubbles in a rodent model. Ongoing work encompassing optimal pressure and bubble concentration threshold and will be presented in the meeting.

P-BBB-2

Topic: Blood-Brain Barrier Opening

Presentation Type: Poster

Mri-contrast enhancement of copper oxide nanoparticles following fus-mediated bbb disruption

Daniel Dahis[1], Galit Saar[1], Iris S. Weitz[2], Natalie Artzi[3], Haim Azhari[1]

[1]Technion Institute of Technology, Haifa, Israel
[2]ORT Braude College, Karmiel, Israel
[3]Harvard Medical School, Cambridge, MA, USA

Background: MRI contrast agents (CA) are widely used for brain tumor imaging as a means to delineate tumor borders, surgery planning, and treatment. While these agents are very important for imaging, they lack anticancer therapeutic abilities. Copper-based nanoscale materials constitute a promising multifunctional candidate for brain tumor imaging and treatment. In addition to multiple anti-cancer therapeutic effects demonstrated in brain cancer cell lines[1] copper oxide nanoparticles (CuO NPs) were demonstrated to increase ultrasonic attenuation to a level detectable by ultrasound and to improve MRI contrast in non-cerebral regions[2].

Thus, this pilot study aimed to assess the in-vivo MRI detection feasibility of CuO NPs accumulation in the brain following focused ultrasound (FUS)-mediated blood-brain barrier (BBB) disruption, in mice.

Materials and Methods: FUS-mediated BBB disruption was performed using a 1 MHz therapeutic probe (Mettler Electronics) coupled with an acoustic lens (Perspex; focal distance: 4 mm; peak negative pressure = 0.8MPa, accounting for the mice skull); pulse length = 50 ms; PRF = 1 Hz). Two C57BL/6 mice were anesthetized using isoflurane and positioned in a stereotaxic platform bed (Stoelting Co.). Evans Blue (EB) was administered intravenously (I.V.) prior to sonication. FUS-mediated BBB disruption (duration = 60 sec) was applied to the left hemisphere. At the beginning of sonication, microbubbles (SonoVue®; 50 uL) were administered as a bolus injection followed by a saline flush. The mice were then transferred to a 9.4T MRI (Bruker Biospec) for scanning. Images were acquired using a T1-weighted RARE sequence (TR/TE=1400/16.22,100 um in-plane resolution, 0.5 mm slice, 16 slices, Avg = 4) prior and following an I.V. injection of CuO NPs (7 nm in diameter; 4mg/kg). The obtained post-injection images were co-registered to the pre-injection image using MIPAV (NIH) software. This was done as the mice were moved in and out of the scanner for the CuO NPs injection. Contrast-to-noise ratio (CNR) was calculated by selecting regions of interest (ROI) within the treated zone and identical-contralateral ROIs and a reference ROI in air (outside the anatomic image of the head). The contrast enhancement at each frame was then calculated by subtracting the contralateral signal from the signal of the treatment ROI.

Results: The MRI images revealed contrast enhancement in the treatment zone post-CuO NPs injection which correlated with the region of Evans Blue extravasation, revealed by gross pathology (Figure 1). For each mouse, three post-injection images were acquired consecutively (acquired within 24± 9 min post-injection). The cross-section images containing the most prominent effect were chosen for processing. Data was transferred to MIPAV software for analysis. The measured averaged CNR enhancement of the six (n=2 mice x 3 frames) time point images was 4.76%± 1.38% when compared to the contralateral untreated ROI.

Conclusions: The in-vivo contrast-enhancing effect of CuO NPs accumulation in the brain following FUS-mediated BBB disruption was demonstrated. To the best of our knowledge, this is the first report on CuO NPs introduction into the brain following FUS-mediated BBB disruption. These preliminary findings can serve for future studies investigating novel theranostic CuO NPs-based strategies for imaging and treatment of brain tumors.

Acknowledgements: Aharon Alfasi, Technion Integrated Cancer Center (TICC), European Association for Cancer Research (EACR), MISTI (MIT-Israel Zuckerman STEM Fund), The U.S.-Israel Binational Science Foundation (BSF) Bination.

Figure 1. Gross pathology of a treated mouse brain depicting EB extravasation in the targeted zone (left) and contrast enhancement MRI image of the treatment region following CuO NPs injection (right).

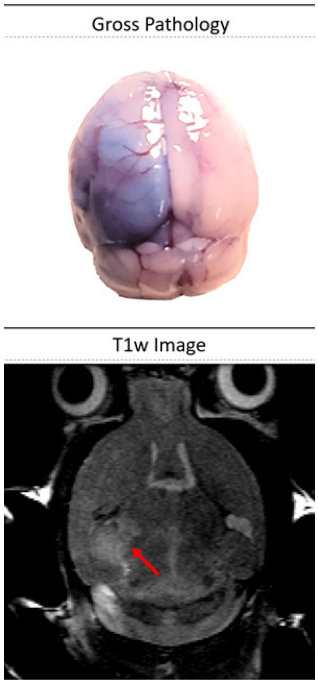

References:

1. Arundhati J. et al. Uptake and Toxicity of CuO NPs in C6. *Neurochem Res*. Published online 2016. doi:10.1007/s11064-016-2020-z
2. Perlman O. et al. CuO NPs as contrast agents for MRI and ultrasound dual-modality imaging. *Phys Med Biol.* 2015;60(15):5767-5783. doi:10.1088/0031-9155/60/15/5767

P-BBB-3

Topic: Blood-Brain Barrier Opening

Presentation Type: Poster

Focused ultrasound-induced augmentation of solute clearance predicted by fluid dynamic model simulation of the glymphatic system

Delaney Fisher, Richard Price

University of Virginia, Charlottesville, VA, USA

Background: The glymphatic system drives waste clearance in the brain by bulk flow of cerebral spinal fluid (CSF) from periarterial spaces across the glia limitans and parenchyma to the perivenous spaces, where solute is further cleared into the subarachnoid space and venous sinuses (Fig. 1). A new study affirms glymphatics in humans by examining contrast agent efflux following focused ultrasound (FUS) blood-brain barrier disruption (BBBD), furthering support for FUS enhancement of brain solute clearance (Ann. Neurol. 86, 975–980; 2019). Recent findings by our group indicate that BBBD via FUS in vivo can increase the size of perivascular spaces, substantiating similar results of pulsed ultrasound on ex vivo brain slices Brain Res. 1646, 543–50; 2016). While many glymphatic parameters remain unknown, computational simulation of solute clearance via this system can inform many FUS-mediated therapeutic approaches: drug/gene delivery, immunotherapy, and neurotoxin removal (e.g. amyloid beta).

Materials and Methods: A fluid dynamics model of glymphatic system clearance was developed using COMSOL Multiphysics software. The model is comprised of 5 compartments representing the periarterial space (16 microns FUS-; 20 microns FUS+), two glial limitans barriers (1 micron), the parenchyma (250 microns), and the perivenous space (10 microns FUS-; 12.6 microns FUS+; Fig. 2). Fully developed, laminar Stokes flow is simulated in the periarterial and perivenous spaces, while flow in porous media is simulated via the Brinkman equation in the glia limitans and parenchyma compartments. Solute transport is modeled for a solute comparable to dextran tracers (effective diffusion coefficient in the parenchyma=1E-11 m^2/s) at a bolus initial concentration of 0.5 mMol in the middle parenchyma compartment. Analysis of perivascular space augmentation post-FUS BBBD was performed on 20x H&E stained brain sections from mice anesthetized with either i.v. injection of albumin-shelled microbubbles (10^5/ g) without FUS sonications or with FUS sonications (0.4 MPa peak-negative pressure, 120-s duration, 10-ms bursts, 0.5-Hz burst rate) stereotaxically targeted to the right striatum. Diameter measurements of perivascular spaces and vessels were recorded. Measurements were made for vessels larger than 5 micron and with clearly visible perivascular spaces. The average ratio of perivascular space diameter to vessel diameter for FUS- (n=44) and FUS+ (n=35) groups were compared.

Results: To determine the effect of FUS on the perivascular space width, the ratio of perivascular space diameter to vessel diameter was measured from H&E images of the striatum from either sham mice or FUS+MB treated mice. H&E analysis revealed that FUS BBBD increases the perivascular space diameter to vessel diameter ratio on average by 26% (Fig. 3A-B; p=0.0002). To investigate how an increase in the perivascular spaces influences fluid dynamics of the glymphatic system, simulations of solute clearance were performed with baseline and 26% larger periarterial and perivascular space widths (Fig. 3C). The increased perivascular space widths augmented the volumetric fluid flow rate in the periarterial glia limitans by 10%, the parenchyma by 9%, and the perivenous glia limitans by 12%. Correspondingly, the FUS+ simulation resulted in a 12% decrease in solute half-life in the parenchyma compared to simulations with FUS- perivascular space widths.

Conclusions: Through computational simulation of the glymphatic system, FUS-induced augmentation of perivascular spaces is predicted to increase solute clearance. While we have currently only explored how changes perivascular space width changes affect clearance, other potential biological alterations stimulated by FUS (i.e. porosity, anisotropy) could also be investigated with this model. Our model has the potential to provide insightful predictions for many FUS applications such as temporal concentration of delivered drug and genes, tumor antigen clearance for immune priming, and amyloid beta clearance in Alzheimer's disease.

Acknowledgements: Supported by National Institutes of Health Grants R01EB020147 and R21EB024323 to R.J.P. D.G.F. was supported by the Cardiovascular Research Training Grant and a Wagner Fellowship.

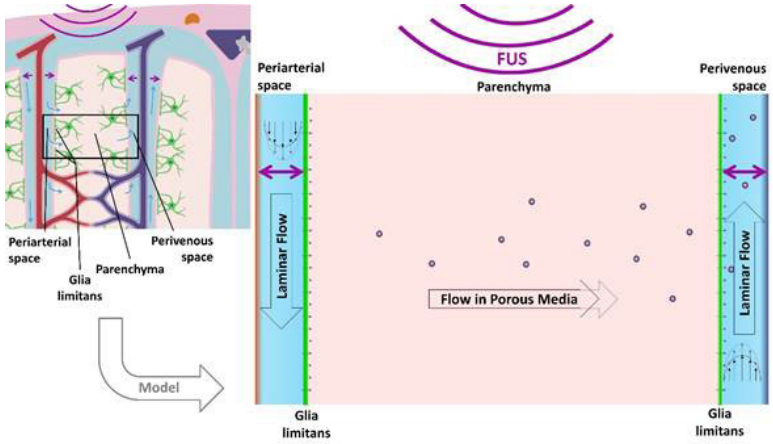

Figure 1. (Left) Schematic diagram of the glymphatic system. (Right) Fluid dynamic interpretation of the glymphatic system for computational model of solute clearance from the brain parenchyma.

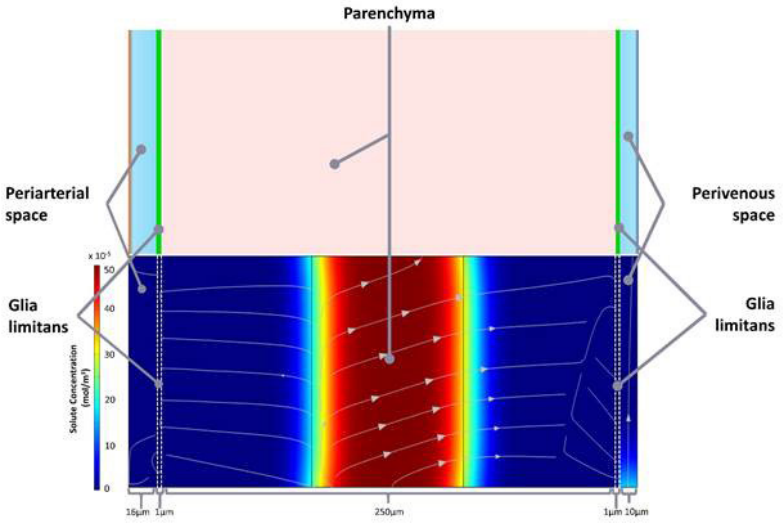

Figure 2. Depiction of glymphatic system compartments and their dimensions in schematic format and in COMSOL model. Rainbow color map indicates solute concentration profile for dextran tracer analog.

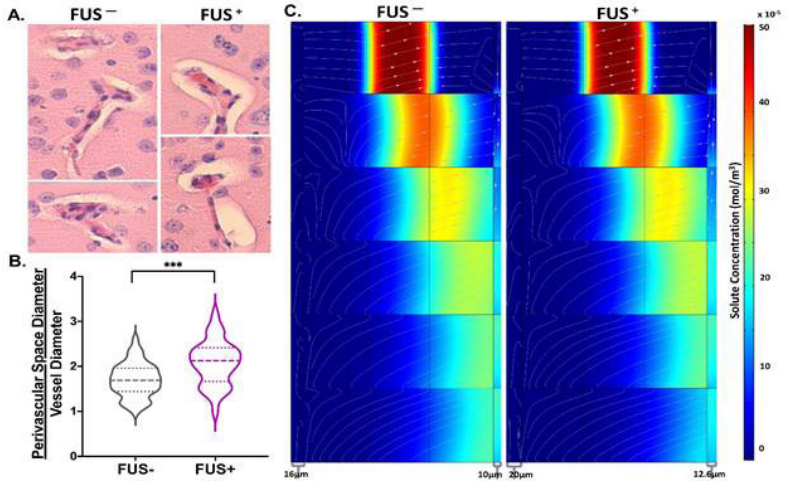

Figure 3. A) Representative H&E stained brain sections. B) Perivascular space and vessel diameter ratio measurements. C) Temporal solute concentration profile for FUS+ and FUS- conditions.

P-BBB-4

Topic: Blood-Brain Barrier Opening

Presentation Type: Poster

Logic-based signaling network model of brain endothelial cells predicts impact of FUS-induced transcriptomic responses on blood-brain barrier protein recycling

Catherine Gorick, Richard Price, Jeffrey Saucerman

University of Virginia, Charlottesville, VA, USA

Background: Focused ultrasound (FUS) has been widely used to transiently disrupt the blood-brain barrier (BBB) to facilitate the targeted delivery of therapeutics for applications such as cancer and neurodegenerative disease. Recent work has demonstrated that disruption of the BBB with FUS may be associated with transcriptome-level alterations in gene sets associated with sterile inflammation, cell-cell junctions, metabolism, and tissue repair. In past studies, boolean logic-based systems of differential equations have been used to model a number of signaling networks and predict the effects of interventional strategies. Here, we develop such a model for brain endothelial cell signaling, which we use to predict how transcriptomic changes resulting from FUS treatment of the brain could impact BBB integrity.

Materials and Methods: A consensus signaling network was reconstructed from manual curation of experimental studies in the literature, with a focus on the brain-derived neurotrophic factor (BDNF) and vascular endothelial growth factor (VEGF) signaling pathways and their role in regulating the transcription or recycling of BBB tight junction proteins (Fig. 1). The network was converted into a predictive computational model using a logic-based ordinary differential equation (ODE) modeling approach, with each node's activity governed by a normalized Hill ODE with default parameters and logic gating. The following in vivo studies informed the model input: FUS was applied to the brains of C57Bl/6 mice to transfect the tissue with an mRuby transgene. 24 hours after FUS, transfected cells were isolated via FACS using the mRuby fluorescence (Fig. 2A). We then conducted single cell RNA sequencing (scRNAseq) of the transfected cells and identified the endothelial cell population (Fig. 2B). Differential gene expression analysis was conducted between the FUS-transfected endothelium and control FUS-naïve brain endothelial cells, and used to identify transcripts significantly upregulated by FUS (Fig. 2C). The gene with the largest significant upregulation was then used as an input for the network model (with other inputs set to a low baseline value), to predict the effects on endothelial cell phenotype and BBB integrity in the days following FUS treatment.

Results: The computational network consists of 40 nodes (including proteins, small molecules, and phenotypes) and 56 edges connecting those nodes (Fig. 1). In vivo transfection of the mouse brain via 0.4 MPa FUS with microbubbles resulted in 12.4% transgene-positive cells in the targeted brain quadrant 24 hours after treatment (Fig. 2A). scRNAseq permitted identification of unique cell populations, including endothelial cells (Fig. 2B). The most upregulated transcript in the FUS-treated endothelium relative to control was cathepsin D (Fig. 2C). A focused literature search identified a function of cathepsin D in upregulating ERK and AKT in endothelial cells. We therefore added a cathepsin D node to the model, and simulated a bolus input of cathepsin D (Fig. 3A). The network predicted that this would result in an increase in cell growth and survival signaling as well as decreased BBB integrity (Fig. 3B), likely due to facilitate increased cell growth or angiogenic processes.

Conclusions: Here, we demonstrate the capacity of computational signaling models to predict cell phenotype outcomes in response to unique molecular inputs, including those informed by in vivo transcriptomic studies. Such models have previously been utilized to predict the responses of cardiac fibroblasts to mechanical stimuli, and we hypothesize that they could prove useful in the field of FUS to estimate long-term signaling changes as a result of short-term transcriptomic alterations, as well as to optimize choices of target genes for delivery in disease contexts.

Acknowledgements: Supported by National Institutes of Health Grants R01EB020147 and R21EB024323 to R.J.P. C.M.G. was supported by American Heart Association Fellowship 18PRE34030022.

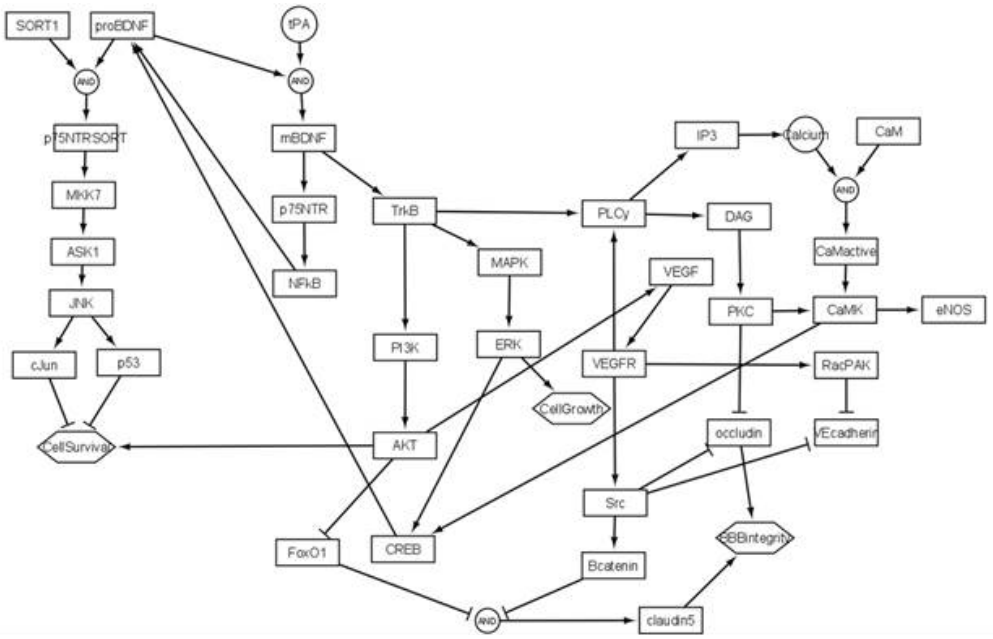

Figure 1. A Boolean logic driven signaling network illustrates the interplay between the BDNF and VEGF signaling pathways and various cell phenotypes, including BBB integrity.

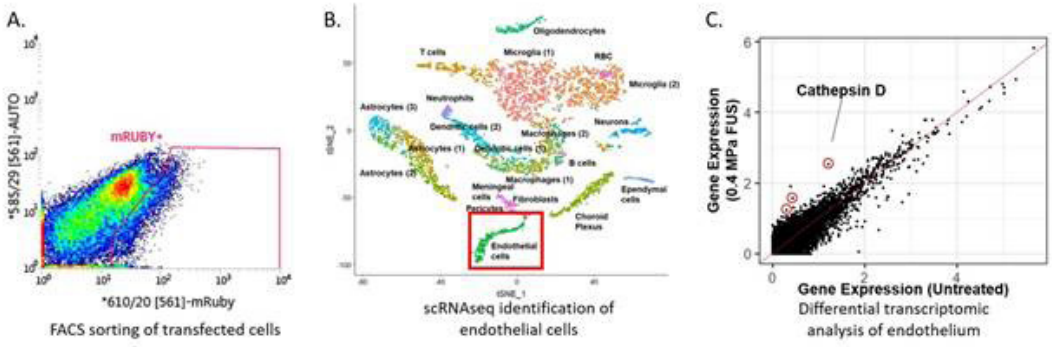

Figure 2. In vivo identification of differentially expressed genes in FUS-treated endothelium.

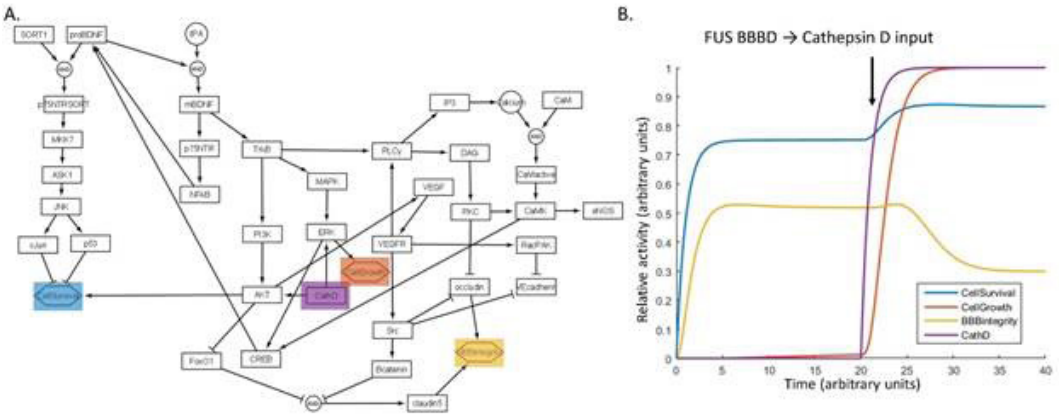

Figure 3. Network model predicts endothelial phenotypic responses to a simplified "Cathepsin D" input, generated by FUS BBBD.

P-BBB-6

Topic: Blood-Brain Barrier Opening

Presentation Type: Poster

Phagocytic response to focused ultrasound-mediated blood-brain barrier opening

Alina Kline-Schoder, Rebecca Noel, Sana Chintamen, Elisa Konofagou

Columbia University, New York, NY, USA

Background: More than 5 million people in the United States and nearly 50 million worldwide are suffering from Alzheimer's Disease (AD) or related dementia, making it the most common neurodegenerative disorder. The signature biological markers of AD are an accumulation of amyloid-beta plaques and hyperphosphorylated protein-tau (p-tau) tangles. A reduction in pathology and improvement in associated behavioral deficits is shown in transgenic AD mice when they are treated with focused-ultrasound (FUS) blood brain barrier (BBB) opening.

Pathology reduction has been suggested to be due to the stimulation of microglia, the central nervous system's main phagocytic cell. However, the increased blood-brain barrier permeability due to FUS may also allow the infiltration of macrophages, which hold a similar phagocytic role in the periphery. Macrophage infiltration is the marker used in this study to quantify the immunogenicity of FUS-mediated BBB opening.

Materials and Methods: C57 wild-type mice (n=5/group) were split into two groups – 1) FUS/MB, and 2) MB only, which acted as the negative control. The FUS/MB group was treated with FUS at a frequency of 1.5 MHz, a peak negative pressure of 450 kPa and a PRF of 2 Hz for 120 sec. Prior to sonication, the FUS/MB group was IV injected with in-house, customized polydispersed microbubbles. The MB group was injected with the microbubbles, but were not treated with FUS and so no BBB opening was expected. All mice underwent a contrast-enhanced MRI (Bruker, 9.4T) to evaluate BBB opening within 1 hour post-opening. 24 hours post-treatment, mice were perfused and the targeted area was extracted, homogenized and flow cytometry (BD FACSCANTO II) was used to quantify the macrophage population.

MRIs were post-processed on Matlab using manual area selection followed by 3-Dimensional K-Means filtering, resulting in a 3-dimensional rendering of the Gadolinium distribution in the brain at the time of imaging. The size of opening was quantified from this rendering.

All flow cytometry analysis was performed on FCS Express 7.0. All FCS files were filtered to exclude debris, doublets and dead cells before the macrophages were quantified due to their CD11B and CD45 positivity.

Results: As expected, all mice in the FUS/MB group had a BBB opening that could be detected with the MRI processing. The openings from this group were quantified to range between 20 and 80 mm3. The MB only group was used as a negative control and had no detectable opening. The mice in the FUS/MB group had a macrophage population between 0.5 and 1.5% of the alive cells as compared to less than 0.7% of the cells as was seen in the MB group. When the size of the macrophage infiltration was plotted as a function of opening volume for the FUS/MB group, a linear correlation emerges (Figure 1). This correlation is found to be statistically significant with a P-value of 0.03 and an R2 value of 0.53.

Figure 1.

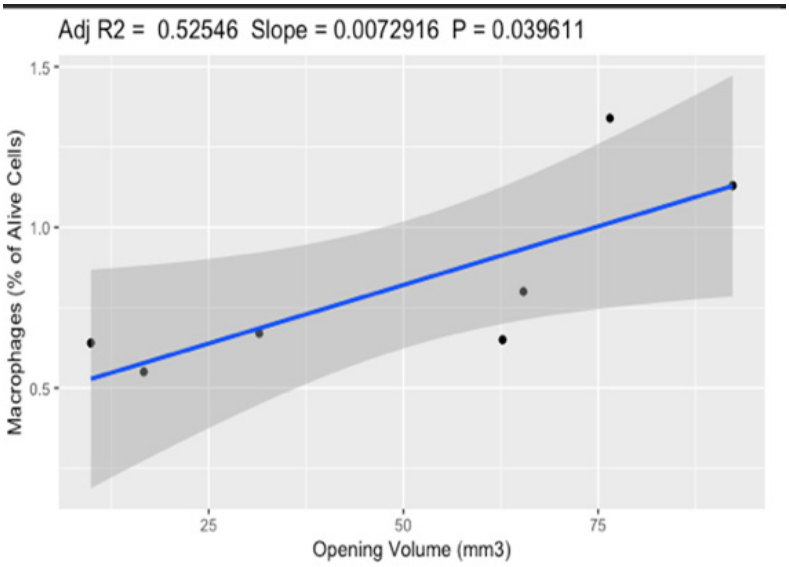

Conclusions: In this study, infiltration of macrophages was hereby detected 24 hours after BBB opening. We also found that this infiltration increases linearly with the opening volume computed 1 hour after FUS. Ongoing efforts include longer time-points post-opening to determine reinstatement of macrophages in the periphery as well as quantify the reactivity of the infiltrating macrophages in conjunction with microglia in order to fully characterize their effects on immunogenicity post-BBB opening.

P-BBB-7

Topic: Blood-Brain Barrier Opening

Presentation Type: Poster

Microvessel rupture induced by high-intensity therapeutic ultrasound exposure in the presence of mi-crobubbles using a novel model, lumbricus terrestris, earthworms

Asis Lopez[1], Yaswitha Mikkilineni[2], Shayna Berman[3], Damir Khismatullin[4], Gregory T. Clement[1], Matthew R. Myers[1]

[1]FDA, Silver Spring, MD, USA
[2]Virginia Commonwealth University, Richmond, VA, USA
[3]Montgomery College, Takoma Park, MD, USA
[4]Tulane University, New Orleans, LA, USA

Background: The blood-brain barrier (BBB) is a vital feature of the brain that prevents the introduction of toxic substances. Tightly bound endothelial cells forming the blood vessel walls serve as gatekeepers, regulating which molecules can pass into the brain. An approach to getting drugs past the BBB involves the use of focused ultrasound in conjunction with gas filled microbubbles. While multiple clinical studies of microbubble-enhanced BBB opening are progressing, the thresholds for vessel damage are not well understood. We present the earthworm as a useful model for studying vasculature rupture induced by High-Intensity Therapeutic Ultrasound (HITU) + Microbubbles.

Materials and Methods: Although vertebrates are indispensable to biomedical research, studies are often limited by factors such as cost, lengthy internal review, and ethical considerations. The earthworm model allows large number of trials that enable identification of the critical characteristics of bubbles, blood vessels, and acoustic fields affecting the threshold for blood-vessel rupture in HITU + Microbubble applications. In the experiments performed, the driving frequencies were 0.5, 1.1, 2.5, and 3.3 MHz, and the pulse repetition frequencies were 1, 3 and 10 Hz. The duty factor was held at 0.1%.

Results: An extensive database of vessel-rupture probabilities and times was created for both HITU and HITU + Microbubbles as a function of critical parameters, including microbubble dosage and size, and ultrasound operating frequency and intensity.

Conclusions: The outcomes of these in vivo experiments are expected to assist in predicting the rupture probability for HITU + Microbubble procedures. They will also inform a computational model of bubble-induced vessel rupture.

P-BBB-8

Topic: Blood-Brain Barrier Opening

Presentation Type: Poster

Blood brain barrier opening for drug delivery – state of the field

Juliette Strubel[1], Kelsie Timbie[2], Suzanne LeBlang[2]

[1]Focused Ultrasound Foundation, London, United Kingdom
[2]Focused Ultrasound Foundation, Charlottesville, VA, USA

Background: The blood brain barrier (BBB) excludes 98% of small molecules, allowing the crossing of only 1% of intravenously injected substances, weighing < 400 Daltons. Focused ultrasound (FUS) is advantageous compared to other drug delivery methods as it is non-invasive yet provides targeted therapy. BBB opening is induced through low intensity focused ultrasound (LIFU) which is different to high intensity focused ultrasound (HIFU), already FDA approved for multiple indications with thermal ablation. Numerous published studies cite the ability of FUS to increase the concentration of neurotherapeutics crossing the BBB that delay disease progression for Alzheimer's Disease, Parkinson's Disease and glioblastomas. Research suggests that opening the BBB with ultrasound is not binary, but rather a continuum with potential to control the extent of BBBO by adjusting ultrasound beam technical parameters. The purpose of this poster is to present the classes and sizes of therapeutics able to cross the BBB.

Materials and Methods: An extensive literature search performed from 2012 to 2020 using the search terms "blood brain barrier opening" and "focused ultrasound", identified 227 preclinical and clinical articles which discussed BBBO for various neurotherapeutics. Examination of reference lists of these studies uncovered additional articles. A summary of the architecture of the neurovascular unit and the physiology of the BBB including the various methods of molecular transport across the BBB will be explained including cellular vesicles for transcytosis, endocytosis, paracellular passages/tight junctions, and cytoplasmic channels in the endothelium. The different classes of molecules including the size and weights of specific subtypes are incorporated into a table (Table 1).

Results: For antibodies, the largest agent was human epidermal growth factor receptor 2 (Her2/erbB2)-185 kDa, and the smallest a dopamine receptor D4 antibody-48 kDa. In gene therapy agents, the largest was the reporter gene AAV-4000 kDa, and vascular endothelial growth factor packaged in plasmids was the smallest-23 kDa. For chemotherapy, the largest agent was unencapsulated Temozolomide (TMZ)-194 kDa, and the smallest unencapsulated BCNU-0.214 kDa. The largest drug was unencapsulated IL-12-70 kDa and the smallest drug, Propofol packaged in a nanoemulsion-0.178 kDa. Under nanoparticles, the largest agent was specialised brain-penetrating nanoparticles (SBPNP), packaged in poly(ethylene glycol),-60nm, the smallest being therapeutic magnetic nanoparticles (MNPs) packaged in polysaccharides,-13nm. Under various cells, Natural Killer (NK) were the largest agents with a diameter varying from 6000-7000nm, and iron-labeled GFP-expressing neural stem cells with a diameter of 60nm, were the smallest.

Conclusions: Knowledge of the specific size and weights of therapeutics that are able to cross the BBB is critical in ensuring safety and efficacy of FUS-induced BBBO. We encourage people to use this illustration and video to better understand BBBO and consider the use of new or repurposed medications which could potentially cross the BBB with the aid of ultrasound and treat a variety of diseases.

	Diameter (nm)	Weight (kDa)
Red Blood Cell	7500-8700	N/A
Microbubble	1000-10000	N/A
Optison contrast agent (Albumin + Perflutren)	3000-4500	N/A
SonoVue contrast agent (sulphur hexafluoride MBs)	2500	N/A

Table 1.

continued, next page

Table 1. (continued)

continued, next page

Therapeutic Size Compared To A Red Blood Cell

Category	Therapeutic Agent	Packaging	Diameter (nm)	Weight (kDa)
Antibodies	Anti-AB (IgG)	Unencapsulated	14.5 nm	150 kDa
	Bevacizumab	Unencapsulated	21.4 nm	150 kDa
	Herceptin / Trastuzumab	Unencapsulated	5 nm	150 kDa
	Dopamine receptor D4 antibodies	Unencapsulated	N/A	150 kDa
	Human epidermal growth factor receptor 2 (HER2/erbB2)	Unencapsulated	N/A	185 kDa
	Amyloid-ß antibodies	Unencapsulated	13 nm	150 kDa
	Endogenous IgG and IgM	Unencapsulated	14.5 nm	150 kDa
Gene Therapy Agents	Reporter Genes	AAV	20 nm	4000 kDa
	GDNF / reporter gene	Liposome	100 nm	26 kDa
	GDNF	Microbubble	5000 nm	24 kDa
	Plasmid DNA (BDNF / reporter gene)	Microbubble	5000 nm	N/A
	BDNF	Neurotrophic factor	N/A	145 kDa
	GDNF / PEI-PEG	Polymeric Nanoparticle	56 nm	N/A
	cc-siRNA-Htt	Unencapsulated	50 nm	N/A
	Vascular endothelial growth factor	Plasmids	4.12 nm (monomer) /5.20 nm (dimer)	23 kDa
	AAV9-GFP	N/A	20 nm	4000 kDa
	AAV2-GFP	N/A	20 nm	4000 kDa
	NTN (Neurturin)	Unencapsulated	N/A	24 kDa
Chemotherapy	DOX	Liposome	N/A	0.543 kDa
	DOX	Liposome (targeted)	N/A	0.543 kDa
	DOX	Liposome (thermosensitive)	N/A	0.543 kDa
	DOX	Microbubble	N/A	0.543 kDa
	DOX	Unencapsulated	N/A	0.543 kDa
	Cisplatin / PAA-PEG	Polymeric nanoparticle	60 nm	N/A
	BCNU	Polymeric nanoparticle	10-20 nm	N/A
	BCNU	Unencapsulated	N/A	0.214 kDa
	DOX/PLGA	Polymeric nanoparticle	80 nm	N/A
	DOX/PLGA	Polymeric nanoparticle (targeted)	100 nm	N/A
	Paclitaxel / PLGA-PEG	Polymeric nanoparticle	170 nm	N/A
	Paclitaxel	Liposome	98.3 nm	N/A
	Cytarabine	Unencapsulated	N/A	0.243 kDa
	Temozolomide (TMZ)	Unencapsulated	N/A	194 kDa
	Methotrexate	N/A	N/A	0.545 kDa
Drugs	Propofol	Nanoemulsion	N/A	0.178 kDa
	IL-12	Unencapsulated	N/A	70 kDa
Nanoparticles	1,3-bis(2-chloroethyl)-1-nitrosourea) (a chemotherapy agent)	BCNU	N/A	0.21 kDa
	Therapeutic magnetic nanoparticles (MNPs)	Polysaccharides	13 nm	N/A
	Specialised brain - penetrating nanoparticles (SBPNP)	Poly (ethylene glycol) (PEG)	60 nm	N/A
	Gold nanoparticles/ nanoparticles with scattering (SERS) capability	N/A	20 nm	N/A
Cells	Iron-labeled GFP-expressing neural stem cells	N/A	60 nm	N/A
	Natural Killer (NK) cells expressing chimeric Her2 antigen receptor	N/A	6000-7000 nm	N/A
	Erythropoetin	N/A	N/A	21-37 kDa
Imaging	PS-PEG	Polymeric nanoparticle	40-60 nm	N/A
	Dextran	Unencapsulated	N/A	70 kDa

Table 1. (continued)

Cells	Iron-labeled GFP-expressing neural stem cells	N/A	60 nm	N/A
	Natural Killer (NK) cells expressing chimeric Her2 antigen receptor	N/A	6000-7000 nm	N/A
	Erythropoetin	N/A	N/A	21-37 kDa
Imaging	PS-PEG	Polymeric nanoparticle	40-60 nm	N/A
	Dextran	Unencapsulated	N/A	70 kDa

Gene Therapy Agents
AAV – Adeno-Associate Virus (used as a vector)
GDNF - Glial cell-derived neurotrophic factor (encoded by GDNF gene)
BDNF - brain derived neurotrophic factor (encoded by BDNF gene)
PEI-PEG – Copolymers

Weights VS Size of Therapeutics
For smaller drugs: usually nm are used, as it is easier to compare these sizes.
For larger drugs: usually Da are used, as therapeutic packaging significantly affects weight.

1. Tan YH, Liu M, Nolting B, Go JG, Gervay-Hague J, Liu G. A Nanoengineering Approach for Investigation and Regulation of Protein Immobilization. *ACS Nano*. 2008;2(11):2374-2384. doi:10.1021/nn800508f
2. Sousa F, Cruz A, Fonte P, Pinto IM, Neves-Petersen MT, Sarmento B. A new paradigm for antiangiogenic therapy through controlled release of bevacizumab from PLGA nanoparticles. *Sci Rep*. 2017;7(1):3736. doi:10.1038/s41598-017-03959-4
3. Timbie KF, Mead BP, Price RJ. Drug and gene delivery across the blood–brain barrier with focused ultrasound. *Journal of Controlled Release*. 2015;219:61-75. doi:10.1016/j.jconrel.2015.08.059
4. Presset A, Bonneau C, Kazuyoshi S, et al. Endothelial Cells, First Target of Drug Delivery Using Microbubble-Assisted Ultrasound. *Ultrasound in Medicine & Biology*. 2020;46(7):1565-1583. doi:10.1016/j.ultrasmedbio.2020.03.013
5. Shen Y, Pi Z, Yan F, et al. Enhanced delivery of paclitaxel liposomes using focused ultrasound with microbubbles for treating nude mice bearing intracranial glioblastoma xenografts. *IJN*. 2017;Volume 12:5613-5629. doi:10.2147/IJN.S136401
6. Samiotaki G, Acosta C, Wang S, Konofagou EE. Enhanced Delivery and Bioactivity of the Neurturin Neurotrophic Factor through Focused Ultrasound—Mediated Blood—Brain Barrier Opening *in vivo*. *J Cereb Blood Flow Metab*. 2015;35(4):611-622. doi:10.1038/jcbfm.2014.236
7. Lin C-Y, Hsieh H-Y, Pitt WG, et al. Focused ultrasound-induced blood-brain barrier opening for non-viral, non-invasive, and targeted gene delivery. *Journal of Controlled Release*. 2015;212:1-9. doi:10.1016/j.jconrel.2015.06.010
8. Burgess A, Shah K, Hough O, Hynynen K. Focused ultrasound-mediated drug delivery through the blood–brain barrier. *Expert Review of Neurotherapeutics*. 2015;15(5):477-491. doi:10.1586/14737175.2015.1028369
9. Iqbal N, Iqbal N. Human Epidermal Growth Factor Receptor 2 (HER2) in Cancers: Overexpression and Therapeutic Implications. *Molecular Biology International*. 2014;2014:1-9. doi:10.1155/2014/852748
10. Chai W-Y, Chu P-C, Tsai C-H, et al. Image-Guided Focused-Ultrasound CNS Molecular Delivery: An Implementation via Dynamic Contrast-Enhanced Magnetic-Resonance Imaging. *Sci Rep*. 2018;8(1):4151. doi:10.1038/s41598-018-22571-8
11. Sierra C, Acosta C, Chen C, et al. Lipid microbubbles as a vehicle for targeted drug delivery using focused ultrasound-induced blood–brain barrier opening. *J Cereb Blood Flow Metab*. 2017;37(4):1236-1250. doi:10.1177/0271678X16652630
12. Fan C-H, Yeh C-K. Microbubble-enhanced Focused Ultrasound-induced Blood–brain Barrier Opening for Local and Transient Drug Delivery in Central Nervous System Disease. *Journal of Medical Ultrasound*. 2014;22(4):183-193. doi:10.1016/j.jmu.2014.11.001
13. Valls-Comamala V, Guivernau B, Bonet J, Puig M. prevents amyloid β-peptide folding into β-sheet to form. :12.
14. Morse SV, Pouliopoulos AN, Chan TG, et al. Rapid Short-pulse Ultrasound Delivers Drugs Uniformly across the Murine Blood-Brain Barrier with Negligible Disruption. *Radiology*. 2019;291(2):459-466. doi:10.1148/radiol.2019181625
15. Tabatabaei SN, Girouard H, Carret A-S, Martel S. Remote control of the permeability of the blood–brain barrier by magnetic heating of nanoparticles: A proof of concept for brain drug delivery. *Journal of Controlled Release*. 2015;206:49-57. doi:10.1016/j.jconrel.2015.02.027
16. Meng Y, Pople CB, Lea-Banks H, et al. Safety and efficacy of focused ultrasound induced blood-brain barrier opening, an integrative review of animal and human studies. *Journal of Controlled Release*. 2019;309:25-36. doi:10.1016/j.jconrel.2019.07.023
17. Todd N, Angolano C, Ferran C, Devor A, Borsook D, McDannold N. Secondary effects on brain physiology caused by focused ultrasound-mediated disruption of the blood–brain barrier. *Journal of Controlled Release*. 2020;324:450-459. doi:10.1016/j.jconrel.2020.05.040
18. Varongchayakul N, Huttner D, Grinstaff MW, Meller A. Sensing Native Protein Solution Structures Using a Solid-state Nanopore: Unraveling the States of VEGF. *Sci Rep*. 2018;8(1):1017. doi:10.1038/s41598-018-19332-y
19. Diez-Silva M, Dao M, Han J, Lim C-T, Suresh S. Shape and Biomechanical Characteristics of Human Red Blood Cells in Health and Disease. *MRS Bull*. 2010;35(5):382-388. doi:10.1557/mrs2010.571
20. Holmes DI, Zachary I. The vascular endothelial growth factor (VEGF) family: angiogenic factors in health and disease. *Genome Biology*. Published online 2005:10.
21. Chen K-T, Wei K-C, Liu H-L. Theranostic Strategy of Focused Ultrasound Induced Blood-Brain Barrier Opening for CNS Disease Treatment. *Front Pharmacol*. 2019;10:86. doi:10.3389/fphar.2019.00086
22. Dziawer Ł, Majkowska-Pilip A, Gaweł D, et al. Trastuzumab-Modified Gold Nanoparticles Labeled with 211At as a Prospective Tool for Local Treatment of HER2-Positive Breast Cancer. *Nanomaterials*. 2019;9(4):632. doi:10.3390/nano9040632
23. Timbie K, Zhang C, Nance E, et al. Ultrasound-mediated delivery of brain-penetrating nanoparticles across the blood-tumor barrier. *J Ther Ultrasound*. 2015;3(S1):P34, 2050-5736-3-S1-P34. doi:10.1186/2050-5736-3-S1-P34
24. Timbie, K - personal communication

P-BBB-9

Topic: Blood-Brain Barrier Opening
Presentation Type: Poster

Computational fluid dynamic model simulation of immunotherapeutic antibody transport through the blood-brain barrier after focused ultrasound

E. Andrew Thim, Richard Price

University of Virginia, Charlottesville, VA, USA

Background: Focused ultrasound (FUS) in combination with intravenously injected microbubbles (MBs) is a proven approach for the safe, effective, and transient disruption of the blood-brain barrier (BBB) for therapeutic drug delivery. While both tight junction disruption and enhanced transcytosis occur during FUS+MBs BBB disruption (BBBD), our understanding of the relative impact of these mechanisms on total drug delivery are poorly understood and likely dependent on numerous parameters. Furthermore, over the course of a transient BBBD (typically 4-6 hours) treatment, drug delivery across the BBB will be temporally affected by changes in interstitial fluid pressure, drug clearance from tissue and tissue permeability. While defining the impact of these factors on drug delivery will ultimately require empirical approaches, we submit that computational fluid dynamic models of drug delivery across the disrupted BBB will allow us to generate therapeutic strategies for optimal delivery.

Materials and Methods: We developed our computational model of antibody transport across the BBB in COMSOL Multiphysics (ver. 5.5) modeling software in conjunction with the microfluidics module. By combining the 2D Brinkman equation (fluid flow) with the 2D diffusion-convection-reaction equation (solute transport) in porous media, we were able to construct a four-layer BBB model: arterial lumen, endothelial lipid bilayer, intracellular endothelial space and interstitial space (Fig 1). To approximate FUS-MB disruption of the BBB, the intrinsic permeability of the lipid bilayer was uniformly ramped up by 10,000-fold over 60 s. This increase in permeability was maintained for another 60 s before a permeability decrease was modeled via mono-exponential decay. The reference antibody and associated values were from literature values for T-DM1 (Trastuzumab) and the injection was approximated as a bolus intravenous injection with clearance modeled as a mono-exponential decay. The solute reaction equations involve free, bound and internalized antibody limited to the interstitial space. The user-defined mesh grid built in COMSOL has a minimum and maximum element size of 1 nm and 1.5 microns. We assumed fully developed laminar flow in the arterial lumen. The endothelial lipid bilayer, intracellular endothelial and interstitial spaces were considered porous media and laminar, low Reynolds number flow was assumed to neglect the inertial terms (Stoke's flow).

Results: Basally, the BBB protectively prevents large molecules from crossing into the interstitial space. In our model, this basal level is represented by an average concentration difference from the arterial lumen to the interstitial space by 9.5 orders of magnitude. By increasing the intrinsic permeability of the lipid bilayer by 100-fold, the concentration difference drops by 2.5 orders of magnitude. This concentration change was, in part, caused by the 2 orders of magnitude change average velocity pre-FUS and immediately post-FUS in the lipid bilayer, intracellular endothelial space and interstitial space.

Conclusions: With this model, we have shown the ability to mimic our FUS-mediated BBBD protocol by altering the intrinsic permeability of the endothelial lipid bilayer. This model predicts both velocity and concentration changes because of the simulated FUS disruption. With this model and its continued development, we will use this as a tool to explore other drug delivery mechanisms like endothelial tight-junction disruption and endocytosis of specific antibodies and small molecules.

Acknowledgements: Supported by National Institutes of Health (NIH) Grants R01EB020147 and R01CA197111. E.A.T. was supported by National Institutes of Health Cardiovascular Training Grant.

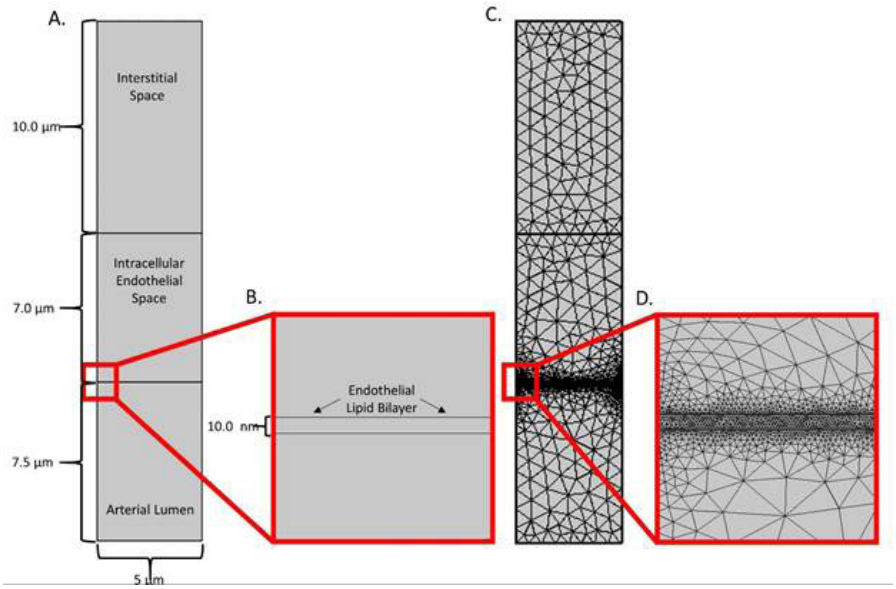

Figure 1. A) General geometric model of the blood-brain barrier (BBB). B) Magnified endothelial lipid bilayer. C) BBB geometry with mesh element overlay. D) Magnified endothelial lipid bilayer.

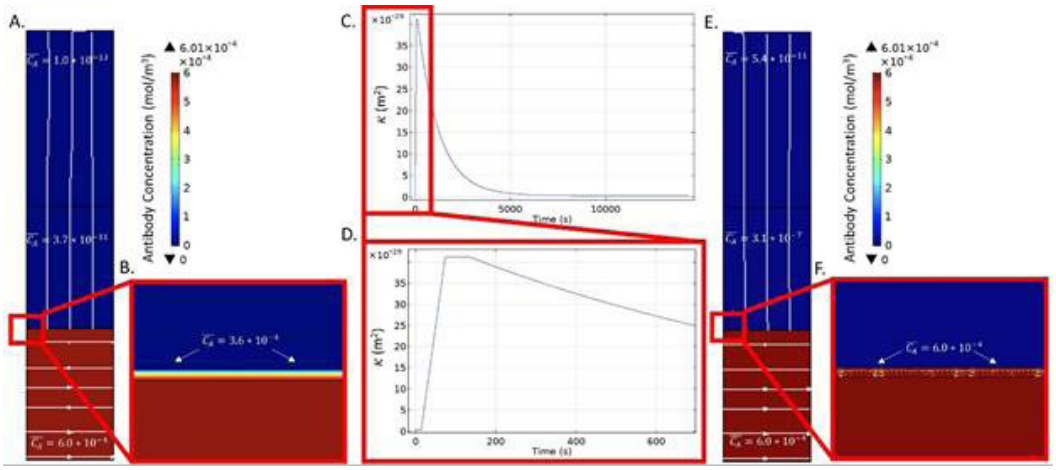

Figure 2. A,B) 2D antibody concentration distribution prior to FUS. C,D) Modeled permeability changes due to FUS BBBD with time (0-4 h). E,F) Antibody distribution post-FUS.

P-BBB-10

Topic: Blood-Brain Barrier Opening

Presentation Type: Poster

Preclinical evaluation of feedback control of ultrasound-induced blood-brain barrier opening via NaviFUS system

Chih-Hung Tsai[1], Wen-Ting Tsai[1], Han-Huei Chen[1], Hsiang-Yang Ma[1], Hao-Li Liu[2]

[1]NaviFUS Co. Ltd., Taipei, Taiwan (Republic of China)
[2]Chang Gung University, Tauyuan, Taiwan (Republic of China)

Background: Focused ultrasound (FUS) with microbubbles has been employed to temporally open the blood-brain barrier (BBB) for brain disease treatment such as brain tumors and Alzheimer's disease. Currently a clinical purposed neuronavigation-guided FUS system, NaviFUS, has been developed for FUS energy guidance. However, the procedure still lacks real-time feedback control to real-time monitor and control the procedure. Therefore, we aim to develop a real-time acoustic emission feedback control algorithm that can be implemented on this system.

Materials and Methods: NaviFUS is designed to transcranially deliver focal energy into the deep brain via multiple transmitting, and real-time receive multiple backscattered RF-channel data through multiple receiving channels. The FUS real-time feedback control procedure includes two stages, i.e. ramp stage and sonication stage. In ramp stage, the acoustic level would be increased until AE change reach ceiling threshold. In the following sonicate stage, the acoustic level would be decreased until AE change less than floor threshold and continuously proceed the exposure until the end of the exposure time. The performance of the developed algorithm was tested via animal experiments including 17 rats and 2 swines. In rat experiment (Fig 1a), we compared the BBB opening efficiency between fixed acoustic level versus the acoustic level real-time controlled by the feedback algorithm. In level fixing group, acoustic levels were fixed ranging from 0.191 to 0.300 MPa. In swine experiment (Fig 1c), we applied two targets, which one located on frontal cortex and the other one on hippocampus. Administration of microbubble was 0.1 ml/Kg intravenous injection before FUS exposure. Evans-Blue (EB) dye was injected following FUS exposure to confirm BBB-opening. T2*-weighted MRI as well as histological examinations were employed to evaluate red-blood cell (RBC) extravasations.

Results: Figure 1B shows typical case of 3 groups of rat experiment. When acoustic level set to 0.191 MPa (left), 1 out of 4 rats was observed to have low BBB-opened occurrence, without any RBC extravasations. When acoustic level set to 0.3 MPa (right), high BBB-opened occurrence can be achieved (4 out of 4 animals), yet histological examinations demonstrated extensive RBC extravasations (100% occurrence, identified as middle- to high-grade extravasations). In the contrast, in group applying real-time feedback control algorithm in FUS exposure procedure, 9 out of 9 rats (100% successful rate) successfully induced BBB-opening, but with low RBC extravasations occurrence rate (22% occurrence rate, identified as very low-grade extravasations) were occurred. In swine experiment (Fig 1d), we applied real-time feedback control algorithm. The successful rate was 100% (2 out of 2 targets) and the occurrence of RBC extravasations in histology was 0%.

Conclusions: We confirmed that NaviFUS can be a reliable and safe system to conduct BBB opening after the implementation of acoustic emission feedback emission control. Implemented real-time acoustic emission feedback control scheme on NaviFUS, the successful rate of FUS induced BBB-opening can reach 100% with minimal hazard concern.

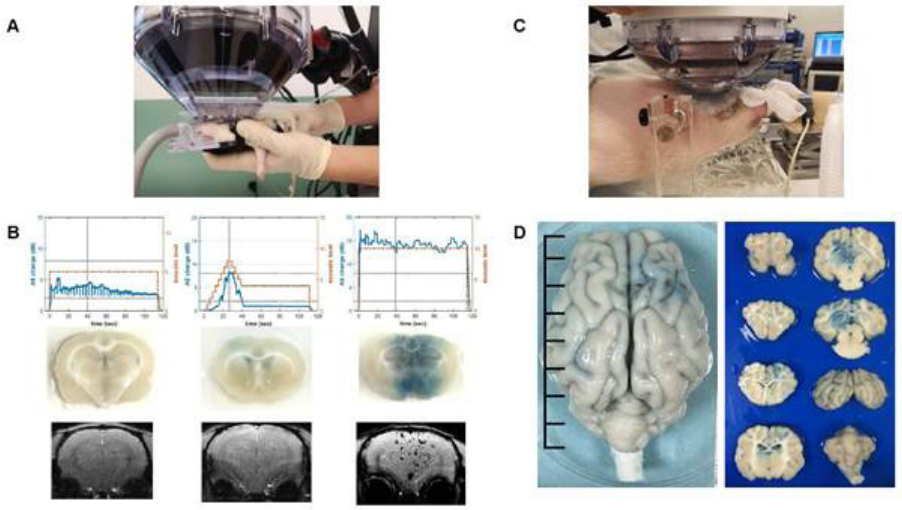

Figure 1. Animal experiment result: (a, b) Rat experiment setup and three groups of rat experiment histology result. (c, d) Swine experiment setup and histology result.

P-BRT-1

Topic: Brain Technical
Presentation Type: Poster

Emergence of diffusion weighted MRI contrast after focused ultrasound thalamotomy: A preclinical study

Steven P. Allen[1], Francesco Prada[2], Zhiyuan Xu[1], Jeremy Gatesman[1], Xue Feng[1], Helen L. Sporkin[1], Yekaterina Gilbo[1], Sydney DeCleene[1], Kim Butts Pauly[3], Craig Meyer[1]

[1]University of Virginia, Charlottesville, VA, USA
[2]Fondazione IRCCS Istituto Neurologico, Milano, Italy
[3]Stanford University, Stanford, CA, USA

Background: Improvements in essential tremor symptoms after transcranial MR-guided focused ultrasound (T-MRgFUS) have yet to equal those of deep brain stimulation. There is a critical need to improve T-MRgFUS efficacy by ensuring tissue necrosis within the entire ablation target. Intraoperative MRI may assist in this goal by visualizing the volume of tissue ablated by a given sonication. However, T-MRgFUS lesions develop T2-weighted (T2-w) contrast over several hours, preventing intraoperative lesion assessment. Previous reports have hypothesized that diffusion-weighted imaging (DWI) may provide early intraoperative detection of thermal ablation in the brain. Here, we test whether DWI can detect thermal lesions within 35 minutes of ablation using a porcine T-MRgFUS thalamotomy model and quantitative assessments of image contrast and apparent diffusion coefficient (ADC), time to the emergence of contrast, and receiver operator characteristic (ROC) analysis.

Materials and Methods: 6 swine craniotomy models were positioned in the focus of a 650 kHz, phased array transducer (ExAblate Neuro, INSIGHTEC, Israel) inside a 3T MR scanner (GE MR750, General Electric, WI) as shown in Figure 1A. 2-3 coplanar thalamic targets in each hemisphere were treated sequentially, for an average of 4.17 targets per animal and 25 targets total. At each target, transmit power and sonication duration were gradually increased until the peak estimated temperature, as measured by MR thermometry, reached or exceeded 60 oC. After ablation, the target was continuously imaged for 35 minutes using previously described custom DW and T2-w imaging sequences. A control monitoring session was also acquired prior to sonication.

T2-w and DW contrasts and ADC values were computed from 3x3 pixel regions of interest (ROI) placed both about the center of each lesion and on untreated locations in the cortex. These values were then subtracted from their respective baseline means and normalized into z-scores by dividing by their respective baseline standard deviations. ROC curves for ADC, DW, and T2-w z-scores were calculated by evaluated the resulting false positive and true positive rates for a series of classification thresholds.

Three reviewers, unaware of the targets' locations, identified apparent visible lesions in each intraoperative image. The earliest time point where two or more reviewers correctly labeled a lesion was termed time to consensus detection.

Results: Treated targets displayed hyperintense contrast on intraoperative T2-w and DW images, as shown in Figure 1B. Times to consensus detection for T2-w and DW contrasts are displayed as violin plots in Figure 2. The majority of targets displayed observable DW contrast within 15 minutes after treatment. The time evolution of DW and T2-w contrast and ADC values in both targets and control ROI's are shown as violin plots in Figure 3. Median values marked by a star are significant at the 0.0083 level. On average, DW contrast emerged within 10 minutes after treatment while T2-w contrast emerged after 20 minutes. Meanwhile, most targets showed a significant decrease in ADC values for all time points after treatment. Figure 4 displays ROC curves for T2-w, DW, and ADC z-scores. The areas under the curve, which equal the probabilities of correct classification, are 0.66, 0.80, and 0.74 for the T2-w, DW, and ADC z-scores, respectively.

Conclusions: Our results indicate that, in at least a preclinical swine model, intraoperative DWI can visualize thermal lesions within 15 minutes of ablation and that thermal lesions display persistent changes in ADC values within a few minutes of lesioning. Finally, ROC analysis suggests that intraoperative DW imaging can provide a more reliable intraoperative classifier of lesioning than intraoperative T2-w imaging.

Acknowledgements: Focused Ultrasound Foundation

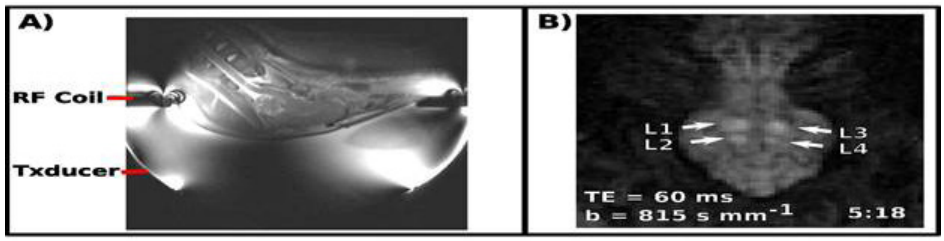

Figure 1. A) Experimental setup. B) Example intraoperative DW image. Thermal lesions (arrows) present hyper-intense contrast. This image was acquired 5:18 after treating the target located at L4.

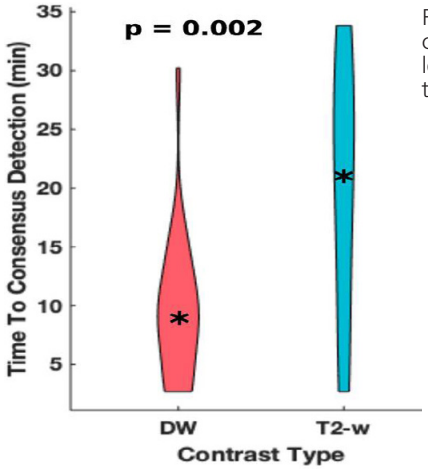

Figure 2. Violin plots of the observed times to consensus detection by image reviewers. On average, lesions observed on DW images produced earlier times to consensus detection.

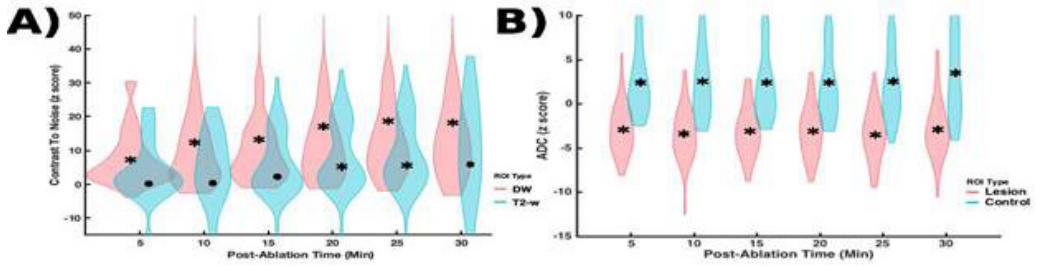

Figure 3. A) Violin plots of T2-w and DW z-scores after ablation. (B) Violin plots of ADC z-scores for lesion and control ROI's. An asterisk indicates statistical significance at the 0.0083 level.

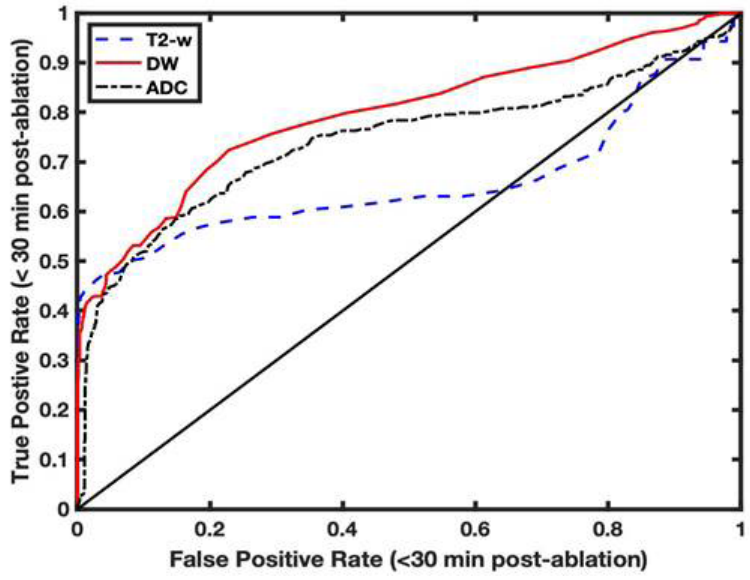

Figure 4. ROC analyses for T2-w, DW, and ADC lesion/no lesion classification thresholds. The DW, ADC and T2-w curves present areas of 0.80 and 0.74 and 0.66, respectively.

P-BRT-2

Topic: Brain Technical
Presentation Type: Poster

Coupling media for improved MR guidance during focused ultrasound surgery

Steven P. Allen[1], Thomas Steeves[2], Austin Fergusson[2], Lauren Arnold[2], Edsall Connor[2], David Moore[3], Richey M Davis[2], Eli Vlaisavljevich[2], Craig Meyer[1]

[1]University of Virginia, Charlottesville, VA, USA
[2]Virginia Tech, Blacksburg, VA, USA
[3]Focused Ultrasound Foundation, Charlottesville, VA, USA

Background: Acoustic coupling baths play important roles during magnetic resonance imaging (MRI) guided focused ultrasound surgery (MRgFUS). However, the bath also degrades MR image quality by introducing imaging artifacts. MRI quality can be improved by adding paramagnetic materials to the coupling bath and thereby suppressing the bath's MRI signal (Figure 1). Iron oxide nanoparticles are particularly attractive because, with a high relaxivity, very small concentrations still produce a suppresive effect. However, increased prefocal cavitation induced by the particles remains a limitation to clinical translation. The ideal nanoparticle design should maintain a high MR relaxivity while decreasing the chance of stabilizing a gas cavity on its surface. Here, we present nanoparticles designed to reduce the chances of prefocal cavitation by expressing a small, hydrophilic surface. We then estimate the MR transverse relaxivity and cavitation probability of these particles.

Materials and Methods: Iron oxide particles were synthesized using the coprecipitation method. To produce a hydrophilic surface coating, the particles were mixed with polymethacrylic acid and then placed in a water bath sonicator (Ultrasonic Bath, 15337410, 110W, 40 kHz, Fisher Scientific) for 30 minutes. To produce small particles and improve purity, the resulting suspension was washed using magnetic sedimentation and deionized water. The suspension was then centrifuged (Sorvall Legend X1R, ThermoFisher Scientific) for 60 minutes at 5000 rcf. The sizes of the resulting particles were then analyzed using dynamic light scattering (Zetasizer Nano ZS). The MR transverse relaxivity of the particles were analyzed (Bruker Minispec, 60 MHz). Finally, the probability of a cavitation event at a given acoustic pressure level was analyzed by first placing a 0.06 mM Fe nanoparticle sample in a hemispherical, 1mm thick polystyrene container at the focus of a 650 kHz transducer (Insightec Exablate, Israel) and then continuously sonicating for 10s at acoustic powers ranging from 5 to 250 W. Eight passive cavitation detectors continuously recorded emission spectra and the root mean square average (RMSA) of acoustic emissions within the 60-500 kHz band were estimated. A cavitation event was assumed to occur when the RMSA exceeded 5 standard deviations of the baseline value. The relative fraction of cavitation events per second of sonication were then subjected to probit analysis.

Results: The particles displayed a hydrodynamic diameter of 48±8 nm and a polydispersity of 0.20±0.08, which is much smaller than the 240 nm of an alternative particle design reported in (Allen et al. Medical Physics, 2019). The estimated MR transverse relaxivity was 590 s-1 mM Fe, which is 3 times larger than the ~175 s-1 mM Fe reported in (Allen et al. Medical Physics, 2019). Meanwhile, the relative fraction of cavitation events for a likely nanoparticle concentration at different dissolved gas levels are displayed in Figure 1 as a function of acoustic power. With the nanoparticles present, the relative incidence of cavitation increased for a large range of sonication powers, suggesting that the nanoparticle are able to stabilize a gas cavity. For equivalent Fe concentrations, the relative fraction of cavitation events observed in this study at each acoustic power level are larger than those reported in (Allen et al. Medical Physics, 2019).

Conclusions: The presented nanoparticles display a small hydrodynamic diameter and a large relaxivity. However, cavitation emissions under continuous sonication conditions suggest a relatively large chance for prefocal cavitation. Future work will include increasing the interfacial tension of the nanoparticle solution, reducing the size of the nanoparticles, and determining the probability of a cavitation event under single cycle (histotripsy) conditions.

Acknowledgements: Focused Ultrasound Foundation, Research reported in this publication was also supported, in part, by the National Center for Advancing Translational Sciences of the National Institutes of Health under Award Number UL1TR003015.

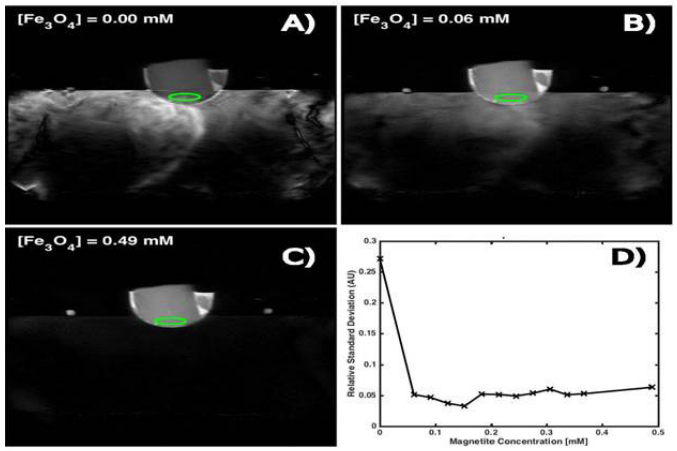

Figure 1. (A-C) Example MR images of a gel in a transducer filled with circulating water. As nanoparticle concentration increases, the water bath signal is suppressed and thus motion artifacts decrease (D).

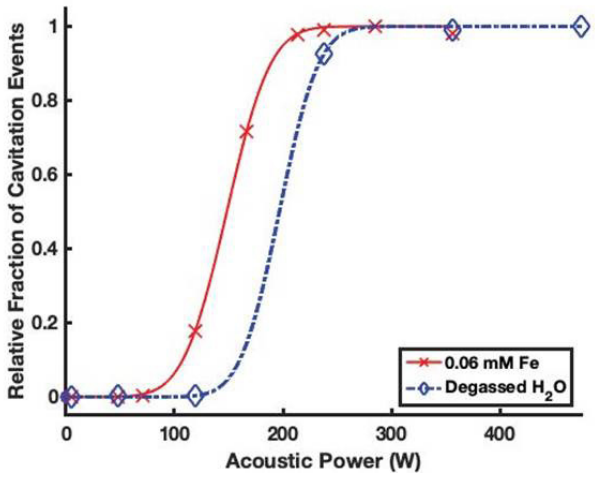

Figure 2. Relative fraction of recorded acoustic emissions that recorded a cavitation event plotted as a function of transmitted acoustic power. Continuous lines represent fits to a probit curve.

P-BRT-3

Topic: Brain Technical
Presentation Type: Poster

Toward improved 3D MRI thermometry: Predicting the effects of eddy currents

Steven P. Allen, Craig Meyer

University of Virginia, Charlottesville, VA, USA

Background: Many magnetic resonance imaging (MRI) thermometry techniques for focused ultrasound surgery employ long duration (>10 ms) data readouts. This design choice improves temperature precision by placing the echo time within the optimal range of 30-50 ms. It also enhances spatial coverage and temporal resolution by sampling high spatial frequency data during periods (~10 ms after excitation) when temperature data presents low relative contrast.

However, long readout designs have yet to translate into clinical use because they also sensitize temperature estimates to magnetic field perturbations such as those predicted by Lenz's law (called eddy currents). These perturbations are challenging because they can vary with scan prescription, sequence design, and transducer position and subsequently blur, shift or bias estimates of focal heating (Figure 1A).

Here, we present a method to characterize and predict the eddy currents produced during a long readout thermometry sequence.

Materials and Methods: Our method models eddy current phenomena as a set of linear, shift invariant systems that, in response to an input magnetic field gradient, introduce additional magnetic fields that are well approximated by a 1st order polynomial in space. We estimated the transfer functions of these systems by comparing the Fourier transforms of a series of triangular input waveforms to the Fourier transforms of the resulting output waveforms using the maximum likelihood estimator in (Vanessjo et al, MRM 2013). The true magnetic field produced in the scanner was estimated by modifying the well-known thin-slice method (Rahmer, J. et al. MRM. 2018) to excite 30, 0.75 mm planes spaced 2 mm apart, perpendicular to the input magnetic field gradient. The resulting unwrapped phase signal, weighted by the signal magnitude, was then projected onto a first order Vandermonde matrix. This analysis produced four transfer functions: one for each physical gradient axis and one for global shifts in the magnetic field.

This method was validated on a GE MR750s system by first measuring the resulting magnetic fields produced by a separate, test waveform and then comparing the results against those predicted by the estimated transfer functions. This validation experiment was conducted under the following conditions: scanning a gel phantom, scanning a gel phantom held at the focus of an Exablat 650 kHz system (Insightec, Israel) in two positions, and scanning a gel phantom with a stereotactic surgical frame.

Results: The designed method produces estimates of the true magnetic field gradient with a precision better than 0.8 mT/m. Example input and output waveforms are shown in Figures 1.B-C. Estimated transfer functions along each Vandermonde basis and physical setup are displayed in Figure 2 and indicate the frequency response of each modeled eddy current system.

On average, we found that the transfer function models could accurately predict linear eddy currents. However, the model poorly predicted global shifts in the magnetic field. Figure 3 displays the input, measured, and predicted linear and global shift waveforms observed using different physical gradient axes and physical setups.

Conclusions: The presented method is able to predict eddy current effects on magnetic field gradients implemented during magnetic resonance imaging guided focused ultrasound. However, the method proved less effective at predicting eddy current effects on global shifts in the magnetic field. Future work will examine the beneficial or deleterious effects of these predictions on the accuracy of MR thermometry during phantom heating.

Acknowledgements: Focused Ultrasound Foundation

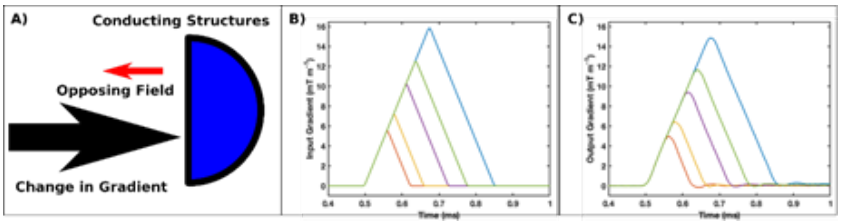

Figure 1. (A) Schematic of the eddy current effect. (B-C). Example input and output gradient waveforms. Eddy currents distort the input waveforms.

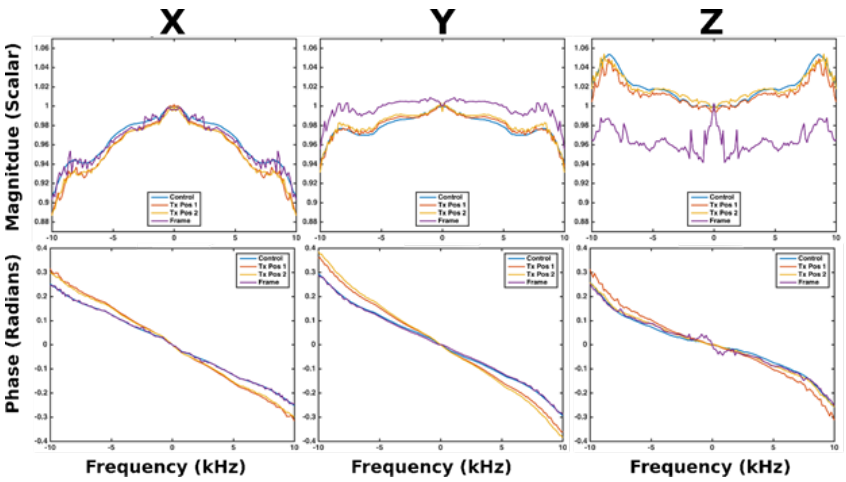

Figure 2. Estimated transfer functions as a function of gradient direction (X,Y,Z) and transducer setup. Control=gel phantom in the scanner bore.

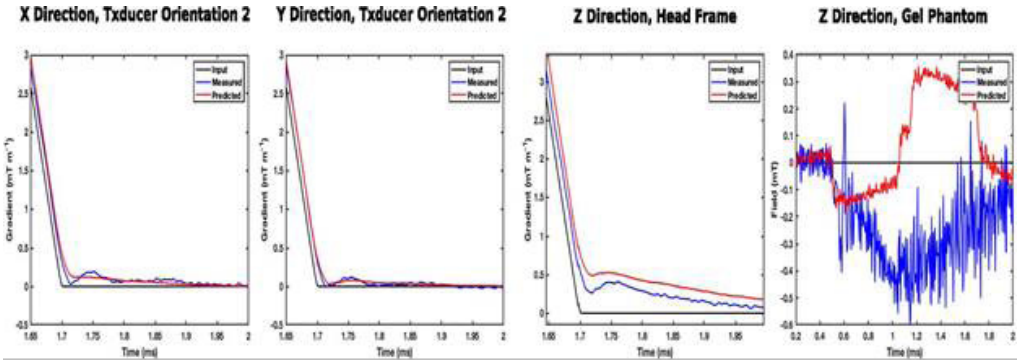

Figure 3. Example plots of the input, measured, and predicted gradient and global shift waveforms for a number of physical gradient directions and experimental setups.

P-BRT-4

Topic: Brain Technical
Presentation Type: Poster

Human skull resolution dependence of the transcranial focused ultrasound propagation accuracy

Alec Batts, Elisa Konofagou

Columbia University, New York, NY, USA

Background: Blood-brain barrier (BBB) opening with focused ultrasound (FUS) is a noninvasive technique for delivering therapeutics to the brain parenchyma. The noninvasive nature of BBB opening in the clinic relies on acoustic wave propagation through the intact skull. However, phase aberration, signal attenuation and beam distortion after transcranial transmission necessitates thorough treatment preplanning, including acoustic wave propagation simulation. Such in silico preplanning involves simulating the acoustic propagation through a model of the patient's skull derived from patient-specific computed tomography (CT) scans and noting the predicted beam distortion and attenuation profile. Since transcranial acoustic wave propagation depends on several skull properties including density, thickness, topographical irregularities and trabecular microstructure, we demonstrate the improved ability of high-resolution micro-CT over conventional CT to better replicate the human skull model in silico.

Materials and Methods: The k-Wave MATLAB toolbox for time-domain modeling of acoustic wave propagation was used to simulate a 1.5 MHz focused transmit in 2D and 3D from a P4-1 phased array transducer through micro-CT and conventional CT scan-based models of the same fragment of human frontal and parietal skull bone. The computational grid resolution of the 2D and 3D simulation was 8 points/wavelength and 6 points/wavelength, respectively, while the resolutions of the micro-CT and conventional CT scans used in the simulation were 0.08 mm and 0.49 mm, respectively. Density, sound speed and absorption maps for both skull models were derived from the Hounsfield unit scale in each CT scan. The simulated P4-1 phased array (96 elements, 0.245 mm element width, 0.295 element spacing, 16 mm elevational aperture) was positioned ~5 mm from the skull surface and the beam was electronically focused at 60 mm in the 2D simulation and 35 mm in the 3D simulation.

Results: Along with the fundamental increase in skull microstructure resolution (Fig. 1A-B), simulations revealed differences in beam distortion and attenuation profiles between transcranial focused transmits through the micro-CT and conventional CT-based human skull models when validated against in vitro measurements. 2D simulations revealed axial focal shifts of 4.25 mm and 1.38 mm, and lateral focal shifts of 0.5 and 0.75 mm from the free-field focal position after transmission through the micro-CT model and conventional CT model, respectively. Additionally, the micro-CT model yielded a 19.32% increase in signal attenuation over the conventional CT model. 3D simulations of acoustic wave propagation through the micro-CT model yielded axial, lateral and elevational focal shifts of 3.25, 1.0 and 0.25 mm, respectively (Fig. 1C-F), along with a 95.51% signal attenuation. The micro-CT model yielded a marked improvement in representing the attenuation profile recorded in vitro at 1.5 MHz of 87.7%.

Conclusions: This study demonstrated the importance of emphasizing human skull microstructure for accurate simulation of FUS transcranial propagation and proper treatment pre-planning. While the reported simulated attenuation profile of the micro-CT model in 2D may underestimate the overall signal attenuation, the simulated attenuation profile in 3D more closely aligns with the attenuation profile recorded in vitro.

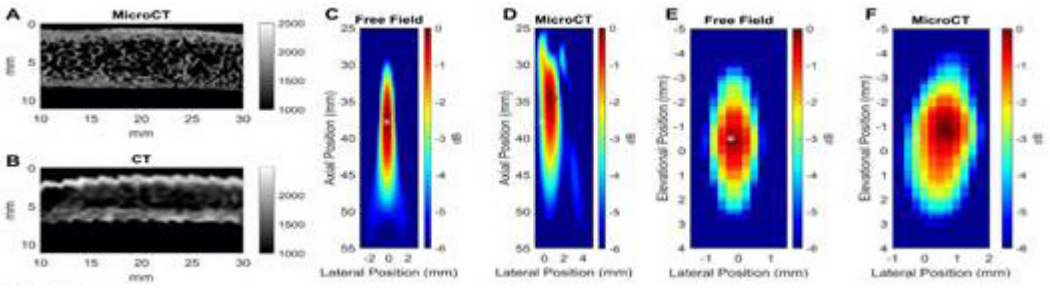

Figure 1. Density maps of (A) Micro-CT and (B) CT scan of human skull. Axial focus profile in (C) free field and (D) micro-CT model. Elevational focus profile in (E) free field and (F) micro-CT model.

P-BRT-5

Topic: Brain Technical
Presentation Type: Poster

Bidirectional platform for precise transcranial ultrasound delivery and optoacoustic monitoring of the mouse brain

Hector Estrada, Ali Özbek, Justine Robin, Shy Shoham, Daniel Razansky

ETH and University of Zurich, Zurich, Switzerland

Background: Transcranial ultrasound (TUS) delivery is commonly used for hyperthermia treatments, opening the blood-brain-barrier or neuromodulation applications. Simultaneous monitoring of the brain is paramount for assessing the treatment efficacy and gaining insight on the physiological mechanisms underlying brain responses to ultrasound. In preclinical settings, the use of bulky focused ultrasound transducers precludes the combination of TUS with advanced neuroimaging methods. Moreover, mice are often targeted with focal spots as large as a whole mouse brain hemisphere (6 mm x 3 mm). Here we show a non-invasive bidirectional platform capable of focusing ultrasound to <400 μm spots anywhere in the mouse brain while acquiring real-time volumetric optoacoustic images of the region of interest . The imaging capabilities could potentially be used to monitor hemodynamic changes, calcium changes from fluorescence reporters, and ultrasound thermal effects.

Materials and Methods: Our platform relies on a spherically focused ultrasound array of 512 elements to deliver ultrasound at a focus located at 4 cm away from the transducer's active surface. The same array is able to detect broadband optoacoustic signals produced by deposition of pulsed laser light delivered through an 8mm aperture in the array. The optoacoustic imaging performance of our platform was tested using 90 μm light absorbing microspheres embedded in an agarose block. In vivo mouse imaging of the brain was also performed at different wavelengths.

We characterized the ultrasound emission capabilities of the array measuring first a single element using chirp excitation and a needle hydrophone (75 μm diameter) to scan the pressure field. The single-element measurement results where then used to build up a linear model of the complete array. Pressure field scans using single cycle (0.1 μs period) excitation were performed to characterize the array's focus and the results compared against the linear model. In addition, the pressure field scans were performed steering the focus up to 2 mm from the geometrical focus. Eventually, we repeated the pressure field scans with an excised mouse skull in the propagation path, in order to evaluate the actual focal properties inside the mouse brain.

Results: Our platform showed optoacoustic volumetric resolution in the order of 200 μm. Mice imaged at different wavelength show an effective field of view covering the entirety of the mouse brain (10 mm x 10 mm). Penetration depth is strongly dependent on the light propagation inside the brain. Illumination at 488 nm produces strong superficial contrast, whereas 900 nm produces slightly lower contrast but deeper penetration.

The array readily generated pressures beyond 5 MPa in free field. A lateral focal size below 200 μm (FWHM) and lower pressures of 2.6 MPa were measured after steering the beam by 2 mm. The prediction of our linear ar model agrees reasonably well with the experimental data, although non-linear effects are already visible in the experimental data. Transcranial pressure fields characterized from 3 to 9 MHz show a non monotonic decay below 25 % of the peak pressure in free-field. Also the focus diameter is increased to about 400 μm in diameter due to skull-induced distortions

Conclusions: Our bidirectional TUS platform is suitable for preclinical studies targeting the mouse brain. It provides unprecedented spatial resolution below 400 μm through the skull in conjunction with brain-wide real time volumetric imaging of the optical absorption contrast. The platform thus offers new possibilities for image-guided TUS applications, such as neuromodulation and targeted blood-brain-barrier opening.

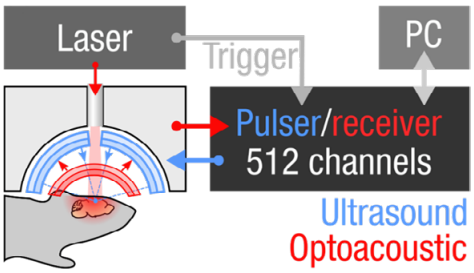

Figure 1. Schematic of the Parallelized Optoacoustic imaging and Transcranial Ultrasound delivery POTUS. Laser light is delivered through the array's aperture to the sample and the optoacoustic signals detected.

Acknowledgements: The authors acknowledge grant support from the US National Institutes of Health (UF1-NS107680) and European Research Council (under grant agreement ERC-2015-CoG-682379).

P-BRT-6

Topic: Brain Technical
Presentation Type: Poster

Assessing the accuracy of magnetic resonance guided focused ultrasound (MRgFUS) thalamotomy with Kranion: An open-source software dedicated to offline analysis and planning of focused ultrasound stereotactic procedures

Samuele Cabras, Andrea D'Auria

Istituto Neurologico Carlo Besta, Milan, Italy

Background: MRgFUS is a technique for creating thermal lesions within dysfunctional brain circuits. Thus, it positively affect the course of neurological disorders such as essential tremor (ET) and tremor-dominant Parkinson's disease (TDPD). To achieve good outcomes without neurological damage high targeting accuracy is mandatory. The currently used device's planning software does not allow to define the target referencing to the bicommissural line system. Therefore, the formulaic methods are used. However, they may hamper the determination of the procedure's accuracy. Kranion is a software that allows the user to simulate MRgFUS treatment and to analyze previous procedures, also by defining the position of a brain area referencing to the bicommissural system. Therefore it could be used to evaluate the procedure's accuracy and plan MRgFUS retreatments.

The aim of this study is to assess the stereotactic accuracy of VIM thalamotomy in a cohort of patients treated for ET and TDPD using Kranion.

Materials and Methods: All patients with ET or TDPD who underwent stereotactic VIM thalamotomy at a single institution between January 2019 and July 2020 were included in the analysis. For all patients, brain pre and post-operative images were loaded in, processed and analyzed with Kranion. The stereotactic coordinates of the definitive lesions were compared with those of the planned targets and accuracy of the stereotactic procedure was determined.

Results: 25 patients with medication-refractory ET and TDPD were included in the analysis. The accuracy of MRgFUS for medication-refractory tremor, as calculated using Kranion was 0.24mm ± 0.98 SD in left-right axis, 2.19mm ± 1.29 SD in anteroposterior axis, 0.75mm ± 1.26 SD in rostro-caudal axis. Mean Euclidean distance between the planned target and the center of the definitive lesion was 2.83mm ± 1.22 SD.

Conclusions: Kranion software allowed effectively to calculate the accuracy of MRgFUS thalamotomies performed in a single-institution cohort of patients with medication-refractory tremor. Our results demonstrate that MRgFUS is highly accurate. In the future, the Kranion software may help functional neurosurgeons in the planning of upfront and repeat MRgFUS treatments as well as in comparing post-operative clinical outcomes with radiological results.

P-BRT-7

Topic: Brain Technical
Presentation Type: Poster

The feasibility and safety of non-invasive brain mild hyperthermia using transcranial MR-guided focused ultrasound with microbubbles in rodents

Bingbing Cheng, Chenchen Bing, David Rushforth, Tadeusz Foniok, Samuel Pichardo, Bruce Pike

University of Calgary, Calgary, Canada

Background: Mild hyperthermia based on magnetic resonance imaging-guided focused ultrasound (MRgFUS) has been investigated preclinically in solid tumors in the body for many years and gradually translated into clinical studies. Its enhanced effects on localized drug delivery and radiation therapy have been clearly demonstrated. It also has a great potential in augmenting the immune response to treat cancers. However, due to the skull barrier, little to no investigations have been done in the brain. The skull absorbs most of ultrasound energy, posing a safety risk. However, it has been demonstrated that microbubbles can help to reduce the required ultrasound energy to produce thermal effects. This study aimed to evaluate the feasibility and safety of non-invasive MRgFUS-induced brain mild hyperthermia in a rodent model and the effectiveness of using microbubbles (MBs) to reduce the required acoustic energy to achieve hyperthermic levels, thus reducing the risk of skull-associated thermal damage.

Materials and Methods: Female wild-type mice (C57Bl/C, 19-25g, n=5) were assigned randomly into three groups: saline control, MB-conc1 (10ul/kg/min), and MB-conc2 (20ul/kg/min). Mild hyperthermia treatment was performed in the mouse brain (10 mins duration) using a small animal MRgFUS system (8-element transducer, 2.5MHz, Image Guided Therapy, France) incorporated into a 9.4T Bruker MRI Scanner. The Proteus software platform for MRgFUS procedures was utilized for real-time control of the hyperthermia delivery. The saline or microbubbles were infused continuously during hyperthermia. The ultrasound power required to achieve mild hyperthermia (42 °C) was compared among the three groups. T2w, T2*w, and gadolinium contrast-enhanced T1w images were acquired to evaluate potential tissue damage.

Results: Ten minutes of brain hyperthermia was achieved with excellent temporal stability (mean±SD = 42.0±1.0 °C) for all three groups (Fig. 1A). A 30.8% and 57.7% power reduction was observed in the MB-conc1 and MB-conc2 group, respectively, compared to the saline control group (Fig. 1B). In the FUS target region, no signs of edema, vascular damage, nor blood-brain barrier permeability change were observed on the MRI. However, in regions close to the skull, some edema was observed, likely due to some skull heating. With the power reduction in the MB-conc1 and MB-conc2 groups, edema was significantly reduced (Fig. 1C).

Conclusions: Non-invasive mild hyperthermia based on MRgFUS is feasible in the rodent brain. Ten-minutes duration did not cause MRI-detectable tissue damage in the target brain region. When combined with microbubbles, the ultrasound power required for hyperthermia can be reduced substantially thereby reducing skull-associated damage.

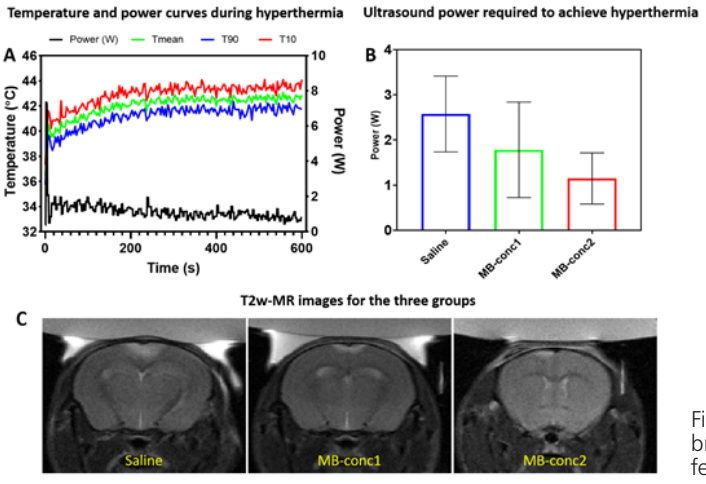

Figure 1. Non-invasive MRgFUS brain mild hyperthermia feasibility and safety

P-BRT-8

Topic: Brain Technical
Presentation Type: Poster

Low-cost 3D hydrophone scanning tank with Matlab GUI control

Sam Clinard, Erin Wettstone, David Moore, John Snell, Frederic Padilla, Matt Eames

Focused Ultrasound Foundation, Charlottesville, VA, USA

Background: Ultrasound research labs often require specialized equipment to characterize their ultrasound devices. One such device is a motorized 3D hydrophone scanning tank, which allows the recording of a transducer's output pressure in 3D space so that a device's acoustic field and other pressure output characteristics can be quantified and visualized. This equipment can cost tens-of-thousands of dollars, often representing a significant portion of a nascent lab's start-up cost or a sizeable portion of a grant application. Labs may, alternatively, commit the time to building a home-grown system at significantly lower cost. Presented here is a validated 3D scanning tank with assembly instructions and a basic Matlab control GUI that can be built for under $1,000 (excluding hydrophone, oscilloscope, function generator, and Matlab license, most of which engineering research labs/institutions have in-place) in roughly 40 person-hours.

Materials and Methods: Materials for assembling the hydrophone scanning tank were sourced from online vendors and consisted of three NEMA 17 stepper motors, limit switches, 20mm aluminum extrusion, linear bearings and associated fittings, an Arduino microcontroller and accompanying CNC "shield", cabling, and 3D printed parts. All parts, vendors, and approximate pricing are detailed in a full inventory table to be included in the presentation.

Results: The performance of the low-cost scanning tank was compared to data collected with a commercial automated scanning tank (AIMS III, Onda Corp, Sunnyvale, CA, USA). A 350kHz focused transducer and a plane 1.1 MHz transducer were evaluated with 2D automated scans with 0.25 mm resolution x/y spacing. The low-cost scanning tank completed the measurement in 45 minutes, as compared to the commercial system's 30 minutes. Representative scans are provided in Fig. 1.

Conclusions: With only moderately longer scan times (and likely some room still to improve scan times) and data that has a percent error of only 19% when compared to that acquired with a commercial system, the low-cost scanning system developed here is a viable solution for ultrasound labs in need of efficient, low-cost spatial quantification of ultrasound transducers.

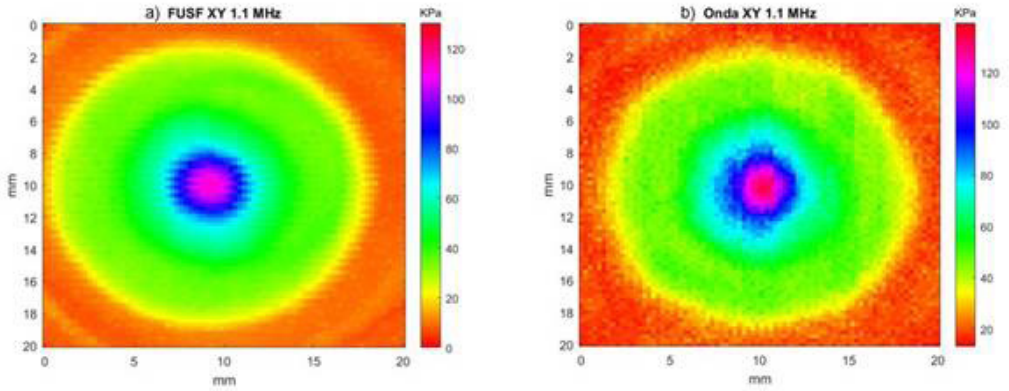

Figure 1. Side-by-side comparison of horizontal 20x20 mm 0.25 mm resolution negative pressure [kPa] scans with a) Focused Ultrasound Foundation (FUSF) low-cost model and b) Commercial Onda model.

P-BRT-9

Topic: Brain Technical
Presentation Type: Poster

Feasibility of ultrasonic thermal monitoring using coded excitations for focused ultrasound hyperthermia

Daniel Dahis[1], Haim Azhari[1], Natalie Artzi[2], Tomer Romano[1], Noy Farti[1]

[1]Technion Institute of Technology, Haifa, Israel
[2]Harvard Medical School, Cambridge, MA, USA

Background: Focused Ultrasound (FUS) thermal treatments offer a non-invasive opportunity to treat neurological diseases such as brain cancer and essential tremor. Thermal monitoring during these procedures is crucial. MRI is the leading method for temperature mapping. However, it is expensive with limited accessibility. Acoustic thermal monitoring could provide a portable cost-effective alternative with higher temporal resolution. However, brain ultrasonic monitoring is challenging due to the skull bone attenuation and induced aberrations, which compromise the wave signal-to-noise ratio (SNR). Coded Excitations (CoE) is a method that could potentially overcome these challenges.

Hence, this study evaluated the feasibility of implementing the Golay CoE sequences as means to non-invasively estimate the temperature changes of the brain, using the therapeutic FUS transducer itself. We hypothesized that these changes could be detected in speed of sound (SoS) related variations of the reflected waves.

Materials and Methods: Golay sequences consist of a pair of complementary coded transmissions that are processed to provide an amplified narrowed signal, even under poor SNR conditions (Figure 1). Importantly, this technique enables implementation in narrow-banded transducers, such as therapeutic FUS. A 1 MHz FUS transducer manufactured by INSIGHTEC was used in this study. The transducer contained a concentrically embedded pulse-echo probe. The FUS was positioned in a water tank. A custom-made 3D-printed holder was mounted on top of the transducer. Plastic containers were filled with ex-vivo bovine brain tissue carefully resected from the cortex (Figure 2). Next, the containers were heated to about 45oC, by immersion in a water-filled beaker. Each container was then positioned in the focal zone of the system and sonicated with Golay sequences every 1 second during cool down, until reaching 30oC. Three thermocouples were used for real-time temperature monitoring of the samples. From the obtained decoded signals, the echo shifts trajectories as a function of temperature were registered.

Results: The results have demonstrated improved SNR of the Golay-derived signals in comparison to the raw RF echoes (Figure 3). Furthermore, a high linear correlation (R2=0.9547) between the estimated normalized cortical SoS and temperature was observed (Figure 4). This indicates the validity of the hypothesis and the possibility of obtaining noninvasive brain tissue temperature estimation using CoE.

Conclusions: The feasibility of CoE-mediated acoustic thermal monitoring using a single FUS transducer for transmission and reception was successfully demonstrated. Importantly, the linear echo-shift trajectories as a function of temperature indicate the possibility of temperature estimation. This approach can serve as a basis for the development of a new tool for brain FUS thermal monitoring, without MRI.

Acknowledgements: Aaron Alfasy, Technion Integrated Cancer Center

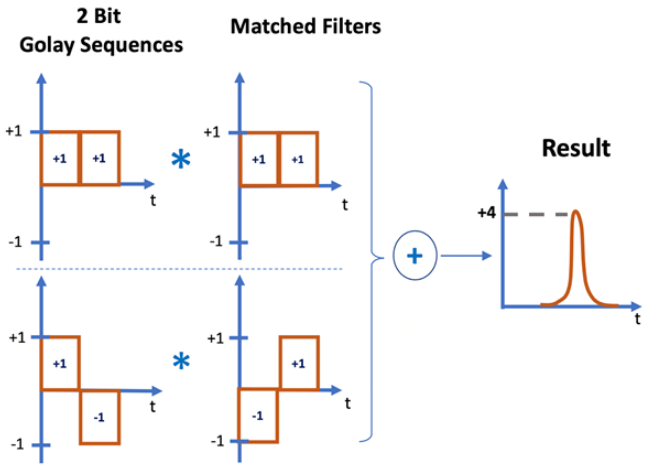

Figure 1. The 2-bit Golay coded excitation pair and improved SNR following signal decoding.

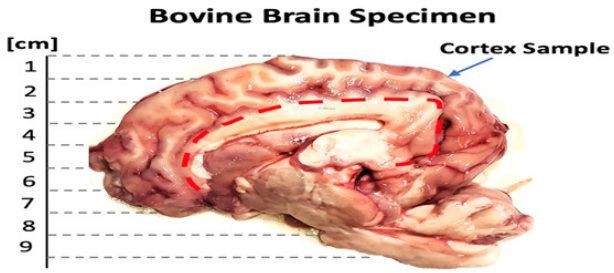

Figure 2. Samples were prepared using bovine cortical tissue.

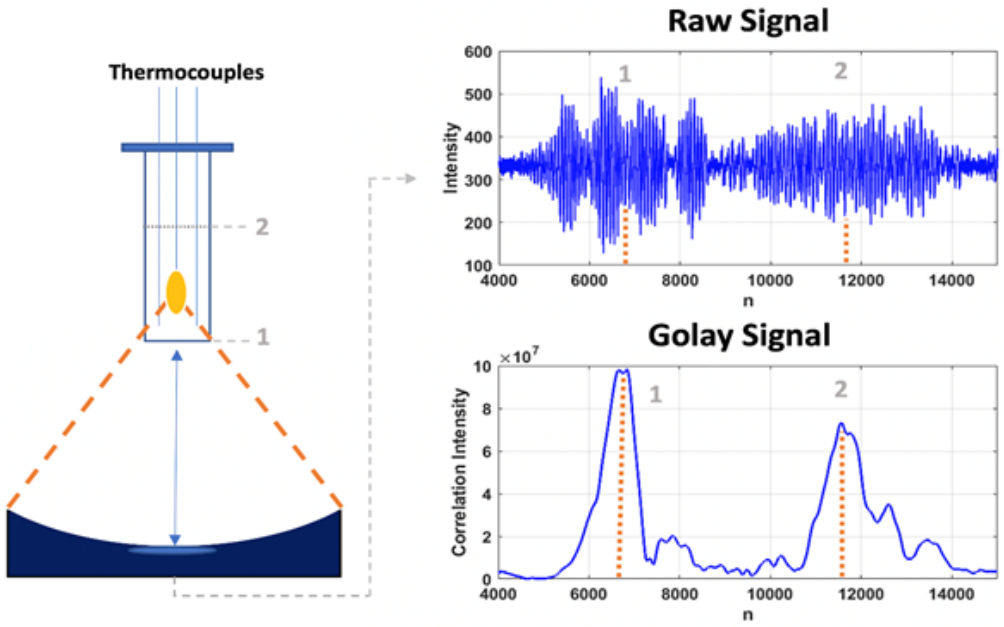

Figure 3. The raw echoes obtained by the FUS transducer (top right) and the correspondent Golay signals obtained following the decoding stage (bottom right).

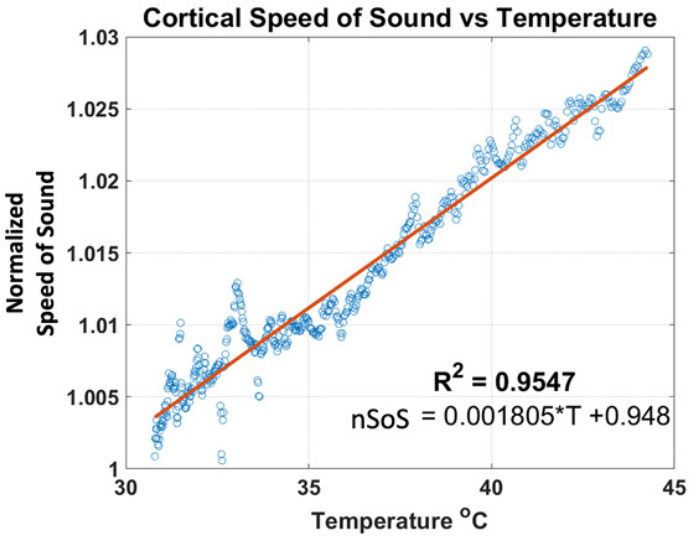

Figure 4. Cortical speed of sound as a function of temperature obtained from the Golay signals. The cortical SoS exhibited linear behavior indicating the possibility of cortical temperature estimation.

P-BRT-10

Topic: Brain Technical
Presentation Type: Poster

Ex-vivo focused ultrasound can induce histologic changes in tissue

Norman M Spivak[1], Bianca Dang[1], Alexander Korb[1], Brendan Bych[1], Eric Johnson[1], Samuel Reyes[1], Negar Khanlou[1], Mark Cohen[1], Martin Monti[1], Mark Schafer[2], Alexander Bystritsky[1]

[1]University of California, Los Angeles, Los Angeles, CA, USA
[2]Sonic Tech, Ambler, PA, USA

Background: Ongoing projects in the lab in patients with temporal lobe epilepsy use intensities upwards of 5760 mW/cm² Ispta.3. Several days after sonication, the sonicated brain regions are surgically resected and the tissue is examined. The skull is known to attenuate up to 90% of the transmitted energy, and so unsurprisingly, there is no detectable damage in these resected tissues. In order to know what intensity levels are safe, one must determine what levels are unsafe, and so this was the premise of the proceeding set of experiments.

Materials and Methods: Tissue blocks came from two sources. The majority came from recently deceased (<24 hours) cadaver temporal lobe. Several blocks came from hemispherectomy surgery. Tissue blocks were divided into several pieces which were sonicated at varying intensity levels (≤ 160 W/cm²) at 100% duty cycle for 60 seconds. After sonication, tissue was placed in formalin for 48 hours. Afterward, tissue was embedded in paraffin wax, sliced at 4μm, and stained using hematoxylin and eosin. For each block, one piece was not sonicated but otherwise went through the same processing steps to serve as a control piece. The investigator who examined the tissue under a microscope was blinded to the sonication intensity of each piece.

Results: Regardless of the source, all tissue that was sonicated below 25 W/cm² was visually indistinguishable from the control pieces. Sonication above 25 W/cm² demonstrated irreversible damage to cells' integrity, evidenced by spongiosis and blood vessel destruction on light microscopy.

Conclusions: It is worthwhile to mention that the tissue did not have a piece of skull in the way to attenuate some of the ultrasound energy. As such, an in-vivo approach would require roughly 250 W/cm² Intensity to effect the same changes in tissue. Even if this is disregarded, at 25 W/cm², there is a great potential that the 90% attenuation by skull will result in significant heating, leading to burns on the skin. For this reason, further safety testing is needed to assess the degree of heating in the skin at these intensity levels prior to commencing with human subjects' work.

Acknowledgements: BrainSonix Corporation

P-BRT-12

Topic: Brain Technical
Presentation Type: Poster

Conformation of ultrasonic vortex beams through the skull using acoustic holograms for particle trapping

Noé Jiménez, Sergio Jiménez-Gambín, Diana Andrés, Francisco Camarena

Universitat Politècnica de València, Valencia, Spain

Background: Acoustic tweezers are a versatile and powerful emerging tool to biomedical applications, such as cell manipulation or drug delivery, as they allow contactless particle manipulation using low-power devices. Single beam acoustic tweezers based on vortex beam require a focused ultrasound beam containing a phase dislocation at its axis. While these beams have demonstrated great potential to trap particles in homogeneous media, phase aberrations produced by strongly heterogeneous and refracting media distorts the wavefront and inhibit the generation of trapping forces. In this work we report a method to conform aberration-free focused vortex beams through the skull for transcraneal particle trapping using acoustic holograms.

Materials and Methods: The method is based on a single-element focused ultrasound source and a spiral-holographic lens. First, using x-ray CT images of an ex-vivo human skull and time-reversal full-wave simulations we model the wave propagation from the desired trapping-location inside the skull towards the location of the focused transducer. The holographic information at 500 kHz is recorded at source location and a holographic lens based on Fabry-Perot resonators is designed using phase-conjugation methods. The acoustic hologram is manufactured using stereolithographic 3D-printing with a 50 μm resolution in a rigid polymer. Then, the target acoustic vortex is generated by exciting the lens with a custom single-element focused transducer of 100-mm aperture and 140-mm focal length. The hologram was excited with a 500-kHz pulsed burst using a duty-cycle of 5 %. The focusing performance of the ultrasonic vortex was evaluated by hydrophone measurements of the acoustic field performed in a water tank using a micro-positioning system, scanning with a resolution of 100 μm over a 2 cm per 5 cm area [measurements shown in Figure 1 for water and Figure 2 for transcranial propagation]. Finally, a series of elastic 3D-printed spheres of apertures from 1 to 0.25 mm in radius were stably trapped at the centre of the acoustic, and calibrated optical tracking techniques were applied to measure its location inside the water bath.

Results: A phase dislocation was identified at the focal area. The magnitude of the field shows a ring-shaped focused spot with a FWHM of 11.36 mm in the axial direction [see Figure 1(a) for water and Figure 2(a) for skull] and 4.9-mm in the transversal direction [see Figure 1(b,d) for water and Figure 2(b,d) for skull], while the topological charge of the measured vortex is the unity [see Figure 1(c,e) for water and Figure 2(c,e) for skull]. In contrast, when using a holographic vortex-lens designed for homogeneous media, the phase aberrations produced by the skull distort the wavefront and the vortex was not observed. A particle was placed at the focal spot [see Figure 1(f) for 1-mm radius sphere trapping] and optical tracking measurements show that in water its position remained stable while the ultrasound transducer was active. The location of the particle matched the location of the phase singularity of the beam in water.

Conclusions: The results show that, by compensating the phase aberrations produced by the skull, wavefront containing phase dislocation can be generated in the cranial cavity. Such a focused vortex beam can be used to trap a solid particle in an arbitrary position. These results open new paths for contactless manipulation of objects in complex biomedical environments such as relocating clots during an ischemic stroke or the propulsion of large drug-delivery vehicles. Beyond particle trapping applications, focusing vortex beams containing phase dislocations opens new venues to transfer angular momentum to brain tissues that might be used for non-thermal therapeutic purposes.

Acknowledgements: This research has been supported by the Spanish Ministry of Science, Innovation and Universities through grants "Juan de la Cierva – Incorporación" IJC2018-037897-I and PID2019-111436RB-C22, by the Agència Valenciana de la Innovació through grants INNVAL10/19/016 and INNCON/2020/009, and by Generalitat Valenciana through grant ACIF/2017/045. Action co-financed by the European Union through the Programa Operativo del Fondo Europeo de Desarrollo Regional (FEDER) of the Comunitat Valenciana IDIFEDER/2018/022.

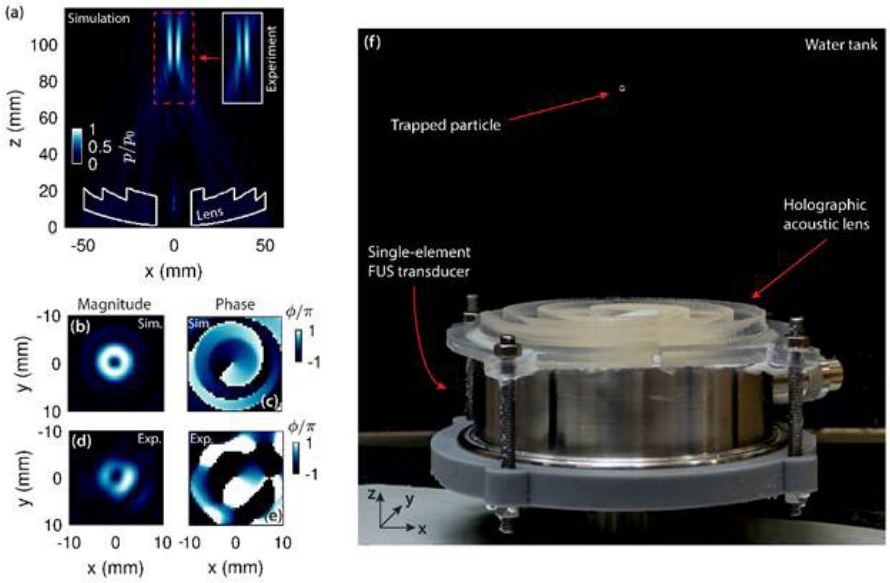

Figure 1. Pressure-field distribution and particle trapping using the acoustic hologram in water. (a) Simulated axial pressure-field distribution at y=0 mm; experimental result shown in the inset.

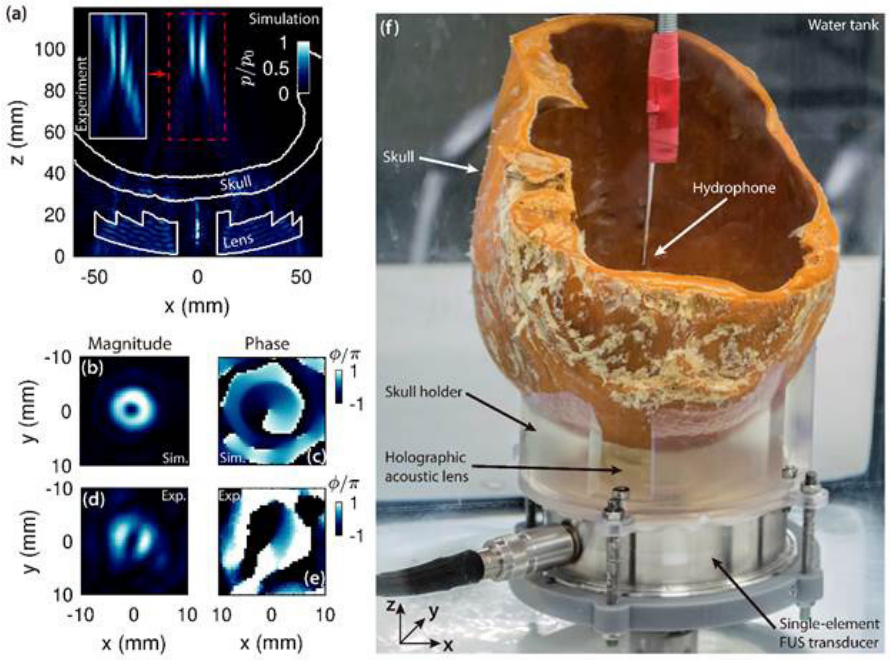

Figure 2. Pressure-field distribution using the acoustic hologram through the skull. (a) Simulated axial pressure-field distribution at y=0 mm; experimental result shown in the inset.

P-BRT-13

Topic: Brain Technical
Presentation Type: Poster

Transcranial ultrasound delivery using dual-mode conversion

Ki Chang Kang[1], Young Hun Kim[1], Kwan Kyu Park[1], Kamyar Firouzi[2], Pierre Khuri-Yakub[2]

[1]Hanyang University, Seoul, South Korea
[2]Stanford University, Stanford, CA, USA

Background: Transcranial ultrasound technique has been researched as a non-invasive treatment for treatments of brain tumors, neuromodulation, and delivery of cancer therapeutics. Focused ultrasound is one of the most common methods for non-invasive treatments, but the present technology generally uses an array of transducers by normal incidence. The general focused ultrasound technique has high transmission loss and heating of the skull because of the normal incidence. We propose an array of wedge transducer consisted of PZT stacks for dual-mode conversion technique, which means that the longitudinal wave in wedge converted to Lamb wave in the skull and the Lamb wave converted to the longitudinal wave in the brain. This technique is able to efficient transmission, to reduce heating of skull, and to extend the focal spot range.

Materials and Methods: We proposed this concept and presented the data proving feasibility in 2017. In order to verify this concept, we have implemented a finite-element method in time transient mode. In the case of normal incidence, the skull angle is parallel to the input pressure, but in the case of wedge incidence, the skull angle is decided by the wedge angle. The wedge angle is calculated by Snell's law; the wedge angle is calculated by the speed of sound in the wedge and the phase velocity of the selected Lamb wave mode. The wedge is the PDMS which has a speed of sound of 1080 m/s. The common skulls have a thickness of 5-7 mm and the skull thickness used in the simulation is 6.5 mm. The phase velocity of A2 mode Lamb wave is 2571 m/s when the center frequency is 500 kHz. The skull angle is determined to 23.61° by calculating based on the speed of sound of PDMS and the phase velocity of the skull. In order to conduct the experiment, we made the 1/8 model with one array consisted of 49 wedge elements. One PZT stack has a size of 1 mm × 1 mm × 3 mm and has a center frequency of 500 kHz. The total wedge angle is determined to 52° by the sum of the skull average angle and the wedge angle. The longitudinal waves irradiated to the skull and mode-converted to the A2 mode Lamb waves. This Lamb waves propagate and leak the energy into the medium. This dual-mode conversion approach makes high transmission efficiency and reduces the heating of the skull.

Results: The FEM results present that the wedge incidence has 21% more efficient transmission than normal incidence. We calculated the pulse integral intensity (PII) for normal incidence and wedge incidence instead of using maximum pressure because of the different waveforms. The PII is calculated by the time integral of the intensity over the measurement time and the intensity is a function of pressure squared. The results of 200 cycles input pressure (1Pa) show that PII of the normal incidence and wedge incidence is 26.9 pW/m^2 and 32.5pW/m^2, respectively.

The 3D scanning experimental results present that the wedge transducer generates the dual-mode conversion. We conducted experiments with a partial wedge transducer using a hydrophone and motorized stage. In the absence and presence of the skull, the maximum RMS pressure is 88.4 kPa and 13.6 kPa, respectively. The total transmission loss including reflection is 16 dB.

Conclusions: We propose a dual-mode conversion technique for enhancing a transcranial ultrasound delivery into the brain using a wedge array method. The dual-mode conversion means that the longitudinal wave in the wedge is converted to Lamb wave in the skull, then the Lamb wave is converted to the longitudinal wave in the brain. From the simulation results, this concept improves the transmission efficiency of the skull. The focal spot is adjusted by changing the radius of the wedge. In addition, sufficient focusing pressure could be acquired by making the full-wedge transducer. We presented the concept and feasibility of the dual-mode conversion transcranial technique.

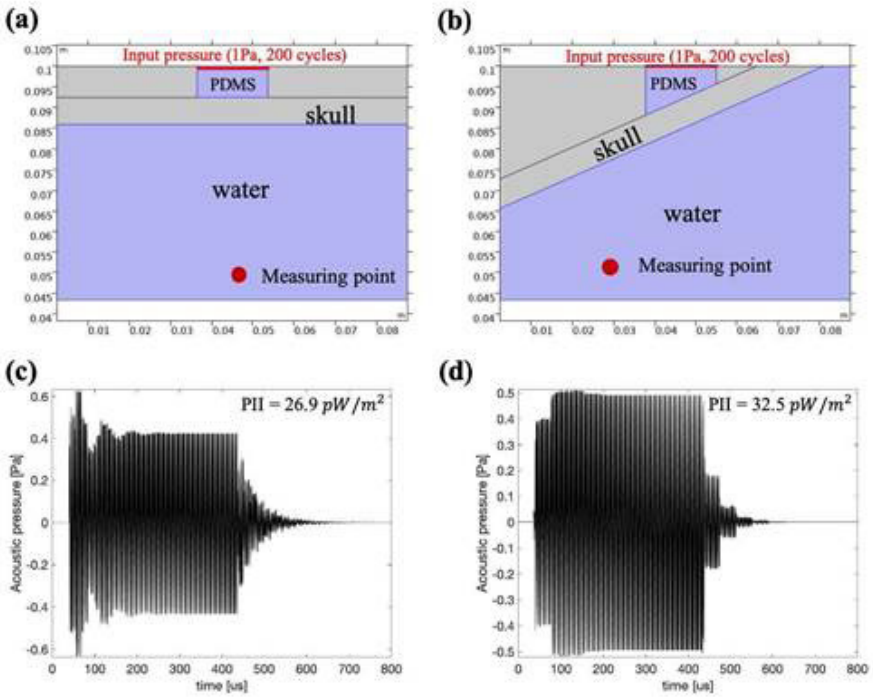

Figure 1. (a) Simulation setup of normal incidence, (b) Simulation setup of wedge incidence, (c) Acoustic pressure data and PII (pulsed integral intensity) of normal incidence.

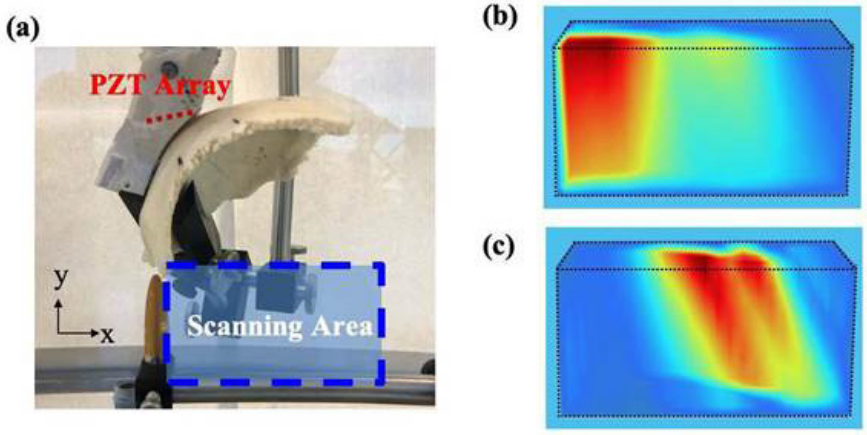

Figure 2. (a) Experiment setup with the wedge transducer, the skull and the hydrophone, (b) 3D scanning results without skull, (c) 3D scanning results with skull.

P-BRT-14

Topic: Brain Technical
Presentation Type: Poster

A figure of merit for ultrasound transmission in transcranial focused ultrasound

Sait Kilinc, Costas Arvanitis, F. Levent Degertekin

Georgia Institute of Technology, Atlanta, GA, USA

Background: Understanding ultrasound transmission through the skull is critical to reduce the detrimental effects such as heating of the skull and to optimize the treatment. Conventional tFUS techniques utilize normal incidence wave transmission through the skull which has limited the treatment envelope to the center of the brain. To overcome this limitation, use of oblique incidence angles for shear mode transmission and plate mode conversion have been previously proposed (Pichardo 2007, Firouzi 2017), but this approach has not been thoroughly evaluated given the wide range of reported skull properties in the literature. The present work is motivated by those studies and aims to develop a figure of merit (FOM) to compare ultrasound transmission techniques and optimize transducer geometry through numerical simulations.

Materials and Methods: Elastic wave propagation through the skull is numerically simulated using a pseudo-spectral finite difference time domain solution (k-Wave) that calculates the discretized wave equation for viscoelastic media on a finite-difference grid. A planar skull model sandwiched between water and brain layers with non-reflective boundaries (Fig. 1 inset) is used to eliminate the impact of complex skull geometry from the ultrasound transmission and temperature map calculations. The temperature maps were calculated from the steady-state particle velocity amplitude and the impact of shear and longitudinal waves on skull heating were separated. Angular dependence of the pressure (and power) transmission coefficients in the 0.5-1.2MHz frequency range for a 1.27cm wide transducer is calculated by integrating the spatial pressure distribution over the entire 2D beam and normalizing it with the no-skull condition on the same plane. This is repeated for a wide range of different shear and compressional attenuation coefficients reported in the literature (White 2006). The ratio of transmitted power to maximum temperature rise in the skull region is used as the figure of merit (FOM) and it is evaluated as a function of incidence angle. Additionally, experimental acoustic pressure transmission measurements were conducted on a degassed human skull specimen in water tank with a custom data acquisition and scanning system to qualitatively verify the calculation approach.

Results: Pressure transmission calculations at 1MHz show that maximum transmission is obtained around normal incidence with a minimum occurring the longitudinal wave critical angle of 33° for all thickness values (Fig 1). Although there are local maxima due to Lamb wave mode conversion, the transmission coefficient is significantly reduced beyond 20°. This is in qualitative agreement with the measured transmission coefficient on a ~7mm thick real skull sample (Fig. 2), which shows reduced transmission beyond the longitudinal critical angle. Temperature map calculations (Fig. 3) show that after 20° incidence angle the maximum temperature rise in the skull is nearly independent of thickness indicating that the most of the heating occurs close to the top of the skull layer and ultrasound quickly attenuates for the particular attenuation parameters. As the incidence angle is increased, the reason for the temperature rise shifts from longitudinal wave attenuation to shear wave attenuation.

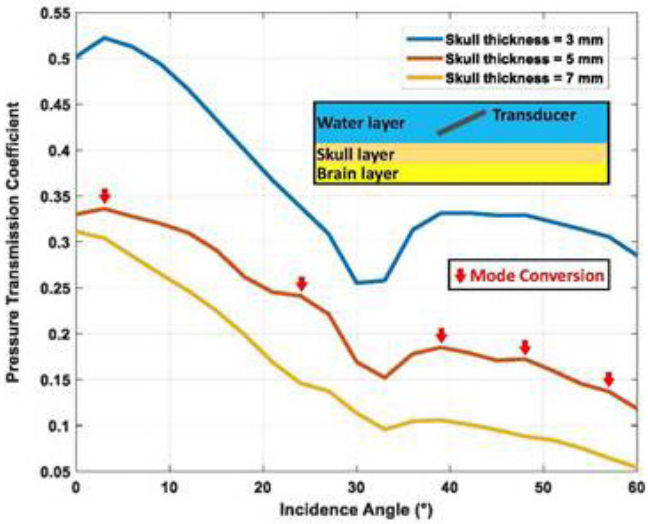

Figure 1. Simulated ultrasound pressure transmission coefficient at 1MHz as a function of incidence angle. Arrows show the angles where reflection coefficient calculations indicate Lamb wave mode conversion.

Conclusions: When the FOM is calculated based on the ratio of ultrasound power transmission through the skull to the maximum temperature rise in the skull layer, one obtains the curve in Fig. 4. Although reasonable power transmission is obtained through mode conversion beyond the longitudinal critical angle, this comes with excessive temperature rise. As confirmed by earlier studies, incidence angles below 15° should be targeted for high FOM. This conclusion is valid even when shear and longitudinal attenuation are considered equal (Fry 1978). Therefore, when used with the typical water coupling methods, Lamb wave mode conversion based ultrasound transmission does not seem to have an advantage for tFUS applications to reduce skull heating

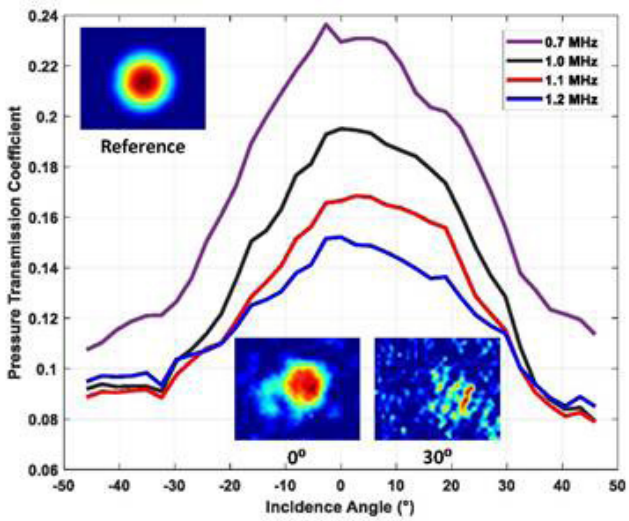

Figure 2. Measured transmission coefficient as a function of incidence angle for ~7 mm thick human skull sample. Insets show the measured 2D scanned transmitted pressure fields with abd without skull at 1MHz.

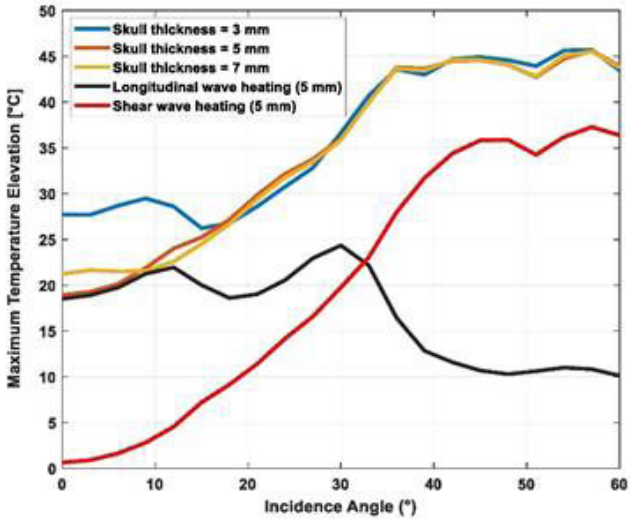

Figure 3. Maximum temperature elevation in skull as a function of incidence angle at 1MHz with attn. coefficients from (White 2006). As incidence angle is increased heating due to shear waves becomes dominant.

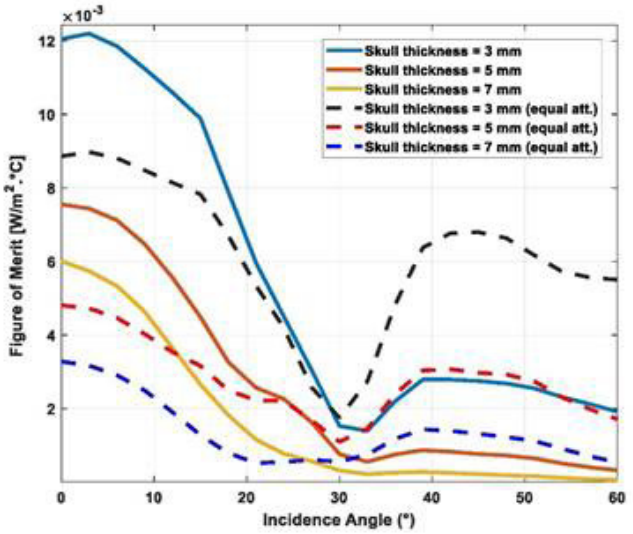

Figure 4. Calculated FOM variation with incidence angle for different skull thicknesses at 1MHz. For equal longitudinal and shear attn. case (Fry 1978) reference is used with higher longitudinal attenuation.

P-BRT-15

Topic: Brain Technical
Presentation Type: Poster

A benchtop focused ultrasound system for drug screening investigations in central nervous system

Hohyun Lee, Scott Schoen Jr, Yutong Guo, Chulyong Kim, Costas Arvanitis

Georgia Institute of Technology, Atlanta, GA, USA

Background: High cost and lack of portability hinder widespread use of magnetic resonance imaging–guided FUS (MRgFUS) both in preclinical and clinical settings; ultrasound-guided FUS (USgFUS) system has the potential to address these limitations in addition to providing real-time guidance during the sonications. Here, we present a portable, cost-effective and autonomous ultrasound system for targeted drug delivery in the central nervous system with sub-millimeter targeting accuracy and closed-loop blood-brain barrier (BBB) disruption capabilities.

Materials and Methods: The proposed system is composed of two subunits. The first is for neuronavigation (i.e. targeting the desired brain structure) and the second for closed-loop targeted drug delivery (i.e. monitoring and controlling the microbubble dynamics) (Fig. 1 A). The neuronavigation subunit uses ultrasound pulse-echo signals and insertion loss of echoed signals to create an ultrasonic image of the mouse head by raster scanning a single-element imaging transducer mounted on a 3D-Positioning system. This image is then registered with published brain atlas to estimate the location of the bregma that is then used to navigate a coaxially aligned therapeutic FUS transducer (0.5 MHz and 1.5 MHz) to desired location in the brain for focal BBB disruption (Fig. 1 B-D). The broadband imaging probe (2.5 MHz -5 MHz) is then switched to passive mode for monitoring and controlling the microbubble dynamics via passive cavitation detection (PCD). The PCD is part of a closed-loop system designed for controlled BBB disruption. Following the FUS pulses, the microbubble acoustic emission level detected by the PCD is used to adjust the transducer pressure in order to attain strong harmonic signal in the absence of broadband emissions. The level of harmonics is correlated with Ktrans values – a measure of BBB permeability extracted by dynamic contrast enhanced MRI – in order to train the closed – loop controller and establish criteria for safe and effective BBB disruption and drug delivery.

Results: In vivo BBB-disruption experiments allowed to compare desired targets with the actual targeted brain locations using contrast enhanced MRI (Fig. 1 D). Our results indicate that our neuronavigation methodology has targeting accuracy of 430 ± 100 μm, which is less than the size of the FUS transverse profile (500 μm). Using PCD during BBB-disruption experiments we were able to capture the cerebrovascular microbubble kinetics and dynamics after a bolus microbubble injection (Fig. 1 E), providing the basis for a closed-loop controller of bubble dynamics (i.e. harmonic level and duration that the controller will be active). Moreover, the 3rd harmonic emissions level, in the absence of broadband emissions, positively correlated with Ktrans measurements ($r2 = 0.59$), supporting the hypothesis that it can provide important real-time information for attaining safe and effective BBB disruption. Importantly, the system had total experimental time (for one target per animal) less than 10 minutes.

Conclusions: We designed, developed, and evaluated an autonomous ultrasound system for targeted drug delivery in central nervous system with sub-millimeter targeting accuracy. The extended capabilities of the proposed system that allows for automatic targeting of brain regions in mice with reduced experimental time makes it ideal for drug screening investigations. Ongoing investigations aim to refine the real-time controller and identify optimum FUS-drug combinations in order to facilitate the effective translation of the FUS technology to the clinics.

Figure 1.

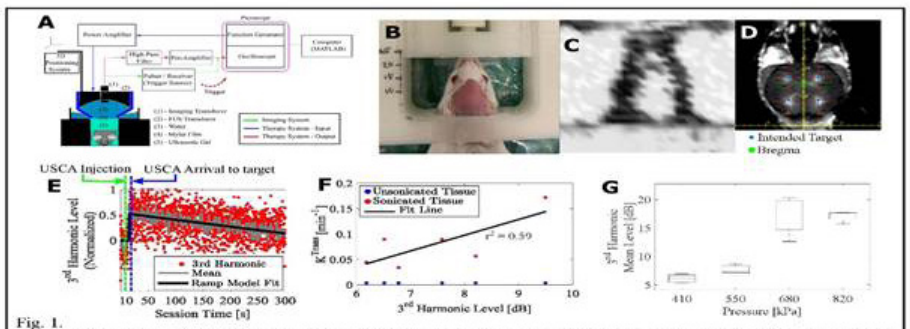

Fig. 1.
A) overall system schematic B) *in-vivo* setup C) created ultrasound image D) contrast - enhanced MRI after 4 sonications E) microbubble kinetics throughout sonications F) correlation of K^{trans} with harmonic level G) mean harmonic level as a function of pressure.

Acknowledgements: Supported by Focused Ultrasound Foundation Global Internship Program (2018, 2019).

P-BRT-16

Topic: Brain Technical
Presentation Type: Poster

Saturated peak negative pressure of shock waves generated from a carbon nano tube composite transducer

Jooho Lee, Dong-Guk Paeng

Jeju National University, Jeju City, South Korea

Background: Sound pressure and frequency band are the important characteristics in therapeutic ultrasound. Shock waves generated by photoacoustic carbon nanotube transducers have the advantages of high sound pressure and broadband frequency. Therefore, the application studies in the field of therapeutic ultrasound using carbon nanotube (CNT) transducers are continuously being conducted. However, peak negative pressure (PNP) of shock wave was saturated to a few MPa even with higher laser energy while peak positive pressure (PPP) increased to several tens of MPa. In this study, the trend of saturated PNP with increased PPP of the shock wave was measured by several CNT transducers and the results were compared with the simulation result to confirm that the PNP was saturated due to the phase delay.

Materials and Methods: Five CNT transducers with a diameter of 2cm were manufactured and used in the experiment. The shock waves from the CNT transducers generated by a laser system (ND:Yag, wave length is 532nm STL-5000Q, StraTek, Korea) were measured by a needle hydrophone(NH0200, Precision Acoustics Ltd, UK) to measure PPP and PNP at the focus with laser energy from 250 to 900 mJ. A measured shock wave signals in the experiment with a laser energy of 250 mJ was used for the simulation study of the phase delay. The shock wave signals were superimposed with 1000 random phase changes within the 100 ns range. The results were then compared with the results without phase delay. Finally, the PPP was normalized to the measured pressure when the laser energy was 900 mJ in the experiment and compared with the experimental results.

Results: In the experiment, the PPP of the shock wave increased as the laser energy increased, while the PNP was saturated. With laser energy of 900 mJ, the PPP of the shock wave was 40 MPa, while the PNP was saturated to -8.33 MPa. The simulated PNP was -22MPa without phase changing. When the phase was randomly delayed within 100 ns, the PNP was -10MPa, which was similar to the experimental results.

Conclusions: In this study, the saturation of the PNP of the shock waves from carbon nanotube transducers in the experiment was assumed to be the phase delay by the different areas of the transducer surface and proved by simulation. In order to prove this assumption of phase delay, new CNT transducers will be designed and fabricated with different backing layers and the additive structures for phase delay control.

Acknowledgements: This research was supported by the Focused Ultrasound Foundation.

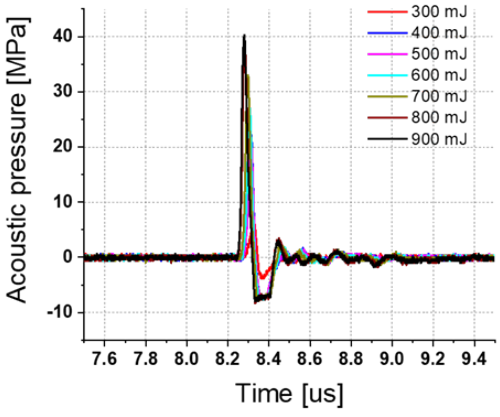

Figure 1. Measured shock wave signals according to laser energy increase in the experiment.

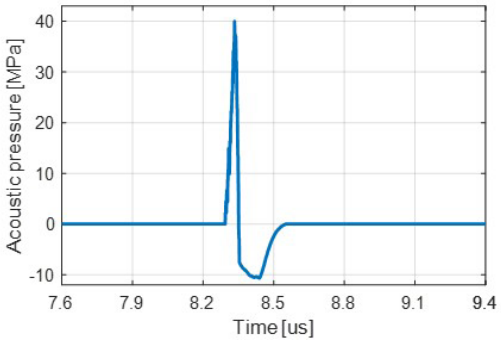

Figure 2. Simulation result about the superimposed signal of Shock wave with 1000 random phase changes within the 100 ns range.

P-BRT-17

Topic: Brain Technical
Presentation Type: Poster

Analysis methods for noninvasive manipulation of the glymphatic system by focused ultra-sound

Anirudh Natarajan, Muna Aryal Rizal, Raag Airan

Stanford University, Stanford, CA, USA

Background: The overall goal is to develop computational methods to analyze the progression of tracer through the brain using MR images acquired before and after ultrasonic manipulation of the glymphatic system. Currently, for this project, our image analysis pipeline uses software such as OsiriX, which is effective but requires manual delineation of the regions of interest, which is prone to errors and bias and requires significant investigator effort. We instead propose a novel analysis pipeline built in Python to greatly simplify and automate this process. As opposed to OsiriX, our application would allow users to simply input a large group of DICOM files and receive a full analysis without any further manual input. To rapidly develop our technique of ultrasonic glymphatic manipulation, we need to be able to efficiently analyze our imaging data without the significant sources of bias and error that come with manual processing.

Materials and Methods: Inputting the pathway to a folder, the program automatically sifts through the hundreds of images in the dataset and then organizes them by time. I made a method that selects the correct scan for analysis, which removes all the scans except the ones with the highest mean, leaving one scan for each position. I then crop the MR images so that just the brain data is being analyzed and use z-scores to normalize the scans. Using these normalized scans, I used a t* equation to calculate statistical significance among the brightness of the pixels and set that as the baseline for the analysis. The program then calculates the intensity and volume over time and presents the user with two charts (Fig 1). All of this works in the program for the initial dataset I used. When using others, everything works fine except the cropping. Cropping is a problem because two images can be the same sequence but be a part of different datasets meaning they were taken on different days. Because of this, there is movement in the location of the brain (Fig 2). This makes cropping extremely difficult, if not impossible. To try and solve this, I tried a number of different things. First I tried to subtract the image from itself offset by one pixel to hope to see some edges. This worked somewhat but was not good enough. I then developed a machine learning algorithm to detect the edges of the image, in hopes that the edges will reveal the central brain structure and I can simply crop around it (Fig 3).

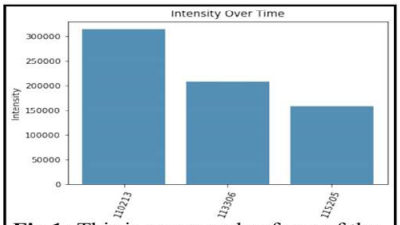

Fig 1: This is an example of one of the graphs the program generates, in this case intensity. The y axis is the time of each set of scans.

Results: Overall, the project was a success and the goal of the project was completed, it just needs to be refined a little bit more so that the cropping step is fully automated. With my limited manual input, the program runs smoothly as planned. I am currently working on refining the algorithm so that the machine learning might be able to work. Some of my next steps also include creating my own software to view the 2D brain data as a 3D object and looking into SPM (statistical parametric mapping) and seeing if it could help my project.

Conclusions: To rapidly develop our technique of ultrasonic glymphatic manipulation, we need to be able to efficiently analyze our imaging data without significant sources of bias and error. Automated post-processing of the imaging data will rapidly speed up and simplify this analysis to allow researchers to focus on optimizing their experimental preparations. Python is rapidly becoming the most common scientific and data processing language and its capabilities are endless. Creating an analysis pipeline in Python will not only ease the development, it will also capitalize upon the most current image analysis algorithms, given the incredibly active Scientific Python community. This program ushers us into the new generation of ultrasound research.

Acknowledgements: Charles Steger Global Internship 2019

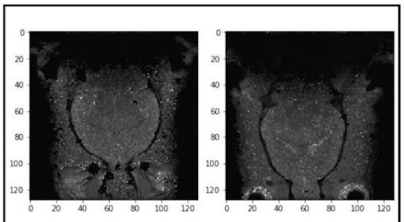

Fig 2: This clearly displays the cropping problem. Both of these scans are the same sequence and yet the one on the left is much higher than the right. This makes a standardized cropping method very difficult.

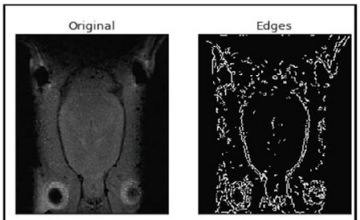

Fig 3: This displays the machine learning model I built and how it detects the edges of the original brain scan. You can clearly see the central structure but it is not clear enough to use it for cropping.

P-BRT-18

Topic: Brain Technical
Presentation Type: Poster

Estimating thickness and speed of sound of layered material using a low-frequency imaging linear-array

Shirshak Shrestha, Laura Curiel, Samuel Pichardo

University of Calgary, Calgary, AB, Canada

Background: Low-Intensity Focused Ultrasound (LIFU) is currently being investigated for non-invasive neurostimulation treatments. LIFU transmits low-intensity waves, which produce a precise ultrasound focus that can deliver a transient and reversible effect on neuron's activity (Neuron, vol. 66, no. 5, pp. 681-694, 2010). LIFU involves ultrasonic waves passing through the skull, a secondary medium, resulting in potential defocusing due to the refraction that can be mitigated using computed tomography (CT) and numerical simulations (Hum. Brain Mapp., vol. 39, pp. 1995, 2018; J. Ther. Ultrasound, vol. 4, 2016). We propose a method based exclusively on ultrasound imaging that will facilitate the development of refocusing algorithms through the human skull, which will avoid radiation and be able to operate in real-time. Here we present estimation of the thickness and speed of sound of layered material, including a skull phantom, using a low-frequency ultrasound imaging linear array.

Materials and Methods: We applied a variable focusing method (J. Appl. Phys., vol. 84, pp. 668, 1998; Phys. Med Biol., vol. 58, pp. 1083, 2013) to locate the inner edge of the skull where the echo signal from the interface is at its maximum (example of the echo signal is shown in Figure 1). The ultrasound time-of-flight between the two edges, free field focus, and the distance of the skull from the transducer, obtained from the echo signal with focus at the inner edge of the skull, were used to estimate the skull thickness and speed of sound (geometry and equations for estimations are shown in Figure 2). We implemented this method using a 32-element 1 MHz linear array transducer and a Verasonics vantage system. We used a low-frequency transducer to ensure that there was enough signal-to-noise ratio to differentiate between the two interfaces of the skull as the ultrasound passes through the skull. We performed tests with plates made of polycarbonate (PC) and high-density polyethylene (HDPE), along with a skull phantom (True Phantom Solutions, Windsor, ON, Canada). The experimental setup is shown in Figure 3. We compared the estimation of thickness with calliper measurements. For the speed of sound, we used the time-difference measured with a hydrophone between water-only and the phantom materials.

Results: The estimated thickness of the PC and HDPE plates was 6.49 mm and 6.38 mm respectively, compared to 6.4 mm measured with a calliper. The speed of sound was 2260 m/s and 2429 m/s, respectively, compared to 2186 m/s and 2347 m/s measured with a hydrophone. The skull phantom was estimated to be 10.56 mm thick and have a speed of sound of 2112 m/s compared to 8.8 mm +/- 0.625 mm, and the speed of sound was at 2467 m/s. The error for the estimated thickness and speed of sound for the plastics was at 1.4% and 3.5% and skull phantom at 20% and 15%, respectively, compared to hydrophone measurements.

Conclusions: The new non-invasive method can estimate individual acoustic properties using a transducer operating at a frequency compatible with transcranial sound transmission. The acoustic information obtained using the proposed method can be used to calculate the phase information to be programmed in a phased array for transcranial ultrasound therapy. This method can avoid in the future the use of CT and simulations while performing the correction in real-time.

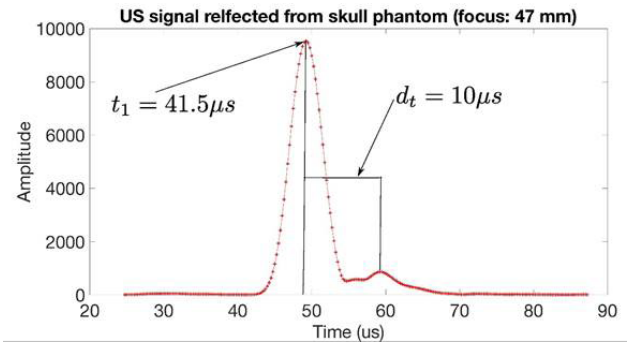

Figure 1. US echo signal from skull phantom when focused at furthest edge. Filtered with bandpass between 0.9 MHz and 1.07 MHz. All of the elements were summed after applying the transmit delay.

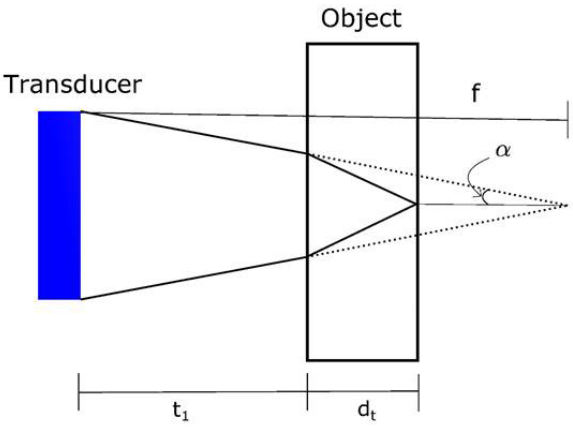

$$\sec(\alpha)(-\sin^2(\alpha) + \frac{c_w^2}{c_o^2})^{\frac{1}{2}} = \frac{c_o d_t}{2f - c_w t_1}$$

c_w : speed of sound in water (m/s)

c_o : speed of sound in object (m/s)

Figure 2. Focused at the back of the object. Equation for calculating the speed of sound of the object.

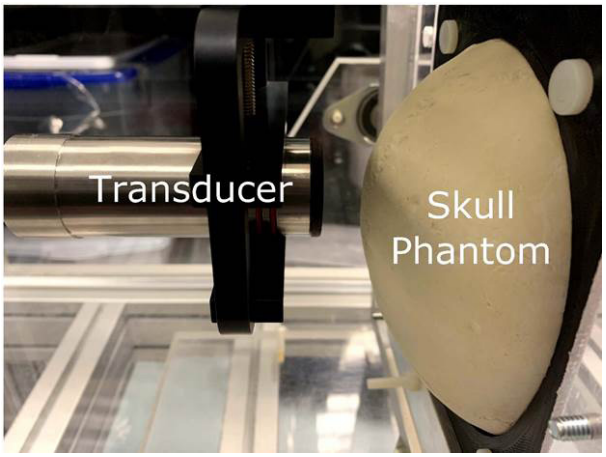

Figure 3. Experimental setup of collecting the ultrasound echo signals using the imaging transducer and the skull phantom.

P-BRT-19

Topic: Brain Technical
Presentation Type: Poster

Comparison by simulations of phase correction methods in transcranial MR-guided focused ultrasound

Emma Slominski, Dennis Parker, Henrik Odéen, Douglas Christensen, Viola Rieke

The University of Utah, Salt Lake City, UT, USA

Background: In neurological treatments using transcranial magnetic resonance-guided focused ultrasound (tcMRgFUS), phase correction is used to ensure the intended target is heated sufficiently to ablate the target. Phase correction is necessary because spatial heterogeneities and variations in skull thickness cause phase aberration and lead to blurring and shifting of the focal spot. By simulating how phase correction improves the sharpness of the focal zone, the increase in achieved temperature can be observed.

Materials and Methods: Patient data from an essential tremor (ET) treatment were used to simulate different phase correction methods. The patient's CT scan was segmented into water, brain, and bone before being rotated and translated into the transducer space to register with the MR images. Using the hybrid angular spectrum (HAS) method, the ultrasound transmitted through the skull to the focus was simulated for the tcMRgFUS system (660-kHz Exablate Neuro, Insightec, Tirat Carmel, Israel) using: (1) no phase correction, (2) time reversal phase correction, and (3) Insightec's phase correction values obtained from the ET treatment log file. Time reversal was applied by backwards propagating ultrasound from a point source at the focal point back to the transducer elements. The last four sonications of the treatment were independently simulated using each of the three methods. The ultrasound power deposition patterns (Q in W/m3) were generated with 1-mm isotropic resolution. These Q patterns were then used in Pennes' Bioheat equation to simulate temperature maps at 1-mm spatial resolution and 1-s temporal resolution.

Results: The peak temperature in space and time was determined for each method of phase correction for the final four of ten total sonications. Figure 1 displays the results for Sonication 9. The average temperature in the volume surrounding the peak temperature was also calculated for Sonication 9, as shown the same figure. This provided the average temperature in a 1 x 1 x 3-mm region, which is the same resolution as the post-processed MRTI for this treatment. In Figure 2, plots of the simulated axial temperature in the focal plane for each correction method show that the focus becomes sharper and more centered corresponding to increasing temperature.

Conclusions: These results indicate that the method of phase correction can significantly affect the obtained temperature. The simulation using no phase correction produced the lowest temperature rise, as expected. The time-reversal method provided a greater improvement than employing Insightec's treatment phases, which is not surprising since it was based on the same simulation procedure and acoustic parameters that produced the forward propagation results. Future experiments are planned that will involve using an ex vivo skull with an enclosed tissue-mimicking phantom to compare simulations with experiments. Insightec's phase correction values and the HAS-calculated phase corrections will be employed in these experiments.

Acknowledgements: This study has been supported by the Summer 2019 FUSF Global Intern program, NIHR01EB028316, Insightec, and the Mark H. Huntsman Chair.

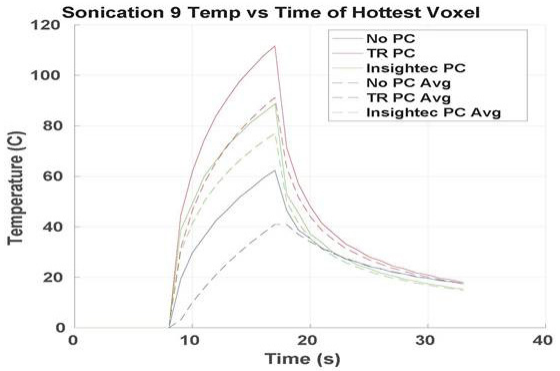

Figure 1. Plot comparing temperature rise in the hottest voxel(solid lines) for Sonication 9 along with the average temperature in the surrounding 1x1x3-mm volume(dashed lines) using each of the three methods.

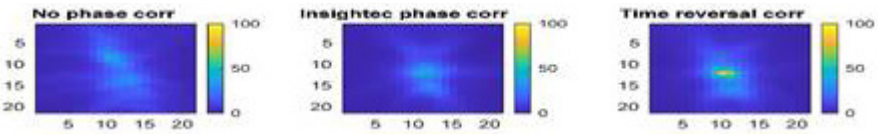

Figure 2. Simulated temperature profiles in the axial focal plane using each phase correction method for Sonication 9. Each image is plotted with a resolution of 1 x 1 mm and with the same temperature scale.

P-BRT-21

Topic: Brain Technical
Presentation Type: Poster

Pressure field estimation by Kranion at the geometrical focal area through the human skulls

Woongbin Kang[1], Changzhu Jin[2], Dong-Guk Paeng[1]

[1]Jeju National University, Jeju, Korea
[2]DGIST-ETH Microrobot Research Center, Daegu, Korea

Background: The transmitted energy is significantly affected by morphological characteristics of the human skull at the focal area. Kranion software was developed for a fast and easy visualization tool of the acoustic rays through the human skull from the elements of array transducers. In this study, we estimated the sound pressure field transmitted through the human skulls using Kranion in order to find the optimal focal area in the brain tissue at the geometric focal area.

Materials and Methods: To estimate sound pressure at the different focal areas through the human skull, sound pressure field at different focal areas inside the skull was computed using the Kranion software. Target focus at a geometric center was moved to 5 mm away from the center each time and the focal pressure and shape were computed with phase information of all 1024 elements of an ExAblate Neuro system. (ROI size: 85x35mm at sagittal planes from the center (0) to 10 and 20 mm away)

Results: We simulated the pressure fields at the geometrical focal areas in the ROIs of the brain tissue by phase correction of the acoustic rays through two human skulls as shown in Fig. 1(a) and (b) in the Kranion software. We numerically obtained the peak pressure, -6dB area in pressure field, intensity and power. Fig. 2 (a) and (b) show the sound intensity fields for data1 and data2, respectively. High intensity was obtained far off the reference center, and the closer the reference center, the lower the sound pressure because the rays were more refracted. The maximum powers were 218W and 291W, and the intensities were 8.3 W/cm2, about 20 times larger than those at the reference center position. The higher power and intensity were mainly from the thinner thickness of the skull, frontal part for data1 and top part for data2. The number of rays and out-of-targeted rays passing by the focal area are the two main reasons, which were validated by homogeneous hemispherical phantom skull.

Conclusions: This research shows the possibility of selecting the optimal focal area by mapping the pressure field in any ROI due to individual skull characteristics using Kranion. This would be helpful for patient selection and verification of failure of thermal ablation after treatment.

Acknowledgements: 2019 Global internship of Focused Ultrasound Foundation

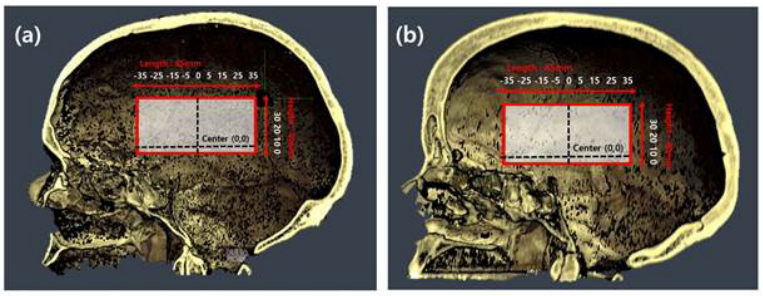

Figure 1. CT and MR images uploaded in Kranion and the coordinates in ROI for data1 provided in Kranion software in (a) and data2 provided by Stanford Medical school in (b).

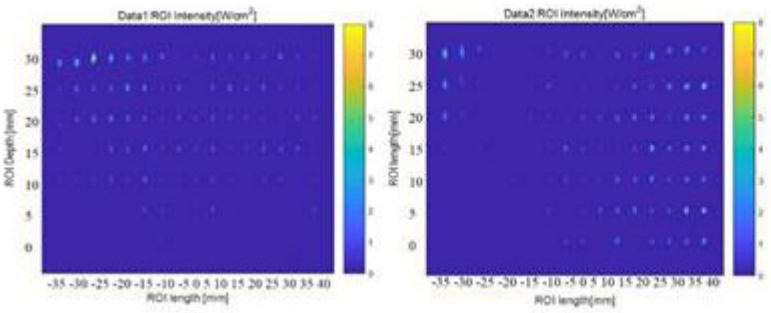

Figure 2. Intensity maps in ROI calculated from the pressure using Kranion for data1 in (a) and data2 in (b).

P-BRT-22

Topic: Brain Technical
Presentation Type: Poster

The effects of skull numerical representation on intracranial fields in transcranial focused ultrasound (tFUS) simulations

Shaikhah Alkhadhr[1], Sumukha B N[1], Sergey Turovets[2], Mohamed Almekkawy[1]

[1]Penn State University, State College, PA, USA
[2]University of Oregon Neuroinformatics Center, Eugene, OR, USA

Background: Neuromodulation and brain stimulation are promising approaches to mitigate the effects of brain-originated diseases. Current studies are focusing the non-invasive Transcranial Focused Ultrasound (tFUS) method in spite of the accompanying challenges caused by the nature of the human skull. Focal specificity and target pressure are two of them. There is a heavy reliance in studies on tFUS simulations. These simulations are crucial to observe the procedure and adjust critical parameters thoroughly investigating the numerical representations of key skull features. Adjusting such parameters will allow better understanding of propagation. Simulations are grounded by accurate measurement of the skull's geometry and acoustic properties. Previous studies have observed the effects of uncertainties and inaccuracies in these measurements. This paper aims to compare numerical representations utilizing Computed tomography (CT) imaging and their impact on predicting the intracranial fields.

Materials and Methods: The performed simulations were carried out with CT image from a 13.5 years old male as part of a pediatric head modeling project in Washington University. The intensity of pixels in the CT images was registered in Hounsfield Units (HU) with accordance to a pediatric head atlas. The average acoustic properties for each of the 3 media (water, skull, brain tissue) were calculated through a known relationship between porosity and CT intensity. Two types of simulations were performed. One that processed the values of acoustic properties as depicted by the HU registration of the CT image creating a heterogenous medium closer to an actual skull composition. The other simulation processed the values of the acoustic properties registered from the HU, all averaged, to create a more homogenous medium for the simulation. Finite Difference Time Domain (FDTD) methods were used to calculate the tFUS propagation from a spherical array transducer. The values of the peak pressure obtained from these simulations were then compared to have an insight on errors caused by different representations of media.

Results: Simulations modeled a 1 MHz 64-element spherical array ultrasound transducer through various representations of the target media. Simulation duration was 150 μs with grid spacing of 100 μm and grid size 2520 x 2520 pixels. CT image resolution was 0.5mm in all directions. A perfectly matched layer was used at the edge of the simulation domain to absorb waves at the boundary. The results show that the use of homogenous values saw a decrease at the focal peak pressure of around 15% and increase in the spread of the focal spot.

Conclusions: The use of homogenous-like values in representing the acoustic properties of the the skull directly affects the values of the peak pressure at the focal point and in the spread of that point causing significant difference in simulating the resulting intracranial fields. Hence, numerical representation of the skull acoustic properties occupies a vital role in tFUS simulations.

P-BTU-2

Topic: Brain Tumors
Presentation Type: Poster

Investigation of the tumoricidal effects of sonodynamic therapy in glioblastoma

Jason Sheehan[1], Kimball Sheehan[1], Darrah Sheehan[1], Mohanad Sulaiman[1], Fred Padilla[1], David Moore[2], Zhiyuan Xu[1]

[1]University of Virginia, Charlottesville, VA, USA
[2]Focused Ultrasound Foundation, Charlottesville, VA, USA

Background: Glioblastoma is the most common primary brain tumor, and, even with treatment, survival is typically 12-18 months after diagnosis. Sonodynamic therapy couples a sonosensitizer molecule and focused ultrasound to cause cancer cell death. We sought to study the effects of sonodynamic therapy using 5-aminolevulinc acid (5-ALA) and high frequency focused ultrasound (FUS) on 2 aggressive glioblastoma cell lines.

Materials and Methods: C6 and U87 glioblastoma cells were grown in culture. Cells were studied under the following conditions: 1. 1mM 5-ALA alone (5-ALA); 2. 10W/cm2 Focused ultrasound alone (FUS); 3. 5-ALA and focused ultrasound (SDT); 4. No treatment. Using a 3D printed holder for the tissue culture plates and a calibrated 1.1MHz ultrasound device, we were able to deliver focused ultrasound to the cells. Studied responses for each condition included cell counts using an MTT (3-(4,5-dimethylthiazol-2-yl)-2,5-diphenyltetrazolium bromide) assay, microscopic changes using phase contract microscopy, and apoptosis staining to quantify cell death. Statistical methods were evaluate for differences between groups.

Results: After treatment with 5-ALA, the glioblastoma cells avidly fluoresced but maintained normal morphology. Ultrasound resulted in some decreased cellular extensions, but SDT led to a marked decrease in cell extension and reduction in cell size. For C6, the MTT assay showed reductions in cell viability for 5-ALA, FUS, and SDT groups of 5%, 16%, and 47%, respectively compared to control ($p<0.05$ between SDT and FUS). For the C6 cells, caspase 3 staining showed the percentage of apoptotic cells were 2.1%, 6.7%, 11.2%, and 39.8% for control, 5-ALA, FUS, and SDT groups, respectively ($p<0.05$ between SDT and FUS). Parp-1 staining showed the percentage of C6 positive cells were 1.9%, 6.5%, 9.0%, and 37.8% for control, 5-ALA, FUS, and SDT groups, respectively. U87 cells showed similar responses to the various treatments.

Conclusions: Sonodynamic therapy using a combination of 5-ALA and focused ultrasound resulted in appreciable glioblastoma cell death in C6 and U87 cells as compared to either 5-ALA or FUS alone. SDT led to apoptosis and death of cancer cells. The approach couples two already FDA approved techniques in a novel way to treat the most aggressive and malignant of brain tumors. Further study of this promising technique is planned.

Acknowledgements: support from University of Virginia and Focused Ultrasound Foundation.

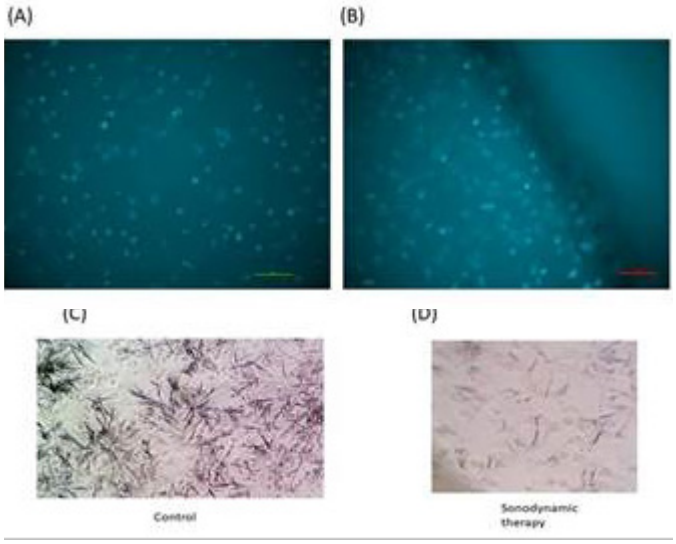

Figure 1. These micrographs demonstrating fluorescence of U87 cells after exposure to 1mM 5-ALA and phase contrast microscopy of control and SDT treated cells.

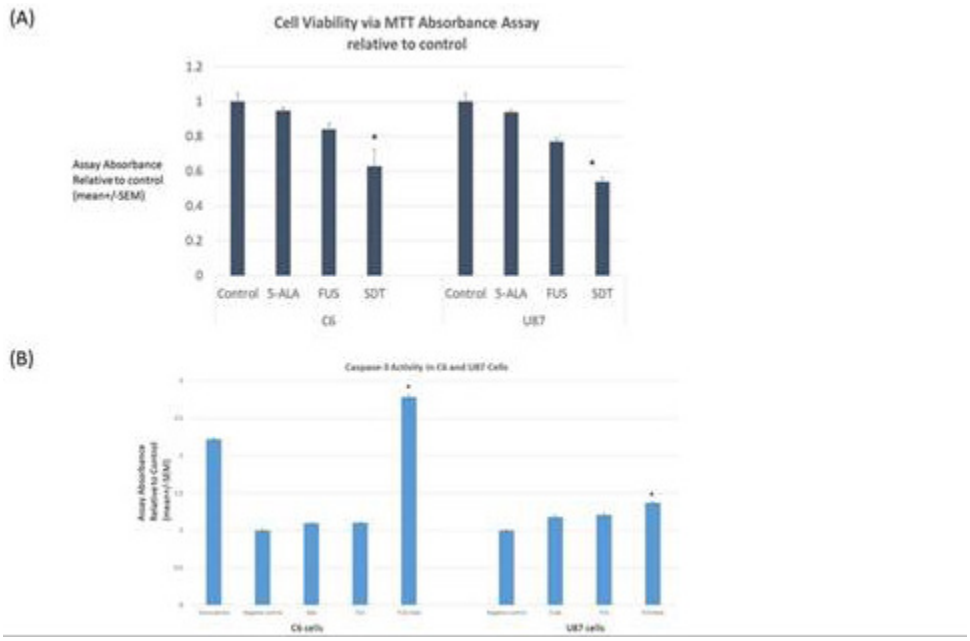

Figure 2. MTT and Caspase 3 Assays for C6 and U87 cells treated with control, 5-ALA, FUS and SDT.

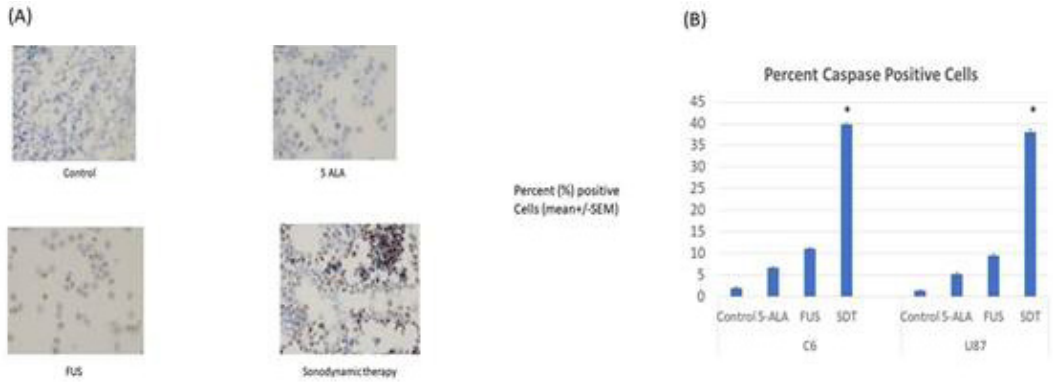

Figure 3. Caspase staining for C6 and U87 cells of control, 5-ALA, FUS, and SDT treated groups.

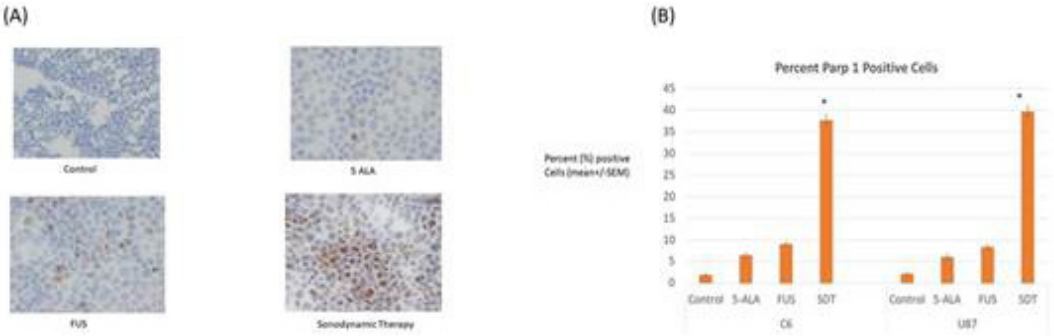

Figure 4. Parp-1 staining for C6 and U87 cells of control, 5-ALA, FUS, and SDT treated groups.

P-BTU-3

Topic: Brain Tumors
Presentation Type: Poster

Focused ultrasound treatment of cerebral cavernous malformations

Petr Tvrdik, Khadijeh Sharifi, Catherine Gorick, Delaney Fisher, Min Park, Richard Price

University of Virginia, Charlottesville, VA, USA

Background: Cerebral cavernous malformations (CCM) are vascular abnormalities of the central nervous system with a prevalence of 0.4–0.5% in general population. There is a strong hereditary component to CCM pathology. Heterozygous loss-of-function mutations in one of three genes (CCM1/KRIT1, CCM2/Malcavernin, and CCM3/PDCD10) cause CCM lesions throughout the brain and spinal cord. Murine models have been developed, recapitulating the human disease. We hypothesize that sonodynamic therapy (SDT) in conjunction with a suitable sonosensitizer can be effective for the treatment of CCM. Aminolaevulinic acid hydrochloride (5-ALA) is one such effective sonosensitizer. Despite of its wide use in the treatment of brain tumors, the FDA-approved 5-ALA has not been explored in the context of sonodynamic therapy of CCM. We will use two CCM mouse models, Krit1 and Ccm2, to address the question of whether focused ultrasound (FUS) and 5-ALA can be successfully used for CCM treatment.

Materials and Methods: To generate the experimental animals, the following crosses are used: PdgfbiCreERT/+; Krit1fl/+ male x Krit1fl/fl female; and PdgfbiCreERT/+; Ccm2fl/+ male x Ccm2fl/fl female. The required mutant genotypes and controls will each segregate at 25%. All newborn mice are injected with tamoxifen subcutaneously at P6 (2 mg/mL tamoxifen in corn oil dosed at 50 µl per 2-3 g body weight pups). One to two months after the induction, the brains are cryo-sectioned at 25-50 µm thickness, stained with cresyl violet (Nissl Stain) and mounted on slides. The slides are scanned to establish the incidence of lesions. In the next step, adult tamoxifen-induced animals are subjected to MRI – guided FUS treatment. The animals are placed in a supine position over a degassed water bath coupled to an MR-compatible small animal FUS system. After localization of the vascular lesions suitable for treatment, a tail vein catheter is inserted to permit intravenous injections of 5-ALA and the MRI contrast agent. A dose of 60 mg/kg 5-ALA or vehicle is then intravenously injected through the tail vein 6 hours before sonication. The cavernomas will be sonicated with low acoustic power. T2-weighted MR images will be recorded to detect potential brain damage and bleeding. One month following the procedure, the animals will be scanned with T1-weighted MRI to re-evaluate the size of the lesions. Volumetric measurements will be performed in OsiriX or Horos.

Results: At this early stage of the project development, we have successfully started creating the genotypes necessary for inducing the brain lesions in the animal model. Tamoxifen dosage has been adjusted for young neonates, resulting in a high survival rate. The first set of six mutants harboring the PdgfbiCreERT/+; Krit1fl/- alelles, surviving the administration of adjusted dose of tamoxifen at postnatal day 6, have reached the adulthood and will be analyzed with Nissl staining and imaging. As soon as the prevalence and distribution of the lesions with our adjusted induction protocol is determined, we will move to the in vivo MRI-guided FUS treatment of animals infused with 5-ALA.

Conclusions: The mouse models of CCM faithfully replicate the human condition. We have established the production of two genetic models of CCM, namely Krti1/Ccm1 and Ccm2/Malcavernin. In later stage of this project, we will be able to test the hypothesis that sonodynamic therapy, involving MRI-guided FUS treatment of 5-ALA infused cavernomas, will reduce the load of vascular lesions without hemorrhage and/or damage to the surrounding tissue. If successful, this project could encourage the development of clinical applications.

Acknowledgements: FUS878

P-CAR-1

Topic: Cardiovascular
Presentation Type: Poster

Electromechanical wave imaging for RVOT arrhythmias characterization in-vivo

Jade Robert[1], Elodie Cao[1], Bruno Quesson[2], Francis Bessière[1], Cyril Lafon[1]

[1]LabTAU INSERM U1032, Lyon, France
[2] IHU Liryc, Bordeaux, France

Background: Abnormal electrical behavior of cardiac cells in the Right or Left Ventricular Outflow Tract (RVOT/LVOT) regions can induce arrhythmias in the right ventricle. In most severe cases, the patient must be treated using RF-catheter ablation. The exact position of the arrhythmogenic focus will influence treatment strategy. However, with the current methods, a few hours might be necessary to determine the treatment target and pathway, which impedes on the actual treatment time. Electromechanical Wave Imaging (EWI) is a fast ultrasound-based method that could provide cardiac activation maps with high precision, as shown in a previous study on ex-vivo beating heart model. This imaging method consists in estimating tissue local displacement to visualize local contraction propagation induced by electrical activity of the cardiac cells: The Electromechanical Wave (EW). This study aims at assessing the feasibility of discriminating arrhythmogenic sources in the RVOT and LVOT using EWI in-vivo.

Materials and Methods: 3 pacing electrodes were screwed on the epicardium at the lateral, antero-lateral and septal parts of the RVOT and one was screwed at endocardial level of the aortic cusp (LVOT activation), on two open-chest swines. These electrodes were successively used to induce arrhythmogenic behavior by pacing at least 10bpm above the natural cardiac rhythm. An intracardiac ultrasound probe (6.25MHz) was inserted into the femoral vein up to the right atria, under fluoroscopic guidance. Imaging plane included cross-sections of aorta and pulmonary artery and some lateral RVOT tissue, where one of the pacing electrodes was screwed. ECG-synchronized ultrasound data were acquired at 2500fps during 320ms (800 frames). In total, 9 acquisitions were performed by pacing at the lateral RVOT and 36 control acquisitions without pacing or while pacing at another part of the RVOT. Inter-frame displacement cineloops of the cardiac tissue was computed using phase-tracking algorithm on IQ data. Propagation of the EW front was tracked and origin of the cardiac displacement was compared to pacing site. As out-of-plane motion could affect ultrasound acquisitions, and thus displacement estimation, data quality was assessed by computing the mean correlation coefficient of a tissue pixel displacement with the displacement of its surrounding pixels. Datasets with an overall average correlation coefficient below 0.8 across all tissue pixels were rejected.

Results: In total, 29 EWI datasets were considered of sufficient quality: 6 with lateral RVOT pacing, 23 with out-of-plane or no pacing. Amongst the 6 acquisitions performed during lateral RVOT pacing, 5 demonstrated a cardiac mechanical activation located near the pacing site, synchronized with the local electrical activity. However, 2 of them also showed simultaneously cardiac displacement at another part of the field of view. On one dataset with lateral RVOT pacing, the EW front could not be visually tracked. Concerning the 23 other acquisitions with no pacing or a pacing site out of the field of view, 6 of them resulted in an unclear EW front, 4 showed an mechanical activation onset both at the lateral RVOT and at another region of the cardiac tissue and 16 successfully depicted an origin of cardiac activation which was not located at the lateral RVOT.

Conclusions: EWI allowed to accurately depict a mechanical activity synchronized with local electrical activity with an onset at the pacing site in the imaging plane for 5 out of 6 acquisitions during lateral RVOT pacing. The control datasets, with no pacing or pacing in other regions of the RVOT, were more challenging to interpret, but demonstrated in majority an onset of mechanical activity in other regions of the RVOT. EWI application on in-vivo models with intracardiac probe raises new challenges, such as global motion, more complex anatomy or even, that might require further data processing. Yet these preliminary results could indicate that EWI might be feasible in-vivo and would be useful to visualize arrhythmogenic foci, with intracardiac probes.

Acknowledgements: FUS Foundation, IHU Liryc

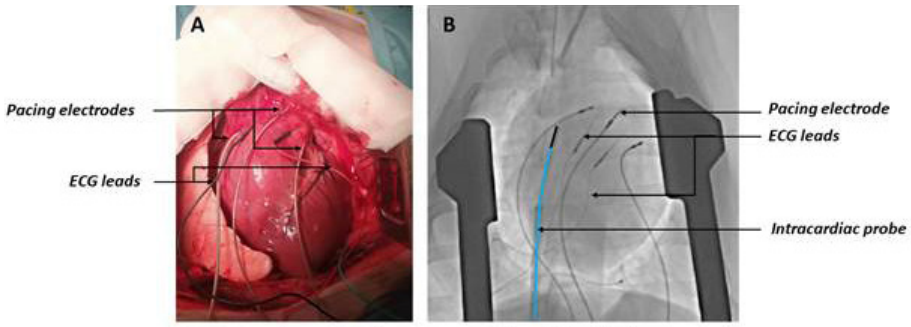

Fig.1 - Experimental in-vivo set-up. A: Epicardial leads placement on open-chest swine's heart. B: Fluoroscopy guidance for intracardiac probe insertion in the right atria.

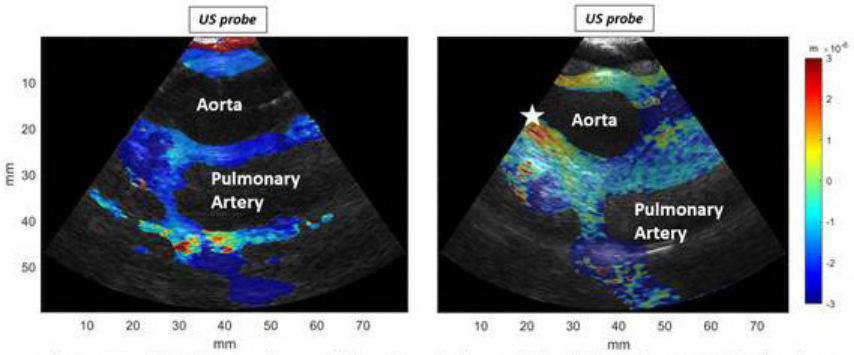

Fig.2 – EWI of the RVOT region overlaid on B-mode image of the field-of-view. A: EWI during sinus rhythm (no pacing). First cardiac activation appears near the pulmonary artery. B: EWI during lateral RVOT pacing (position of the pacing electrode indicated by white star). Cardiac activation seems to originate from lateral part of the aorta, near the pacing site.

P-CAR-2

Topic: Cardiovascular
Presentation Type: Poster

Characterization and performance evaluation of a transesophageal HIFU probe for cardiac applications: Ex vivo experiments

Elodie Cao[1], Jade Robert[1], Maxime Cheppe[2], Claire Bantignies[3], Francis Bessière[1,3], Cyril Lafon[1]

[1]LabTAU, INSERM, Centre Léon Bérard, Université Lyon, Lyon, France
[2]Vermon SA, Tours, France
[3]Hospices Civils de Lyon, Hôpital Cardiovasculaire Louis Pradel, Lyon, France

Background: Catheter ablation is the gold standard to treat focal ventricular tachycardia. This method however remains invasive and has a high recurrence rate. The main difficulty is to guarantee treatment efficacy as the arrhythmia focus localization can be either on the endocardium, on the epicardium or in the middle layer of the myocardium. HIFU is a promising alternative therapy as it could induce thermal lesions in the cardiac tissue at distance and throughout myocardium thickness. Based on these requirements and numerical simulations, a transesophageal HIFU probe guided by ultrasound was designed. Preliminary ex vivo experiments were conducted on myocardium slices. The present study aims at characterizing the transducer, validating the probe ability to produce transmural lesions with HIFU and at detecting the lesion with passive elastography.

Materials and Methods: The transesophageal HIFU probe (Vermon, Tours, France) is composed of a plane 3-MHz piezocomposite transducer, cut into 32 rings truncated at 13.8 mm. An unused cross-shape zone is included in the annular array. The probe is driven by a Verasonics Vantage system. Qualitative and quantitative pressure fields are obtained using respectively a novel method to image focused ultrasound fields in real time and a hydrophone. Results are compared to ultrasound pressure field simulation computed with Rayleigh integral method. Probe acoustic intensity and electro-acoustic performance are determined using an acoustic radiation force balance and a brush target. For ex vivo experiments, 90s-long HIFU sonication, at an acoustic power of 76 W and a focus of 45 mm, is performed on 2-cm myocardium slices. The tissue temperature was maintained at 37°C using a thermoregulator, to reproduce biological conditions. A cooling system was used to avoid excessive temperature rise of the transducer surface. Diffuse shear wave field was generated into the tissue using an external vibrator, for passive elastography purposes. Ultrafast ultrasound data were acquired at 600fps for 1sec with an imaging probe (3MHz, 46 elements) before and after each HIFU shot.

Results: Imaged and measured pressure fields agreed with simulation. HIFU beam can be focused at a distance between 20 and 100 mm. The probe can reach an acoustic intensity of 14.04 W/cm2 and an electro-acoustic performance of 60%. In total, 8 lesions were achieved and confirmed by gross pathology. The average lesion size was 8.12±0.6mm in length, 7.12±0.6mm in width and 14.5±3.9mm in thickness. Amongst these lesions, 8 were transmural. Qualitatively, passive elastography can detect the lesions on 50% of the cases, but further processing should be conducted to validate this result.

Conclusions: The characterization demonstrates that the transesophageal probe complies with focusing and acoustic power requirements to treat arrhythmogenic areas at 20 to 100 mm depth. Transmural thermal lesions could be achieved on ex vivo cardiac tissues using this prototype. These lesions were confirmed by gross pathology and also seen in 50% of the cases by passive elastography, which depicted the change of tissue thickness after the lesion formation. These preliminary ex vivo results give hopeful insight of cardiac HIFU applications. However, therapeutic transducer should still be tested during in vivo experiments to clearly assess its capability.

Acknowledgements: This work is supported by ANR-17-CE19-0017-CHORUS.

Figure 1. (top) Schematic view of the probe and pressure fields in water with an electronic focusing at 100 mm: (i) simulated using Rayleigh integral method, (ii) imaged with L7-4, (iii) measured with hydrophone.

Figure 2. (bottom) Two transmural lesions in myocardium.

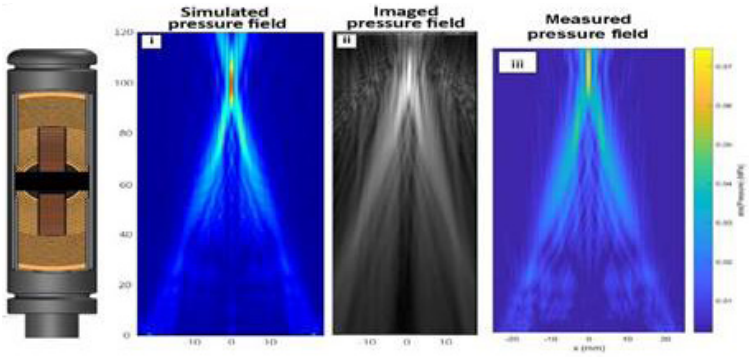

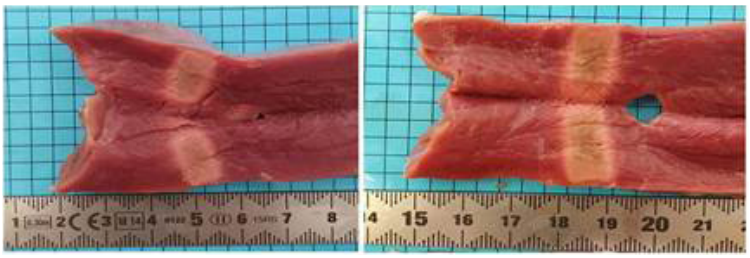

P-CAR-3

Topic: Cardiovascular
Presentation Type: Poster

Cavitation characteristics of phase change nanodroplets activated by pulsed focused ultrasound in sono-thrombolysis

Jinwook Kim, Ryan DeRuiter, Paul Dayton

The University of North Carolina at Chapel Hill, Chapel Hill, NC, USA

Background: Phase-change nanodroplet (ND) is a hundred-nanometer sized, liquid-filled contrast agent that converts to a gaseous state upon excitation by thermal and acoustic energy. Unlike conventional microbubble (MB) contrast agents, the smaller size and a liquid core of nanodroplets allow them to function more sustainable cavitation nuclei with improved circulation and permeation towards the blood clot fibrin network. For optimal use of ND as a cavitation agent, it is crucial to clarify the ND cavitation characteristic compared to the free-field cavitation or MB cavitation. We hypothesized that ND cavitation exhibits higher intensity or larger cavitation cloud size compared to ultrasound alone or MB-mediated ultrasound. Here we tested this hypothesis by in vitro sonothrombolysis experiments with active cavitation imaging.

Materials and Methods: We used bovine blood clots (304±19 mg) in a venous flow model (flow rate of 80±15 ml/min). Thrombolysis efficacy tests were conducted with four test groups: 1) control (only flow), 2) ultrasound (US) alone, 3) US+MB, and 4) US+ND. For 20 min treatment, each group was tested with two insonation conditions: 1) low-pressure, long-pulse condition (1.2 MPa pressure and 3% duty cycle) and 2) high-pressure, short-pulse condition (8.0 MPa pressure and 0.018% duty cycle). Lipid-shelled decafluorobutane (DFB) microbubbles (MB, ~1 μm diameter) and nanodroplets (ND, ~250 nm in diameter) were prepared and diluted in saline water (1:10) for continuous infusion (80 μl/min) in a flow channel. For active cavitation imaging, the five different acoustic conditions were tested: the spatial-peak temporal-average intensity (ISPTA) of 8.7 W/cm2, 8.9 W/cm2, 13.4 W/cm2, 14.5 W/cm2, and 26.9 W/cm2. The cavitation clouds were monitored by 7.8 MHz B-mode imaging. Maximum intensity projections (MIPs) of the differences between 300 consecutive frames were used to visualize the cavitation clouds.

Results: The thrombolysis efficacy of low-pressure, long-pulse condition showed no significant difference between the four test groups (figure 1). Although the negative pressure of 1.2 MPa is sufficient to induce inertial cavitation of both MB (rupture) and ND (vaporization and rupture), the cavitation magnitude is likely insufficient to exhibit noticeable clot fragmentation. A clear difference among the four test groups was observed by the high-pressure, short-pulse insonation. The US+ND case showed an approximately 135% thrombolysis rate of the US+MB case. This result correlated with the cavitation imaging results (figure 2) that ND cavitation clouds have larger cloud sizes with higher pixel intensity than MB clouds for all the five acoustic conditions (e.g. >120% larger cloud size in the case of 8.7 W/cm2). We interpreted this result as a correlation with enhanced shock scattering bubble nucleation by evaporating nanodroplets.

Conclusions: We observed the cavitation characteristics of nanodroplets with pulsed focused ultrasound. In comparison with US alone and US+MB cases, ND-mediated pulses generated consistently larger cavitation clouds with higher intensity, which is possibly evaporating nanodroplets functioning as scatterers for additional bubble nucleation. This feature resulted in a higher clot dissolution efficacy of ND-mediated focused ultrasound thrombolysis than MB-mediated treatment. This study may lay the foundation for optimizing the ND-mediated sonothrombolysis technique for effective, rapid treatment of thrombo-occlusive diseases.

Figure 1. (top) In vitro thrombolytic efficacy test results in terms of percent clot mass reduction during 20 min-treatment (n=3) with two insonation groups. The asterisk (*) indicates a significant difference ($p<0.05$).

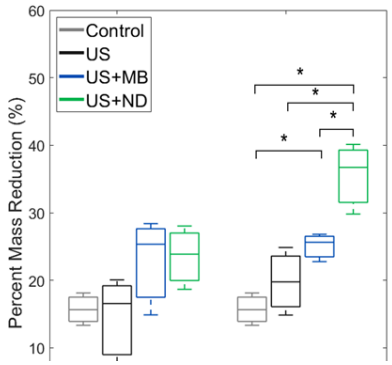

Figure 2. (bottom) Active cavitation imaging results with 8.7 W/cm2 (5.9 MPa-0.75%) insonation. The green-colored-pixels indicate the area of cavitation clouds. The blue circles denote the inner area of a tube.

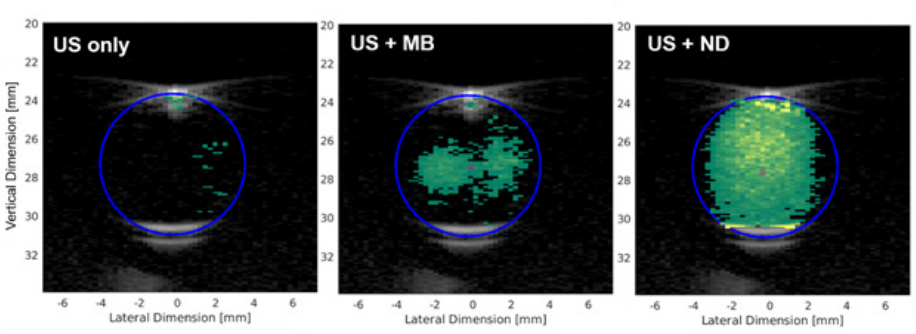

Acknowledgments: This work was supported in part by grant R01 HL141967 from the National Institutes of Health and National Center for Advancing Translational Sciences (NCATS), National Institutes of Health, through Grant Award Number UL1TR002489. The content is solely the responsibility of the authors and does not necessarily represent the official views of the NIH.

P-CAR-4

Topic: Cardiovascular
Presentation Type: Poster

Is currently available high-intensity focused ultrasound imaging adequate for treatment of pe-ripheral vascular malformations?

Ralf Seip[1], Brian Lee[1], Naiem Nassiri[2]

[1]SonaCare Medical LLC, Charlotte, NC, USA
[2]Yale University School of Medicine, New Haven, CT, USA

Background: No definitive cure or FDA-approved treatment modality currently exists for peripheral vascular malformations (VM). Commonly employed techniques – such as surgical excision, debulking, and/or embolization - vary widely depending on physician specialty, experience, and preference. Outcomes remain variable. A safe, more durable therapeutic modality with lower morbidity is needed. High Intensity Focused ultrasound (HIFU)-mediated coagulative necrosis of vascular endothelial cells is one such possible modality. Herein, we aimed to assess the ultrasound imaging requirements and quality of currently available intervening-tissue-sparing HIFU technology in visualizing peripheral VMs in preparation for a follow-up safety and efficacy HIFU clinical study for VM therapy.

Materials and Methods: The current effort focused on determining whether a commercially available, mechanically-scanned, 6.5MHz ultrasound imaging/4.0MHz HIFU probe [SonablateTM, SonaCare Medical] could be used to adequately visualize peripheral VMs for HIFU ablation targeting and treatment monitoring. This effort also focused on addressing workflow-specific considerations pertinent to a future safety and efficacy study, such as: determining the difficulty of probe placement and probe/patient coupling, clinician's ability to align VM targets within the HIFU transducer focal zone, proximity of critical structures to the VM targets, and impact of patient motion on targeting accuracy and therapy delivery. Utilizing commercially available devices for this investigation has the advantage of drastically reducing the introduction time of this technology into clinical practice. This investigation was accomplished under an IRB-approved clinical pilot study in which 10 VM subjects were imaged with MRI, a commercial ultrasound imaging device (18-6MHz), and the HIFU probe. The resulting images and workflow questionnaires were then analyzed for their suitability in targeting and guiding the HIFU delivery for VM therapy.

Results: Subjects with peripheral VMs were imaged immediately prior to their embolization procedure. When using features of the pre-procedure MRI and ultrasound scanner images as markers, the VMs could be identified with the HIFU probe in all cases. Adjusting the volume of the water in the probe's coupling bolus allowed for positioning the VM target in the probe's focal zone from the skin surface up to a depth of 45 mm. Motion was deemed to minimally impact HIFU delivery only for VMs located on the patient's upper trunk, where breathing resulted in relative target/probe motion of up to 5 mm. Probe/patient coupling and probe focal zone/VM target alignment was deemed satisfactory for treatment in all observed cases, making ample use of the probe's articulated probe arm and stepping mechanism for gross and fine alignment, as needed.

Conclusions: Valuable insights on HIFU probe placement, patient coupling, workflow, and the effects of patient motion were obtained in this initial study. These encouraging results have demonstrated that the HIFU probe, its ultrasound imaging performance, and the device's treatment planning functionality could likely be extended to be used for the non-invasive treatment of VMs, paving the way for a follow-up study in which the safety and efficacy of the HIFU probe will be evaluated for VM ablation.

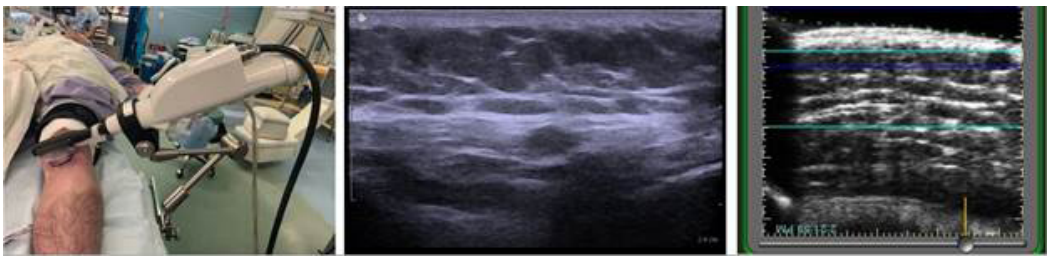

Figure 1. HIFU probe for VM imaging (left). VM image from a commercial ultrasound scanner (center). Equivalent image acquired with the HIFU probe (right), showing VM target placement in the probe's focal zone.

P-DRD-1

Topic: Drug Delivery
Presentation Type: Poster

Preclinical evaluation of a multifocused ultrasound therapeutic approach for improved microvascular permeabilization and drug delivery in breast cancer

Lokesh Basavarajappa, Girdhari Rijal, Kenneth Hoyt

University of Texas at Dallas, Richardson, TX, USA

Background: Focused ultrasound (FUS) exposure of microbubble (MB) contrast agents can transiently increase microvascular permeability allowing anticancer drugs to extravasate into the targeted tumor tissue. Either fixed or mechanically steered in space, most studies to date have used a single element focused transducer to deliver the ultrasound (US) energy. The goal of this study was to investigate various multi-FUS strategies (use of multi-focal zones) and assess impact on microvascular permeabilization and drug delivery using a preclinical murine model of breast cancer.

Materials and Methods: Various multi-FUS strategies (use of multi-focal zones) were implemented on a programmable US scanner (Vantage 256, Verasonics Inc) equipped with a linear array for image guidance and a 128-element therapy transducer (HIFUPlex-06, Sonic Concepts). The multi-FUS strategies included multi-FUS with sequential excitation (multi-FUS-SE) and multi-FUS with temporal sequential excitation (multi-FUS-TSE) and were compared with single-FUS and sham US therapies. Athymic nude mice were implanted with breast cancer cells (N = 20) and allowed to grow until about 6 to 8 mm in size. FUS therapy experiments were then performed for 10 min after a solution containing MBs (Definity, Lantheus Medical Imaging Inc) and near infrared (NIR) dye was injected via the tail vein (surrogate drug). Fluorescence was imaged in live animals using an optical imaging system (Pearl Trilogy, LI-COR) to quantify intratumoral dye accumulation at baseline and again at 0.1, 24, and 48 h after receiving US therapy. Animals were then euthanized for ex vivo dye extraction analysis.

Results: At 48 h, fluorescent tracer accumulation within the tumor space for the multi-FUS-TSE therapy group animals was found to be 67.3%, 50.3%, and 36.2% higher when compared to sham, single-FUS, and multi-FUS-SE therapy group measurements, respectively. Also, dye extraction and fluorescence measurements from excised tumor tissue found increases of 243.2%, 163.1%, and 68.1% for the multi-FUS-TSE group compared to sham, single-FUS, and multi-FUS-SE therapy group measures, respectively.

Conclusions: Preclinical findings were encouraging and revealed that for a multi-FUS sequence, increased microvascular permeability is considerably influenced by both spatial and temporal aspects of the US treatment plan.

P-DRD-2

Topic: Drug Delivery
Presentation Type: Poster

Ultrasound molecular imaging for the guidance of ultrasound triggered release of liposomal doxorubicin and its treatment monitoring in an orthotopic prostatic tumor model in rat

Alexandre Helbert[1], Philippe Bussat[1], Florence Séchaud[1], Matthew von Wronski[1], Emmanuel Gaud[1], Jean Louis Mestas[2], Samir Cherkaoui[1], Jean-Marc Hyvelin[1], Isabelle Tardy[1], Thierry Bettinger[1], Cyril Lafon[2], Frederic Padilla[3]

[1]Bracco Suisse SA, Plan-les-Ouates, Switzerland
[2]LabTAU INSERM U1032, Lyon, France
[3]Focused Ultrasound Foundation, Charlottesville, VA, USA

Background: The aims of this study were 1) to guide ultrasound triggered release of liposomal doxorubicin (L-DXR) by the mean of Ultrasound Molecular Imaging (USMI) with BR55, a targeted ultrasound contrast agent against the vascular growth factor receptor 2 (VEGFR-2), 2) to demonstrate the increased therapeutic efficacy of confocal ultrasound (USconfocal) combined with L-DXR versus L-DXR alone, and 3) to demonstrate the potential of USMI to monitor the response to the treatment in a orthotopic prostatic G Dunning rat tumor model.

Materials and Methods: Orthotopic tumors in Copenhagen rats were obtained by the injection of G Dunning R 3327 tumors cells in the left ventral lobe of the prostate. Home made sonosensitive [1,2-dierucoyl-sn-glycero-3-phosphocholine]-based liposomes encapsulating doxorubicin were produced, and their behavior was evaluated in blood, healthy prostate and tumor. USMI with BR55 was used to guide ultrasound triggered release of doxorubicin from liposomes accumulating in the tumor 48 h after injection. Local release was triggered using a dedicated confocal ultrasound device composed by two focused transducers (frequency 1.1 MHz) which delivers, at focus, peak positive and negative pressures of 20.5 MPa and 13 MPa, respectively. Tumor perfusion and VEGFR 2 expression in response to the treatment were evaluated by USMI with BR55 over a two-week period. Immunohistochemistry of CD31 and VEGFR 2 was performed on tumor and confocal microscopy was performed to visualize localization of doxorubicin after release.

Results: Home made sonosensitive liposomes have an extended circulation time in blood in comparison to free drug, with 8 % of initial dose of L-DXR still in circulation after 72 h versus only ~0.5 % after 24 h for the free DXR. A 9 fold increase drug accumulation was observed with the L-DXR in the tumor compared to healthy prostate. One week post-treatment, tumor size increased a 2.2-fold and 1.5-fold in the control and confocal ultrasound alone groups respectively. Tumor size remained unchanged in animal treated with free DXR, and decreased 3-fold in the DXR USconfocal group. Over a two-week period, the tumor size decreased by 20 % (compared to Day 0), and by 70% in the L-DXR + USconfocal groups ($P<0.01$).

USMI and immunohistochemistry did not show any substantial variation of perfusion and VEGFR 2 expression over 14 days. Confocal microscopy revealed a strong distribution of DXR in poorly perfused area at tumor periphery, and low DXR signal in the well perfused tumor core.

Conclusions: Ultrasound molecular imaging can provide precise guidance for ultrasound triggered release of liposomal doxorubicin mediated by a confocal ultrasound device. The combination of L-DXR with cavitational ultrasound treatment increases efficacy of doxorubicin, resulting in a significant reduction in tumor size compared to treatment with L DXR alone.

Treatment response monitoring can be performed by USMI with BR55 and can provide supplemental information to identify areas of the tumor that remained viable. USMI imaging did not reveal variations in terms of perfusion and late phase enhancement but allows accurate delineation of the tumor border. In addition, immunohistochemistry staining confirmed absence of VEGFR 2 expression variation.

P-DRD-3

Topic: Drug Delivery
Presentation Type: Poster

B-mode ultrasound-guided pulsed focused-ultrasound-mediated local gene therapy reduces neointimal hyperplasia restenosis after laser angioplasty of advanced atherosclerosis

Hossein Mehrad

Islamic Azad University, Tabriz, Iran

Background: Excessive intimal cell hyperplasia due to smooth muscle cell proliferation is the dominant cellular event in the restenosis process after laser angioplasty of advanced atherosclerotic severe stenosis. In this study, we developed an experimental pulsed- focused ultrasound local gene therapy (transfection therapy) system and investigated its effectiveness on neointimal hyperplasia reduction, wherein diagnostic ultrasound is combined with focused ultrasound, with a goal of increased safety.

Materials and Methods: Briefly, Golden Syrian hamsters were submitted to advanced atherosclerotic severe stenosis by primary intravascular radiofrequency (F= 23.7 MHz, P= 10 W) thermal balloon angioplasty- mediated endothelial injury at the abdominal aorta (approximately 0.5 cm superior to the iliac bifurcation) followed by a 1.5% cholesterol-rich diet injury for 12 weeks. Histopathology results showed the formation of advanced atherosclerotic plaque with foam cells- derived macrophages, smooth muscle cells and neovessels that resulted to severe stenosis (> 70%) in all of the hamsters´ arteries. Then treatment group underwent ArF excimer laser (193 nm) angioplasty followed by pulsed-focused ultrasound (F= 750 KHz, P= 15 W, PD= 200 ms) accompanied by intravenous Synthetic Antisense Oligodeoxynucleotides (ODN)- loaded PESDA (Perflurocarbon-Exposed Sonicated Dextrose Albumin) microbubbles (100ml/kg, 2-5 ×105 bubbles/ml) administration and simultaneously ultrasound imaging.

Results: Results from B-mode ultrasound imaging concurrent with ultrasound transfection therapy, showed the generation of inertial cavitation in the abdominal aorta. Also, histopathology results showed a significant reduction in the mean value for macrophages and smooth muscle cells density in the intimal layer of transfection therapy group compared with the other groups ($p< 0.05$).

Conclusions: Local gene therapy with Synthetic Antisense Oligodeoxynucleotides (ODN)-loaded PESDA microbubbles and inertial cavitation effect of microbubbles, induced by pulsed- focused ultrasound can cause to reduce the intimal macrophages and smooth muscle cells density and significantly dilate the luminal cross- sectional area. Ultrasound- mediated transfection therapy is a feasible and efficient method for the vascular neointimal hyperplasia reduction after laser angioplasty of advanced atherosclerotic plaque with severe stenosis.

P-DRD-4

Topic: Drug Delivery
Presentation Type: Poster

Local gene therapy with phosphomimetic endothelial nitric oxide synthase-loaded microbubbles-mediated B-mode ultrasound-guided dual-frequency sonication improves the artery endothelial dysfunction

Hossein Mehrad

Islamic Azad University, Tabriz, Iran

Background: Local gene therapy by ultrasound (transfection therapy) has enormous potential for the treatment of vascular disease. We developed an experimental transfection therapy protocol using dual-frequency focused ultrasound system and investigated its effectiveness on the endothelial dysfunction improvement.

Materials and Methods: Briefly, Golden Syrian hamsters underwent balloon dilatation injury at the abdominal aorta. Then arteries treated by dual- frequency focused ultrasound (I= 3w, F= 3MHz, PD= 30 ms and I= 30 W/cm2, F= 150 KHz, PD= 150 ms) accompanied by Phosphomimetic Endothelial Nitric Oxide Synthase- loaded PESDA (perfluorocarbon exposed sonicated dextrose albumin) microbubbles administration, wherein diagnostic ultrasound imaging system is combined with the therapy system, with a goal of increased safety. In order to evaluate endothelial-dependent relaxation, acetylcholinemediated dilation (AMD) was measured during the infusion of acetylcholine at a rate of 0.5 μg/kg/min and endothelial independent relaxation was evaluated by measuring nitroglycerin mediated dilation (NMD) during the infusion of nitroglycerin at a rate of 5 μg/kg/min.

Results: Results from ultrasonography showed significant differences in AMD between the treated and the non-treated rabbits ($p<0.05$), whereas there were no significant differences in NMD between the treatment and normal groups ($p>0.05$). Also, results from histopathology showed a significant reduction in the macrophages density within the lesion in the treatment group compared with the non-treatment group ($p<0.05$). No microscopic intimal lesions were seen in the normal and treated rabbits, but intimal thickening was observed in the histological studies in the non-treated hamsters.

Conclusions: Transfection therapy with dual- frequency focused ultrasound accompanied by Phosphomimetic Endothelial Nitric Oxide Synthase- loaded PESDA microbubbles administration resulted in significant enhancement of protein expression and nitric oxide synthesis. Ultrasound- mediated transfection therapy is a feasible and efficient method for the vascular endothelial dysfunction improvement.

P-DRD-6

Topic: Drug Delivery
Presentation Type: Poster

Effects of encapsulated gas in lipid-based microbubbles on brain-targeted drug delivery

Daiki Omata, Tamotsu Maruyama, Fumiko Hagiwara, Lisa Munakata, Saori Kageyama, Yuno Suzuki, Kazuo Maruyama, Ryo Suzuki

Teikyo University, Itabashi-ku, Japan

Background: The blood brain barrier (BBB) is a major obstacle to achieve an effective treatment for brain diseases, because most drugs cannot cross the BBB. Recently, the combination of ultrasound (US) and microbubbles (MBs) has attracted an attention for brain-targeted drug delivery by enhancing the permeability of BBB. US devices are important and have been developed to establish non-invasive and efficient brain-targeted drug delivery system. MBs also play an important role in BBB opening. Previous reports demonstrated that particle size and shell components of MBs affected the efficacy of brain-targeted drug delivery. However, the effect of encapsulated gas in MBs on brain-targeted drug delivery is not well evaluated. In this study, we prepared lipid-based microbubbles (LBs) containing perfluoropropane (C3F8), perfluorobutane (C4F10) or sulfur hexafluoride (SF6) with same phospholipid shell (LB-C3F8, LB-C4F10 or LB-SF6) and examined the effects of each LBs on brain-targeted drug delivery.

Materials and Methods: Preparation of LBs: Liposomes composed of 1,2-distearoyl-sn-glycero-phosphocholine (DSPC), 1,2-distearoyl-sn-glycero-phosphoglycerol (DSPG) and N-(carbony-methoxypolyethyleneglycol 2000)-1,2-distearoyl-sn-glycero-3-phosphoethanol amine (DSPE-PEG2000) were prepared by lipid hydration method (DSPC: DSPG: DSPE-PEG2000 = 30: 60: 10, molar ratio). A homogenizer was inserted into a tube containing liposomes, and the head space was replaced with each gas. The liposomes and gases were mixed using the homogenizer at 15,000 rpm for 5 min. The number and size of LBs were measured using coulter counter.

Brain-targeted drug delivery: The mixture of evans blue (EB) (100 mg/kg), as a model drug, and LBs (3×109 particles/kg) was injected into mice. Immediately, non-focused US (Frequency: 3 MHz, Intensity: 0.5 W/cm2, Duty: 50%, Pulse repetition frequency: 10 Hz, Time: 3 min) was applied to the right side of brain. After 1 h, mouse was perfused, and the brain was collected. The EB transferred to the brain was observed and determined.

Results: The average sizes of each gas loaded LBs were approximately 2.5 μm. Therefore, in this study, the effect of size of LBs on brain-targeted drug delivery would be excluded. To evaluate the effect of gas in LBs on brain-targeted drug delivery, we examined the EB delivery efficacy to the brain using different gas loaded LBs and US. When LB-C3F8 and LB-C4F10 were administrated, EB was distributed in wide area of the brain compared with LB-SF6. Furthermore, we extracted and determined the EB contents in each side of the brain. As a result, the treatment of LB-C3F8 and LB-C4F10 with US showed significantly higher EB contents in the right side of brain, which is exposed to US, compared with the left side. Otherwise, the combination of LB-SF6 and US did not significantly increase EB contents in the right side of brain. These results suggested that MBs containing C3F8 or C4F10 would efficiently deliver drugs into the brain.

Conclusions: We prepared LB-C4F10, LB-C3F8 and LB-SF6 with identical outer shell and similar size and demonstrated that LB-C3F8 and LB-C4F10 could efficiently deliver EB into the brain with US. Our results suggested that C3F8 and C4F10 would be useful for developing MBs to achieve efficient brain-targeted drug delivery.

Acknowledgements: This study was partially supported by JSPS KAKENHI Grant Number 19K20717 and 17H07119. Traveling expenses was supported by The Research Foundation for Pharmaceutical Sciences.

P-DRD-8

Topic: Drug Delivery
Presentation Type: Poster

Localized mild hyperthermia using MRI guided high intensity focused ultrasound in tumour-bearing mice for potential cancer therapies

Maryam Siddiqui[1], Donna Senger[1], Ngoc Ha Dang[1], Jennifer King[1], Jennifer Rahn[1], Tadeusz Foniok[1], David Rushforth[1], Stephen Robbins[1], Warren Foltz[2], Benjamin Keunen[3], Karolina Piorkowska[4], Michael Dunne[2], Adam. C. Waspe[4], Christine Allen[2], Samuel Pichardo[1]

[1]University of Calgary, Calgary, Canada
[2]University of Toronto, Toronto, ON, Canada
[3]SickKids, Palmerston, ON, Canada
[4]The Hospital for Sick Children, Toronto, ON, Canada

Background: Alveolar soft part sarcoma (ASPS) is a rare type of soft tissue sarcoma. Tumour resection is not possible in 45% of patients, requiring treatment alternatives. MRI guided Focused Ultrasound (MR-FUS) concentrates mechanical energy in a small volume of tissue and can induce localized hyperthermia (temperature is raised to about 42-43°C for a prolonged period). MRI allows monitoring of temperature changes non-invasively and in real-time. ThermoDox is a thermosensitive liposomal encapsulated formulation of Doxorubicin (a common chemotherapy drug used in a variety of cancers) that only releases its content in heated regions. The drug is released at temperatures greater than 41.5°C. Combining the induction of MR-FUS-based localized hyperthermia with the administration of ThermoDox can enhance targeted drug delivery to ASPS tumours as drug is only released at the tumour site, and healthy tissue are protected from drug toxicity.

Materials and Methods: We performed first a pilot study where we delivered hyperthermia in healthy mice (C57BL, n=19), heating the leg muscle (42.5°C for 30 minutes) using a small-animal MR-FUS device (IGT, Bordeaux, France) with a transducer operating at 2.5MHz. We conducted treatment-planning and thermal therapy using our in-house software Proteus. We collected FLASH T1-weighted images throughout the procedure plus 8 minutes post-heating, and T2-weighted images before and after heating to check for tissue damage. Post-procedure, we immediately euthanized the mice. In a second ongoing study, we performed hyperthermia treatment in tumour-bearing CB17 SCID mice. We injected the mice with ASPS cells from a human cell line (SM3762), subcutaneously in the flank of the mouse. We monitored tumour growth and when the tumours reached a size of about 7mm, we placed them into one of four groups (n=5 per group): hyperthermia plus encapsulated drug, hyperthermia plus free drug, no hyperthermia plus encapsulated drug and no hyperthermia plus free drug. We placed a piece of chicken on the skin to increase distance from the transducer. We heated tumours for 10 minutes using the same parameters as before and collected FLASH and T2-weighted images. When the temperature stabilized at 42.5°C, we infused drug (dose: 5mg/kg) through the tail vein. Post-treatment, we euthanized the mice and performed blood perfusion. We resected the tumour and major organs and froze them at -80°C for drug analysis.

Results: For the pilot study, temperature maps showed controlled heating that was mainly limited to the target region on the muscle. Time-temperature plots showed a stable average temperature maintained throughout the treatment. Repeatability of these results were shown in 7 animals (heating duration: ≥17 minutes, average temperature: 42.5±3°C) with no tissue damage. For the tumour study, 12 mice underwent hyperthermia treatment: 5 from the hyperthermia plus encapsulated drug group, 5 from the hyperthermia plus free drug group, one that was a control mouse and was only injected with saline, and one extra mouse that had to be added to the hyperthermia plus encapsulated drug group due to the drug not get fully injected in one of the mice. For 9 out of 12 mice, the average temperature was maintained throughout the treatment (average temperature: 42.5±3 °C). 4 out of 12 mice were treated with no damage. However, 4 got a skin burn and in 5 mice edema was evident in T2W imaging.

Conclusions: Hyperthermia can be established in precise locations in the body using MR-FUS in a non-invasive manner. The temperature is well-maintained and homogenous in the region of interest. The position of the target is important to ensure safe delivery of hyperthermia. Targets that are close to bones or the skin make it difficult to induce hyperthermia without causing damage. Therefore, although MR-FUS is very good at maintaining hyperthermia in precise locations, the position of the tumour in CB17 SCID mice must be carefully planned. Coupling localized hyperthermia with chemotherapy using

temperature-sensitive drug-carriers demonstrates a therapy for cancer treatment that is non-invasive and can potentially improve targeted drug-delivery.

Acknowledgements: Canadian Institutes of Health Research

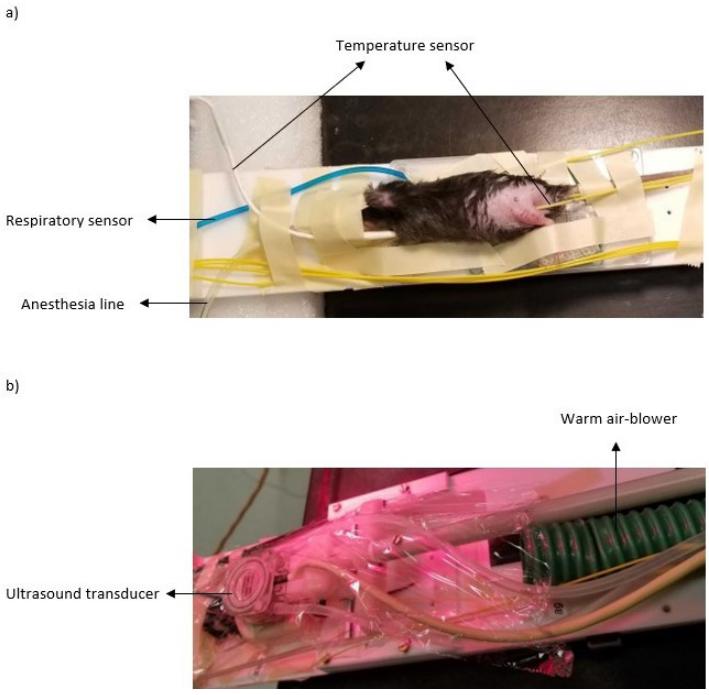

Figure 1. a) Mouse positioned on HIFU bed with sensors attached for monitoring vitals b) Final set-up showing transducer placed on the mouse and an air-blower to keep the mouse warm during treatment.

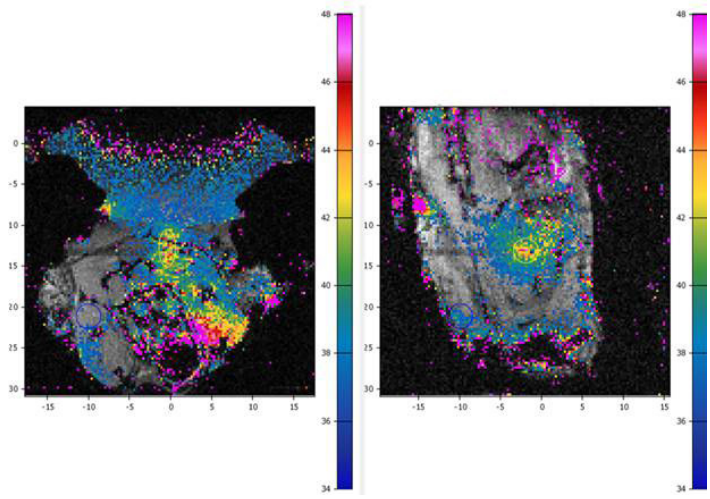

Figure 2. MRI images showing thermal map of heating in axial (left) and coronal (right) planes of imaging. The yellow ellipse and the yellow circle represent the region of interest for heating.

P-DRD-9

Topic: Drug Delivery
Presentation Type: Poster

Perfusion-guided sonopermeation of neuroblastoma: A novel strategy for monitoring and predicting liposomal doxorubicin uptake in vivo

Aditi Bellary[1], Arelly Villarreal[1], Rojin Eslami[1], Quincy J. Undseth[1], Bianca Lec[2], Ann M. Defnet[2], Naina Bagrodia[2], Jessica J. Kandel[2], Mark A. Borden[3], Sumbul Shaikh[4], Rajiv Chopra[4], Theodore W. Laetsch[5], Lauren J. Delaney[6], Colette M. Shaw[6], John R. Eisenbrey[6], Sonia L. Hernandez[2], Shashank R. Sirsi[1,4]

[1]University of Texas at Dallas, Richardson, TX, USA
[2]University of Chicago Medical School, Chicago, IL, USA
[3]University of Colorado, Boulder, CO, USA
[4]University of Texas Southwestern Medical Center, Dallas, TX, USA
[5]Harold C. Simmons Comprehensive Cancer Center, University of Texas Southwestern Medical Center and Children's Health, Dallas, TX, USA
[6]Thomas Jefferson University, Philadelphia, PA, USA

Background: Neuroblastoma (NB) is the most common extracranial solid tumor in infants and children, and imposes significant morbidity and mortality in this population. The aggressive chemoradiotherapy required to treat high-risk NB results in survival of less than 50%, yet is associated with significant long-term adverse effects in survivors. Over the last two decades, Image-guided drug delivery (IGDD) using focused ultrasound with "microbubble" ultrasound contrast agents (UCAs) is an increasingly popular method of targeting a wide variety of diseases, including cancer. This technique, known as sonopermeation, mechanically augments vascular permeability, enabling increased penetration of drugs into target tissue. However, to date, methods of monitoring the vascular bioeffects of sonopermeation in vivo are lacking. In this study, we assess tumor vasculature changes associated with sonopermeation and describe how they can be used to evaluate and predict drug uptake and response to therapy.

Materials and Methods: To monitor the therapeutic efficacy of sonopermeation in vivo, we developed a novel system using 2D and 3D quantitative contrast-enhanced ultrasound imaging (qCEUS). 3D tumor volume and contrast enhancement was used to evaluate changes in blood volume during sonopermeation. 2D qCEUS-derived time-intensity curves (TICs), were used to assess reperfusion rates following sonopermeation therapy. Intratumoral doxorubicin (and liposome) uptake in NB was evalauted ex vivo along with associated vascular changes. After gauging initial perfusion, matrigel plugs were sonopermeated using a therapeutic ultrasound machine at 3 W/cm2 (1 MHz, 10% duty cycle) for 10 minutes with a high dose of microbubbles (1x109 MBs) mixed with 25 mg/kg L-DOX. Tumors (along with liver, contralateral kidney, and heart) were excised to assess drug uptake using an acidified isopropanol extraction to recover doxorubicin. The doxorubicin was quantified with a fluorescent plate reader. Ex vivo analysis of tumor tissue was used to evaluate associated vascular changes at 30 minutes and 24 hours.

Results: In the course of this study, we show that contrast-enhanced focused ultrasound therapy can effectively promote nanoparticle uptake in experimental neuroblastoma by ~5-fold, and that qCEUS imaging can function as an effective predictor of sonopermeation efficiency in vivo. Changes in reperfusion rates immediately after sonopermeation increased by ~2-fold when using tumor-free Matrigel plug models, but decreased by ~2-fold when using neuroblastoma tumor models. Changes in total perfusion volume did not fluctuate significantly in either Matrigel plugs or neuroblastoma xenografts following sonopermeation. Although overall perfusion did not change significantly from pre- to post-treatment, we show that initial tumor perfusion can be a critical determinant of total chemotherapeutic uptake. Our results indicate that liposomal doxorubicin can effectively be delivered using focused ultrasound and microbubbles without significant vascular damage.

Conclusions: Our results suggest that significant L-DOX uptake can occur by increasing tumor vascular permeability with microbubble sonopermeation without otherwise damaging the vasculature, as confirmed by in vivo qCEUS imaging and ex vivo analysis. The use of qCEUS imaging to monitor sonopermeation efficiency and predict drug uptake could potentially provide real-time feedback to clinicians for determining treatment efficacy in tumors, leading to better and more efficient personalized therapies. Finally, we demonstrate how the IGDD strategy outlined in this study could be implemented in human patients using

a single case study.

Acknowledgements: The work performed in this study has been supported by the National Institute of Health through the NIBIB and NCI (R21EB015040, R01CA232154, R01CA238241, and 1R01CA199937), as well as the Pediatric Cancer Foundation.

P-DRD-10

Topic: Drug Delivery
Presentation Type: Poster

Development of effective drug delivery system by the combination of liposome-loaded microbubble and ultrasound

Yuno Suzuki, Daiki Omata, Lisa Munakata, Saori Kageyama, Fumiko Hagiwara, Tamotsu Maruyama, Kazuo Maruyama, Ryo Suzuki

Teikyo University, Itabashi-ku, Japan

Background: Anticancer drug-encapsulated liposomes have been approved for cancer therapy. However, the most of liposomal drugs have not provided enough therapeutic effects. Therefore, it is necessary to develop a novel drug delivery system. It is reported that the mechanical effect by the cavitation of microbubbles (MBs) under ultrasound field loose the tight-junction between endothelial cells. In tumor tissue, it is expected that this mechanical effect could enhance liposomal drugs accumulation into the tumor tissue. To achieve the efficient liposomal drugs delivery, it is important that the liposomes are loaded on MBs. The liposomes-loaded MBs is expected to deliver drugs actively because of the release of liposomes from MBs and the blood vessels opening in tumor. In this study, we prepared the doxorubicin encapsulated liposomes-loaded microbubbles (D-Lipo-MB) and assessed the feasibility of active drug delivery by the combination of D-Lipo-MB and ultrasound for pancreatic cancer therapy.

Materials and Methods: Lipid suspension (DSPC:PEG40-monostearate:DSPE-PEG(2k)-biotin = 90:10:1 in molar ratio) was put into a vial. The air in head space of the vial was replaced with perfluorobutane gas. Then, the vial was vigorously shaken with VIALMIX® to form MBs. The MBs were incubated with avidin to make avidin modified MB. To prepare D-Lipo-MB, avidin modified MB and biotinylated D-Lipo (DPPC: Cholesterol: DSPE-PEG(2k)-biotin = 55: 40: 5 in molar ratio) were mixed. To confirm D-Lipo loading on MBs, the D-Lipo-MB was observed with a fluorescence microscope. In the drug delivery experiments, D-Lipo-MB was added to pancreatic cancer cells (PAN02). Immediately, ultrasound (Frequency; 1 MHz, Intensity; 0.5 W/cm2, probe diameter; 6 mm, Exposure time; 10 sec, Duty; 50%) was exposed to D-Lipo-MB and cells. After incubation for 1 day, the cell viability was assessed with MTT assay. Furthermore, intracellular doxorubicin at 4 hours after the treatment was observed with confocal laser scanning microscope.

Results: D-Lipo-MB was observed with a fluorescence microscope to confirm whether D-Lipo was loaded on MBs. The doxorubicin-derived fluorescence was detected on the MB surface. This result suggested that D-Lipo was loaded on MBs. In addition, we observed intracellular doxorubicin after treatment of D-Lipo-MB with or without ultrasound. Intracellular doxorubicin in the treatment of D-Lipo-MB with ultrasound was significantly higher than that without ultrasound. To assess the cancer cell growth suppression with this delivery system, we examined the cell viability after the treatment. The cell viability did not reduce in the treatment of D-Lipo-MB or Lipo-MB (without doxorubicin). On the other hand, the cell viability significantly reduced in the combination of D-Lipo-MB and ultrasound. From these results, it was thought that the ultrasound triggered liposome-release from MBs was induced and resulted in delivering doxorubicin into cancer cells.

Conclusions: We succeeded to prepare D-Lipo-MB to be able to enhance the drug delivery efficiency for cancer cells with ultrasound. Our D-Lipo-MB could effectively deliver doxorubicin into cytosol of pancreatic cancer cells by the combination of ultrasound. Accordingly, the cancer cell growth was effectively suppressed. Therefore, it is expected that the combination of D-Lipo-MB and ultrasound would be an effective anticancer drug delivery system for pancreatic cancer therapy.

Acknowledgements: This study was partially supported by JSPS KAKENHI Grant Number JP17K19501.

P-DRD-11

Topic: Drug Delivery
Presentation Type: Poster

Effect of lipid composition on the stability of microbubbles

Tamotsu Maruyama, Daiki Omata, Lisa Munakata, Saori Kageyama, Fumiko Hagiwara, Yuno Suzuki, Kazuo Maruyama, Ryo Suzuki

Teikyo University, Itabashi-ku, Japan

Background: The combination of microbubbles (MBs) and ultrasound (US) is a promising technology for non-invasive and efficient diagnostic and therapeutic system. The behaver of MBs such as oscillation and collapse under the US field can be applied for US imaging, drug delivery and ablation therapy. However, MBs usually have the short lifetime as blood flow US imaging agent, and it could be one limitation for efficient diagnosis and therapy. The lifetime of MBs relies on components such as the shell and the encapsulated gas. The shell in the most of MBs was frequently constructed with lipids. Thus, the lipid composition of MBs as shell should be optimized to be stable. To improve the stability of MBs, we referred to enhance the membrane stability of liposomes by using 1,2-distearoyl-sn-glycero-3-phosphoglycerol (DSPG). In this study, we prepared the lipid-based microbubbles (LMBs) composed with DSPG at different ratios and assessed the effect of lipid composition on the stability of LMBs in vivo.

Materials and Methods: Preparation of LMBs: Liposomes composed of 1,2-distearoyl-sn-glycero-phosphocholine (DSPC), DSPG and 1,2-distearoyl-sn-glycero-3-phosphoethanolamine-N-[methoxy (polyethylene glycol)-2000] (DSPE-PEG2k) were prepared by lipid hydration method (DSPC: DSPG: DSPE-PEG2k = 90: 0: 10, 60: 30: 10, 45: 45: 10, 30: 60: 10, and 0: 90: 10, molar ratio). A homogenizer was inserted into a tube containing liposome suspension, and the head space was replaced with perfluoropropane. The liposomes and perfluoropropane were mixed with the homogenizer at 15,000 rpm for 5 minutes. The average diameter of LMBs was measured with coulter counter.

In vivo assay for LMBs stability: LMBs at various DSPG molar ratio, Sonazoid, or SonoVue were intravenously injected into the mice under isoflurane anesthesia. To assess the stability of LMBs, we evaluated the lifetime of LMBs as US imaging agent in blood flow. The blood flow in the kidneys was observed under the contrast mode of ultrasonography. The contrast images were analyzed to obtain signal intensity using ImageJ software.

Evaluation of biodistribution: DiR-labeled LMBs or Sonazoid were intravenously injected into mice. The distribution of DiR-labeled LMBs was observed with in vivo imaging system at each time point. The fluorescence signal intensity in the liver was quantified, and the average value of fluorescence in the area showing the intensity from the maximum to 35% was measured.

Results: The average diameter of LMBs at various DSPG molar ratios was approximately 2.5 μm, while Sonazoid and SonoVue were a little bigger than LMBs. We examined the stability of LMBs in blood flow at various lipid compositions. LMBs with 60% of DSPG (DSPG60-LMBs) had sustained lifetime in blood flow compared with LMBs at other DSPG ratios. In addition, DSPG60-LMBs had long lifetime in blood flow compared with Sonazoid and SonoVue. Next, we evaluated the biodistribution of DSPG60-LMBs and Sonazoid. Sonazoid was distributed to the liver at 15 minutes after injection. On the other hand, LMBs was lower distribution in the liver at 30 minutes after injection. Thus, DSPG60-LMBs showed less distribution to the liver compared with Sonazoid. These results suggested that adding DSPG would enhance stability in blood flow.

Conclusions: We succeeded the development of LMBs with high stability in blood flow. Adding DSPG to the shell increased the stability of the LMBs, and DSPG60-LMBs prolonged the lifetime in blood flow compared with Sonazoid and SonoVue. In addition, DSPG60-LMBs had lower distribution in the liver compared with Sonazoid. It is suggested that DSPG60-LMBs could escape to be uptaken by the liver. Thus, DSPG60-LMBs would be applicable for development of an effective US diagnostic and therapeutic system.

Acknowledgements: This study was partially supported by NEXT-Support Program for the Strategic Research Foundation at Private Universities, 2013-2017. Grant Number SI1311015 and JSPS KAKENHI Grant Number JP16H03196 and JP17K19501.

P-EPI-1

Topic: Epilepsy
Presentation Type: Poster

Ultrasound mediated ionic modulation in the brain

John Cressman, Monica Gertz, Parag Chitnis

George Mason University, Fairfax, VA, USA

Background: Focused ultrasound stimulation (FUS) for non-invasive neuronal modulation offers greater resolution and penetration than other current stimulation methods, making it an attractive platform both in basic research and clinically. The diverse set of effects attributed to ultrasonic stimulation are most likely due to a variety of underlying mechanisms. Here we utilize a computational model of neuronal tissue that accounts for the body force produced by acoustic radiation. The model reproduces experimental results and provides a detailed explanation of the mechanisms of action.

Materials and Methods: Acute rat hippocampal slices were stimulated in the CA1 region using a 35MHz focused ultrasound transducer at varying intervals, with stimulation durations ranging from 0.1 - 2 s. We used oxygen- and potassium-sensitive electrodes to measure the metabolic demands of FUS as compared to electrical stimulation.

The computational model includes dynamics for acoustic radiation force induced changes on the extracellular volume in a slab of neuronal tissue composed of neuronal and glial cells. Neuronal and glial compartments were modeled with Hodgkin-Huxley conductances and Nernst-based reversal potentials. A number of other mechanisms including co-tranporters, ion pumps, tortuosity, and diffusion are also included to replicate the behavior seen in experiments.

Results: Experimental slice experiments demonstrate that FUS can produce large increases in the extracellular potassium concentration. Increases exceeding 50 mM were observed, however, they were only sustained for a few seconds returning to baseline within ten seconds. The rapid return to baseline is not indicative of the prolonged seizure discharges or spreading depression one might expected in the presence of such highly elevated extracellular potassium.

Although the accompanying increase in oxygen consumption is significant, it is small compared to the increase induced by electrical stimulation resulting in similar potassium changes.

The model is able to reproduce large transient responses in the extracellular potassium concentration in response to the FUS mediated acoustic radiation force. The model also produces a modest concomitant oxygen response.

Conclusions: The weak metabolic response to the large potassium extrusions produced by FUS can be understood through our model as due to an interplay between volume dynamics and osmotic effects produced by mobile and immobile extracellular ions. The model demonstrates that the main flux of concentration altering mobile ions is due to transmembrane currents. Though transient, these dramatic ionic shifts can elicit strong control over neuronal excitability. A better understanding of these effects will lead to more precise and effective applications for FUS to modulate neuronal activity.

Acknowledgements: NSF-GRFP

P-IMM-2

Topic: Immuno-oncology
Presentation Type: Poster

Development of effective cancer therapy by the combination of sonotherapy and immunotherapy

Ryo Suzuki, Lisa Munakata, Daiki Omata, Tamotsu Maruyama, Yuno Suzuki, Saori Kageyama, Fumiko Hagiwara, Kazuo Maruyama

Teikyo University, Itabashi, Japan

Background: Microbubbles have various behaviors under ultrasound field such as oscillation and inertial cavitation. This inertial cavitation can directly induce the damage of tumor cells, it would be applied for cancer therapy. Actually, we showed that the combination of the intratumoral injection of microbubbles and ultrasound exposure significantly suppressed the tumor growth. In this therapy, we reported that the cellular immunity mainly contributed to the tumor growth suppression. This immune response would be induced by the release of tumor associated antigens from the damaged tumor cells. Therefore, we thought that the injection of dendritic cells (DCs) into the damaged tumor tissue would effectively prime the anti-tumor immune response and result in the enhancement of tumor growth suppression. In this study, we examined the enhancement of anti-tumor effect by the combination of microbubble mediated sonotherapy and DC-based immunotherapy.

Materials and Methods: We assessed the DC maturation by tumor cell damaged with microbubbles and ultrasound (1 MHz, 4 W/cm2, 2 min). The conditioned media of Colon-26 cells treated with microbubble and ultrasound was added to immature DCs. After 48 hr, the expression of maturation markers (CD40/80/86) on the DCs were measured with flowcytometory. In the experiment of tumor growth suppression, we utilized the Colon-26 cells (mouse colon carcinoma) inoculated mice. After 8 days of tumor cell inoculation, microbubbles were intratumorally injected and ultrasound was transdermally exposed toward tumor tissue. Immatured DCs were intratumorally immunized on days 9, 10, 11, and 13 after tumor inoculation. The anti-tumor effect was evaluated by measuring tumor volume.

Results: In the DCs incubated with the conditioned media of Colon-26 cells treated with microbubble and ultrasound, the expression of CD40/80/86 which were maturation markers significantly increased. The upregulation of these molecules was similar to the DCs (positive control) treated with lipopolysaccharide which could induce the DC maturation via toll-like receptor 4. This result suggested that the combination of microbubble and ultrasound treatment would directly damage the tumor cells and result in inducing the DC maturation. Thus, we examined the enhancement of anti-tumor effect by the combination of sonotherapy and DC-based immunotherapy. Neither ultrasound therapy with microbubbles nor DC-based immunotherapy had significant anti-tumor effect. On the other hand, the combination of ultrasound therapy with microbubbles and DC-based immunotherapy efficiently suppressed tumor growth.

Conclusions: It seems that microbubble mediated sonotherapy would induce the immunomodulation in tumor tissue. Then, it was thought that DC-based immunotherapy could enhance the antitumor effect after the sonotherapy. Therefore, the combination of microbubble mediated sonotherapy and DC-based immunotherapy would be a useful strategy for cancer therapy.

Acknowledgements: This study was partially supported by JSPS KAKENHI Grant Number JP 21700511 and JP 20H04519.

P-MIS-1

Topic: Miscellaneous Indications
Presentation Type: Poster

Characterization of intracellular calcium dynamics during pulsed focused ultrasound (pFUS) sonication: Implications for regenerative medicine and stem cell therapies

Rebecca Lorsung, Robert Rosenblatt, Gadi Cohen, Joseph Frank, Scott Burks

National Institutes of Health, Bethesda, MD, USA

Background: Non-ablative pulsed focused ultrasound (pFUS) enhances stem cell homing to muscle and kidneys through NFkB-dependent production of cytokines, chemokines, trophic factors (CCTF) and cell adhesion molecules (CAM). pFUS activates mechanosensitive plasma membrane TRPC1 channels whose currents activate voltage-gated calcium channels (VGCC) to generate cytosolic calcium transients. However, the intracellular calcium dynamics (release from intracellular stores, extrusion from the cytosol, and refilling of stores) that ultimately lead to NFkB activation remain unknown. This study characterizes intracellular calcium dynamics during pFUS sonication and their effects on downstream NFkB activation.

Materials and Methods: TCMK1 kidney cells were transfected with an NFkB-GFP reporter and treated in vitro with pFUS (1 MHz, 3 MPa peak-negative-pressure, 100 pulses at 10% duty cycle and 10 pulses/s). Cells received pFUS alone or pFUS in combination with pharmacological inhibitors or genetic knockdowns. Genetic knockdown lines were transfected with specific shRNA sequences while control cells were transfected with a scrambled sequence.

Results: pFUS increased cytosolic calcium and NFkB activation in naïve TCMK1 cells. Inhibiting TRPC1 or VGCC blocks calcium transients and prevents NFkB activation. Depleting endoplasmic reticulum (ER) calcium with thapsigargin inhibited pFUS-induced calcium flux and NFkB activation. Furthermore, blocking ryanodine receptors (RyR) with ryanodine, phospholiase C (PLC) with U-73122, or IP3 receptors with shRNA inhibited cytosolic calcium transients and NFkB. Knockdown of ORAI1 slightly decreased cytosolic calcium and NFkB, while knockdown of cytosolic calcium extruding mechanisms (plasma-membrane-calcium-ATPase or sodium/calcium exchangers) slightly increased NFkB.

Conclusions: pFUS activates NFkB through cytosolic calcium transients that rely on extracellular calcium entry which initiates endoplasmic reticulum (ER) calcium release through both calcium-induced-calcium-release (via RyR) and IP3 signaling following PLC activation. Cytosolic calcium extrusion mechanisms are necessary to modulate appropriate NFkB activation levels, while data suggest store-operated channels (ORAI1/STIM1) play a negligible role initially, but could be necessary if biological effects were increased by multiple pFUS treatments. These data provide insight into calcium-handling dynamics that generate CCTF and CAM necessary for pFUS-induced stem cell homing.

Acknowledgements: Intramural Research Program at the National Institutes of Health Clinical Center

P-MIS-2

Topic: Miscellaneous Indications

Presentation Type: Poster

Pediatric applications of focused ultrasound

Rohan Janwadkar[1], Suzanne LeBlang[2]

[1]Florida Atlantic University, Charles E. Schmidt College of Medicine, Boca Raton, FL, USA
[2]Focused Ultrasound Foundation, Charlottesville, VA, USA

Background: Focused ultrasound (FUS) is a non-invasive therapeutic technology that uses ultrasonic energy via an external transducer to precisely target tissues deep in the body without any incisions or radiation, making it especially advantageous in the pediatric population. Focused ultrasound treatments can also be performed on an outpatient basis with minimal discomfort and fewer complications due to the absence of incisions, allowing for rapid recovery. There are currently over 131 clinical indications for the use of focused ultrasound at various stages of development, most of which are for adult populations. However, similar to many novel therapeutics, investigations of this technology in pediatric populations trails behind. According to the Focused Ultrasound Foundation State of the Field Report 2019, there were 3 pediatric indications in 2012, 9 in 2017 and 14 in 2018. The purpose of this study is to review the current status of focused ultrasound treatments in the pediatric population.

Materials and Methods: A literature review was conducted to identify English language studies as of January 2015, using combinations of the following search terms: 'pediatric,' 'focused

ultrasound,' 'treatment,' and 'high intensity focused ultrasound.' In addition to these 20 articles, examination of reference lists of these studies uncovered additional studies. Studies were evaluated if the patients/subjects being treated were pediatric patients (age 0-18 years) with some adult patients (>18 years) being included in relevant studies regarding focused ultrasound treatment of typical pediatric age diseases. In order to understand the mechanisms of action of focused ultrasound applications in pediatric patients, preclinical studies were included as well. The various diseases were separated into the following major categories: musculoskeletal (MSK), cardiovascular, hematologic-oncologic, and neurological applications. A summary of the existing FUS literature for each specific disease within each category will be provided along with case examples.

Results: Focused ultrasound treatment was found to be feasible, safe, and effective in pediatric patients across many specialties. Pediatric MSK applications of FUS utilize thermal ablation and high intensity focused ultrasound (HIFU) to treat osteoid osteoma, desmoid tumors, bone metastases, and sacral chordomas. Pediatric cardiovascular applications of FUS utilize ablation and vascular occlusion to treat arteriovenous malformations and twin-twin transfusion syndrome via Pediatric hematologic-oncologic applications of FUS utilize ablation and targeted delivery of chemotherapies and immunotherapies to treat sarcomas and neuroblastomas. Pediatric neurological applications of FUS include treatment of intracranial tumors and epilepsy via ablation with HIFU of targets such as hypothalamic hamartomas, or neuromodulation with low intensity focused ultrasound in the hippocampus. Future clinical trials will study targeted drug delivery with blood brain barrier opening for diffuse intrapontine gliomas.

Conclusions: Focused ultrasound therapy in pediatric patients provides a unique advantageous therapeutic platform with no radiation exposure and no incisions. A variety of mechanisms of action allow applications across different diseases and various medical and surgical specialties. In addition to thermal ablation and neuromodulation, clinical trials will further explore the ability of FUS to enhance targeted drug delivery with a variety of chemo- and immunotherapies to improve the quality of life and overall survival for children suffering from malignancies.

P-MIS-3

Topic: Miscellaneous Indications

Presentation Type: Poster

Development of a pair of turnkey platforms for 3D ultrasound-guided focused ultrasound (USgFUS) therapy in preclinical research

Peter Kaczkowski[1], Jon Daigle[1], Kyle Morrison[2]

[1]Verasonics, Inc., Kirkland, WA, USA
[2]Sonic Concepts, Inc., Bothell, WA, USA

Background: In 2017, Verasonics (Kirkland, WA, USA) and Sonic Concepts (Bothell, WA, USA) launched a new product line [HIFUPlex™] that combined a pair of ultrasound transducers (a high power and efficient FUS array combined with a coaxially mounted imaging array) to the Vantage ultrasound system with custom software for ultrasound-guided focused ultrasound therapy (USgFUS) applications. These six pairings offer f1 HIFU transducers operating at 0.5, 1.1, and 2.0 MHz in two different sizes suitable for working with small and large subjects in preclinical research (Fig 1). Capable of a wide range of acoustic regimes including imaging, mild hyperthermia, thermal ablation and boiling histotripsy, the HIFUPlex pairings provide an effective solution to the challenge of assembling a USgFUS experimental capability. To complete the system and provide a truly turnkey platform [HIFUPlex PLUS™], the companies collaborated with the FUS Foundation to add required elements.

Materials and Methods: The small animal configuration (Fig 2) has the transducer assembly mounted in an upward-facing configuration, coupled through water and membrane to a bath. The transducer assembly is rigidly mounted to an X-Y (horizontal) motion stage below, and the annular array provides displacement of the focal zone in the Z (vertical) direction. The imaging array can be rotated with respect to the frame by a gear-coupled motor for a 3D view composed of a sequence of 2D planes. Centering of the applicator is done under image guidance, followed by a rotary scan of the region of interest.

In the large animal configuration (Fig 3), the transducer applicator includes a 2D HIFU array and is mounted on an articulated arm with a distal hinged and ball jointed segment that is servo-locked via manual actuation of electrical switches (buttons) on the handle. Pressing and holding the buttons unlocks the friction arm and permits freely moving the applicator to the region of interest and, under image guidance, optimizing coupling and imaging of the target zone; releasing the buttons locks the arm and freezes the applicator in position. The equipment cart contains the ultrasound system and the water conditioning unit (WCU) which provides temperature controlled degassed water to the transducer applicator for both the large and the small configurations.

The software enables key elements of an experimental workflow via a graphical interface.

Figure 1. Table of HIFUPlex™ Transducer pairings.

Standard HIFUPlex transducer bundles

Verasonics® The leader in Research Ultrasound™ SONIC CONCEPTS

1D USgFUS

Solutions for small animal and intermediate target applications, featuring adjustable FUS focal depth and 2D imaging

HIFUPlex Transducer Bundles	-01	-02	-03
Includes	FUS Array Imaging Array Cone & Target	FUS Array Imaging Array Cone & Target	FUS Array Imaging Array Cone & Target
FUS Array			
Frequency (MHz)	0.5	1.1	2.0
Type	Annular Array	Annular Array	Annular Array
Axial Steering	50mm	50mm	50mm
Imaging Array			
Type	Phased Array	Phased Array	Phased Array
Frequency (MHz)	5.0	5.0	5.0
# of Elements	64	64	64
Compatibility	Vantage 64 LE, 128 & 256 HIFU	Vantage 64 LE, 128 & 256 HIFU	Vantage 64 LE, 128 & 256 HIFU

3D USgFUS

Solutions for large animal and deep target applications, featuring 3D FUS focal positioning and 2D imaging

HIFUPlex Transducer Bundles	-04	-05	-06
Includes	FUS Array Imaging Array Cone & Target	FUS Array Imaging Array Cone & Target	FUS Array Imaging Array Cone & Target
FUS Array			
Frequency (MHz)	0.5	1.1	2.0
# of Elements	64	128	128
Axial Steering (mm)	115	57	40
Lateral Steering (mm)	22 mm from the axis	10 mm from the axis	8 mm from the axis
Imaging Array			
Type	Phased Array	Phased Array	Phased Array
Frequency (MHz)	3.5	3.5	3.5
# of Elements*	64	128	128
Compatibility	Vantage 64 LE, 128 & 256 HIFU	Vantage 256 HIFU	Vantage 256 HIFU

*Only 64 elements used with HIFUPlex-04

Results: The project is a work in progress; development is nearing completion at the time of this writing. Various metrics of interest are under evaluation, including performance parameters such as image quality for the imaging modes (focused beams, unfocused beams, harmonic imaging, Doppler), spatial accuracy of delivered therapy, exposure compensation for attenuation and steering range, thermal strain imaging sensitivity, effectiveness of the user calibration on thermal accuracy, as well as ergonomic factors for the software and hardware components.

Conclusions: The small and

large HIFUPlex PLUS™ platforms are turnkey systems for preclinical research in focused ultrasound therapeutic applications. The software provides access to imaging and FUS therapy controls, and facilitates typical experimental workflows including ultrasound-guided positioning of the applicator, 3D imaging using a series of 2D slices for therapy planning, 3D therapy delivery with control over parameters for each focal exposure, therapy monitoring conventional imaging or Thermal Strain Imaging, and experimental data management. It is hoped that the availability of these turnkey systems will ultimately serve to advance adoption of focused ultrasound as a clinical therapeutic modality.

Acknowledgements: Focused Ultrasound Foundation

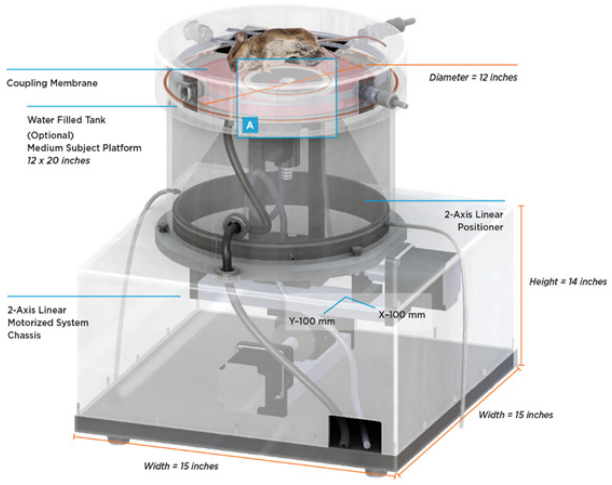

Figure 2. Sketch of the HIFUPlex PLUS™ 1000 platform for small subject preclinical USgFUS research.

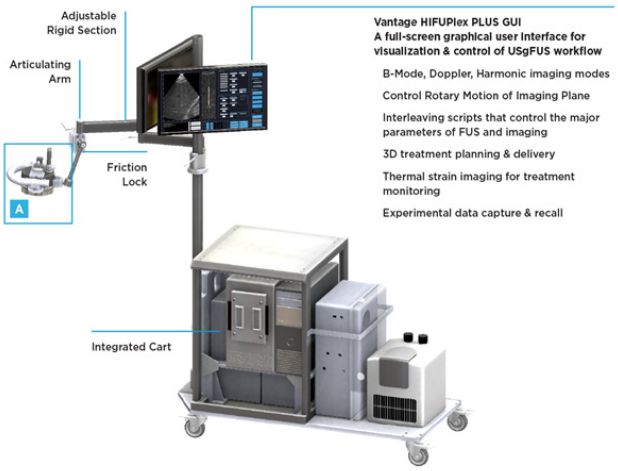

Figure 3. Sketch of the HIFUPlex PLUS™ 3000 platform for large subject preclinical USgFUS research.

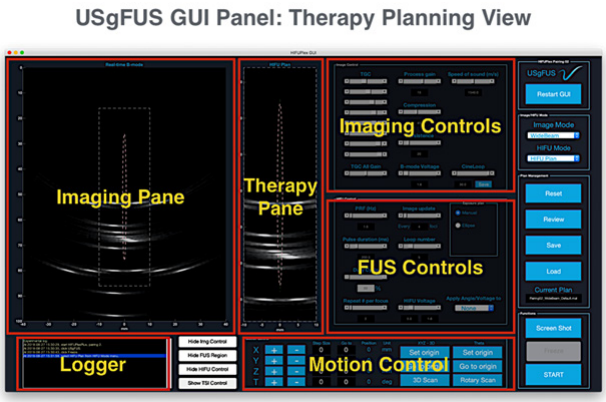

Figure 4. Example from HIFUPlex PLUS™ graphical user interface, here showing the therapy planning screen.

P-MIS-4

Topic: Miscellaneous Indications

Presentation Type: Poster

Evaluating how focused ultrasound and hypoxia cause deformation of mouse brain endothelial cell nuclei

Rajwinder Kaur[1], Graham Ferrier[1], Eugene Park[2], Andrew Baker[2], Jahan Tavakkoli[1]

[1]Ryerson University, Toronto, ON, Canada
[2]St. Michael Hospital, Toronto, ON, Canada

Background: Traumatic brain injury (TBI) begins with a primary mechanical insult triggering a cascade of secondary cellular processes, which can lead to long-term adverse outcomes. Various in vivo and in vitro models have been developed to investigate altered biochemical signaling pathways involved in TBI at the molecular level. Brain endothelial cells (an essential component of the blood brain barrier), being sensitive to mechanical injury and susceptible to hypoxia, can be investigated for any morphological changes in their nuclei following TBI. In this work, we investigate the significance of a sublethal primary mechanical injury induced by pulsed high intensity focused ultrasound (pHIFU) and mechanical stretching to mouse brain endothelial cell (bEND.3) nuclei in vitro followed by secondary hypoxia. After exposing bEND.3 cells to normoxic and hypoxic conditions and incorporating two methods of primary mechanical injury, the corresponding circularities and areas of bEND.3 nuclei are evaluated.

Materials and Methods: A focused acoustic field was generated using a single-element, hemispherical, 1-MHz pHIFU transducer that was driven by a function generator, and amplified efficiently using a matching network and an RF power amplifier. Calibration and characterization of the pHIFU field at various input powers were performed using a calibrated ONDA needle hydrophone (active element diameter of 400 μm). A MATLAB-based simulation tool was used to evaluate the corresponding acoustic pressures, intensities, and beam width within the focal region (2 mm x 10 mm). A monolayer of bEND.3 cells, cultured on a flexible and acoustically transparent silastic membrane of a six-well Flexcell® plate, was targeted at 5 distinct regions in each well. Initially, cells endured no primary injury (control) or primary mechanical injury using one of two methods: pHIFU or mechanical stretch. In the second method, a Model 94A Cell Injury Controller (Commonwealth Biotechnology, Richmond, VA) was used to inject air pressure to inflate the membrane, thereby stretching the monolayer of cells. Secondary injury was then induced by exposing cells to hypoxic (5% O2) conditions for 6 h. Temperature was maintained at 37°C using a circulating water bath. To study morphological changes due to primary and secondary injuries, the ImageJ (https://imagej.nih.gov/ij/) image processing tool was used to analyze DAPI-stained nuclei to determine their circularities and areas at 6 h and 24 h post-treatment.

Results: Morphological scatterplots (Area vs. Circularity) were obtained using ImageJ for three primary treatments (Control, pHIFU, and mechanical stretch – Fig. 1). After each primary treatment, cells were either fully normoxic for 24 h or subjected to a 6 h hypoxic environment followed by recovery in an 18 h normoxic environment. When cells remained normoxic post-treatment, the percentage of irregular nuclei (Circularity < 0.7 and Area < 380 μm2) varied insignificantly ($p > 0.05$) after all primary treatments. However, after cells endured the hypoxic environment, the percentage of irregular nuclei increased significantly ($p < 0.05$) compared with that after the 24 h normoxic regimens (Fig. 2a). In the absence of primary injury, hypoxic cell nuclei recovered significantly to their normal circularity after an 18 h normoxic recovery (Fig. 2b). However, when primary injury was present, the percentage of irregular nuclei increased irreversibly to ~19% during the hypoxic-normoxic regimen.

Conclusions: The circularity results show that pressures imposed by pHIFU (0.57 MPa acoustic pressure) and mechanical stretch (0.013 MPa static pressure) were insufficient to directly deform bEND.3 nuclei, but sufficient to irreversibly affect the integrity of bEND.3 nuclei. Therefore, bEND.3 nuclei became more vulnerable to hypoxia – a well-known secondary process in TBI. When bEND.3 cells endured primary injury followed by a 6 h secondary hypoxic regimen and an 18 h normoxic recovery, bEND.3 nuclei did not regain their original circularity. When this hypoxic-normoxic regimen was not preceded by a pHIFU (or mechanical stretch) primary injury, nuclei recovered their original shape successfully.

Acknowledgements: NSERC CRSNG, iBEST (Institute of Biomedical Engineering, Science and technology), St. Michael's Hospital.

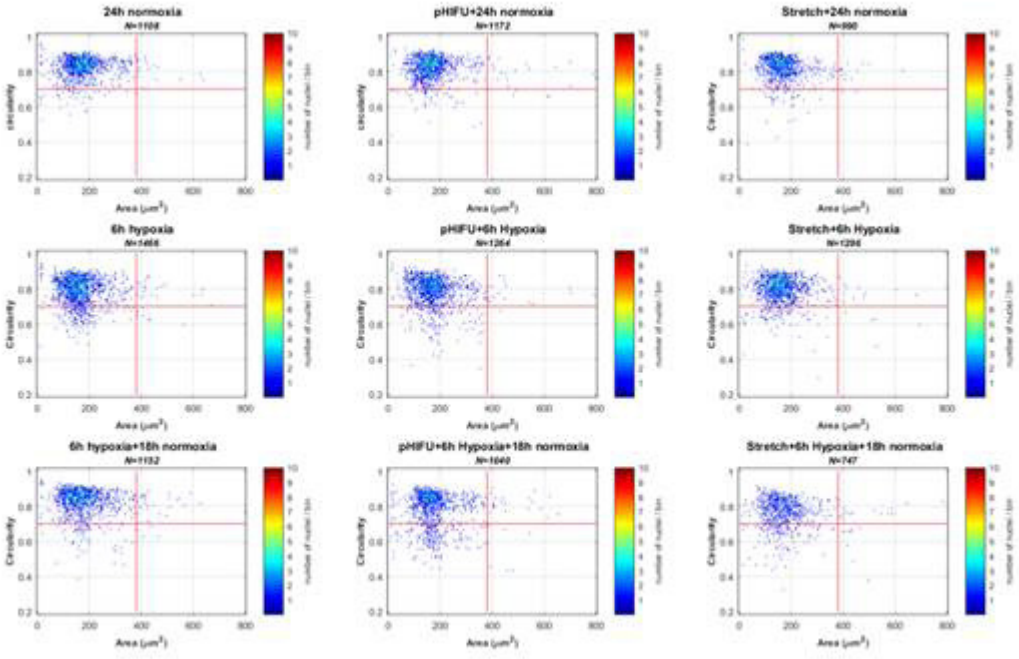

Figure 1. Scatterplots showing distribution of nuclei w.r.t. area and circularity. Irregularly-shaped bEND.3 nuclei in the lower-left quadrant, with area cut-off = 380 μm2, circularity cut-off = 0.7.

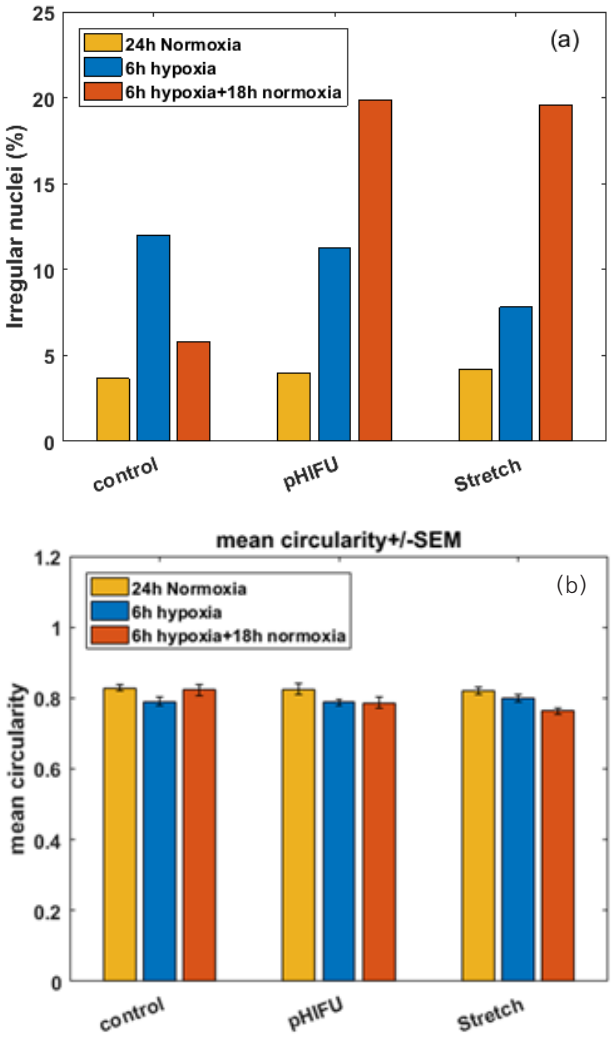

Figure 2. Variation in the (a) % of irregular nuclei (b) mean circularity for three primary (x-axis; acoustic or mechanical) and three secondary conditions (colours; normoxic-3 wells each and hypoxic-4 wells each.

P-MIS-6

Topic: Miscellaneous Indications
Presentation Type: Poster

Image-guided histotripsy treatment of abscesses in a large animal model

Yak-Nam Wang, Tatiana Khokhlova, Daniel Leotta, Andrew Brayman, Matthew Bruce, Adam Maxwell, Brian MacConaghy, John Kucewiz, Keith Chan, Wayne Monsky, Thomas Matula

University of Washington, Seattle, WA, USA

Background: Infected abscesses are common sequelae of complications in the settings of surgery, trauma or other diseases. The Agency for Healthcare Research and Quality reported that >262,000 U.S. patients were hospitalized for abscess treatment, accruing >$6.2B in aggregate U.S. hospital charges in 2011 alone. Current treatment is typically limited to antibiotics with invasive catheter drainage or surgical wash-out. Percutaneous catheter drainage involves inserting drains into the abscess under CT or US guidance. Drains usually remain in place for several weeks, during which catheter care and repeat procedures may be needed. In addition, it is often unsuccessful when the absessal contents are too viscous. Histotripsy can liquefy pus and deactivate bacteria, potentially obviating the need for long-term catheterization. The objective of this study was to use the latest ultrasound advances to characterize abscess development and evaluate the use of histotripsy for treatment in a novel porcine model.

Materials and Methods: Intramuscular and subcutaneous abscesses were generated in domestic swine by inoculating with a bimicrobial mixture of Bacteroidies fragilis and Escherichia coli with dextran particles as an irritant. Up to eight sites were inoculated in each animal. Shear wave, Doppler and B-mode ultrasound imaging was performed at least weekly to monitor abscess development (structure, size, stiffness and vascularity) and maturity, the latter reached at 2-6 weeks. On the day of treatment, animals were anesthetized and a 1.5 MHz HIFU transducer integrated with coaxially aligned ultrasound imaging probe was used for histotripsy treatment. Real-time B-mode was used for targeting and monitoring the bubble cloud during treatment. Two histotripsy pulsing regimes were tested: cavitation histotripsy (CH) (7-33 microseconds pulse duration, 1% duty cycle, n=8 treatments) and boiling histotripsy-like (BH) (10 ms pulse duration, 1% duty cycle, n=5), at the peak power outputs allowing for cavitation bubble cloud and vapor bubble formation. Ultrasound imaging was performed immediately prior to and after the treatment to evaluate the changes resulting from treatment. Pus samples were aspirated, using an 18G needle, prior to and again after treatment, and cultured to quantify bacterial viability. At the end of the study, the animals were euthanized and the abscesses were removed en block for histopathological evaluation. Whole-mount sections were stained with H&E, Masson's trichrome or gram stain.

Results: Ultrasound imaging was able to monitor the development of intramuscular and subcutaneous abscesses in a novel porcine model as abscesses matured from a region of tissue inflammation to an encapsulated organized mass of viscous pus. Mature abscesses were characterized by an avascular mixed echogenic core surrounded by a highly vascular hypoechoic rim (Fig 1). BH resulted in a larger volume of pus liquefaction than did CH. Histopathological evaluation of treatments revealed features characteristic of histotripsy lesions; homogenized cells with a lack of structural features found in untreated tissue (Fig.2). Samples from both BH- and CH- treated regions were easy to aspirate with an 18G needle following treatment, whereas the pre-treatment contents were substantially more viscous and harder to aspirate. CH produced a log bacterial kill of 0.89 +/- 0.23 (mean +/- s.d.). BH bactericidal effects were highly variable, but most often negligible (Fig 3).

Conclusions: Cavitation histotripsy and boiling histotripsy were both successful at liquefying viscous pus, providing a potential treatment involving simple aspiration. Cavitation histotripsy was more successful than boiling histotripsy in reducing the bacterial load, most likely due to using a higher treatment dose (a single combined treatment that essentially doubled the treatment time resulted in a mean log kill of 3.3). The results of this pilot study suggest that focused ultrasound may be a viable technology for in situ treatment of acoustically accessible abscesses, potentially reducing the need for percutaneous drainage.

Acknowledgements: Work supported in part by NIH grants 5R01EB019365, 2R01EB007643

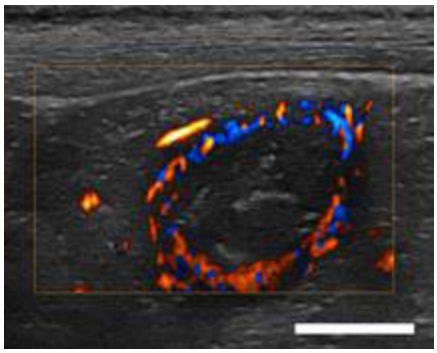

Figure 1. Color Doppler image of a well-circumscribed intramuscular abscess displaying salient features common to larger abscesses. Scale bar represents 1 cm.

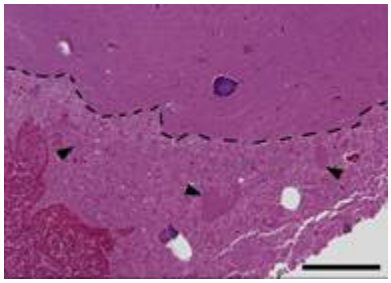

Figure 2. Representative image of Masson's Trichrome stained section showing the border (black dashed line) of a BH treated region (above the dashed line). Scale bar represents 200 um.

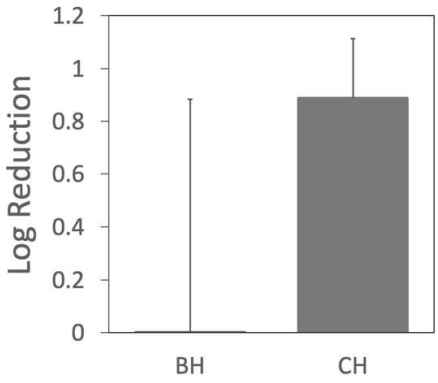

Figure 3. Log reduction in bacteria viability resulting from BH and CH treatments.

P-MIS-7

Topic: Miscellaneous Indications

Presentation Type: Poster

Ultrasound cavitation threshold detection in excised porcine lung tissue at 0.2, 0.5, and 1.0 MHz frequencies

Malia Sanghvi, Adam Morris, Ralf Seip, Narendra Sanghvi

SonaCare Medical, Fort Wayne, IN, USA

Background: The year is 2020, and the COVID-19 pandemic has taken ahold of our world. COVID-19 attacks the respiratory system, forming obstructions in lung tissue, which can cause difficulty breathing. This disease has no truly effective widespread treatment method, only treatments to ease symptoms. These treatments include ventilation and isolation. We propose the use of focused ultrasound for the treatment of this patient population by means of sustained cavitation with minimum side effects. This experimental research is to establish the required minimum cavitation threshold pressure at 0.2, 0.5 and 1 MHz ultrasound frequencies in freshly excised porcine lung tissue.

Materials and Methods: Freshly excised porcine lung tissue obtained from Knightstown Meats and Catering, (Knightstown, IN). The freshly excised tissue was cut into a 9cm x 4cm x 3cm piece and placed in a nitrile glove with sterile water which was placed in a tissue holder. This was done once for each transducer. The tissue holder was placed in a tank filled with degassed water, between a transducer and a hydrophone (figure 1). The hydrophone was connected to the spectrum analyzer and oscilloscope for data acquisition in real-time. The tissue was imaged with ultrasound probe for linear and transverse images prior to sonication for cavitation measurements (figure 2). Three different transducers operating at 0.2, 0.5 and 1 MHz frequencies were used to quantify cavitation thresholds. The Sonablate 500 LoFU program was used with 1 MHz probe. However, for the other two transducers operating at 0.5 and 0.2 MHz, a manual setup consisting of a function generator, an oscilloscope, a spectrum analyzer, and a power amplifier were used for data collection. All transducers were characterized for total acoustic power (TAP in Watts) for input RF drive voltage. The beam areas for all transducers were simulated to calculate peak intensities required for cavitation. For each transducer/frequency level, the tissue was exposed with different amounts of power to observe at what point cavitation began to occur, signified by the presence of half-harmonics on the spectrum analyzer (figure 3).

Results: Cavitation was observed when total acoustic power delivered was 15 W, 17.4 W, and 2.8W for 1 MHz, 0.5 MHz and 0.2 MHz frequencies respectively. Cavitation thresholds for 1, 0.5 and 0.2 MHz were found at 750, 6, and 1.2 W/cm2, respectively.

Conclusions: Lung tissue can be successfully imaged by high frequency diagnostic ultrasound. Cavitation in lung tissue can be maintained at very low ultrasound power at the frequencies of 0.2 and 0.5 MHz. The application of focused ultrasound technology in lung tissue is possible.

Acknowledgements: Sonacare Medical, Focused Ultrasound Foundation, Charles Steger Global Scholars Program.

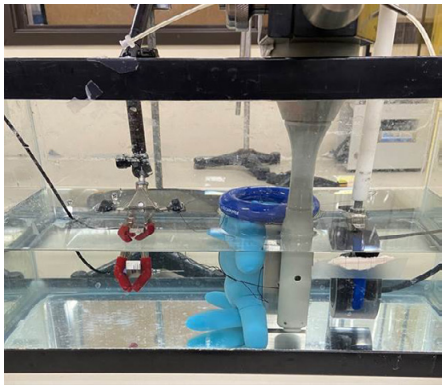

Figure 1. Experimental setup with hydrophone, tissue in globe, imaging probe, and transducer.

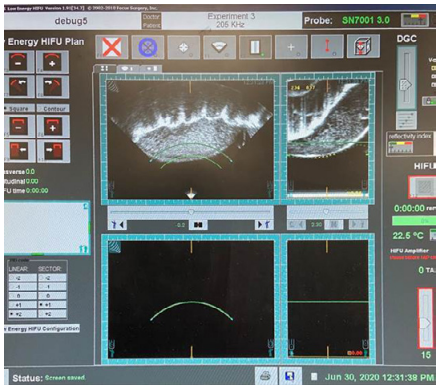

Figure 2. Ultrasound image of freshly excised porcine lung tissue.

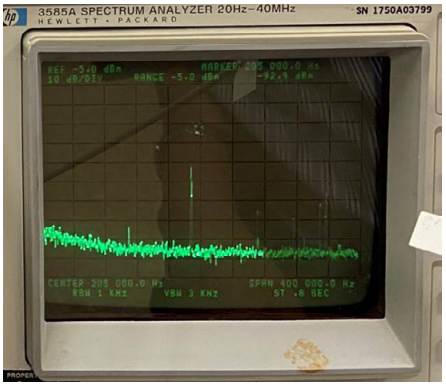

Figure 3. Example of a half-harmonic (cavitation indication) with a center frequency of 205 kHz on a spectrum analyzer, total acoustic power delivered is 7.8 W.

P-MIT-1

Topic: Miscellaneous Tumors

Presentation Type: Poster

Cytosolic Ca2+ transients during pulsed focused ultrasound generate reactive oxygen species and cause DNA damage in tumor cells

Robert Rosenblatt, Joseph Frank, Scott Burks

National Institutes of Health, Bethesda, MD, USA

Background: Mechanical forces from non-ablative pulsed focused ultrasound (pFUS) generate pro-inflammatory tumor microenvironments (TME) characterized by cytokines, chemokines, and trophic factors, as well as immune cell infiltration and reduction of tumor growth rates. pFUS also causes DNA damage in murine B16 melanoma and 4T1 tumors in vivo. DNA damage can be a potent activator of immunity and could contribute to changes in the TME. This study sought to understand biological mechanisms behind mechanotransduction of pFUS that causes DNA damage in several tumor cell types.

Materials and Methods: 4T1 (murine breast tumor), B16 (murine melanoma), C6 (rat glioma), or MDA-MB-231 (human breast tumor) cells were sonicated in vitro (1.1MHz; 6MPa PNP; 10ms pulses; 10% duty cycle; 300 pulses). DNA damage was detected by TUNEL, apoptosis was measured by immunocytochemistry for cleaved caspase-3. Calcium, superoxide, and H2O2 were detected by fluorescent indicators and modulated by BAPTA-AM, mtTEMPOL, or Trolox, respectively.

Results: pFUS significantly increased TUNEL reactivity (range=1.6–2.7-fold) in all cell types except C6 and did not induce apoptosis in any cell line. All lines displayed cytosolic Ca2+ transients during sonication. pFUS increased superoxide (range=1.6–2.0-fold) and H2O2 (range=2.3–2.8-fold) in all cell types except C6. In cell types that exhibited increased DNA damage and ROS production following pFUS (i.e., B16, 4T1, and MDA-MB-231), BAPTA-AM blocked increased TUNEL reactivity, superoxide and H2O2 formation, while Trolox also blocked increased TUNEL reactivity increased after pFUS. mtTEMPOL allowed H2O2 formation and did not block increased TUNEL reactivity after pFUS. Unsonicated C6 cells had higher baseline concentrations of cytosolic Ca2+, superoxide, and H2O2, which were not associated with greater baseline TUNEL reactivity than the other cell lines.

Conclusions: Mechanotransduction of pFUS directly induces DNA damage in tumor cells by cytosolic Ca2+ transients causing formation of superoxide and subsequent H2O2 and further suggest potential clinical utility for pFUS in anti-tumor therapy. However, the lack of pFUS-induced DNA damage in C6 cells demonstrates a range of potential tumor responses that may arise from physiological differences such as Ca2+ or redox homeostasis.

Acknowledgements: Intramural Research Program of the National Institutes of Health Clinical Center

P-MIT-2

Topic: Miscellaneous Tumors

Presentation Type: Poster

PCCA induced vascular disruption visualized by acoustic angiography

Phillip Durham, Jordan Joiner, Paul Dayton

University of North Carolina at Chapel Hill, Chapel Hill, NC, USA

Background: High intensity focused ultrasound is routinely used clinically in the noninvasive ablation of uterine fibroids, and is in clinical trials for the treatment of breast cancer. Acoustically active microbubbles oscillate in an acoustic field, imparting several biological effects. Like microbubbles, acoustically active phase-change contrast agents (PCCA), comprised of a condensed liquid perfluorocarbon core encapsulated by a lipid shell, have demonstrated therapeutic potential. Cavitation agents have been shown to reduce the energy input needed to achieve the same therapeutic ablation effect through the amplification of acoustic cavitation. PCCA are more stable in circulation than microbubbles, and their small size affords them the potential to extravasate near compromised vasculature. As we investigate the immunotherapeutic potential of PCCA, we have observed vascular perfusion defects following therapeutic ultrasound treatment when assessed by acoustic angiography.

Materials and Methods: PCCA were prepared by condensation of microbubbles. Briefly, lipids DSPC and DSPE-PEG2000 (9:1 ratio) were dissolved in a mixture of PBS, glycerol and propylene glycol. The lipid solution was transferred to sealed vials and degassed under vacuum. The vial headspace was filled with decafluorobutane gas. Microbubbles were generated by mechanical agitation (Vialmix). The vials containing microbubbles were cooled to -11°C in a chilled ethanol bath and pressurized to 45 PSI with compressed nitrogen, condensing the gas core resulting in nanoscale PCCA. Size and concentration were determined by single particle optical sizing (Accusizer FX Nano). Subcutaneous pancreatic tumors were inoculated in mice (C57Bl/6J wildtype, n=4) and were monitored until ~65mm3 volume. Acoustic angiography was performed prior to and following therapy on a Sonovol Vega imaging system in Density scanning mode with contrast via tail vein catheter. Therapeutic ultrasound was administered via a Therapy and Imaging Probe System (TIPS, Philips). An 8-element annular array (focal distance 80mm) was aligned over the center of the tumor. To activate PCCA, the transducer was driven at 1 MHz, 100Hz pulse repetition frequency (PRF) at 10% duty cycle, with the first two cycles at a peak negative pressure (PNP) of 1 MPa and the remaining cycles at 0.5 MPa. Animals were treated (5 minutes) following IV injection of 50μL of PCCA. Animals were reassessed via acoustic angiography after completion of treatment.

Results: Tumors were segmented in 3 dimensions using B-mode scans. Tumor density was assessed by proportion of pixels in the volume above a threshold (% positivity). Contrast density decreased after treatment by an average of 17.25 % positivity. The difference was not statistically significant ($p=0.0524$) when assessed with a paired t-test (two-tailed). Tumors with a higher starting perfusion saw the greatest decrease in perfusion, whereas tumors with the lowest perfusion saw the smallest decrease. A visual comparison of the before and after volumes show distinct areas of vessel compromise (Figure 1).

Conclusions: Acoustic angiography is a non-invasive tool for measuring vascular morphology and density non-invasively. Vascular disruption with focused ultrasound and cavitation agents temporarily compromise vascular integrity. While acoustic angiography has been investigated previously as a predictor of treatment response to cancer therapy, here we demonstrate that immediately following disruption, vascular patency can be imaged and visualized with acoustic angiography to confirm successful treatment and treatment location.

Acknowledgements: Carolina Center of Cancer Nanotechnology Excellence, Lineberger Comprehensive Cancer Center

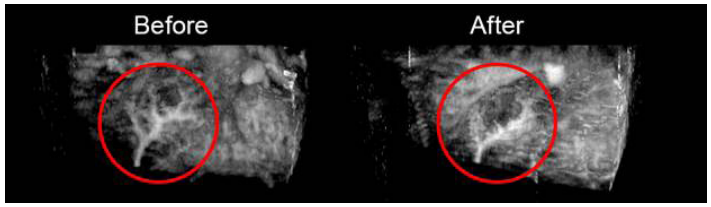

Figure 1. Vascular disruption visualized through 3D acoustic angiography. The large vessel over the tumor (Before, red circle) exhibits considerable disruption after (After) focused ultrasound with PCCA.

P-MIT-3

Topic: Miscellaneous Tumors

Presentation Type: Poster

Magnetic resonance-guided high intensity focused ultrasound (MR-HIFU) hyperthermia for primary rectal cancer – a virtual feasibility analysis

Kaitlyn Perry[1], Samuel Pichardo[2], Robert Staruch[3], Yuexi Huang[1], Merrylee McGuffin[1], Ari Partanen[3], Shun Wong[1], Greg Czarnota[1], Kullervo Hynynen[1], William Chu[1]

[1]Sunnybrook Health Sciences Centre and University of Toronto, Toronto, ON, Canada
[2]University of Calgary, Calgary, AB, Canada
[3]Profound Medical, Mississauga, ON, Canada

Background: Magnetic resonance-guided high intensity focused ultrasound (MR-HIFU) is a non-invasive, outpatient modality being used for thermal treatment of both benign and malignant tumors. In MR-HIFU, a specially designed external transducer is used to focus a beam of ultrasound energy into a small volume at a specific target site in the body (Figure 1). The focused beam results in rapid, localized heat deposition, and is used as a definitive treatment by thermally ablating the targeted tumour(s). At mild hyperthermic temperatures (40-42°C), the addition of heat enhances the cytotoxic effect of radiation (thermal radiosensitization) and chemotherapeutic drugs (thermal chemosensitization) by improving tumour blood flow and reoxygenation. The primary objective of this study was to create a workflow and software solution to virtually simulate primary rectal cancer patients and determine the feasibility of utilizing MR-HIFU hyperthermia.

Materials and Methods: With institutional research ethics approval, the anatomic characteristics and surrounding structures of rectal tumours diagnosed at Sunnybrook Health Sciences Centre from 2014-2019 were retrospectively reviewed to determine targetability by MR-HIFU. Three orthogonal views of MR images were used to determine the potential ultrasound beam path and organs at risk for the 105 available data sets. In part 2 of the study, the gross tumour volume (GTV) was delineated for 30 randomly selected rectal tumours (10 low, mid, high). Image datasets were imported into the Sonalleve® MR-HIFU workstation (Profound Medical, Canada) for virtual simulation to determine tumour targetability and coverage, optimal patient set-up parameters and ultrasound transducer positioning. The MR-HIFU virtual planning and analysis was first performed for single-cell treatment plans, and then repeated allowing for multiple hyperthermia treatment cells (2 to 4 cells) to cover larger tumour volumes (Figure 2).

Results: Of the 105 tumours analyzed, 36, 52, and 17 were lower-rectal (0-5cm), mid-rectal (5.1-10cm), and high-rectal (10.1-15cm), respectively. Figure 1 shows planning images in treatment software. The average width of the acoustic window (sciatic notch) for the US beam path was 5.8 ± 1.4cm, average tumour length was 5.24 ± 2.0cm, and average beam path length (tumour depth from skin to closest tumour edge) was 7.3 ± 1.9cm. 81% of tumours were ≤ 0.3cm from an organ at risk. Of the 30 virtually simulated tumours, 9/10 lower, 7/10 mid, and 1/10 upper rectal tumours were targetable by MR-HIFU. An average of 24% of lower and mid rectal tumours were in the direct hyperthermia beam path with one volumetric sonication. When multiple treatment cells were added to the targetable lesions, hyperthermia beam coverage increased to 47% and 38% in lower and mid rectal tumours respectively (Figure 2). Figure 3 shows examples of 3D rendering of coverage of GTV with treatment cells.

Conclusions: This is the first virtual analysis to evaluate MR-HIFU hyperthermia targetability in primary rectal cancer. We identified that lower and mid-rectal tumours are targetable by MR-HIFU, while upper-rectal tumours are more difficult and will require a different approach. We have created a workflow and software solution for virtual therapy planning that can be applied to a diagnostic MRI of potential patients prior to having them on the MR-HIFU tabletop. Virtual therapy planning can potentially improve patient selection for MR-HIFU, reduce the time needed for treatment set-up and planning, and treatment cost. Virtual MR-HIFU hyperthermia treatment planning is feasible and can be used in future studies of primary rectal cancer and other targets.

Acknowledgements: This study has been funded by the Canadian Cancer Society. Robert Staruch and Ari Partanen are employees of Profound Medical.

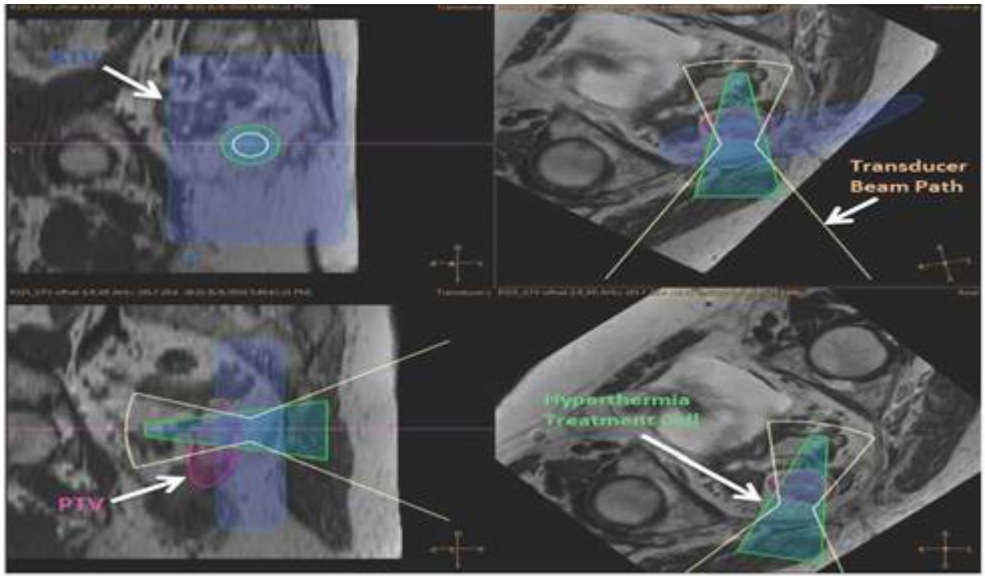

Figure 1: Example of virtually simulated treatment plan across 4 planes.

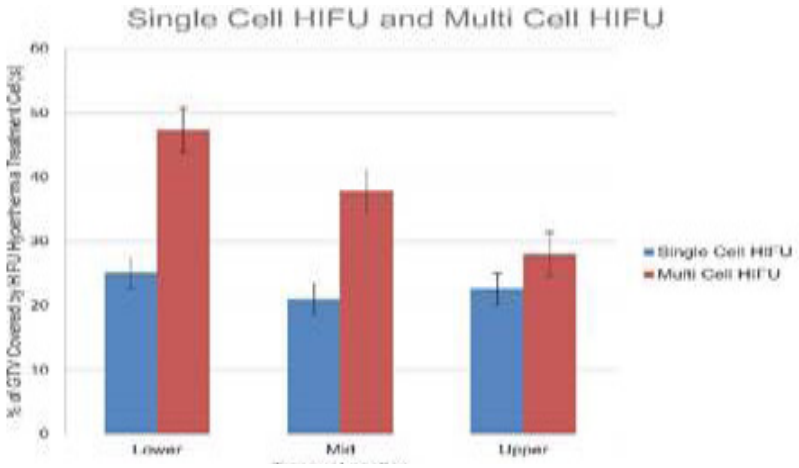

Figure 2: Single and multi-cell HIFU hyperthermia average % GTV coverage for the lower (average of 9 cases), mid (average of 7 cases) and upper (1 data point) that were considered targetable.

Figure 3: 3D rendering of planning examples showing overlap of GTV and hyperthermia treatment cells. A: single treatment cell covering 13.3% of GTV. B: Multiple treatment cells covering 41.1% of GTV.

P-MIT-4

Topic: Miscellaneous Tumors

Presentation Type: Poster

Effect of therapeutic ultrasound on cytoskeletal elements and cell crawling in murine 3LL and 4T1 cancer cells

Marie-Hélène Tomé, Saurabh Singh, Chandra Karunakaran, Claudia Gutierrez Chavez, Indranil Basu, Chandan Guha

Albert Einstein College of Medicine, Bronx, NY, USA

Background: Malignant cells utilize the actin cytoskeleton in order to crawl from the tumor microenvironment into the bloodstream. Cell migration persistence has been linked to cell cycle progression and metastatic potential in cancer cells. Cells that migrated for long periods of time utilizing cell crawling were found to proliferate more rapidly and have a higher metastatic potential. Chemical disruption of the cytoskeleton alters cell shape, disorients cells, and inhibits their ability to move directionally. Here, we will assess if low intensity focused ultrasound (LOFU) has a similar effect on cancer cells using 3LL (murine lung cancer) and 4T1 (murine breast cancer) cells. It has been found that the combination of LOFU and HIFU reduces the frequency of cancer metastasis. In this study, we propose that LOFU's impact on the cytoskeleton and cell crawling reduces the proliferative and metastatic potential of cancer cells.

Materials and Methods: The proposed study includes treating 3LL and 4T1 cell lines in vitro with LOFU and performing immune cell proliferation assays. Cells will be pelleted in thin-walled PCR tubes and submerged in degassed water. LOFU treatment will be performed using the Phillips Therapy and Imaging Probe System (TIPS, Philips Healthcare, Briarcliff Manor, NY) in a grid fashion to cover the whole pellet. Based on our previous studies and published literature, a range of LOFU parameters (3W – 9W of total acoustic power and 75% - 100% duty cycle) will be utilized for each cell type. The viability and proliferation of cells in each treatment group will be monitored with MTT and clonogenic assays. Isotropic cytoskeletal element expression after LOFU treatment will be measured using live-cell fluorescent imaging. Flow cytometry will be used after live-cell imaging to measure actin concentration. Cell crawling experiments will be conducted to assess 3LL and 4T1 cells' ability to navigate a 3D environment after LOFU treatment.

Results: Since LOFU has been postulated to modulate the immune system, the effect of LOFU on the cell crawling and chemotaxis of neutrophils and macrophages will be examined. As cell crawling is central to both cancer cell proliferation and immune response, the immunomodulatory properties of LOFU are expected to stem from its impact on the expression of cytoskeletal elements and thus cell crawling. Previously established non-lethal LOFU parameters are expected to modulate cytoskeletal actin expression of 3LL and 4T1 cells. Like chemical disruption, in vitro LOFU treatment is expected to impair cell crawling of murine lung and breast cancer cells as well as their ability to integrate external signals and navigate a complex 3D environment.

Conclusions: The comparison between 3LL and 4T1 cells will give insight into the commonality of the cell crawling mechanism of metastasis among different cancer types. The establishment of the bioeffects of LOFU on the cytoskeleton and cell crawling will help in developing future treatment methods to mitigate the risk of metastasis and cancer recurrence. The proposed study will help to characterize the effect of LOFU on the cytoskeleton and the cell crawling mechanism of cancer metastasis in murine models and predict the most translationally effective focused ultrasound therapy for controlling primary and systemic tumor growth.

Acknowledgements: Einstein Institute for Onco-Physics and Summer 2020 Focused Ultrasound Foundation Global Internship Program

P-MIT-5

Topic: Miscellaneous Tumors

Presentation Type: Poster

Desmoid tumor volumetric analysis for disease response post ablation with magnetic resonance guided high intensity focused ultrasound

Caitlin Tydings[1], Pavel Yarmolenko[1], James Geller[2], Joseph Pressey[2], John Racadio[2], Haydar Celik[1], Matthew Lanier[2], Karun Sharma[1], AeRang Kim[1]

[1]Children's National Hospital, Washington, DC, USA
[2]Cincinnati Children's Hospital Medical Center, Cincinnati, OH, USA

Background: An objective measure of treatment response is crucial to the clinical evaluation of cancer therapy. Currently, the most widely accepted method is Response Evaluation Criteria in Solid Tumors (RECIST), a unidimensional measurement of a tumor's largest dimension. This may be suitable for more uniform solid tumors, but its limitations are most notable when evaluating treatment response for irregularly shaped, heterogeneous tumors, particularly following targeted local therapies. Desmoid tumors are irregularly shaped, infiltrative and can cause significant morbidity from pressure effects and obstruction of nearby structures. MR-HIFU ablation has been used to target areas of larger tumors thought to be contributing most to morbidity with resultant ablation zone appearing to lack perfusion on contrast-enhanced MRI. Measuring total, perfused and non-perfused tumor volumes using volumetric analysis may provide a better objective measurements of tumor response to local therapy.

Materials and Methods: This is a retrospective review of MRI images from 9 patients, with histologically diagnosed recurrent, refractory and symptomatic desmoid tumors from Children's National Hospital (CNH) and Cincinnati Children's Hospital Medical Center (CCHMC). All patients were treated with MR-HIFU on a clinical trial (NCT02076906) or compassionate use protocol. Unidimensional measurements were per-formed using digital calipers on Synapse (CCHMC) and Osirix (CNH) for patients from CNH and CCHMC, respectively. Volumetric analysis was performed using Osirix software. Total tumor volume (TTV) was segmented and calculated by manually outlining the tumor in axial plane on post-contrast T1-weighted images. Non-perfused tumor volume (NPTV) was similarly measured in axial plane using subtraction images generated from pre- and post-contrast T1-weighted images. Per-fused tumor volume (PTV) was measured as the subtraction of NPTV from TTV.

Table 1: Volumetric Analysis of total tumor, perfused and non-perfused volume as well as RECIST response

	Pre-Treatment 1		Treatment 1 Day			One month Post-Treatment 1			
Patient	TTV (cm3)	RECIST response (cm)	TTV (cm3)	PTV (cm3)	NPTV (cm3)	TTV (cm3)	PTV (cm3)	NPTV (cm3)	RECIST response (cm), percent change (%)
1	135.7	13.4	137.5	81.2	56.4	157.1	115.2	41.9	12.4, -7.5
2	80.5	9.6	76.4	47.3	29	87.3	62.7	24.7	9, -6.2
3	642.7	51	611.8	389.5	222.2	675.7	605.1	70.6	*N/A, N/A
4	19.7	4.4	25.4	17.6	7.8	23	19.8	3.2	4.4, 0
5	657.6	12.9	655.2	240.2	415	612	274.2	337.8	12.7, -1.6
6	176.4	8.5	182.3	161.4	20.9	181.3	173.8	7.6	9, +5.9
7	96.9	12.2	91.8	81.9	9.9	111.1	104.3	6.8	*N/A, N/A
8	262.8	17.2	**218.6	157.2	61.4	286.6	244.7	41.9	17.8, +3.5
9	329.8	11.1	352.8	192.6	160.2	370.1	328.7	41.4	11.7, +5.4

TTV = Total tumor volume, PTV = Perfused tumor volume, NPTV = Non-perfused tumor volume

*Unable to perform due to image acquisition/quality
**MRI does not include entire tumor

Results: Nine patients (median age 15.3 years, range 6-23 years; 4 males) underwent treatment (tx) with MR-HIFU (n=3, 1 tx; n=5, 2 tx; n=1, 3 tx). Tumors were located in the lower extremities (n=6) or body wall (n=3). The median pretreatment TTV was 176.4 cm3 (range 19.7 - 657.2 cm3) and NPTV was considered negligible. Immediately post-treatment, median PTV was 157.2 cm3 (range 47.3 – 389.5 cm3) and median NPV was 56.4 cm3 (range 7.8 - 160.2 cm3). At one month post-treatment, the median TTV was 181.3 cm3 (range 23 - 675.7 cm3), median PTV was 173.8 cm3 (range 19.8 – 605.1 cm3) and median NPTV was 41.4 cm3 (range 3.2 – 337.8 cm3). There were no objective RECIST responses immediately post-treatment. At one month post-treatment, the median percent change in RECIST was 0% (range -7.5 - 5.4%). Table 1 shows individual volumes for all patients. Figure 1 demonstrates volumetric analysis for patient 1 including outlined TTV (white) and NPTV (red).

Conclusions: Patterns of desmoid tumor response after MR-HIFU ablation, assessed by volumetric analysis of both perfused and non-perfused tumor tissue, were subjectively found to be more detailed and meaningful to treating clinicians compared to RECIST. Since TTV did not change as much as the perfused/non-perfused portions of the tumor following treatment, volumetric analysis appears to better reflect effects of MR-HIFU ablation therapy. These volumes are useful measurements that can be followed over time to establish how changes in total tumor volume relate to perfused and non-perfused tumor components. Future work is needed to ascertain and validate reproducibility of these measurements and determine their relation to disease-free survival.

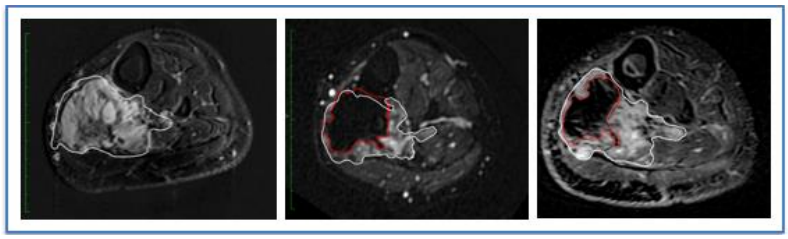

White: TTV, Red: NPTV

Figure 1: Patient 1 Volumetric Analysis before treatment, immediately following treatment and at 1 month follow up.

P-MIT-6

Topic: Miscellaneous Tumors

Presentation Type: Poster

Non-invasive surgical treatment of lung cancer – preliminary results

Jaime Mata[1], Lauren Powlovich[2], David Moore[2], Linda Martin[1]

[1]University of Virginia, Charlottesville, VA, USA
[2]Focused Ultrasound Foundation, Charlottesville, VA, USA

Background: Malignant lung cancer carries a poor prognosis (median survival of about 10 months) with rare cases of complete cure and a 5-year survival rate of about 18 percent. Surgical resection therapy was shown to have the greatest impact on survival and consists of removing the entire lobe or segment of the affected region of the lung, but unfortunately the majority of the lung cancer patients (about 60-70%) do not qualify for or cannot tolerate surgery.

This method proposes an innovative minimally invasive procedure for the transcutaneous ablation of lung tumor masses with complete removal or significant debulking of the masses, without the use of traditional open lung resection surgery. This technique does not require flooding of the lung in order to get an acoustic window for the Focused Ultrasound (FUS), which can pose serious immediate and long term risks for the patient (i.e. pneumonia, sepsis, among other complications).

Materials and Methods: Two Yucatan mini pigs (~30Kg) had both main bronchi selectively intubated, and while the left lung was mechanically ventilated, the right lung was purposely collapsed, followed by a controlled right hydrothorax in the chest cavity with saline in order to create an acoustic window for the FUS beam. At the end of the Magnetic Resonance guided Focused Ultrasound (MRgFUS) ablation, using the InSightec ExAblate 2000 Body System, the saline was drained in a method identical to the drainage of a clinical pleural effusion. Animal #1 received six transcutaneous MRgFUS ablations of the right lung, in six different locations. Each location received a different amount of acoustic power in order to determine the optimal power with minimal side effects (i.e. skin burns). Animal #2 received two transcutaneous MRgFUS ablations in a large area on the upper lobe of the right lung. An intercostal approach with different angulations was used in order to target the transcutaneous beam without distortion and attenuation caused by the ribs. One week after the ablation, each animal received a MRI of the lung to assess the success of the ablation; the animals were then euthanized and a histopathological examination of the lungs was performed to correlate with the results of the MRI.

Results: Ablations were done successfully on both animals. The locations and sizes of the ablations as determined by post treatment MRI and gross histology, correlated well with the initial target locations and the power doses applied (Figs 1-2). The escalation test done on animal #1, was very useful to determine the power and the duration of the treatments. This information was used on animal #2 with immediate success (Figs 1-2) but further refinement of the doses and treatment times is necessary to avoid skin lesions. This should be accomplished in the near future on new animal studies.

Figure 1. (top) Multiple MR images taken one week post MRgFUS treatment of animal #2. Pulmonary lesions produced by MRgFUS marked with arrows.

Figure 2. (bottom) Gross pulmonary lesions marked with arrow. These lesions correlate with the lesions marked on the MR images of Figure 1.

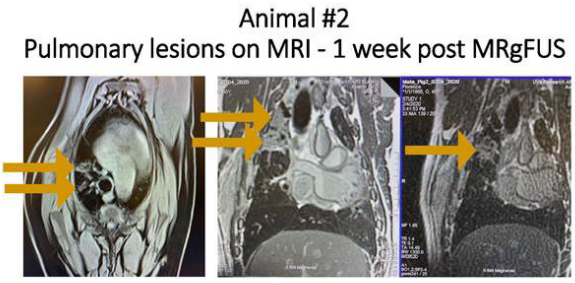

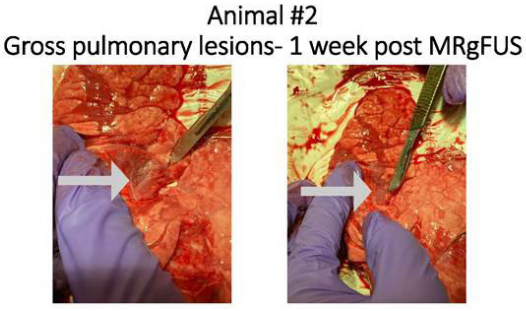

Immediately after MRgFUS treatment, the saline in the chest cavity was drained with only a small volume of ~10% (~50-60cc) remaining inside the cavity. Both animals recovered very well from the MRgFUS treatment with no significant side-effects besides a skin lesion on animal #2 at the place where the transducer was located.

Conclusions: These preliminary results are very encouraging. This new procedure could increase lung cancer survival rates and at the same time decrease morbidity and side effects associated with current treatment therapies like radiosurgery and chemotherapy, since it will permit nonsurgical tumor ablation or tumor debulking. It will also provide a viable treatment for a large group of patients that cannot tolerate resection surgery, radiotherapy and chemotherapy, or who have had prior radiation and cannot have additional radiation to that region. For this large segment of the patient population, palliative care, not full treatment, was traditionally the therapy of choice. The proposed procedure may create new hope for these patients.

Acknowledgements: Focused Ultrasound Foundation

P-MOV-1

Topic: Movement Disorders

Presentation Type: Poster

Quantitative measures of reaching and proprioception following MRgFUS thalamotomy for tremor

Catherine Swytink-Binnema, Bruce Pike, Davide Martino, Samuel Pichardo, Sean Dukelow, Zelma Kiss

University of Calgary, Calgary, AB, Canada

Background: Essential tremor (ET) is a common condition and when unresponsive to medication and disabling, can be treated by magnetic-resonance guided focused-ultrasound (MRgFUS) ablation of the thalamic ventral intermediate (Vim) nucleus. Although MRgFUS minimizes risks associated with open surgeries, balance and gait disturbances have emerged as significant risks. The Vim nucleus is a relay in the proprioceptive pathway and contains kinesthetic cells. Therefore, it may not be surprising that Vim thalamotomy may impact not only tremor but proprioception. However, this has never before been quantitatively measured.

Our aim was to quantify proprioception (kinesthesia and position sense) and reach in ET patients undergoing MRgFUS Vim thalamotomy. We hypothesized that MRgFUS thalamotomy alters proprioception based on the sensorimotor Vim being lesioned.

Materials and Methods: In an ongoing study, proprioception and reach was measured using the Kinarm exoskeleton robot (BKIN Technologies, Kingston, Ontario), pre-operatively, 1 day, 3 months, and 1 year after MRgFUS Vim thalamotomy. Patients were seated, with their arms supported and moving only in the horizontal plane, while they completed three tasks: 1) a visually-guided reaching task, 2) an arm position-matching task, and 3) a kinesthetic-matching task. Based on age-, sex-, and handedness-matched controls, data were transformed into normally-distributed z-scores and compared using repeated-measures one-way ANOVA with post-hoc paired t-tests (with Bonferroni correction).

Results: Because of small sample size at the one year time-point (N=6), only pre op (N=16), day1 (N=15), and month3 (N=14) results were analyzed. Only visually-guided reaching demonstrated significant changes: posture speed, which represents hand tremor, varied significantly with time ($F(2, 24)=5.2$, $p=0.013$, $(\eta\_g)^2=0.18$), decreasing from pre-op to day1 (4.23 ± 1.70 to 2.21 ± 1.63, $t(12)=-3.2$, $p\_adj=0.021$). By month3, posture speed (2.84 ± 2.24) was not significantly different from either pre-op or day1 (Figure 1). Movement time also varied over time ($F(2, 24)=5.5$, $p=0.011$, $(\eta\_g)^2=0.10$), increasing significantly from pre-op to day1 (1.37 ± 1.74 to 0.01 ± 1.90, $t(12)=2.8$, $p\_adj=0.048$), with no significant difference by month3 (-0.46 ± 1.82) (Figure 2). There were no significant changes in position-sense- or kinesthesia-related parameters.

Conclusions: This is the first quantitative assessment of reaching and proprioception following MRgFUS Vim thalamotomy. These preliminary results suggest that MRgFUS Vim thalamotomy does not degrade proprioception and, as expected, decreases tremor. Although posture speed increased slightly at month3 and was not significantly different from pre-op, this is likely due to the higher variability at month3. Vim thalamotomy increased movement time, similar to what has been observed with historical thalamotomies. While statistically significant, the increase remains within the range of what is normal and, thus, is likely not clinically relevant. Further analysis, as more data are collected, will better clarify the long-term effects of Vim thalamotomy.

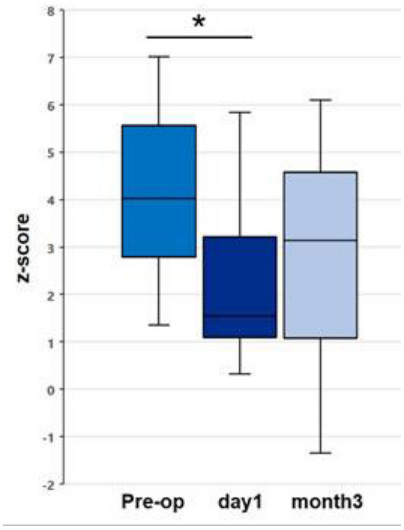

Figure 1. Posture speed decreased significantly following Vim thalamotomy (4.23±1.70 to 2.21±1.63, t(12)=-3.2, p_adj=0.048), but at month 3 (2.84±2.24) was not significantly different from either pre-op or day 1.

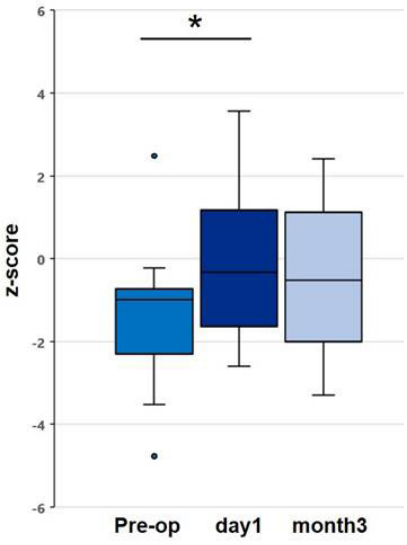

Figure 2. Movement time increased significantly following Vim thalamotomy (-1.37±1.74 to 0.01±1.90, t(12)=2.8, p_adj=0.021), but at month3 (-0.46±1.82) was not significantly different from either pre-op or day 1.

P-MSK-1

Topic: Musculoskeletal
Presentation Type: Poster

A standard test phantom for magnetic resonance guided high intensity focused ultrasound (MRgHIFU)

Simone Ambrogio[1], Piero Miloro[2], Bajram Zeqiri[2], Fiammetta Fedele[1], Kumar Ramnarine[1]

[1]St Thomas Hospital, London, United Kingdom
[2]National Physical Laboratory, London, United Kingdom

Background: MRgHIFU effectively ablates tissues by targeting a selected region while preserving the surrounding tissues. Different clinical systems have received FDA approval and CE marking for non-invasive thermal therapy. As the use is becoming widespread, there is an increasing need to standardise the way in which the delivery of the therapy is described and reported. Development of reliable test objects may be crucial for supporting calibration and definition of high standard of practice. Where the primary mechanism of induced biological effect is thermal, the quantification of the treatment can be described in terms of thermal dose, a parameter that accounts for the heat deposited in a time interval. Consequently, a HIFU test object may consist of a device that allows accurate quantification of temperature as a function of time, in a reference material. The aim of this study is to develop a standard test phantom to perform thermal dose QA on HIFU systems.

Materials and Methods: A phantom consisting of 3D printed bone-equivalent disks (VeroWhitePlusTM, Stratasys Ltd, Minnesota, USA), IEC agar based tissue mimic material (TMM) and four fine wire type-T thermocouples placed in relevant positions (adjacent to the bone and in the tissue mimic) was manufactured. The thermocouples have a junction size of 75 μm to minimise viscous heating artefact, and were connected to a data-logger USB TC-08 (Pico Tecnology, Eaton Socon, UK) through 5 meters of extender cable. The data-logger was kept outside the MR environment to avoid potential artefacts in MR thermometry. The phantom was sonicated with a clinical Sonalleve MR-HIFU system (Philips, Eindhoven, Netherlands) using different acoustic powers and therapeutic configurations: "bone metastasis" and "uterine fibroids". Experiments were performed on four different days to assess reproducibility. The Quality Control automatic protocol was performed before each experimental day, in accord with Manufacturer instructions. Figure 1 shows the experimental set-up on the MR-HIFU system. Sonications were performed on TMM and bone-equivalent regions both far from the thermocouples and on the thermocouples.

Results: MR-thermometry temperature estimates from coronal, sagittal and transverse MRI-Thermometry planes differed by up to 50%. Thermocouple measurements variability across multiple experiments was within 20%. Treatment power of 30W for 16s exposure resulted in peak temperature increase of 18°C, the target temperature elevation for thermal ablation therapy. An acoustic power of 20W in the bone-mimic resulted in peak temperature increase of 35°C (Figure 2), comparable to 31°C found in previous studies in-vivo with the same MRgHIFU system. MRI-Thermometry, performed with proton resonance frequency method, variability across multiple experiments was within 40%. Results are summarised in Figure 3.

Conclusions: A cost-effective and portable test object for MRgHIFU applications was developed. Materials have tissue-like ultrasound properties (e.g. absorption, attenuation, speed of sound and B/A parameter), remain stable over time and provided a satisfactory MR signal with minimum artefacts. The test object allowed the quantification of temperature rise induced by the HIFU source in soft tissue and bone mimic material. Results highlight its potential for supporting calibration, QA, training, optimisation and validation of MRgHIFU procedures thereby ensuring safe and effective HIFU treatment.

Acknowledgements: Authors acknowledge funding support from the National Measurements System, the UK Department for Business, Energy and Industrial Strategy, the Chief Scientific Office (England), the Therapy Ultrasound Network for Drug Delivery & Ablation Research (ThUNDDA).

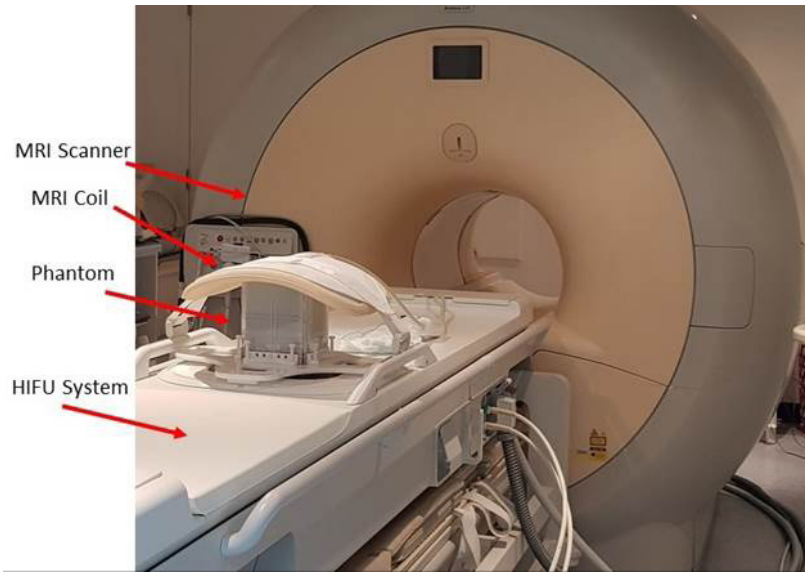

Figure 1. Experimental set-up - Phantom positioned on Sonalleve MR-HIFU system (Philips, Eindhoven, Netherlands).

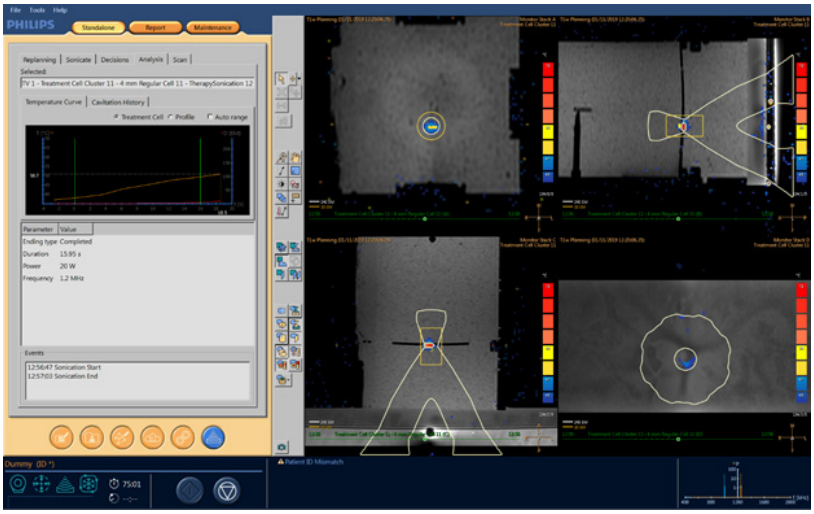

Figure 2. Screenshot of the Sonalleve MR-HIFU (Philips, Eindhoven, Netherlands) console after a 20W sonication on the bone-mimic.

	Input Power (W)	N° of sonication	Peak Temperature - Termocouple - Average (°C)	Peak Temperature - Termocouple - StDev (+/-)	Peak Temperature - Termocouple - Error (%)	N° of sonication	Peak Temperature - MRThermometry Average (°C)	Peak Temperature - MRThermometry StDev (+/-)	Peak Temperature - MRThermometry Error (%)
Exposure on Bone	20	3	34.91	6.51	18.64	10	31.82	4.52	14.22
	30	3	59.67	12.02	20.14	6	35.33	6.94	19.65
	40	1	65.52	-	-	1	48.73	-	-
Exposure on TMM	20	5	11.99	2.24	18.71	5	5.42	1.41	25.98
	30	6	17.79	1.88	10.56	6	9.52	3.97	41.71
	40	4	24.43	3.47	14.21	15	11.76	3.88	32.98
	50	1	37.53	-	-	9	21.47	8.90	41.43

Figure 3. Peak temperature average, standard deviation and percentage error calculated on multiple sonication with thermocouples and MR thermometry.

P-MSK-2

Topic: Musculoskeletal
Presentation Type: Poster

Histotripsy treatment of primary osteosarcoma: Feasibility study in excised canine tumors

Lauren Arnold[1], Alissa Hendricks[1], Sheryl Coutermarsh-Ott[2], Jessica Gannon[1], Nikolaos Dervisis[2], Shawna Klahn[2], Irving C Allen[2], Joanne Tuohy[2], Eli Vlaisavljevich[1]

[1]Virginia Tech, Blacksburg, VA, USA
[2]Virginia Maryland College of Veterinary Medicine, Blacksburg, VA, USA

Background: Osteosarcoma (OS) is a highly metastatic bone tumor affecting dogs and humans. Standard of care treatment for both species includes surgical resection of the primary tumor via limb amputation or limb-salvage surgery, and chemotherapy for treatment of metastatic disease. Canine OS shares many biologic similarities to human OS, and OS prognosis is poor. Human survival rates have remained stagnant for decades; in canines, a ~45% one-year survival rate is expected with definitive treatment. Histotripsy is a non-thermal, non-invasive focused ultrasound method that uses highly controlled acoustic cavitation to mechanically disintegrate tissue. In this study, we investigated the feasibility of treating primary OS tumors with histotripsy using a custom-designed therapy transducer on excised canine OS tumor samples. This study forms the foundation for in vivo studies of histotripsy for treating canine OS, which will provide essential proof-of-concept for human OS treatments.

Materials and Methods: Canine OS samples were harvested after surgical procedures at the Virginia Tech Veterinary Hospital, with all samples treated within 48 hours of harvest. Samples were embedded in gelatin tissue phantoms and treated with a custom 500 kHz histotripsy system (Fig.1A,B) using 1-2 cycle pulses at a pulse repetition frequency of 250 Hz. The location of the bubble cloud was verified using real-time ultrasound imaging, and an automated volumetric ablation was performed (4000 pulses per focal location) (Fig.1C). Separate experiments were also conducted to test the effects of histotripsy on normal canine bone and nerve. After treatment, histopathological evaluation of the samples was completed by a board-certified veterinary pathologist (Fig.1D,E,F). To demonstrate the feasibility of treating canine OS tumor on an intact limb, one final trial applied histotripsy to a limb affected by OS with overlying tissues and skin present.

Results: The generation of precise bubble clouds was achieved at the focus in all tumor samples at peak negative pressures of 30-40 MPa. Histopathology showed effective cell ablation in treated areas for OS tumors, with no evidence of cell death or tissue damage for normal canine cortical bone or nerve tissues. For the treatment conducted on the intact limb, results showed generation of a well-confined bubble cloud and ablation zone inside the OS tumor through tissue and skin. A higher cavitation threshold was observed for the intact limb treatment compared to tumor samples without overlying tissue, with a peak negative pressure of 39.8 MPa applied during treatment.

Conclusions: Results demonstrate the feasibility of treating canine OS tumors while preserving adjacent normal tissues. Based on these preliminary results, ongoing studies are underway to investigate the in vivo feasibility of histotripsy for treating primary canine OS.

Acknowledgements: This work received support from the Virginia Tech Institute for Critical and Applied Technology Doctoral Scholars Program, the American Kennel Club, and the Focused Ultrasound Foundation.

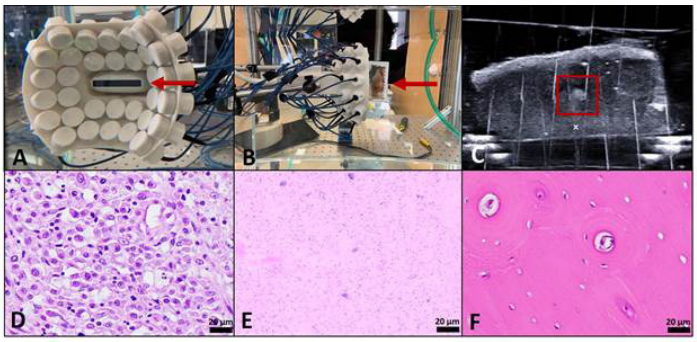

Figure 1: (A-C) Treatment set-up. (D-F) Histology (D) Untreated OS, (E) treated OS, (F) treated bone.

P-MSK-3

Topic: Musculoskeletal
Presentation Type: Poster

Could low intensity pulsed ultrasound improve irradiated mandibular bone healing?

Aline Desoutter, Anne Gaëlle Chaux, Stephan Langonnet, Laura Barrot, Jean-Christophe Bera

Labtau, Centre léon Bérard, Lyon, France

Background: The mandible is often included in the radiation fields in case of head and neck squamous cell carcinomas. External radiotherapy can lead to osteonecrosis, which still represents a threatening adverse effect that may impact quality of life. Its pathogenesis is partially explained by a decrease of cell activity, a decrease of vascularization and an increase of collagen excretion, resulting in bone weakening. The incidence of osteoradionecrosis has decreased to 1-5%. However, its treatment remains controversial and partially unsatisfactory and invasive. Several surgical and non-surgical treatments have been proposed, like the Pentoclo® protocol or hyperbaric oxygen therapy. Several radiation schemes have been developed in the literature, with various results. As Low Intensity Pulsed UltraSounds (LIPUS) seem to stimulate bone healing and vascularization, the hypothesis that LIPUS could enhance post-surgical bone healing in irradiated mandibular bone has been proposed.

Materials and Methods: First step: validation of an animal model of irradiated mandible. Nineteen rabbits (female New Zealand white) were used. The radiation protocol consisted of 5 sessions delivering 8.5 Gy each. MicroCT was performed at D0, D7, D14, D28 and D42 for the control group and D0, D28 and D42 for the irradiated group. A modified Perry's score was determined on histologic samples, and comparison between microCT and histological findings was performed.

Second step: validation of the LIPUS protocol and evaluation of LIPUS' effects. A bibliographic search was performed in Medline via Pubmed, Scopus, EMbase and the grey literature. The LIPUS protocol, animal model used, effects of LIPUS and main conclusions were reported. After selection, 3 experimental studies remained for analysis. The animal model was the dog, and the aim of the studies was prevention or treatment of osteoradionecrosis. The LIPUS protocol (30 mW/cm2, 1.5 MHz, pulse 1:4, frequency 1 kHz) consisted in 20 sessions of 20 minutes, from D0 to D14 postoperatively. We choose to perform 10 sessions with the same parameters. Animals were sacrificed at D28 and D42 to highlight the differences between the irradiation + LIPUS group and the irradiation alone group.

Results: First step: The bone mineral density and the trabecular number were decreased after radiotherapy whereas trabecular separation increased. The main differences between irradiated and non-irradiated rabbits were observed at Day 28 and 42. There was a strong correlation between imaging and histologic findings.

Second step: The preliminary results seem to show a greater heterogeneity in irradiated bone healing with LIPUS. They seem to increase the trabecular number. LIPUS have a probable effect on pain, as Irradiated +LIPUS group presented with modifications of food intake. There is a great heterogeneity in these preliminary results.

Conclusions: Radiation seems to cause a delay in bone healing. It decreases bone quality and mineral density. Five sessions seem to be a valuable compromise between tissues effect and feasibility. This model seemed to be valuable for evaluating postextractional bone healing in the irradiated rabbit. Our first results seem to indicate LIPUS has a positive impact on trabecular number. Despite major heterogeneity in the LIPUS protocols proposed in the literature for bone healing in non-irradiated bone, the LIPUS protocols reported in irradiated bone seemed more consensual. LIPUS seemed to improve early stages of irradiated bone healing and vascularization and play a role in bone healing in case of osteoradionecrosis. Our results need to be consolidated.

Acknowledgements: FUS, IFRO, Eusapharma, Gueules Cassées

P-MSK-4

Topic: Musculoskeletal
Presentation Type: Poster

On the acoustic characterization of skull: An acoustic microscopy approach

Minoo Kabir[1], Kamyar Firouzi[2], Kwan Kyu Park[2], Pierre Khuri-Yakub[1]

[1]Stanford University, Stanford, CA, USA
[2]Hanyang University, Seoul, South Korea

Background: Transcranial focused ultrasound is being used for both imaging and therapeutic applications; including high intensity focused ultrasound and neuromodulation. The presence of skull, in non-invasive transcranial focused ultrasound applications, distorts the ultrasound beam depending on the acoustic characteristics of the skull. The size, thickness, and level of heterogeneity of skulls varies substantially among patients and even at different spots on the same skull, which could considerably change the acoustic properties of skull samples. An in-situ characterization of skull is essential for simulating ultrasound beam traversing the skull and designing the system for effective delivery of ultrasound to the brain. Here, we propose an acoustic microscopy technique that is able to measure directly both shear and longitudinal velocities and attenuations.

Materials and Methods: We have developed a quantitative acoustic microscopy system for in-situ characterization of the skull. In this method, a large aperture focused transducer is scanned towards the material, and the output voltage variation as a function of distance between the focal plane of the transducer and the substrate surface is measured to form a response curve for the material. An in-house designed spherical transducer with center frequency of 1.2 MHz and maximum aperture angle of 30 degree is used for experimental measurements. Due to the large aperture, the ultrasound beam impinges on the sample at a wide range of angles and excites a wide range of Lamb waves, which then leak back into the coupling medium and are measured at the transducer. This procedure is schematically illustrated in Figure 1. By measuring the complex voltage value at each depth, the reflectance function of the material is inverted. Finally, the acoustic properties, including longitudinal and shear velocities and attenuations are estimated using an inversion algorithm that optimizes the experimental measurements data and theoretical reflectance function for a fluid-loaded material. The proposed technique is first validated on attenuative plastic samples that present similar acoustic behavior as skull, such as acrylic, high density polyethylene (HDPE) and polycarbonate at a variety of thicknesses; then, measurements are conducted on human skull samples with different thicknesses.

Results: We have experimentally measured the response curve and inverted the reflectance function for the plastic samples. The traces of the minima on the spectrum of reflectance function perfectly matches the theoretical dispersion curve of each sample. The experimental result for the 6mm HDPE sample is presented in Figure 2. The amplitude of the reflectance function is further analyzed to calculate the longitudinal and shear velocities and attenuation for each sample. These results are consistent with the reported numbers in the literature and present a better confidence interval in the estimates. Measurements on human skull samples with different thicknesses illustrate unique features that represent different modes of Lamb wave propagating in the samples (Figure 3); however, due to the high attenuation these features tend to smooth out. Our numerical simulation results suggest designing the system at frequency of 500 kHz for a more accurate measurement of acoustic properties for skull.

Conclusions: Our experimental results demonstrate the promise of the acoustic microscopy technique for in-situ characterization of skull. The present technique directly measures acoustic properties including both shear and longitudinal speed of sound and attenuations for attenuative samples in a simple way, where the spectrum of the reflectance function is obtained in a single scanning measurement. Moreover, this system can be cost-effective and portable, paving the path for future point-of-care ultrasound treatments such as neuromodulation or BBB opening.

Figure 1. Schematic diagram of experimental setup for acoustic microscopy to characterize the skull, illustrating Lamb wave modes excitation at different angles

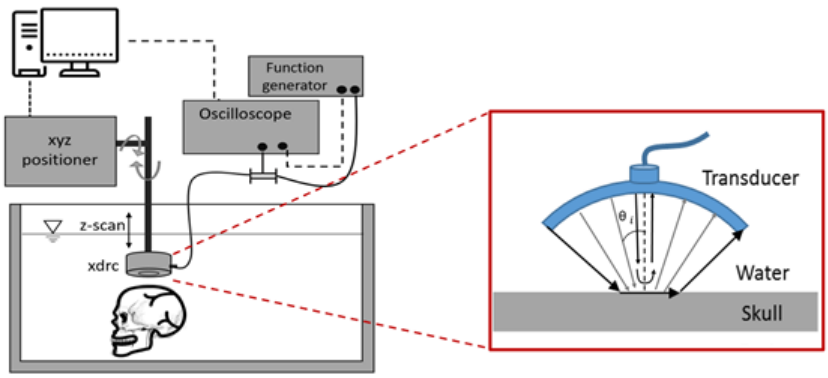

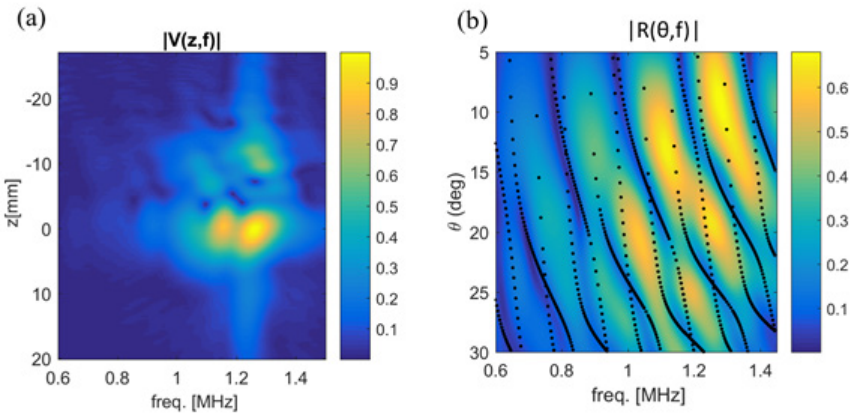

Figure 2. Experimental results, (a) the response curve, and (b) the spectrum of inverted reflectance function of the 6 mm thick HDPE plate, and the theoretical dispersion curve of the sample in vacuum is shown in black dots

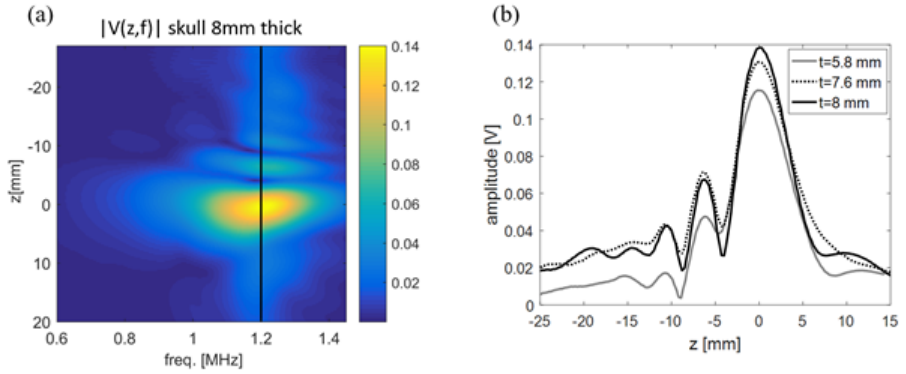

Figure 3. (a) Response curve spectrum of the 8mm thick skull sample, (b) response curves of skull samples with different thicknesses measured at frequency of 1.2 MHz

P-MSK-5

Topic: Musculoskeletal
Presentation Type: Poster

Design of a focused ultrasound system for the non-invasive treatment of injured tendons

Chitra Meduri[1], Alex Simon[1], Lance De Koninck[1], Mela Coffey[1], Eliette Claros[1], Mariah Velazquez[1], P. Gunnar Brolinson[2], Bradley McCrady[2], Eli Vlaisavljevich[1], Vincent M. Wang[1]

[1]Virginia Tech, Blacksburg, VA, USA
[2]The Edward Via College of Osteopathic Medicine, Blacksburg, VA, USA

Background: Tendinopathy is a degenerative condition characterized by collagen disorganization and altered matrix composition, attributable to aberrant cellular responses. Currently, rehabilitative strategies (eccentric loading exercises) are among the few effective long-term therapies for pain mitigation and restoration of tendon function. While non-invasive mechanical loading from therapeutic ultrasound treatment has shown promise in accelerating tendon healing, the low intensities used in such therapies result in modest improvements in healing. Very few studies have explored the use of focused ultrasound (FUS, using much higher ultrasonic intensities) for tendon healing. Therefore, the current study was designed to develop a custom, single element transducer system to precisely target and treat injured Achilles tendons in a pre-clinical mouse model.

Materials and Methods: Our objective is to utilize FUS for treatment in our established murine Achilles tendinopathy model. The primary design targets were an applied radiation force of 0.6N (i.e., ~5% of failure load), peak frequency of 1MHz and a desired treatment volume consistent with the tendon dimensions (Figure 1). Two transducers were built, consisting of 32mm piezoelectric elements, with 30mm and 50mm focal lengths and 1.1MHz frequency. The efficacy of element construction was validated using impedance and beam profile tests which determined the focal zone and maximum pressure profiles achieved by the transducer. Alignment tests were performed to ensure that the desired pressure was applied at the focal point of the treatment area. Upon verification of design functionality, CAD models of the experimental setup were designed.

Results: Impedance tests for both elements showed the frequency curves beginning near infinity, peaking at 1.2MHz and slowly reaching zero. Since the resonant frequency of the piezoelectric elements used was 1.1MHz, the peak frequency test was verified to be accurate. Beam profiles of the transducer were successfully verified using a hydrophone (HNR-500, Onda) in a degassed water tank (Figure 2). Plots of pressure versus distance in x, y and z directions confirmed peak values at the home position (x = y = z = 0, corresponding to thickness, width and length of tendon, respectively) (Figure 3).

Conclusions: The robust experimental setup presented herein appears to be highly suitable for targeted treatment of murine tendon. Using this design, we plan to study thermal and mechanotransduction bioeffects of FUS on injured Achilles tendons (Figure 4). In addition to verifying that mice can well tolerate FUS treatment, we will evaluate tendon biomechanical and structural properties, as well as cellular responses to assess efficacy of the treatment. Using this setup with a custom high frequency imaging system (Daxsonics), the thermal and mechanical effects of FUS on tendon healing can be studied, which is otherwise not possible using commercially available ultrasound systems.

Acknowledgements: This investigation was supported by a grant from The Edward Via College of Osteopathic Medicine (VCOM) and Institute for Critical Technology and Applied Science (ICTAS) at Virginia Tech.

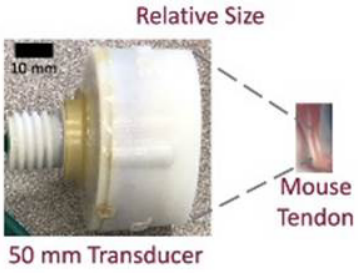

Figure 1: Focal zone encompassing mouse Achilles tendon dimensions.

Figure 2: Beam profile testing using a hydrophone in a degassed water tank to determine focal zone and peak pressures.

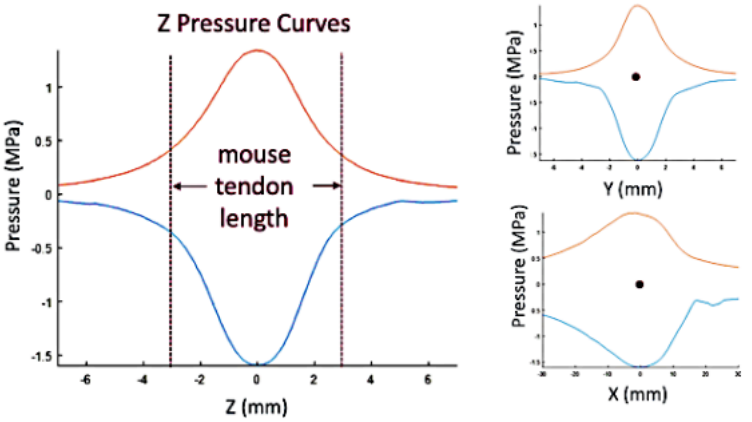

Figure 3: Pressure curves in the Z (left), Y (right, top) and X (right, bottom) directions in a beam profile test. Z curve indicates that the applied pressure spans the entire length of the tendon.

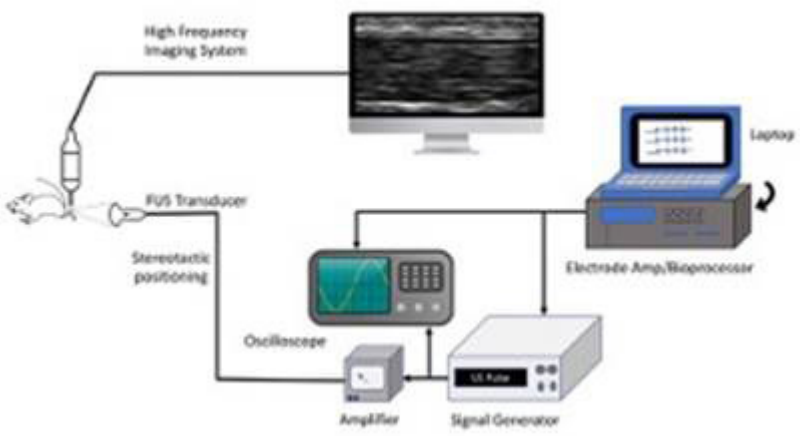

Figure 4: Schematic of our custom-built small animal FUS system allowing interchangeable transducers and driving systems (for different FUS exposures) attached to a high frequency imaging system.

P-MSK-6

Topic: Musculoskeletal
Presentation Type: Poster

Focused ultrasound for the remote modulation of nitric oxide release from injectable composite hydro-gels

Kaylee Meyers[1], Rupak Rajachar[1], Eli Vlaisavljevich[2]

[1]Michigan Technological University, Houghton, MI, USA
[2]Virginia Tech, Blacksburg, VA, USA

Background: Minimally invasive injectable hydrogels composed of polyethylene glycol (PEG)-fibrinogen and S-Nitroso-N-acetyl penicillamine (SNAP)-fibrin μ-particles that have the capability to release nitric oxide (NO) provide an innovative approach to accelerating wound repair in tendon related injuries by regulating extracellular matrix (ECM) turnover via NO presentation. Since the delivery of NO from the SNAP-fibrin μ-particles can be modulated with thermal and mechanical stimulus this work investigates the ability of focused ultrasound (FUS), an ideal combination of these stimuli, to elicit the remote spatial and temporal controlled release of NO.

Materials and Methods: To evaluate the potential of FUS to elicit thermally and/or mechanically induced NO release from SNAP-fibrin μ-particles, a nitrite quantification assay (Griess assay) was used to test thermal release from μ-particles and μ-particles incorporated in hydrogel matrices as an indirect means of determining NO concentrations. A FUS targeting system was then assembled with a 700kHz Histosonics transducer, amplifiers and circuit boards, and 3D printed ultrasonically conductive sample holders. FUS treatment parameters (i.e. duty cycle, peak negative and positive pressures, etc.) were adjusted to optimize the thermally induced release of NO from SNAP-fibrin μ-particles and thermocouples were utilized to quantify the heating effects of different FUS treatment parameters and durations on samples.

Results: Results indicate that both SNAP-fibrin μ-particles and hydrogels containing SNAP-fibrin μ-particles incubated at 37°C for 1.5 hours released significantly higher amounts of NO when compared to similar samples incubated at 20°C (Fig. 1 A, B, and C). Thermocouple measurements were taken with sample holders filled with PBS (Fig. 2 A). The targeted well (2-4) was warmed for 3 minutes and treated at approximately 41°C for 5 minutes with FUS. A control probe was placed in the water tank outside of the sample holder. Results indicate tight spatial and temporal control of FUS treatment targeting as indicated by the near instantaneous transition between warming, treatment, and cooling phases as well as minimal heating of surrounding wells in the sample holders (Fig. 2 B). Current studies are in progress to fully characterize thermally induced NO depletion of SNAP-fibrin μ-particle with FUS.

Conclusions: In this work, a FUS system was used to evaluate the ability of FUS to remotely modulate NO release from injectable composite hydrogels. Future studies will explore the in vitro and in vivo feasibility of using this FUS stimuli-responsive platform for enhancing tendon repair via reestablishing the balance in ECM synthesis and degradation with controlled NO release.

Acknowledgements: This work was supported in part by grants from the NIH (award numbers R15-GM112082 and R15GM137298) and a Focused Ultrasound Foundation (FUSF) Global Internship (KMM). The authors would also like to thank Alex Simon for assistance with FUS systems and Dr. Hal Holmes for help in designing the sample holders.

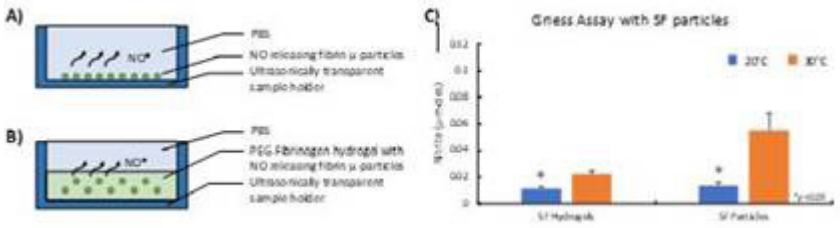

Figure 1. (top) SNAP-fibrin particles were placed in the custom sample holder (A-B) and incubated for 1.5 hours. Griess assay results indicated significantly higher NO release from 37°C samples (C) ($p<0.05$).

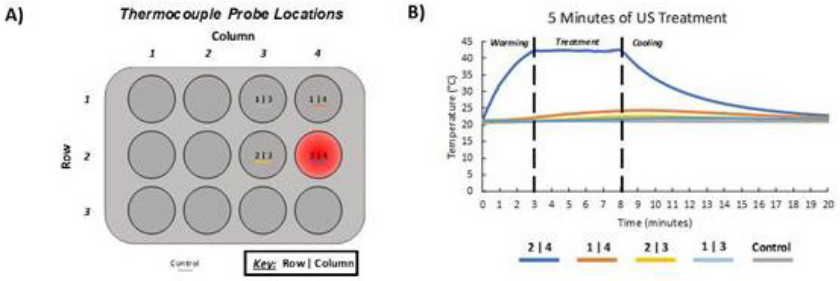

Figure 2. (bottom) Thermocouples were inserted in the wells of the sample holder and the FUS targeted well (2-4) was warmed for 3 minutes and treated at approximately 41°C for 5 minutes (D-E).

P-MSK-7

Topic: Musculoskeletal
Presentation Type: Poster

Histological examination of focused ultrasound disruption of ex vivo tendons

Molly Smallcomb, Jacob Elliott, Sujata Khandare, Ali Butt, Meghan Vidt, Julianna Simon

Pennsylvania State University, University Park, PA, USA

Background: Tendon injuries comprise 45% of the 66 million musculoskeletal injuries each year with an annual cost of $114 billion. Conservative therapies to treat injured tendon, such as dry needling, produce microtrauma in the tendon matrix to induce a healing response, but success rates are mixed. Focused ultrasound has the potential to noninvasively create microtrauma in the tendon through the creation, oscillation, and collapse of bubbles; it may also improve collagen alignment. However, highly collagenous tissues, like tendon, have shown resistance to the mechanical disruption from focused ultrasound. Our objective here is to histologically evaluate whether mechanical disruption by focused ultrasound is achievable without thermal denaturation in rat tendons.

Materials and Methods: Achilles tendons (AT) and supraspinatus tendons (ST) were extracted from Sprague Dawley rats and immersed in a degassed, deionized water tank for ex vivo experimentation. Four groups (n=5/group for each tendon type) were exposed to 1.5 MHz focused ultrasound pulses with peak pressures of p+ = 69 MPa and p- = 24 MPa with 0.1-10 ms pulses repeated at 1-100 Hz for 15-60 s; sham treatments were conducted in 5 tendons of each type. A research ultrasound system (Vantage, Verasonics, Kirkland, WA) and ATL P4-2 transducer was used to monitor for hyperechogenicity, or bubble activity, during the treatment. Tendon samples were frozen fixed and stained with Hematoxylin and Eosin (H&E) for cellular morphology analysis and alpha-nicotinamide dinucleotide diaphorase (αNADH-d) for enzymatic activity analysis.

Results: B-mode ultrasound showed focal hyperechogenicity for all treated samples; however, not all samples showed histological evidence of injury. Of those samples showing injury, shorter pulse lengths at higher pulse repetition frequencies (PRFs) delivered for 60 s resulted in localized tendon fiber disruption in 2/5 AT and 1/5 ST samples for 0.1 ms at 100 Hz, or 3/5 AT and 1/5 ST samples for 1 ms at 10 Hz (Fig. 1). When the pulse length increased to 10 ms at 1 Hz with a reduced treatment time of 15 s, only slight localized fiber disruption was observed with no evidence of thermal injury in 2/5 AT and 2/5 ST samples (Fig. 2). Upon increasing the treatment time to 30 s (10 ms pulses at 1 Hz), focal injury was observed in 4/5 AT and 3/5 ST samples, with focal coagulative necrosis in 1 of AT and 3 of ST samples (Fig. 3). There were no marked differences between the injury types observed between the AT and ST samples. No histological evidence of injury was observed in sham samples.

Conclusions: Presence of hyperechogenicity in B-mode imaging showed bubbles were successfully created in tendons; however, the presence of bubbles did not always equate to histologically detectable injury. When treatment time was increased, thermal injury dominated over mechanical effects. It is unclear why some samples treated with the same parameters showed injury whereas others did not. It is possible signs of injury were occluded by artifact from the histological processing. Future work includes investigating how focused ultrasound influences the mechanical properties of tendon and investigating whether focused ultrasound induces a healing response in in vivo rat tendons.

Acknowledgements: Work supported by NIH NIBIB EB027886, and NSF GRFP DGE1255832 (Smallcomb)

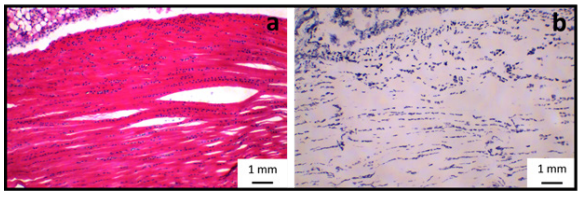

Figure 1. 4/10 samples exposed to 1 ms pulses repeated at 10 Hz for 60 s showed detectable damage as localized fiber separation, indicated in spacing between fibers in both a) H&E staining and b) NADH staining.

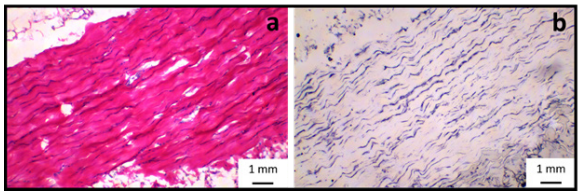

Figure 2. 4/10 samples exposed to 10 ms pulses repeated at 1 Hz for 15 s showed localized fiber disruption shown as disruptions to the fiber pattern in a) H&E staining; b) NADH staining shows no thermal injury.

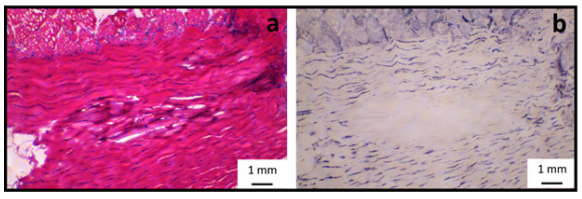

Figure 3. 3/10 samples exposed to 10 ms pulses repeated at 1 Hz for 30 s showed focal coagulative necrosis indicated by an eosinophilic (darker pink) area in a) H&E staining and b) lack of NADH stain uptake.

P-MSK-8

Topic: Musculoskeletal
Presentation Type: Poster

Standardised method to calibrate multivendor MR-HIFU systems used in randomised controlled trial of bone pain palliation study

Janina Strobel, Lukas Sebeke, Edwin Heijman, Holger Grüll

University of Cologne, Cologne, Germany

Background: The European Union funded project "FURTHER" is the first randomised controlled multicentre trial which compares efficacy of radiation therapy to MR-HIFU and the combination of both for pain alleviation in patients suffering from bone metastasis. As MR-HIFU systems from two different vendors are used and treatment protocols differ, we developed a standardised method consisting of a phantom, sonication protocol and temperature mapping sequence to compare and standardise the MR-HIFU treatment protocols across sites and vendors.

Materials and Methods: The phantom consists of a high temperature-resistant polyurethane-based polymer embedded in a polyacrylamide hydrogel (Figure 1A). The phantom was positioned on a Sonalleve MR-HIFU tabletop (Profound Medical) and sonicated multiple times varying acoustic output power and sonication time as well as treatment cell size. During each sonication temperature maps were acquired and analysed to obtain different parameters. To investigate the effect of the different heating strategies (on target vs. behind target) the focal spot was positioned on the surface of the absorber or behind the absorber.

Results: Figure 1B shows comparable mean temperature elevation of 8mm sonication cell (40W, 20s, 1.2MHz) repeated 20 times over a period of 11 weeks. No clinically relevant differences were found between the different heating strategies.

Conclusions: We demonstrated that the phantom is stable and allows repeatable and reproducible measurements allowing the comparison and eventual calibration of different MR-HIFU systems.

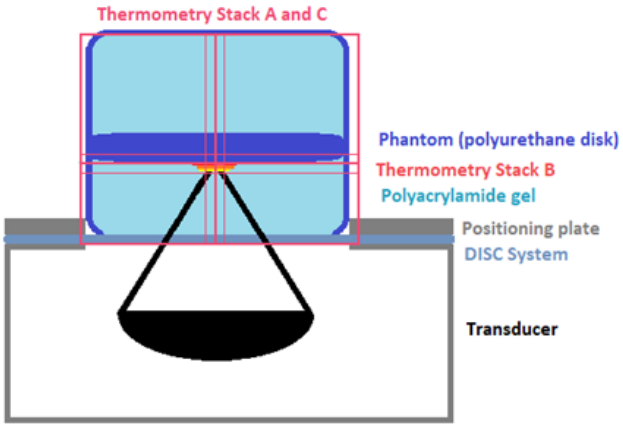

Figure 1A. Schematic model of the phantom

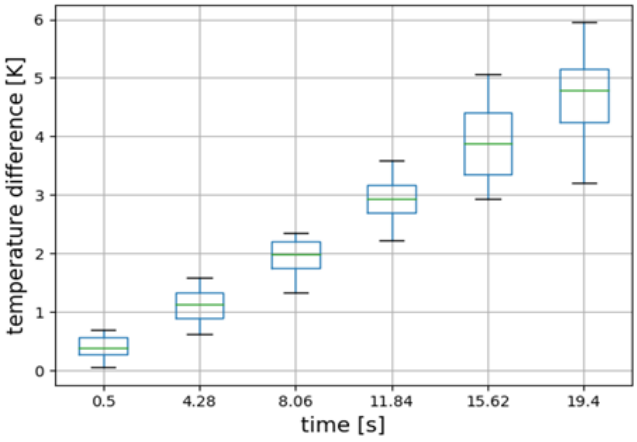

Figure 1B. Mean temperature elevation near the phantom (n=20 sonications over a time period of 11 weeks.

P-MSK-9

Topic: Musculoskeletal
Presentation Type: Poster

Sonication of the shoulder does not lead to dangerous heating

Norman M Spivak[1], Mark Cohen[1], Alexander Korb[1], Taylor Kuhn[1], Mark Schafer[2], Martin Monti[1]

[1]University of California, Los Angeles, Los Angeles, CA, USA
[2]BrainSonix, Ambler, PA, USA

Background: Prior work in the lab demonstrated the ex-vivo safety of transcranial focused ultrasound (tFUS) at intensities of up to Ispta.3 = 25 W/cm^2. As the skull attenuates up to 90% of the ultrasonic energy, we were concerned that the deposition of this energy would result in excessive heating and increase the potential for burns on the skull and skin surface. Because the scapula is, on average, double the thickness of the temporal squama, it would act as an excellent comparator for measuring tFUS-related heating.

Materials and Methods: Subjects were asked to lie supine on a bed. Three thermistors were placed on the subject's back: one over the left scapula, one over the right scapula, and one directly over the spine. Two identical transducers were placed: one on each scapula over the thermistor. The right scapula was the active one, while the left scapula and the spine served as controls. Temperature was measured for 10 seconds before, during, and after sonication. 5 sonications were performed at 5 Ispta levels: 6, 8, 10, 12, 14 W/cm^2. Each sonication lasted 60 seconds and used the following parameters: Pulse Duration=0.5ms, PRF= 100 Hz (5% Duty cycle).

Results: There was no significant relationship between tFUS intensity level and temperature change. The greatest demeaned temperature change was seen at Ispta= 12 W/cm^2 of 1.45 degrees Celsius. The safety cutoff, at which point the sonication would have been stopped and the subject dismissed, was 5 degrees Celsius. No subject exceeded this limit at any point during the study.

Conclusions: Because temperature change was not intensity-dependent, it is likely that there is a dynamic process that acts to carry away heat from the body surface-transducer interface. Regardless, no subject reported any sensations whatsoever during the study, and the heating was sufficiently minimal that it can be presumed non-significant and safe in future work.

Acknowledgements: Tiny Blue Dot Foundation

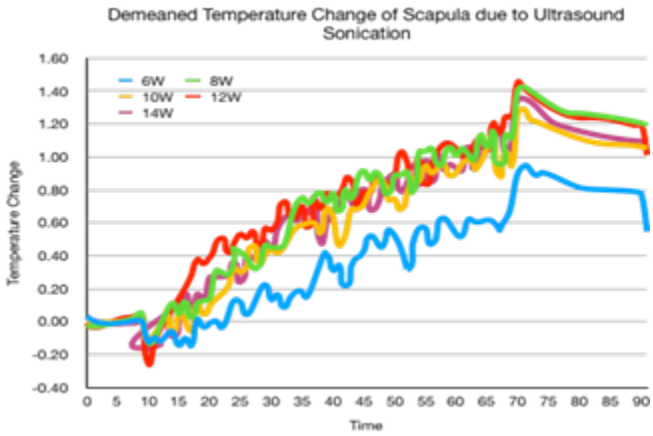

Figure 1. Demeaned Temperature of Scapula due to Ultrasound Stimulation

P-MSK-10

Topic: Musculoskeletal
Presentation Type: Poster

Influence of bone properties on transcranial propagation

David Moore[1], John Snell[1], Sylvain Chatillon[2], Cyril Lafon[3], Frederic Padilla[1]

[1]Focused Ultrasound Foundation, Charlottesville, VA, USA
[2]Commissariat à l'énergie atomique et aux énergies alternatives, Palaiseau, Île-de-France, France
[3]INSERM U1032, Lyon, France

Background: For transcranial focused ultrasound therapeutic, such as treatment of essential tremor via local thermal ablation of a small volume in the thalamus, acoustic energy is focused through the skull using a phased-array transducer. Per-element phase delay is derived using individual patient's skull CT to compensate for skull heterogeneity in geometry and acoustical properties, but MRI thermometry is still required for precise targeting and localization of the focal spot. An accurate simulation system would help to improve the refocusing of the beam in the targeted zones.

Through a parametric study, we investigated how variations of the acoustic properties of the skull, due to uncertainties of their estimates, may translates into errors in spatial positioning and focal gain at the treatment spot.

Materials and Methods: The parametric study examined the influence of density, speed of sound, attenuation, and fluid vs elastic models of the skull. The simulation method employed the CIVA Healthcare simulation platform – a software platform which uses dynamic ray tracing method to model linear acoustic propagation through the skull.

The transducer was modeled on an ExAblate Neuro 650 kHz (Insightec) clinical system.

Results: The results of the parametric simulation study indicate that the uncertainty in the acoustic properties of the skull determined from CT scans translate into significant errors in focalization quality for clinical applications. The disagreement among proposed relationships between density and acoustic velocity produces errors in the acoustic field up to 25%, as shown in Figure 2. Errors in spatial positioning were found to be less than 0.5mm for all values of density and velocity, as shown in Figure 3.

Conclusions: The result of the parametric study quantifies the sensitivity of focal intensity and position to uncertainty in acoustic properties of the human skull used for numerical simulations for transcranial applications. These findings illustrate the importance of accurately determining the relationship between density and acoustic velocity in ray-tracing models of transcranial ultrasound.

Acknowledgments: This work is supported by funding from the Focused Ultrasound Foundation.

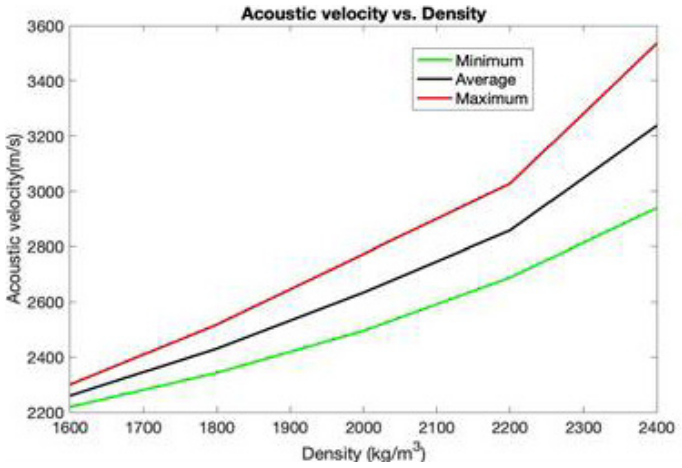

Figure 1. Range of predicted acoustic velocity as a function of density across all proposed models. Simulations were performed at all 3 velocity values in density intervals of 200kg per cubic metre, with the phase delay profile calculated based on the average acoustic velocity.

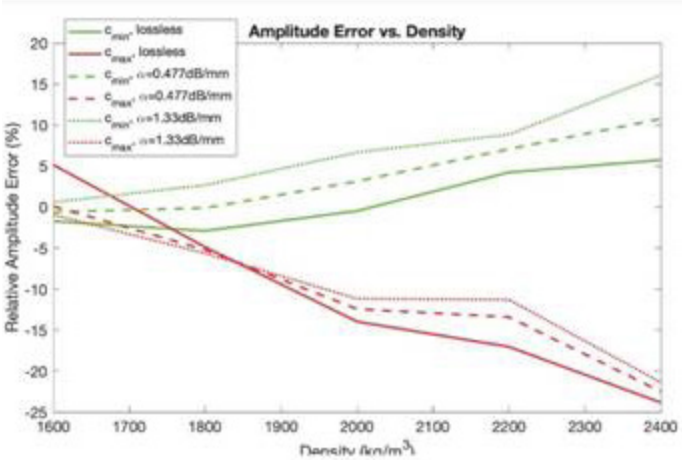

Figure 2. Amplitude error vs density, with three different values of attenuation: 0, 0.48 and 1.33 dB/mm, where the latter two values are average and maximum attenuative values for the skull. Amplitude error is calculated with reference to results from simulations performed with skull acoustic velocity equal to the average speed give Figure 1, which was used to determine the phase delay profile.

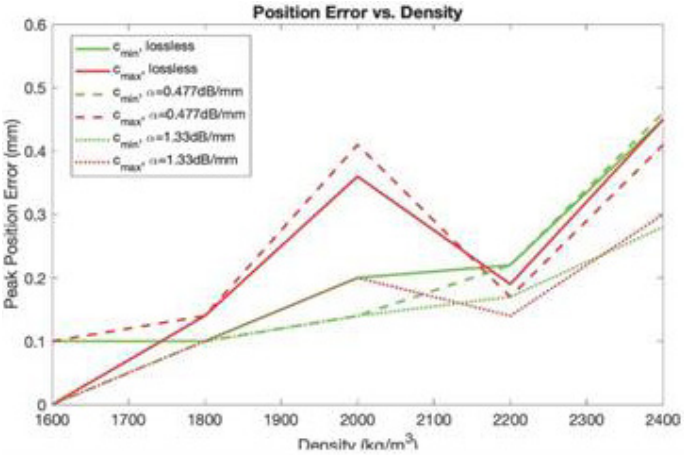

Figure 3. Peak position error vs density for various density values, with three different values of attenuation: 0, 0.48 and 1.33 dB/mm, where the latter two values are average and maximum attenuative values are average and maximum alternative values for the skull.

P-NDG-1

Topic: Neurodegenerative Disorders

Presentation Type: Poster

Towards treating MS and dementia with neuromodulatory ultrasound

Pierre Mourad

University of Washington, Seattle, WA, USA

Background: Multiple sclerosis (MS) and various forms of dementia (including Alzheimer's disease [AD]) represent important disease burdens, with the latter growing in prevalence as the world's population ages. There exist medications that partially ameliorate MS; none to date have had a meaningful impact on AD. Here we summarize published results that show that near-diagnostic ultrasound that activates central neurons can have a positive effect on these diseases - in mouse models thus far.

Materials and Methods: Regarding MS, we used a Cuprizone-based mouse model, where the copper in the cuprizone drove temporary demyelination of the mouse brain. Regarding AD, we used a common AD mouse model (5XFAD) that has within their brains an excess of human amyloid beta plaque (but not neurofibrillary tangles). We repeatedly applied, via transcranial exposure, near-diagnostic ultrasound to anesthetized mice in a way that produced during acute studies measurable EEG signals tied to the application of the ultrasound. After chronic application of the same mouse models for each of five days (30 minutes for MS mice; one hour per hemisphere for AD mice), we sacrificed the mouse for subsequent histological analysis.

Results: We observed a statistically significant acceleration of remyelination in a mouse model of MS. We observed statistically significant (a) acute activation of microglia that (b) after five days of application (one hour per application) reduced the amyloid beta plaque burden by ~50% in a mouse model of AD

Conclusions: transcranial ultrasound, without adjunctive agents of any sort, demonstrated improved histological structure of the brains of MS and of AD mouse models. Given the increased evidence for the safety of comparable ultrasound protocols, including after application to human brain, and given the near-diagnostic nature of these ultrasound protocols, we can anticipate eventual application of these protocols to patients with these diseases after optimization of their effects.

Acknowledgements: NIH 5R21EY027557-02

P-NDG-2

Topic: Neurodegenerative Disorders

Presentation Type: Poster

FUS-BBB opening for targeted delivery of Huntington's disease gene therapeutics

Nick Todd[1], Tao Sun[1], Jaymin Upadhyay[2], Kimberly Kegel-Gleason[3]

[1]Brigham and Women's Hospital, Boston, MA, USA
[2]Boston Children's Hospital, Boston, MA, USA
[3]Massachusetts General Hospital, Charlestown, MA, USA

Background: Huntington's disease (HD) is a devastating neurodegenerative disorder caused by a mutation of the huntingtin gene, which leads to production of the neurotoxic mutant huntingtin protein (mHtt). Accumulation of mHtt occurs in several cell types throughout the brain, leading to the onset of motor and cognitive deficits in middle age, and ultimately death. Gene therapies aimed at lowering the expression level of mHtt offer the possibility of treating HD at its source. Micro-RNA (miRNA)-based and antisense oligonucleotides (ASO)-based gene therapies have entered clinical trials, but neither cross the blood-brain barrier (BBB) and so are delivered either by direct neurosurgical injection or intrathecal injection.

Here we demonstrate the ability of focused ultrasound (FUS)-BBB opening to improve the brain penetrance of systemically injected adeno-associated virus (AAV) vectors, with the goal of delivering a miRNA-HTT construct for lowering mHtt expression levels in a mouse model of HD.

Materials and Methods: Study 1: FUS parameter optimization. AAV1 carrying green fluorescent protein (AAV1-GFP) was injected via tail vein to N=17 wild type mice at a dose of 5.5e11 vg/mouse (2.2e10 vg/g). FUS-BBB opening was targeted to the right striatum at three pressure levels (0.32/0.36/0.40 MPa) and two microbubble doses (Optison, 100/200 μL/kg). BBB disruption was assessed by contrast MRI immediately after FUS sonication and AAV distribution was assessed by fluorescence imaging and cell type staining 3 weeks later.

Study 2: AAV delivery in HD model mice. AVV1-GFP or AAV9-GFP was injected via tail vein to the YAC128 mouse model of HD (N=23). FUS-BBB opening was targeted to the right striatum at the optimized FUS parameters of 0.32 MPa pressure and 200 μL/kg microbubble dose. BBB disruption was assessed by contrast MRI and AAV distribution will be assessed by immunohistochemical staining and immunofluorescence imaging.

Results: Control results from Study 1 are shown in Figure 1, where it is confirmed that it is only the combination of focused ultrasound BBB-opening with AAV1-GFP injection that leads to successful transduction.

Figure 2 shows the results from the FUS parameter optimization study. BBB opening, as determined by contrast MRI, exhibited the expected pattern of stronger opening at higher pressures and larger microbubble doses. The AAV1-GFP distribution did not follow the same pattern. Based on the uniform distribution and spread to the contralateral hemisphere, we concluded that the optimal FUS parameters were 0.32 MPa and 200 μL/kg microbubble dose.

Figure 3 shows example contrast MRI images from the initial results of Study 2. No significant differences were seen in the extent of BBB opening in the YAC128 HD model mice compared to wild type mice undergoing FUS-BBB opening with the same FUS parameters. The analysis of GFP signal distribution by fluorescence imaging is currently being performed.

Conclusions: FUS-BBB opening enhances the penetrance of AAV vectors into the mouse brain. Initial results suggest that delivery of a gene therapy can be safely achieved with this approach in both wild-type and HD model mice under the same set of FUS parameters. These results will form the basis of our next study, which will be to use a micro-RNA delivered in an AAV9 vector, ss-AAV9-miRNA-HTT-GFP, to target knockdown of the HTT protein.

Acknowledgements: NIH grant K01EB023983, The Hereditary Disease Foundation, The Brigham Research Institute.

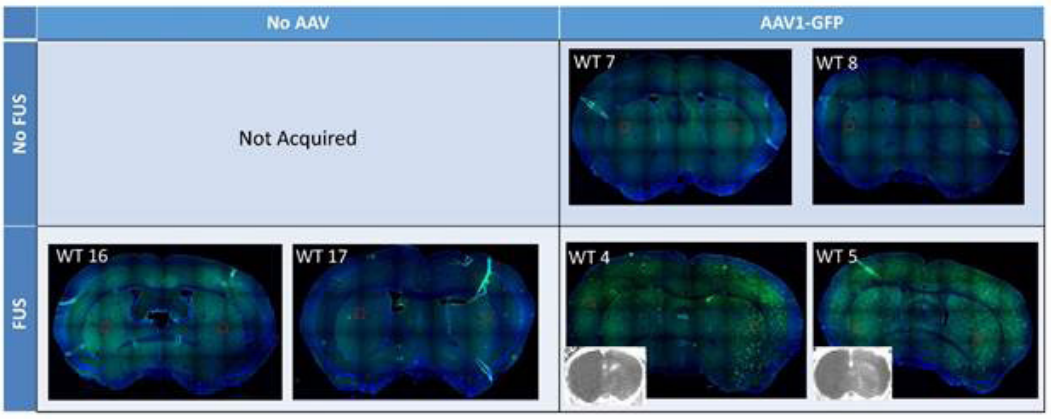

Figure 1. Fluorescent images showing extent of AAV1-GFP transfection under three conditions: FUS alone, AAV1-GFP injection alone, FUS + AAV1-GFP injection (N=2 mice per condition).

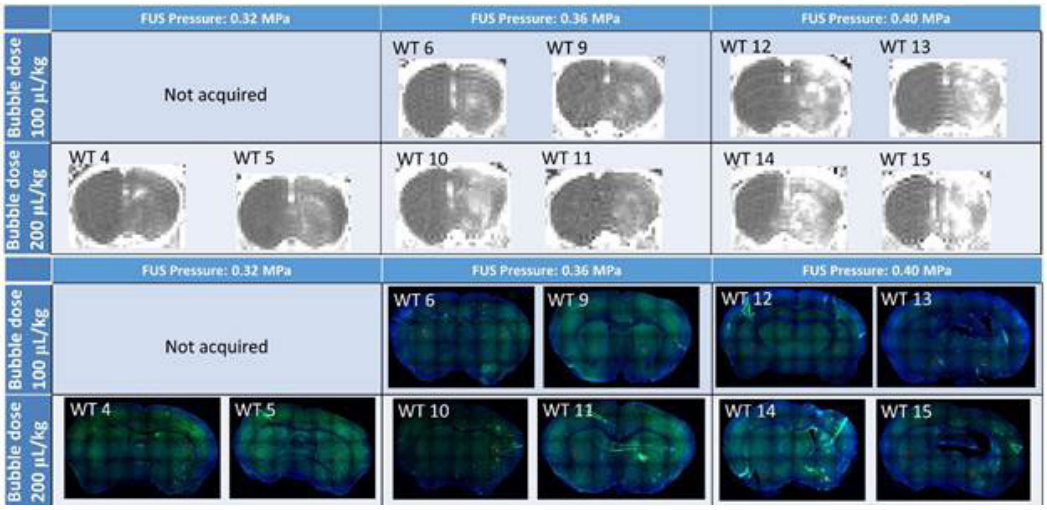

Figure 2. Optimization of focused ultrasound parameters for delivery of AAV1-GFP. Top images show contrast MRI images immediately after FUS-BBB opening; bottom images show GFP fluorescence.

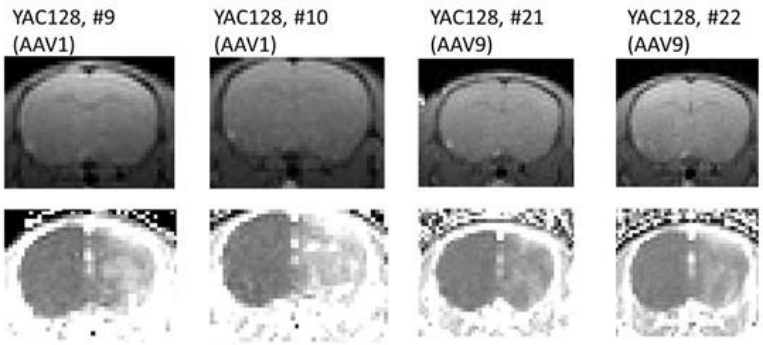

Figure 3. MRI images from four representative YAC128 mice after focused ultrasound BBB opening. Top row shows brain anatomy on T1-weighted images, bottom row shows contrast images depicting BBB opening.

P-NMD-1

Topic: Neuromodulation
Presentation Type: Poster

Transcranial multifocal acoustic holograms

Diana Andrés, Sergio Jiménez-Gambín, Noé Jiménez, Francisco Camarena Femenía

Universitat Politècnica de València, Valencia, Spain

Background: Focused ultrasound have shown great efficacy in the treatment of many neurological disorders. Through thermal ablation of thalamic and subthalamic areas, treatments have been developed for essential tremor, Parkinson's disease or chronic pain, while at moderate intensity they are used for neuromodulation or blood-brain barrier opening to deliver drugs in a safe and localized manner.However,focusing therapeutic ultrasound into the central nervous system has been limited by two major drawbacks: the aberrant and attenuating effects of the skull and the large mismatch between the volume of the brain structure to be treated and the volume of the ultrasonic beam focus, which forces multiple sonications to cover the desired area. In addition, current technology does not allow the simultaneous sonification of two or more spatially separated volumes.In this work, we present a method based on 3D-printed acoustic holograms to generate multifocal ultrasound beams which match the target structures.

Materials and Methods: Holograms were designed to cover bilateral targets in one single sonication, while minimizing the acoustic field outside. Three experiments were performed, each one corresponding to a different bilateral target: left-and-right hippocampi, putamen, and caudate nuclei, as sketched in Fig. 1(a). The volume of each bilateral target was segmented from MRI images. Then, time-reversal simulations were performed from the selected targets inside the skull towards the location of the ultrasound transducer using CT images of an ex-vivo human skull and pseudo-spectral time-domain methods. The holographic information at 500 kHz was recorded at source location and a phase-only lens based on Fabry-Perot resonators was designed using phase-conjugation methods. The holographic lenses were manufactured with resin photopolymer (FLGPCL04, Formlabs) using stereolithography with a resolution of 50 μm (Form2, Formlabs). The lenses were adapted to a custom 500-kHz piezoelectric focused transducer with an aperture of 100 mm and a focal length of 140 mm. The acoustic field was measured inside an ex-vivo human skull using a needle hydrophone with an active diameter of 500 μm (HNR-500, Onda) and a 3D stepper motor (L-511 PI GmbH) to move the hydrophone using a step of 0.1 mm. A 3D printed support with columns matching the surface of the skull was manufactured to guarantee the relative location between the lens and the skull, as show in Fig. 1(b).

Results: First, left-and-right hippocampi is selected as therapeutic targets, Fig. 2(a). First, left-and-right hippocampi is selected as therapeutic targets, Fig. 2(a). The acoustic field measured experimentally agrees with theory and simulations both in water and considering the skull. The segmented volume of the target is 22.84 mm3. The total sonicated volume, defined as the volume were the pressure is higher than half the peak pressure, is 5.05 mm3, corresponding to 22 % of the selected target volume. Similar results are observed when targeting at putamen, Fig. 2(b), with a volume of 14.48 mm3, and where transcranial focusing using holograms covers a volume of 3.4 mm3 (25 % of the target volume). For the caudate nuclei, Fig. 2(c), with a volume of 16.35 mm3, the sonicated volume is 3.85 mm3 (24 % of the target volume). The emitter-lens system is located always located at center of the parietal-occipital area, demonstrating the steering capabilities of transcranial holograms.

Conclusions: Using acoustic holograms coupled to ultrasonic transducers the shape of the acoustic field can be adapted to complex therapeutic targets in a simple and robust manner. Acoustic holograms compensate the aberrations of the wavefront produced by the skull while, simultaneously, allow bilateral sonications whose acoustic field fits to deep-brain structures such hippocampi, putamen or caudate nuclei. In this work, numerical and experimental results show that more than 20 % of the volume of bilateral targets inside the brain can be covered with a single configuration. Furthermore, the steering capabilities of the acoustic holograms have been demonstrated by focusing at three different structures using one single transducer-skull position.

Acknowledgements: This research has been supported by the Spanish Ministry of Science, Innovation and Universities (MICINN) through grant "Juan de la Cierva - Incorporación" (IJC2018-037897-I) and PID2019-111436RBC22, by the Agencia Valenciana de la Innovació through grants INNVAL10/19/016 and INNCON/2020/009. Action cofinanced by

the European Union through the Programa Operativo del Fondo Europeo de Desarrollo Regional (FEDER) of the Comunitat Valenciana 2014-2020 (IDIFEDER/2018/022).

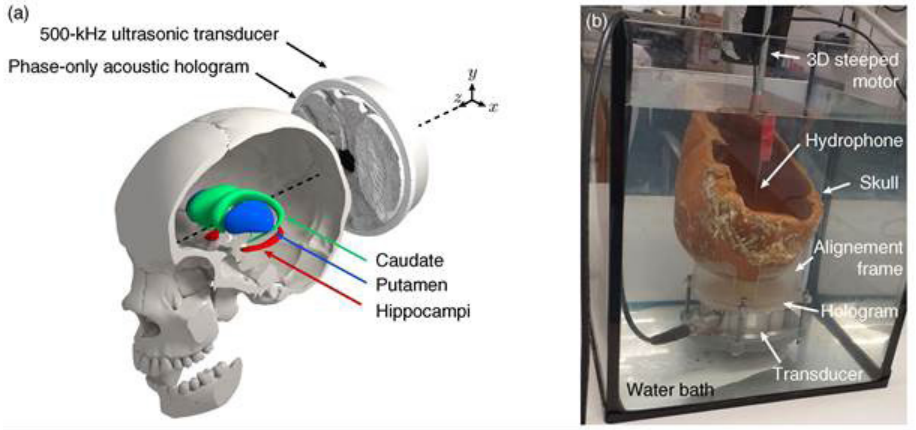

Figure 1. (a) Diagram of the CNS organs to be treated within of the skull and the location of the transducer with the lens to focus the putamen. (b) Experimental setup for the acoustic field measurement.

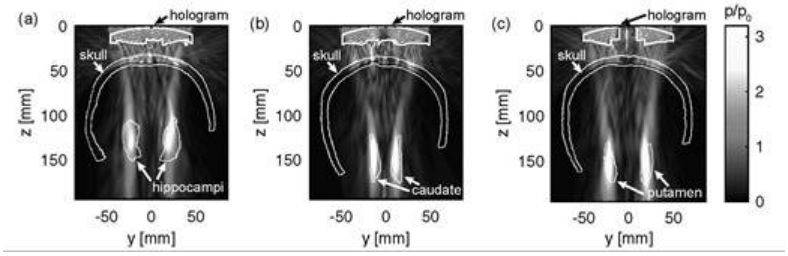

Figure 2. (a) Acoustic field focused at both hippocampi simultaneously. (b) Acoustic field focused at both caudate nuclei. (c) Acoustic field focused at both putamen nuclei.

P-NMD-2

Topic: Neuromodulation
Presentation Type: Poster

Biophysical mechanisms of focused ultrasound neuromodulation

Hongchae Baek[1], Yaoheng Yang[1], Christopher Pacia[1], Lu Xu[1], Yimei Yue[1], Michael R. Bruchas[2], Hong Chen[1]

[1]Washington University in St. Louis, St. Louis, MO, USA
[2]University of Washington, Seattle, WA, USA

Background: Great progress has been made in developing and applying focused ultrasound (FUS) neuromodulation technique, but at the same time researchers have noticed the multifaceted and low-replicability characteristics of this technique. In efforts to elucidate its mechanism, investigators have been categorizing biophysical effect of FUS into dichotomy: mechanical and thermal. However, there might be no clear distinction as thermal effect inevitably accompanies mechanical effect of FUS, and even nonsignificant temperature rise might also affect biophysical mechanisms of neural tissue. The objective of this study was to better understand the biophysical mechanisms of FUS neuromodulation by comparing mechanical and mechanothermal effects of FUS in inducing motor response.

Materials and Methods: Wildtype mice (n = 32) were divided into two FUS parameter groups: short-sonication duration for the mechanical group, and long-sonication duration for the mechanothermal group. FUS pulsing parameters for the mechanical group were as follows: 1 MHz center frequency, 50 % duty cycle, 10 Hz pulse-repetition frequency, 0.3 s sonication duration, 5 s inter-stimulus interval, and four levels of Isppa (4.1, 7.8, 14.0, and 22.7 W/cm2). Mechanothermal group extended sonication duration and inter-stimulus interval to 15 s and 80 s respectively, and kept all the other parameters the same (Fig 1). The anesthetic depth was controlled at the optimal level through electrocardiographic (ECG) monitoring to facilitate the induction of FUS-mediated motor responses. Pulsed FUS stimulation targeted at the deep cerebellar nucleus (DCN) to induce tail motor response, as recorded by tail electromyography (EMG) and tail movement. We estimated EMG latency as the elapsed time from FUS onset to where EMG signal reached the threshold (3 x standard deviation of the baseline). The EMG amplitude (root mean square) from each stimulus was normalized by EMG amplitude acquired from pre-stimulation baseline. The success rate of EMG induction for each mouse was calculated as the percentage of successful EMG elicitation out of total 10 repeated stimulations in the mechanical and 5 stimulations in the mechanothermal group. The target tissue temperature was measured by in vivo magnetic resonance (MR) thermometry.

Results: In the mechanical group, one EMG was elicited from one stimulus; however, the mechanothermal group showed one or two EMG (short-latency and long-latency EMG) from one stimulus (Fig2. A, B). The latency of short-latency EMG (0.2 ± 0.1s–1.4 ± 0.9s) was not statistically different from that of the mechanical group (39.6 ± 8.6ms–132.4 ± 54.2ms). However, the latency of long-latency EMG was statistically longer than that of the short-latency EMG as well as that of the mechanical group at 7.8, 14.0, and 22.7 W/cm2. The amplitude of long-latency EMG was statistically higher than that of mechanical group at 14.0 and 22.7 W/cm2. The threshold for near 100% EMG success rate in the mechanical group was at 22.7 W/cm2 for 96.6 ± 2.3%, whereas the threshold for 100% success rate at the mechanothermal group was at 4.1 W/cm2. Tail response rate reached 100% at 14.0 W/cm2 in mechanothermal group, whereas the highest response rate in the mechanical group was at 22.7 W/cm2 for 48.8 ± 14.0% (Fig2. C, D).

Conclusions: This study compared motor response evoked by FUS neuromodulation under mechanical and mechanothermal mechanisms. The short-latency mechanothermal EMG was not significantly different from that of the mechanical group in most comparisons of EMG indexes implying that mechanical effect could be the dominant mechanism for the short-latency EMG in the mechanothermal group. Also, short-latency EMG showed maximum amplitude and success rate at 14.0 W/cm2 with 3.3 ± 0.9°C of temperature rise which is lower than at 22.7 W/cm2 with 3.9 ± 0.4°C. Future study is needed to further investigate the mechanothermal mechanism of FUS in the neural tissue for synergizing both mechanical and thermal effects of FUS into a FUS-mediated neuromodulation therapy.

Acknowledgements: This work was supported by the National Institutes of Health (NIH) grants R01EB027223 and R01MH116981.

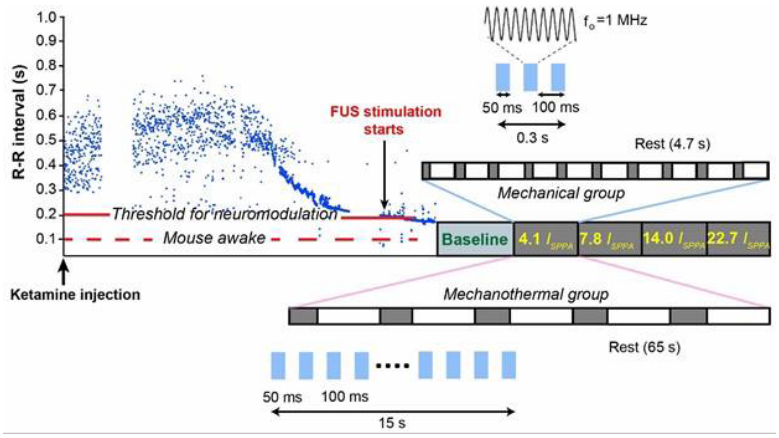

Figure 1. Experimental procedure. Sonication procedure for both mechanical and mechanothermal groups. Anesthesia depth was monitored by R-R interval in ECG recording.

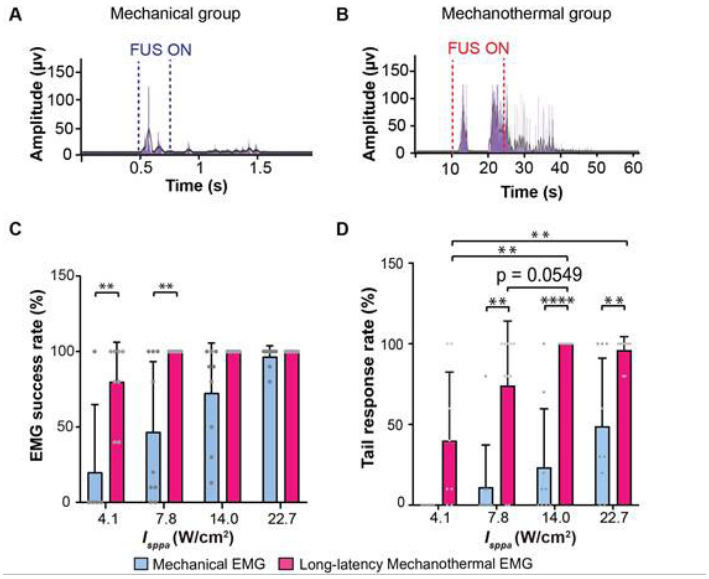

Figure 2. Comparison of EMG signals and tail movement between the mechanical and mechanothermal group.

P-NMD-3

Topic: Neuromodulation
Presentation Type: Poster

Transcranial brain focused ultrasound of anesthetized mice reversibly modulates cardiac and respiratory activity

Ethan Bendau, Hermes Kamimura, Christian Aurup, Elisa Konofagou

Columbia University, New York, NY, USA

Background: Numerous in vitro neuronal studies have shown that temperature changes are associated with modulation of excitability and can result in spontaneous firing. We have previously reported that pulsed transcranial focused ultrasound (FUS) can induce motor and sensory evoked responses, indicating its potential as a modulator of neural excitability in vivo. Thermal modulation of the central nervous system (CNS), more specifically of the autonomic regulation system, via FUS has, however, been largely unexplored. In this study, low-intensity FUS was used to produce focal temperature rise in the brain of anesthetized mice while monitoring heart and respiratory rates. The regulation of autonomic activity using FUS has not been previously demonstrated and we have shown that it can be used to transiently control heart and respiratory rate.

Materials and Methods: A single-element, 2 MHz FUS transducer (focal size: 1 mm lateral by 8.5 mm axial) was used with continuous-wave transmission to sodium pentobarbital-anesthetized wild-type C57BL/6 mice in brain regions related to arousal as well as thermal and autonomic regulation (thalamus, hypothalamus). The transducer was pulsed at 50% duty cycle with a pulse duration of 120 s until the mouse showed signs of alertness. Heart rate (HR) and respiratory rate (RR) were monitored via pulse oximetry. FUS pressure fields within the mouse skull anatomy derived from a micro-CT scan (520x520x520 grid size, 0.08 mm/pixel, ~5 scatterers per wavelength) were calculated in k-wave [1] (, an open-source MATLAB toolbox designed for acoustic simulations (MATLAB, MathWorks, Natick, MA). Density and speed of sound values for the simulated propagation medium were derived by converting Hounsfield units to density in kg/m^3. The bioheat equation function was then solved to compute the temperature profile at pressures ranging within 0.43-1.2 MPa. Simulation findings were validated using a thin needle thermocouple inserted in the sub-arachnoid space during 120-s continuous-wave FUS at each pressure. Sonication of a motor-related region encompassing the primary motor cortex (M1) and caudate putamen (CP) was used as a negative control.

Results: FUS at 0.43 MPa, 0.85 MPa, and 1.2 MPa resulted in respective peak temperature rise of approximately 0.6°C, 1.7°C, and 3.3°C sustained during 120 s at the focal region as estimated in simulations. During FUS (shaded region) of the thalamus/hypothalamus both the heart rate (HR) (Fig. 1a) and respiratory rate (RR) (Fig. 1b) increased steadily with pressure (2-5% ΔHRmax and 5-15% ΔRRmax). FUS in the negative control regions resulted in minimal changes in vital signs, despite similar temperature increase.

Conclusions: In conclusion, temperature rise through FUS pressure increase in HR and RR regulating brain regions was shown to increase both HR and RR, with the latter more significantly. This study provides insight into the application of focused ultrasound for safe, non-invasive, thermally-mediated neuromodulation. This mechanism is separate from mechanical mechanisms found in pulsed FUS neuromodulation by employing very long pulse durations and expands the capabilities of FUS neuromodulation.

Acknowledgements: National Institute of Health

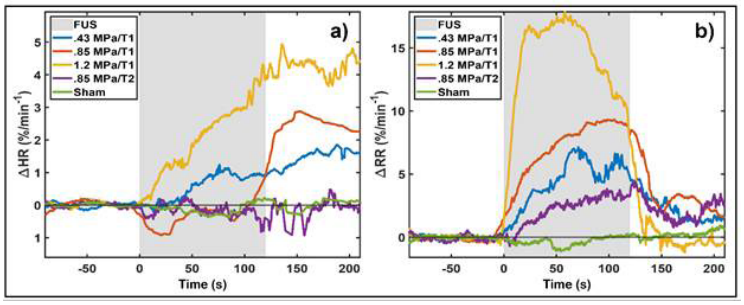

Figure 1. Median change in heart rate (a) and respiratory rate (b) during sonication (gray box) across all mice for each group. T1: thalamus/hypothalamus, T2: M1 and caudate-putamen.

P-NMD-4

Topic: Neuromodulation
Presentation Type: Poster

Spatio-temporal description of electrphysiological responses stimulated by Focused Ultrasound (FUS) using microlelectrode arrays (MEA)

Ivan M. SUAREZ CASTELLANOS[1], Elena Dossi[2], Jeremy Vion-Bailly[1], Jean-Yves Chapelon[1], Alexandre Carpentier[3], Gilles Huberfeld[2], William Apoutou N'Djin[1]

[1]INSERM, Lyon, France
[2]College de France, Paris, France
[3]Pitie Salpetriere Hospital, Paris, France

Background: Neurostimulation by focused ultrasound (FUS) is a field currently attracting much attention for the treatment of several diseases of neurological nature because of its inherent capability for non- or minimally-invasive targeting of cortical and deep brain structures. However, the underlying biological mechanisms regulating this phenomenon remain largely unknown. The objective of this study was to develop a mixed MicroElectrode Array (MEA)/FUS platform to study and describe the spatio-temporal characteristics of the electrophysiological signals generated by FUS stimulation on acute hippocampal brain slices from mice.

Materials and Methods: The FUS system consisted of a 15 mm diameter transducer with focal length of 15 mm. The MEA chip contained a grid of 60 electrodes spreading every 200 micrometers. The hippocampus of the slices (≈ 300-400 µm thick) were carefully placed on top of the electrode grid and continuously perfused with artificial cerebrospinal fluid (aCSF). A micropositioner was used to place the focus of the FUS transducer on the MEA electrode grid and thus on the hippocampus of the slices. A cone filled with agarose gel was used to couple the FUS transducer to the aCSF in the MEA chip. The slices were exposed to FUS pulses (1.78 MHz, 1.1 MPa, 284-568 cycles, PRF: 0.2-1 Hz) and the resulting signals were compared to responses along the Schaffer Collaterals obtained through electrical stimulation of the CA3 region of the hippocampus (5 Vpeak-peak biphasic pulse: 100 µs negative and 100 µs positive, PRF: 0.1-1 Hz). The spatio-temporal characteristics of the FUS-induced responses were described by measuring the amplitude, latency and slope of the generated field Excitatory Post-Synaptic Potentials (fEPSP) across the MEA electrode matrix.

Results: The responses from FUS stimuli, observed in several electrodes, were similar to those obtained through electrical stimulation, though exhibiting much larger variations in fEPSP amplitude, latency and slope. FUS-generated responses were characterized by fast negative deflections observed across the electrode matrix corresponding to FUS artifacts, often followed by fiber volleys (fig. b: latency≈1-5 ms), subsequent slow fEPSPs (fig. c: Amplitude ≈ 100-800 µV) and a slow return to the pre-stimulation baseline observed in fig. a (fig. d). The responses were localized (present in several adjacent electrodes), repeatable over several consecutive FUS pulses, and capable of generating both positive and negative fEPSPs. The distribution of the fEPSPs within the hippocampal brain slice, resulting from a single FUS pulse, suggest that neural structures other than the Schaffer Collaterals can be stimulated (i.e. interneurons, glial cells).

Conclusions: The preliminary results of this study corroborate the use of mixed FUS/MEA platforms as promising tools for real time description of the spatio-temporal electrophysiological mechanisms involved in FUS neurostimulation. Future work using this novel platform will help elucidate the biophysical mechanisms involved in FUS neurostimulation while identifying different biological actors capable of regulating this process.

Acknowledgements: This project was supported by the French National Agency for Research (ANR - 16-TERC-0017), the LabEx DevWeCan, and the Focused Ultrasound Foundation (Centers of Excellence).

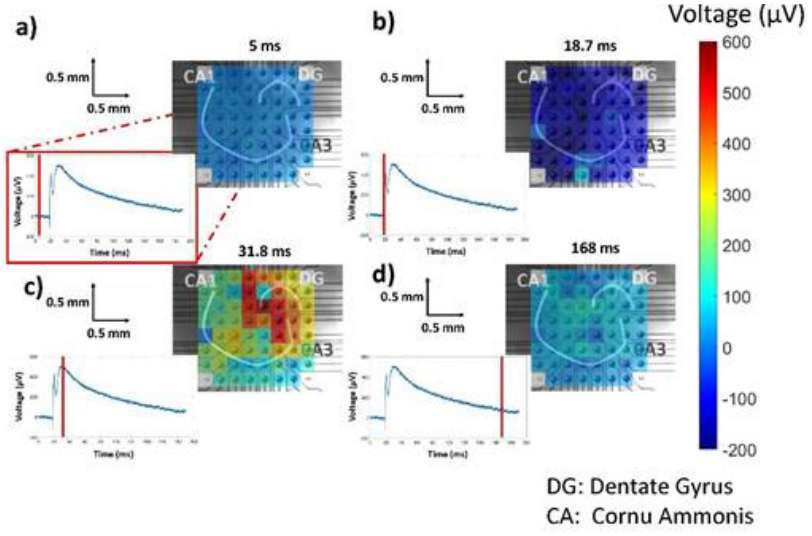

Figure 1. High-speed (50kHz sampling rate) reconstruction of signals recorded by all 60 electrodes during a single FUS pulse

P-NMD-5

Topic: Neuromodulation
Presentation Type: Poster

Design of mixed focused ultrasound (FUS)/patch clamp platform for the the study of electrophysiological activity in neurostimulation/ neuromodulation by FUS

Ivan M. SUAREZ CASTELLANOS, Magali Perier, Jeremy Vion-Bailly, Jean-Yves Chapelon, William Apoutou N'Djin

INSERM, Lyon, France

Background: Neurostimulation/Neuromodulation by focused ultrasound (FUS) is a promising technology for the treatment of several diseases of neurological nature characterized by its inherent capability for non- or minimally-invasive targeting of cortical and deep brain structures. However, the As a result, full description of the mechanisms underlying neurostimulation/neuromodulation by Focused Ultrasound (FUS) is essential for further development of this promising technology. The objective of this study was to integrate a FUS-system to a patch-clamp platform for the study of FUS-stimulated/modulated electrophysiological activity from individual neurons in vitro.

Materials and Methods: Mouse primary neurons and human neural progenitor cells were plated onto 35-mm diameter Petri dishes and bathed in artificial cerebrospinal fluid. A mixed FUS/patch clamp recording system was built on an inverted microscope for US treatment of patch-clamped neurons (fig.a). The US system consisted of 2.2 and 1.1 MHz planar transducers (ø:10-mm) applying 0.5-10 ms pulses at low pressures of 6-50 kPa. A cone filled with agarose gel was used to couple and focus the US field created by the planar transducer to the extracellular medium in the Petri dish. The electrophysiological activity of FUS-treated neurons was recorded using a whole-cell configuration in current-clamp mode. Neuromodulation studies consisted in measuring FUS-induced changes in the activation threshold to electrical stimulation (current density capable of triggering action potentials: AP), while neurostimulation experiments consisted of measuring FUS-stimulated electrophysiological responses in the form of APs or electrical discharges from the patch-clamped neurons. To generate electrically-stimulated APs, the patched neuron was excited by electrical pulses of 500 pA to 3 nA in amplitude for durations of 0.5 to 10 ms.

Results: Neuromodulation results showed that the activation threshold required for triggering APs could be elevated or lowered by approximately 25% following FUS treatment (fig.b). Furthermore, the treatment also appears to have had an effect on the latency of electrically-generated APs as the delay of the response (time between the stimulation artefact and peak of the AP) decreased by approximately 2 ms. In neurostimulation studies, 10 ms FUS pulses of 25 kPa were sufficient for disturbing the membrane potential of the patched neuron while occasionally depolarizing its membrane by up to 70 mV (fig.c). Therefore, FUS is capable of generating both strong, immediate responses in the patched neuron (fig.c) as well as weak, delayed membrane perturbations (fig.d). Whereas immediate responses may be the result of direct interactions between FUS biophysical effects and the neuron, delayed responses may reflect responses generated elsewhere in the network and transmitted to the patched neuron.

Conclusions: These results confirm our FUS/patch clamp platform as a viable tool for study of FUS-stimulated/–modulated electrophysiological activity in individual neurons. Using the platform, we aim at studying and identifying specific biological processes and cellular structures involved in both neuromodulation and neurostimulation by FUS at the level of individual neurons.

Acknowledgements: This project was supported by the French National Agency for Research (ANR - 16-TERC-0017), the LabEx DevWeCan, and the Focused Ultrasound Foundation (Centers of Excellence).

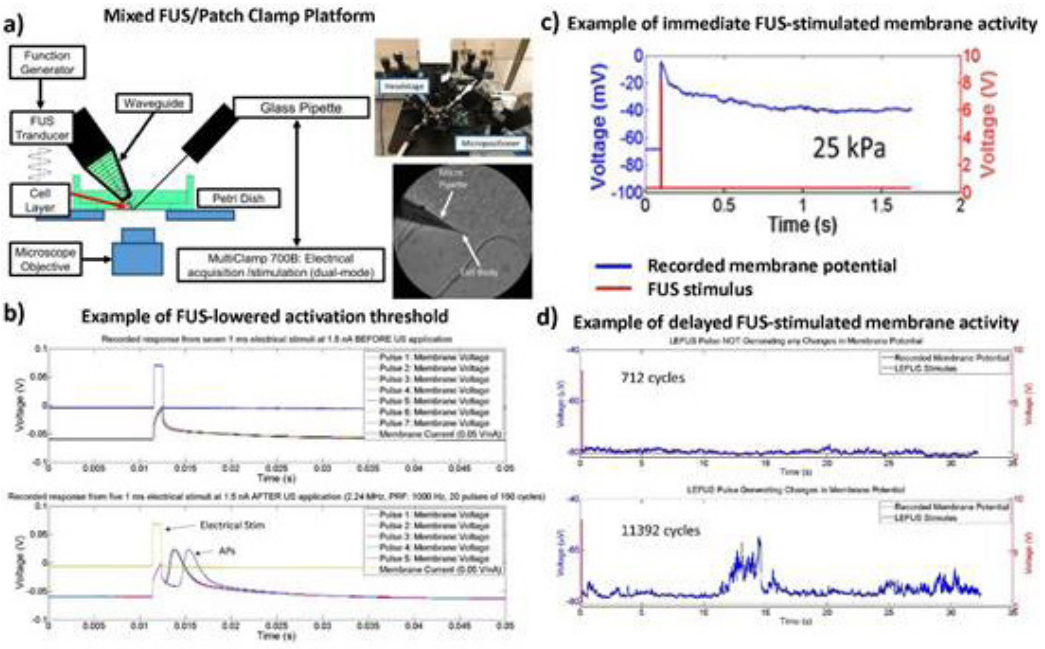

Figure 1. High-speed (50kHz sampling rate) reconstruction of signals recorded by all 60 electrodes during a single FUS pulse

P-NMD-6

Topic: Neuromodulation
Presentation Type: Poster

Transcranial ultrasound stimulation: A simulation study for non-invasive neuromodulation of the hippocampus

Xinghao Cheng[1], Christopher Butler[2], Robin Cleveland[1]

[1]University of Oxford, Oxford, United Kingdom
[2]Imperial College London, London, United Kingdom

Background: Neuromodulation is an important technique for neurological studies. In order to conduct experiments on healthy volunteers, non-invasive methods that can target specific sites are needed. Transcranial ultrasound stimulation (TUS) employs focused ultrasound to evoke neurostimulation and has been shown effective in studies using in-vitro cell models, pre-clinical trials and clinical trials.

The transcranial ultrasound waves need to propagate through the inhomogeneous head tissue to reach the target sites. The variation in acoustic properties in different tissues of the head distorts the ultrasound field with the skull being the major barrier. This study aims used numerical simulations to determine an appropriate lens to target the hippocampus using transcranial ultrasound neuromodulation. The simulations were also used to confirm safety and accuracy of the ultrasound delivery.

Materials and Methods: The simulations were performed in a MATLAB acoustic toolbox: k-Wave. The simulations used the linear fluid-based acoustic solver in the toolbox. T1-weighted MRI data of the human participants were segmented into scalp, skull, CSF, grey matter and white matter in order to generate a 3D medium input for the simulations. The acquired MRI data had a spatial resolution of 1 mm which was interpolated onto a 0.5 mm grid for accuracy of the 500 kHz ultrasound frequency used in the simulations. This is the frequency that previously has been shown to have safely and successful transcranial ultrasound stimulation of superficial brain targets in healthy volunteers.

Target sites were specified in the anterior hippocampus and perirhinal cortex. A virtual point source was placed at the target and time reversal techniques were used to determine the location and phase of an extracorporeal transducer with an acoustic lens. Several transducer sizes were also tested to find the optimal source diameter.The acoustic lenses were designed based on the phases required for focusing at the desired target site as well as accounting for the inhomogeneity of the tissues in the path of propagation. Several potential materials (ABS, PMMA and PDMS) for lens were tested to determine to optimal one to be used. The optimal transducer and lens was then simulated to assess the resulting focal pressure field in the head.

Results: The acoustic lens material with the most promising results was PDMS. It can be made easier to be acoustically homogeneous for the unique geometry that each lens possesses. The optimal diameter of the piston transducer was 65 mm. Using the lenses, the focusing occurs with 0.5 mm of the target site in the simulations with a -6 dB volume of less than 30 mm^3. In comparison using a single element transducer with a fixed radius of curvature produce a focal volume greater than 1300 mm^3. The gain (pressure at target divided by the effective source pressure) at the target with the lens was 2.5 which is much less than the gain of 17 that would occur in water for a single element transducer. The dominant processes that affected the gain were losses (both due to reflection and attenuation) in the lens and the skull and attenuation in the soft tissue.

Conclusions: Acoustic simulations employing time-reversal, where by a virtual source was placed at a target location in realistic head models, were performed to find the optimal source placement to target the hippocampus. The simulation results showed that use of a lens with a single element 500 kHz transducer can target the anterior hippocampus and perirhinal cortex. Targeting was accurate to within 1 mm with a focal volume less than 30 mm^3. This motivates developing and validating a lens based TUS with neuromodulation of the hippocampus.

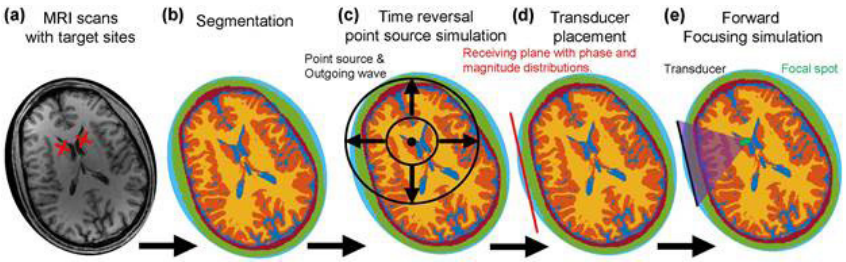

Figure 1. Flowchart for the simulation pipeline.

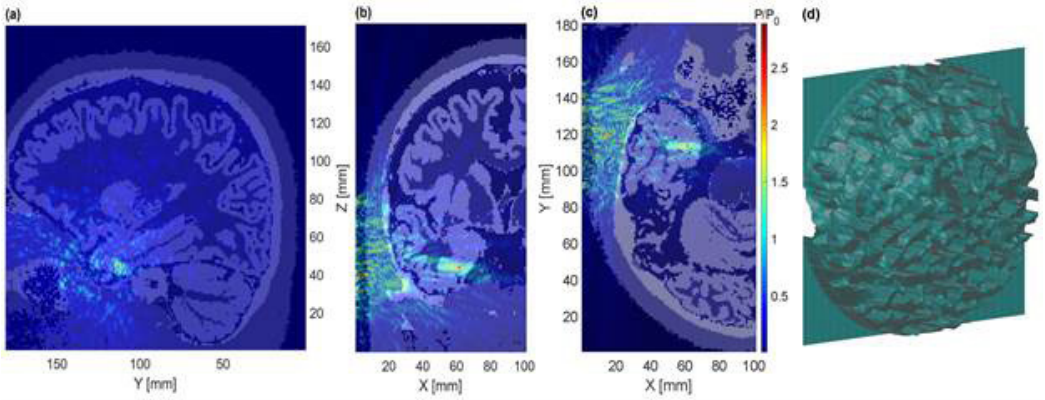

Figure 2. 3D pressure distributions through the target site: perirhinal cortex. (a) Sagittal view. (b) Coronal view. (c) Axial view. (d) The lens geometry in 3D.

P-NMD-7

Topic: Neuromodulation
Presentation Type: Poster

Non-invasive cognitive neural prosthetics improve amygdalar cerebral perfusion

Bianca Dang, Norman M Spivak, Sergio Becerra, Maya McNealis, Ben M Rosenberg, Sonja Hiller, Andrew Swenson, Luka Cvijanovic, Michael Sun, David Kronemyer, Rustin Berlow, Nanthia Suthana, Martin Monti, Susan Y Bookheimer

University of California, Los Angeles, Los Angeles, CA, USA

Background: Neurostimulation is an emerging therapy in treating psychiatric and neurological disorders via methods such as TMS and ECT (Fox 2013). However, most non-invasive transcranial stimulation techniques are limited to the range of disorders they can treat due to their inability to reach deeper brain regions (George 2013), which is currently only achieved by invasive, high-risk & surgery-intensive deep brain stimulation (Rabins 2009). This study sought to determine whether MR-guided low-intensity tFUS can selectively increase regional cerebral perfusion in the amygdala. As the brain's main contributor to emotional response and regulation, the amygdala's modulation and connectivity have great clinical potential. This study sought to determine whether MR-guided low-intensity tFUS can selectively increase regional cerebral perfusion in the amygdala. This is a very preliminary step towards validating tFUS as a non-invasive treatment tool for a wide range of psychiatric and neurologic disorders.

Materials and Methods: This study sought to determine whether MR-guided low-intensity tFUS can selectively increase regional cerebral perfusion in the amygdala while using the entorhinal cortex (ErC) as its subcortical control. A randomized, double-blind, within-subject crossover study was conducted to investigate whether tFUS can selectively increase regional blood perfusion in the amygdala or the entorhinal cortex and their functionally associated regions. The study sample consisted of a total of six healthy subjects (N = 6) with an average age of 61.8 years (SD: 8.25) and comprised of 50% female participants. Subjects were scheduled for two visits, exactly two weeks apart, for two tFUS sessions: one session targeting one targeting the amygdala (AG) and the entorhinal cortex (ERc). The tFUS was administered under MR guidance using a Siemens 3T Prisma scanner.

The tFUS was administered using the BX Pulsar 1002 (BrainSonix Corp, Sherman Oaks, CA). The parameters were as follows: 650 kHz, 720 mW/cm2 ISPTA.3, 5% DC, with a PRF of 10 Hz for AG and 100 Hz for the ErC. The transducer was a circular, single-element, and spherically focused, with an active aperture of 61 mm, 65 mm nominal focal length, with a hydrophone-measured -6 dB focal width of 4 mm in water and - 6 dB depth range of 50.4 - 80.5 mm. Arterial Spin Labeling (ASL) MRI was collected before and after tFUS to measure regional perfusion. ASL data was then processed using FSLv6.0 using various standard processing techniques.

Results: ASL results revealed increased perfusion in the region of the brain targeted by tFUS and not in the control region (ie. increased ERc perfusion without increased AG when targeting ERc and vice versa). Increased perfusion was also seen in regions known to be functionally connected to the targeted areas. AG-focused tFUS increased AG and medial PFC perfusion. ERc-focused tFUS increased ERc and hippocampal perfusion.

The amygdala receives its primary source of arterial blood through the anterior choroidal artery (AChA). As a result, increases in ASL perfusion of the amygdala will cause an increase in the amount of blood flowing through AChA.

Conclusions: These very preliminary data suggest that tFUS may be able to selectively increase perfusion in the targeted region. The relationship between increased perfusion and tFUS-related changes in functional connectivity or behavioral outcomes remains an important focus of our ongoing investigations. Replication in larger samples is needed and work on this study is ongoing to study the potential tFUS has to directly enhance memory and emotion regulation via modulation of the entorhinal cortex and amygdala. While very preliminary, these findings offer novel and exciting insight into the potential future application of tFUS as an accessible, safe, and non-invasive therapeutic device for a wide variety of patient populations.

Acknowledgements: UCLA Staglin IMHRO Center for Cognitive Neuroscience

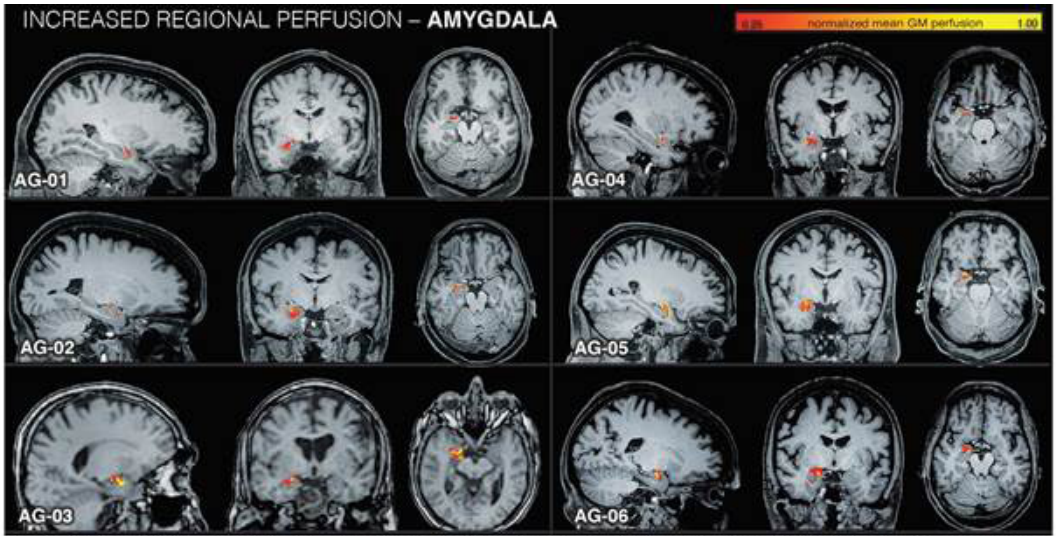

Figure 1. Increased AG Perfusion Post tFUS Targeting

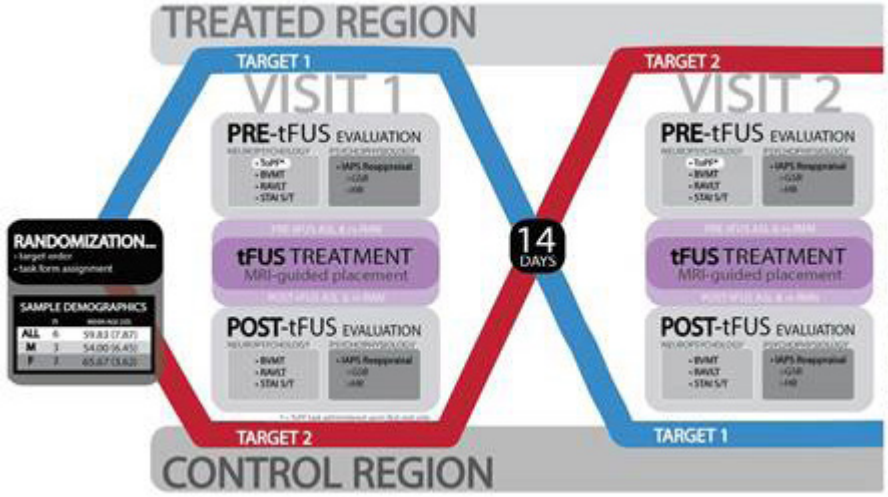

Figure 2. Double-Blind, Controlled Crossover Experimental Design

P-NMD-8

Topic: Neuromodulation
Presentation Type: Poster

Identifying auditory artifacts in small rodent focused ultrasound neuromodulation

Jake Hesselink[1], Amine Benaceur[1], Chris Krasnichuk[2], Zelma Kiss[3], Samuel Pichardo[3]

[1]University of Calgary, Regina, Canada
[2]Lakehead University, Calgary, Canada
[3]University of Calgary, Calgary, Canada

Background: Neuromodulation has proven a powerful technique in the treatment of various neurological disorders; however, current methods suffer from certain drawbacks. Deep brain stimulation involves invasive surgery, while transcranial magnetic stimulation offers little ability to target deep-brain areas accurately. Focused ultrasound (FUS) neuromodulation offers a spatially specific, non-invasive neurostimulation technique. Current studies in mice often record motor response to FUS neurostimulation. The fidelity of such motor responses was called into question by a study that found FUS caused widespread auditory activation within the cortex that may underlie the motor responses (Sato et al. (2018). Neuron, 98(5), 1031-1041.). Here, we hypothesize that FUS stimulation causes vibrations in the skull within the audible range of the animal and, accordingly, motor activity will be seen in response to FUS stimulation of both the motor and visual cortices.

Materials and Methods: To test this hypothesis, 477 kHz ultrasound, with a pulse repetition frequency (PRF) of 1.5 kHz and a spatial-peak temporal average intensity of 4.2 W/cm2, was delivered to visual cortex or motor cortex targets of C57BL/6 mice. We used a stereotactic-guided ultrasound device from FUS Instruments [RK-50]. Motor responses to each stimulation were recorded with video and with electromyography (EMG), while vibrations in the skull were recorded using a small contact microphone.

Results: As hypothesized, distinct motor responses to both targets were captured on EMG and video. There was no significant difference in response rate between the motor (M = 8.41 +/- 3.73 %) and visual (M = 14.49 +/- 14.12 %) cortices. Clear audio signals containing 1.5, 3.0, and 4.5 kHz frequencies were seen in 9 of 15 animals, although the presence of this signal had no effect on response rates.

Conclusions: This vibratory artifact provides evidence for a possible mechanism of indirect auditory activation. Though motor responses were seen, their inconsistency calls for further investigation into the mechanism underlying FUS-induced motor activation.

Acknowledgements: Natural Sciences and Engineering Research Council of Canada, FUS Instruments (Dallas, TX)

P-NMD-9

Topic: Neuromodulation
Presentation Type: Poster

A genetic targeted mechanogenetics by noninvasive ultrasound

Xuandi Hou, Zhihai Qiu, Shashwati Kala, Jinghui GUO, Jiejun Zhu, Ting Zhu, Lei Sun

The Hong Kong Polytechnic University, Hong Kong, China

Background: Techniques for noninvasive and remote brain stimulation have long been desired for both probing brain functions and treating brain dysfunctions. Potential technologies candidate for brain stimulation include optical, magnetic, electric, and acoustic brain stimulation. Of these, ultrasound brain stimulation is considered among the most promising technologies since ultrasound can non-invasively penetrate through the skull into deep brain structures with high spatiotemporal resolution. Recently, ultrasound neuromodulation has gained increasing attention, although the spatial resolution of ultrasound is sufficient for region-specific brain stimulation, it lacks cellular and molecular specificity.

Materials and Methods: Here, we developed an ultrasonic mechanogenetic tool to manipulate the neuronal activity and signaling with excellent precision by introducing gas-filled nanostructures, gas vesicles (GVs). GVs have unique size which can induce highly localized ultrasonic pressure gradient, unique microstreaming and shear stress in low intensity ultrasound field. In this study, we customized low intensity low frequency pulsed ultrasound stimulation system and a high-speed fluorescence microscopy was employed for calcium imaging. Neuronal calcium concentration was monitored simultaneously as a readout under ultrasonic stimulation.

Results: We hypothesized that the GVs could oscillate and consequently trigger widespread and reversible firing of neurons when exposed to ultrasound field. We showed that GVs mediated ultrasound can directly activate cultured neurons and initiate calcium influx. Further, the induced calcium response could be significantly suppressed by inhibiting the mechanosensitive ion channels with ruthenium red (RR), indicating that these ion channels mediated this kind of neuron activation. To manipulate target cells activities, we further sensitized the neurons by overexpression of MscL, a mechanosensitive ion channel. It showed that MscL-neurons could be activated under much lower ultrasound intensity and c-Fos expression significantly increased in the MscL-transfected cells, compared with the control. Furthermore, the parameters of ultrasound excitation we used do not affect cell viability or cell membrane integrity and temperature change.

Conclusions: Altogether, our findings demonstrated that under low intensity ultrasound irradiation, local ultrasound pressure will be significantly intensified where the oscillating GVs are placed and this GVs mediated ultrasound system can activate mechanosensitive ion channels and control calcium release in neurons. Moreover, the activity of mechanosensitive ion channels such as MscL stimulated by ultrasound is an important contributor to its ability to stimulate specific cells in vitro.

P-NMD-10

Topic: Neuromodulation
Presentation Type: Poster

Molecular mechanism of ultrasound neuron stimulation

Jiejun Zhu[1], Zhihai Qiu, Jinghui GUO, Shashwati Kala, Quanxiang Xian, Xuandi Hou, Lei Sun

The Hong Kong Polytechnic University, Hong Kong, Hong Kong (China)

Background: Ultrasound is a promising tool for both probing brain function and treating brain diseases with the advantage of non-invasiveness. However, the minimum focal spot of an ultrasound beam is much larger than a single neuron or a specific small set of neurons. These make it difficult for the ultrasound to probe or target the complex neural circuits entangled with interdependent different neurons. The underlying mechanism of ultrasound neuron modulation is thus the key issue for the best usage of ultrasound neuron modulation in both the basic and clinic neurosciences. Due to the nature of mechanical force of ultrasound, the mechano-sensitive ion channel displayed a promising candidate. Piezo family is so far the most sensitive mechanical ion channel, that could respond quickly to forces as low as 10 pN which is consistent with the scale of ultrasound induced forces. Base on this, piezo family is likely to be a factor modulates the ultrasonic neural modulation.

Materials and Methods: Firstly, 293T was used to test whether piezo1 mediates the ultrasound effect on cells. To further confirm whether the ultrasound neuron modulation is also mediated by piezo1, primary neurons were adopted. The endogenous expression of piezo1 in the primary neurons were tested by immunofluorescent staining. And the function of piezo1 was assessed by calcium imaging with a piezo1 agonist Yoda1 and a piezo1 antagonist GsMTx-4 . The ultrasound bio-effect was then tested with or without the GsMTx-4. The expression of c-Fos in the primary neurons are tested afterward. To further explore the signalling implications of piezo1-mediated ultrasound neuron modulation,the protein expression of phospho-CaMKII, phospho-CREB and c-Fos were tested in CLU199 by western blot.

Results: Overexpressing the piezo1 in the 293T induce the calcium influx whereas the unexpressed one has little response to ultrasound.In primary neurons, the ultrasound could activate piezo1, initiating calcium influx with a dose depend of ultrasound intensity. And these effects can be blocked by GsMTx-4 . Similarly, the ultrasound increased nuclear c-Fos expressions in primary neurons with a dose depend of ultrasound intensity. And these effects can be reduced if the neurons were pre-treated with GsMTx-4. These findings demonstrated that the piezo1 mediates the ultrasound neuron modulation in primary neurons.The protein level test further showed that the ultrasound increased the expression of phospho-CaMKII, phospho-CREB and c-Fos in a dose dependent manner of ultrasound intensity. But piezo1 knockdown significantly reduced this effect.

Conclusions: Our research indicate the piezo1 mediated ultrasound neuron modulation in vitro and may also provide a possible mechanism of ultrasound brain modulation in vivo. By controlling the expression of piezo1 we may able to target specific neuronal pathways or nuclei in both the basic and clinical neurosciences.

P-NMD-11

Topic: Neuromodulation
Presentation Type: Poster

Effect of skull on pattern interference radiation force (PIRF) based on focused transducer using fresnel lens

Young Hun Kim[1], Ki Chang Kang[1], Kamyar Firouzi[2], Kwan Kyu Park[1], Pierre Khuri-Yakub[2]

[1]Hanyang University, Seoul, South Korea
[2]Stanford University, Stanford, CA, USA

Background: Using focused ultrasound transducer is one of the most preferred methods for neurostimulation. Due to its high spatial resolution and high penetration depth, ultrasound, along with other methods, is suitable for non-invasive brain neurostimulation and is widely used. Generally, in the case of brain stimulation using a focused transducer, only one transducer was used or all the transducers were facing one direction for the focusing. Unlike the previous cases, neurostimulation using pattern interface radiation force (PIRF) uses more than two focused transducers and make standing wave pattern inside the brain for neurostimulation. In this paper, a study on the change according to the skull on PIRF which is made of focused transducers using the Fresnel lens was conducted.

Materials and Methods: The transducer was designed using size of 100 mm × 80 mm ×2.2 mm PZT with the center frequency of 1 MHz and the Fresnel lens was made of polydimethylsiloxane (PDSM). The frame of all the transducer were 3-D printed with polylactide (PLA) and the mold of the Fresnel lens was made with resin. The Fresnel lens was designed to have 4 binary step with diameter of 90 mm and f-number of 0.7 and the minimum thickness of 3 λ (4.5 mm) and each step with thickness of 0.66 mm difference. The minimum thickness of the Lens was determined not to be damaged in the process of manufacturing the lens. The PZT is covered with thin PDSM layer at the front and the backside is exposed to the air medium to transfer the power generated by the PZT to the front side as possible. The rubber ring was used between the cover of the transducer frame to store the air inside the transducer. The transducer was designed to be interchangeable lenses so that we can use different kinds of lenses with the same transducer. A thin gap was given to avoid trapping bubbles between the transducer and the lens. For measuring the pressure, we used the membrane hydrophone (GAMPT, Germany) and the lipstick hydrophone (Onda, USA). Simulations using COMSOL were conducted to verify the design of the lens.

Results: The input voltage to the transducer was about 54 V_ppwith 20 cycles at 1 MHz. The power amplifier was used to apply enough voltage to the transducer. All the image was measured by mechanical scanning with the hydrophone. For 1-D scanning, the pressure was measured by 0.1 mm steps and for 2-D scanning, the pressure was measured by 0.5 mm steps. The 3-dB spot size of a single transducer from the experiment was measured to be about 6.8 mm ×1.4 mm. And the 3-dB spot size of the focal point from the experiment using the skull increased to about 10 mm ×2.5 mm. The maximum pressure at the focal point was 2.63 MPa_pp and it decreased to 162.6 kPa_pp after placing the skull in front of the transducer. The thickness of the skull was 6 mm ~ 7 mm as the thickness is not uniform. The attenuation of the skull was -37.2 dB/cm. The maximum radiation force calculated from the standing wave pressure field without the skull was about 4.66 N/m^3.

Conclusions: By using two transducers with the same design, we have measured the standing wave at the focal point without the skull, and how the pressure field changes as it passes through the skull with one transducer. But due to its short focal length, we were not able to measure the difference caused by the skull. We are designing more lenses with different focal lengths and frequencies for various experiments. The attenuation of the skull slightly changes depending on the position and the shape of the skull due to the large size of the transducer. Further simulation and experiments are needed to observe changes in the internal pressure field by the changes in the shape and thickness of the skull.

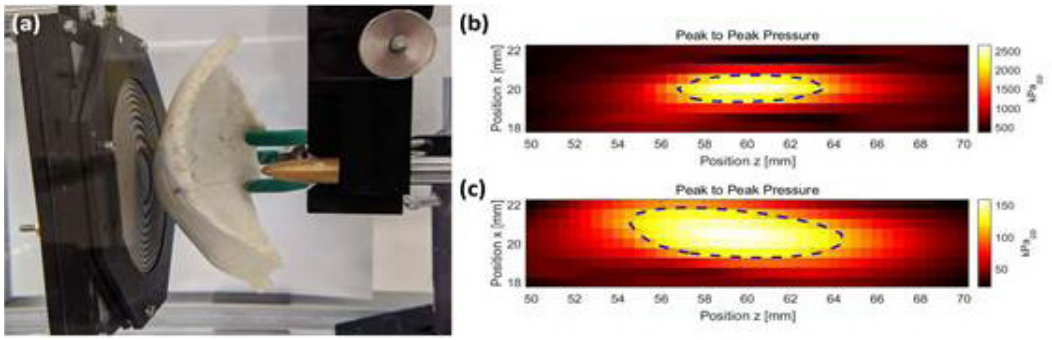

Figure 1. (a) Experiment setting image using single transducer (b) Pressure field measured without the skull (c) Pressure field measured with skull.

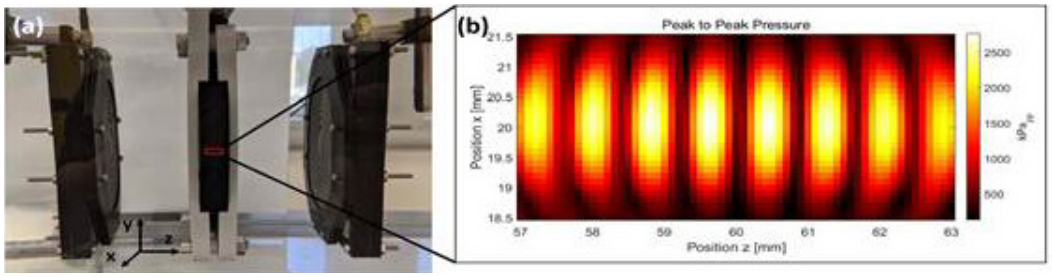

Figure 2. (a) Experiment setting image using two transducers (b) Pressure field measured at the focal point.

P-NMD-12

Topic: Neuromodulation
Presentation Type: Poster

Optimal pulse length of ultrasound for Piezo1 activation and intracellular calcium response

Defei Liao, Ming-Yen Hsiao, Gaoming Xiang, Pei Zhong

Duke University, Durham, NC, USA

Background: Sonogenetics have been successfully demonstrated to control the activity of target cells which are modified to express mechanosensitive (MS) ion channels. Among the possible ultrasound (US)-responsive MS ion channels, Piezo1 is an eminent candidate due to its diverse expression pattern in mammalian cells, high specificity, sensitivity, and temporally precision to mechanical force. Although previous studies have shown that Piezo1 could be elicited by US with or without microbubbles, the optimal US parameters and protocol for its activation with minimal adverse effects have not been identified. Here, we utilized a novel vertically deployed surface-acoustic-wave (VD-SAW) technique to investigate the effect of ultrasonic pulse length (PL) on Piezo1 activation by monitoring the intracellular calcium (Ca2+) change. We aim to determine the optimal PL for safely activating Piezo1 and investigate the underlying mechanism.

Materials and Methods: SAW was generated by a 33 MHz focused interdigital transducer and transmitted into culture medium, eliciting leaky pressure waves toward individual cells grown in a glass-bottom petri dish (Fig.1A). Fluorescence images were taken to monitor the intracellular Ca2+ transient (fura-2) and membrane poration (propidium iodide (PI) uptake), as well as tracking the cell displacement (Liao et al., BBRC, 2019). Under 20% duty cycle (DC) and thus a constant total acoustic energy, pulse repetition frequency (PRF) was varied from 0.2 Hz to 20 kHz to adjust the PL from 1 s to 0.01 ms (Fig. 1B&C). HEK293t cells with Piezo1 either genetically knocked out (P1KO) or transfected (P1TF) were treated by SAW for 60 s at an estimated peak pressure of 1.6 MPa and associated shear stress of 50 dyne/cm2 (Fig.1D).

Results: Under the same total insonification energy and treatment time (60 s), We found PL = 20 ms produces the highest Piezo1 activation probability (34%) and the strongest normalized calcium ratio change (94%) with < 10% cell detachment or membrane injury. We found the time-integral of the cell displacement (CDTI) rather than the maximum cell displacement (CDmax) calculated based on image analysis correlates well with Piezo1 activation and intracellular calcium response (Fig. 3A-E). We further developed a mathematical model to understand how the intrinsic properties of Piezo1 affect its response to pulsed US. The model was built through the adaption of previous membrane current measurement and the four-state Piezo1 gating mechanisms including open, close, inactivation I, and inactivation II (Lewis et al., Cell Reports, 2017). The time-integral of current calculated by the model predicted the same peak of calcium change at 20 ms PL (Fig.4A-F).

Conclusions: We have discovered that the PL of ultrasound plays an important role in the activation of Piezo1 and modulating the resulting Ca2+ response. This PL-dependence is highly correlated to the CDTI presumably associated with the viscoelastic properties of the target cells and the intrinsic property of the Piezo1, especially its inactivation states.

Acknowledgements: Dr. Jorg Grandl provided the HEK293T Piezo1 knockout cell line. This study was supported in part by NIH R37DK052985.

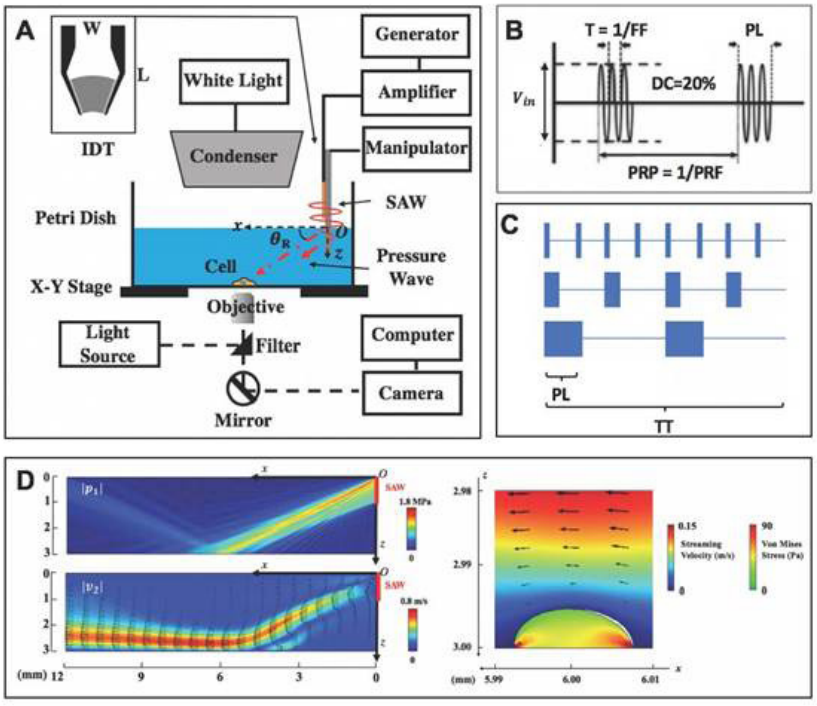

Figure 1. A: VD-SAW experimental setup; B: US parameters; C: US protocol to maintain a constant total ultrasound energy; D: finite-element stimulation.

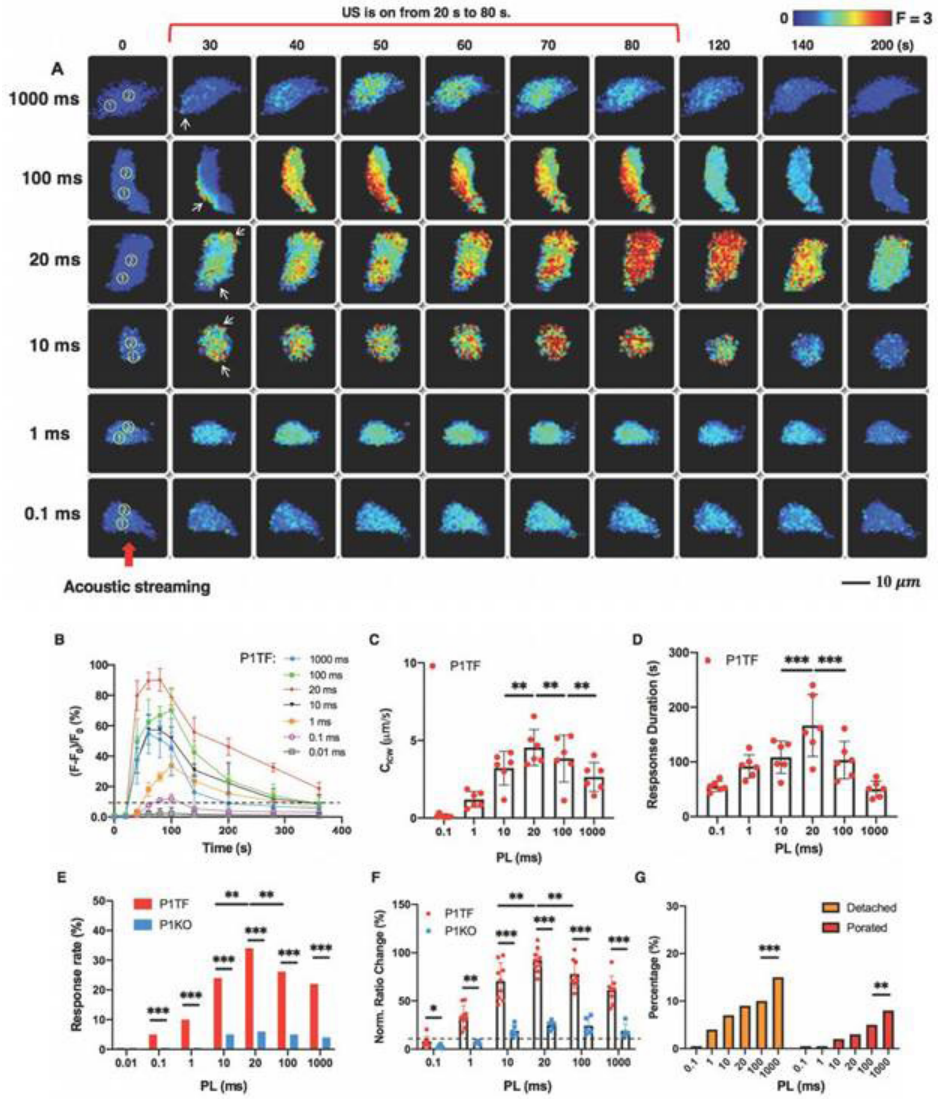

Figure 2. A: Image sequences of intracellular calcium response; B-G: Charactieristics of intracellular calcium response, Piezo1 acitvation and cell detachement and poration at different PL.

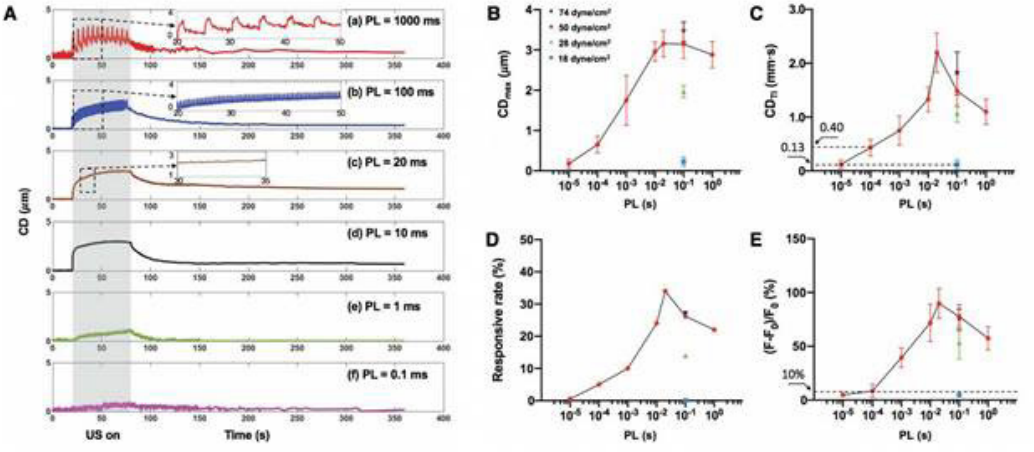

Figure 3. A: Cell displacement change over time produced by different PL; B: CDmax, C: CDTI, D: Piezo1 responsive rate and E: peak of the normalized intracellular calcium ratio at different PL.

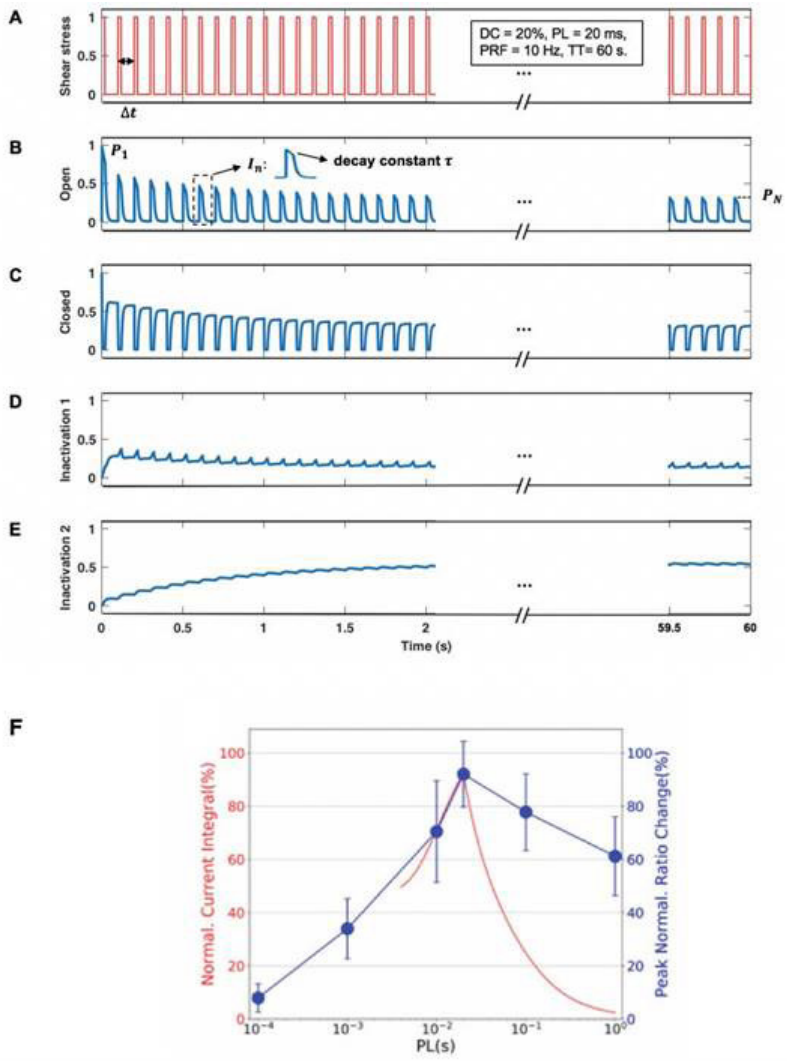

Figure 4. A: Normalized shear stress; B-E: Piezo1 at four states; F: Time-integral of current (red) and peak calcium ratio change in experiments (blue).

P-NMD-13

Topic: Neuromodulation
Presentation Type: Poster

Targeted surface and deeper brain stimulation by non-invasive ultrasound

Quanxiang XIAN, Zhihai Qiu, Shashwati Kala, Jinghui Guo, Jiejun Zhu, Lei Sun

The Hong Kong Polytechnic University, Hong Kong, Hong Kong (China)

Background: Manipulating specific targeted neural activity by physical intervention is a powerful method to gain causal insight into brain functions and treat brains disorders. It can be non-invasively steered and focused into mm-scale regions across the human skull, facilitated to produce controlled modulation of neuronal activity. However, it still remains challenging to stimulate well-defined neurons in a desired brain area without significant surgical invasion. Here, we introduce a non-invasive and selective neural excitation strategy using ultrasound, through the specific activation a mutant of the large-conductance mechanosensitive channel.

Materials and Methods: Methods included ultrasound stimulation, cell culture, viral transduction, patch clamp, calcium imaging, virus injection, immunocytochemical staining.

Results: Calcium ion (Ca2+) imaging showed that low-intensity ultrasonic stimulation was able to activate mechanosensitive ion channels in 293T cells and mouse primary cortical neurons. Ultrasonic stimulation of a cortical region in the brains of mice induced in neurons (identified by c-Fos expression) expressing mechanosensitive ion channels compared to a vector control. When the dorsomedial striatum (DMS) was made to express mechanosensitive ion channels and stimulated by ultrasound, we found activation only in that region, and not in the cerebral cortex directly above it or in either contralateral region.

Conclusions: Thus, we demonstrate an effective non-invasive approach for activating neurons in the intact brain using ultrasound. This experiment confirmed the ability of ultrasound generated by our setup to penetrate regions of the brain deeper than the cortex, making it suitable for in vivo use in areas of the brain both relatively superficial and deep.

P-NMD-14

Topic: Neuromodulation
Presentation Type: Poster

TRPV1-mediated sonogenetics for cellular-level neuromodulation in rodent brain in vivo

Yaoheng Yang[1], Christopher Pacia[1], Dezhuang Ye[1], Lifei Zhu[1], Hongchae Baek[1], Yimei Yue[1], Jinyun Yuan[1], Mark J Miller[1], Jianmin Cui[1], Joseph P. Culver[1], Michael R. Bruchas[2], Hong Chen[1]

[1]Washington University in St. Louis, St. Louis, MO, USA
[2]University of Washington, Seattle, WA, USA

Background: Spatiotemporally precise and noninvasive control of activity in a well-defined neuron type is a long-sought goal for investigating neural systems and treating neurological disorders. Focused ultrasound (FUS) is a promising technique for noninvasive control of neural activities. However, there are various types of cells within the FUS focal region, and the lack of cell-type selectivity hinders its application in revealing the causal links between neural activity and behavior. Sonogenetics, which combines FUS with genetics to selectively control neurons genetically modified with ultrasound-sensitive ion channels, can be a powerful cell-type specific neuromodulation tool. However, no study has demonstrated sonogenetic control of neuronal activity in mammalian brains in vivo. The objective of this study was to test the hypothesis that thermosensitive transient receptor potential vanilloid 1 (TRPV1) is an ultrasound-sensitive ion channel and develop TRPV1 mediated sonogenetics (Fig. a).

Materials and Methods: We first tested the TRPV1 ion channel in HEK293T cells in vitro using a customized microscopic system for simultaneous FUS stimulation and fluorescent calcium imaging. FUS (1.7 MHz, 1 MPa, and 40% in duty cycle) was applied to the cells and TRPV1 activation was quantified based on calcium imaging. Following the in vitro study, we injected lentiviruses to the mouse brain to selectively express TRPV1 in the excitatory neurons in the transgenic mice (Thy1-GCaMP6f) using the CaMKII promoter. The calcium indicator GCaMP6f in the transgenic mice allowed direct observation of neural activity. After TRPV1 virus expression, repeated FUS stimulations were applied to the TRPV1 expressing neurons (TRPV1+, n = 17), and the activities of every TRPV1+ neurons were recorded using a two-photon microscope (Fig. c) and compared to neurons without TRPV1 overexpression (TRPV1-, n = 16) as control group. Multiple FUS parameters including both pulsed wave (PW) and continuous wave (CW) with 1, 4, 7, and 15 s stimulation duration were investigated to determine the success rate, activation latency and relaxation time. Tissue temperature within the FUS-targeted brain area was measured by in vivo real-time magnetic resonance thermometry to evaluate the correlation between local temperature and the success rate of neural activation. The safety of the FUS sonication was evaluated using histological and immunohistochemical staining.

Results: FUS activated the TRPV1+ HEK293T cells in vitro with the calcium signal increase ($\Delta F/F$) of 45.6 ± 9.3% (Fig. b). In the in vivo mice brain, FUS selectively activated TRPV1+ neurons, while did not affect the nearby TRPV1- neurons as recorded by two-photon imaging (Fig. c). Both PW (15 s) and CW (7 s) FUS activated TRPV1+ neurons with comparably high success rate of 75.0 ± 6.8% and 88.0 ± 7.3% respectively, which were significantly higher than 9.2 ± 3.8% of the control group (TRPV1-). The activation latency of neurons sonicated by CW-FUS were 2.5 ± 0.3 s which was significantly shorter than the latency by PW-FUS (4.7 ± 0.5 s). The success rate of sonogenetic activation had a strong linear correlation (R = 0.97) with FUS-induced temperature rise. The peak temperatures achieved by the different FUS parameters were within the range of 38.5 ºC to 43.8 ºC, which did not cause detectable cell apoptosis, inflammation, or neuronal integrity change.

Conclusions: This work demonstrated that TRPV1 is an ultrasound sensitive ion channel and TRPV1 based sonogenetics achieved noninvasive, cell-type specific, precise control of mammalian neural activity in vivo. Compared with the existing FUS neuromodulation, which uses FUS alone to stimulate brain in tissue level, sonogenetics is able to activate specific types of cells in the brain. Sonogenetics can accelerate the achievement of the ultimate goal of neuroscience in understanding intact neural circuits and enable potential clinical applications. TRPV1, as a biogenic ultrasonic sensor, could lead to broad applications in the remote control of various types of cells, such as tumor cells, T cells, and stem cells.

Acknowledgements: This work was supported by the National Institutes of Health (NIH) BRAIN Initiative (R01MH116981) and NIBIB (R01EB027223).

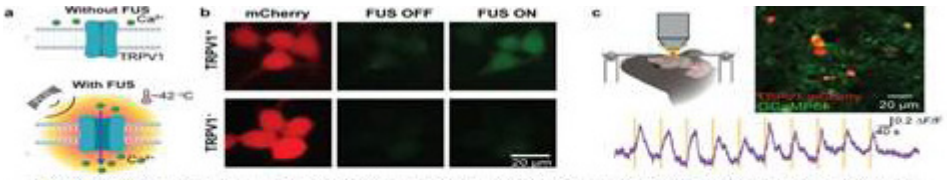

Figure. (**a**) Schematic illustration of TRPV1 mediated sonogenetics. (**b**) TRPV1 enabled FUS activation of HEK293T cells *in vitro*. Red: HEK293T cells expressing the fluorescence reporter mCherry with the TRPV1 ion channels (TRPV1+) or without the TRPV1 (TRPV1-). Green: Intracellular calcium signal before and during FUS stimulation. (**c**) Sonogenetics in the mouse brain *in vivo*. The mouse head was fixed in the stage for simultaneous FUS stimulation and calcium imaging using a two-photon microscope. The co-expression of TRPV1 and GCaMP6f was observed *in vivo*. The calcium signal (ΔF/F) shows that FUS repeatedly activated TRPV1+ neurons. The orange bars indicate the FUS ON.

Figure 1.

P-NMD-15

Topic: Neuromodulation
Presentation Type: Poster

Noninvasive spinal cord stimulation via focused ultrasound modulates corticospinal excitability

Evgenii Kim, Jeungeun Kum, Hyungmin Kim

Korea Institute of Science and Technology, Seoul, South Korea

Background: Focused ultrasound (FUS) is gaining traction as a noninvasive alternative to conventional neurostimulation techniques. Compared to current noninvasive methods utilizing magnetic and electrical means, the acoustic-based stimulation provides a higher spatial resolution and depth penetrability. Previous reports demonstrated that FUS over the brain has the ability to both excite as well as suppress neural circuits. The sonication of the sciatic nerve facilitated the motor response when using a low pulse repetition frequency, while the response is suppressed with rapid pulsation. Acoustic stimulation has also been used to modulate neural signaling in the peripheral organs to regulate specific physiological functions. Despite the broad application of FUS stimulation, there are very few studies dedicated to the investigation of FUS on the spinal cord. In this study, we present the effect of FUS on the spinal cord during corticospinal tract stimulation.

Materials and Methods: The study was performed on anesthetized 6 week-old mice (ketamine/xylazine cocktail, 80:10 mg/kg). Stimulation of the corticospinal tract was achieved by applying an electrical current to the hind limb region of the motor cortex. A 30 ms electrical pulse train consisting of 0.1 ms pulses with a repetition rate of 300 Hz was delivered to the brain using a bipolar electrode triggering a hind limb twitch. The muscle twitch was recorded using electromyography (EMG) electrodes attached to the contralateral hind limb.

Noninvasive spinal cord stimulation was performed using a single-element focused ultrasound transducer with a fundamental frequency of 3 MHz. The transducer was placed above the mouse dorsum targeting the L3 spinal cord segment within the T13 vertebra. The acoustic stimulation is given as a 100 ms acoustic pulse train with a pulse repetition rate of 1 kHz and a duty cycle of 16% (Isppa = 57.5 W/cm^2). The interstimulus interval was set to 2 sec. The FUS modulation of corticospinal excitability was evaluated by comparing hind limb twitch power before, during, and after sonication.

Results: The averaged EMG signal over 100 trials from three different conditions is shown in Fig 1. Results indicated that the spinal cord sonication is able to temporarily suppress the corticospinal pathway, as it can considerably weaken the muscle twitch. Suppression lasted an additional several seconds after the end of sonication. The motor response before and 5 min after stimulation has no visible difference.

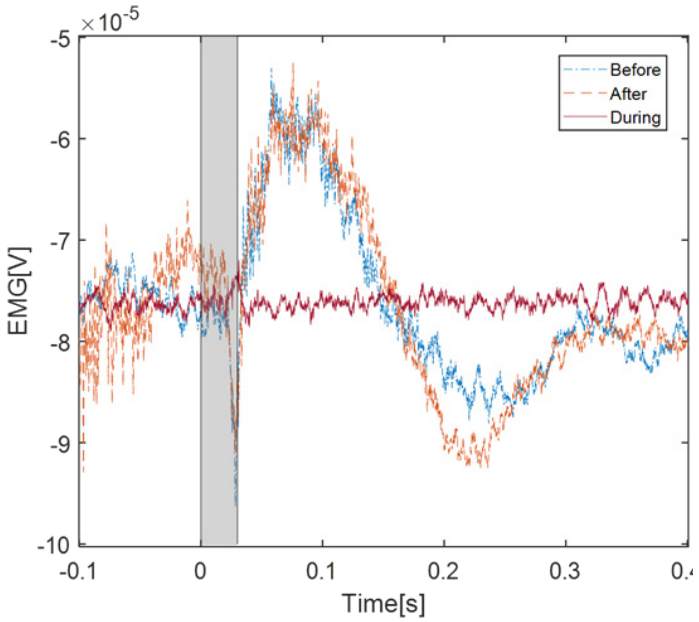

Figure 1. Hind limb EMG signal before, during, and after sonication. Gray region represents the electrical stimulation.

Conclusions: In this work, noninvasive spinal cord stimulation was performed using focused ultrasound. The sonication on the L3 spinal cord segment suppressed the hind limb movement induced by electrical stimulation of the motor cortex. Although the study still requires additional investigation for finding optimal sonication parameters, the noninvasive modulation of spinal cord activity has great potential in various medical applications including chronic pain syndrome and spinal cord injury.

Acknowledgements: This research was supported by the National Research Council of Science & Technology (NST) grant by the Korea government (MSIT) (No. CAP-18-01-KIST).

P-PAC-1

Topic: Pancreatic Cancer
Presentation Type: Poster

Establishing a SCID-like porcine model of human cancer for novel therapy development: a pilot study with pancre-atic adenocarcinoma

Irving C Allen[1], Alissa Hendricks[2], Sheryl Coutermarsh-Ott[1], Margaret Nagai-Singer[1], Kiho Lee[1]

[1]Virginia Maryland College of Veterinary Medicine, Blacksburg, VA, USA
[2]Virginia Tech, Blacksburg, VA, USA

Background: New therapeutic paradigms to treat pancreatic cancer are direly needed. One of the largest factors impeding the development of efficacious therapies is the lack of an effective pre-clinical animal model that can recapitulate the anatomy and physiology of human patients. Likewise, there is a general lack of tumor tissue available from human patients for ex vivo studies. These are both significant limitations in the biomedical device field. To address these limitations, we have developed IL2/RAG2 deficient pigs using CRISPR/Cas9 as a novel, large mammal model for use in cancer xenograft studies of human pancreatic adenocarcinoma.

Materials and Methods: We generated six IL2/RAG2 deficient pigs using CRISPR/Cas9 and raised the animals in sterile, gnotobiotic isolators until tumor injection. Human Panc01 cells were cultured and injected subcutaneously with Matrigel behind the ears of each animal. Tumors were allowed to progress for 38 days following injection. The subcutaneous tumors were measured 3 times per week using calipers. Likewise, the tumors were imaged using ultrasound. Following euthanasia, animals were necropsied and tissues were prepared for either histopathology or ex vivo tumor assessments. Pigs were genotyped for RAG2 and IL2RG post-study.

Results: In initial proof-of-concept studies, discussed here, these novel pigs were successfully generated using on-demand genetic modifications in embryos, circumventing the need for breeding and husbandry. Genotyping revealed that all six animals were IL2RG/RAG2 deficient. Using this novel model, human Panc01 cells injected sub-cutaneously into the ears of IL2/RAG2 deficient pigs demonstrated 100% engraftment, with all pigs developing palpable tumors by the second week of the study. The tumors continue to grow through day 38, when the average tumor size reached 1cm. Tumor growth rates were similar to those typically observed in NOD-scid gamma (NSG) mice. Histopathology analysis revealed no immune cell infiltration and tumor morphology was highly consistent with the NSG mouse models. The subcutaneous tumors provided ample, high quality pancreatic cancer tissue for utilization in subsequent ex vivo tumor ablation studies.

Conclusions: The anatomical features, including size, of the RAG2/IL2RG pigs is more similar to that of humans compared to most other pre-clinical animal models, making these swine ideal for prototype testing of medical devices targeting the pancreas, including focused ultrasound and histotripsy, without the need for a significant scale down. The proof-of-concept studies presented here demonstrate the technical capabilities of the model, show the potential engraftment efficiencies, and provide insight into growth rates for the Panc01 cells. Together, these data support the next phase of studies, which includes the generation of orthotopic tumors in the pancreas and tumor ablation therapeutic assessments.

Acknowledgements: We would like to thank the Focused Ultrasound Foundation for their support of this project. We would also like to acknowledge the Virginia Maryland College of Veterinary Medicine, the Virginia Tech Institute for Critical Technology and Applied Science, and the Center for Engineered Health for their continued support.

P-PAC-2

Topic: Pancreatic Cancer
Presentation Type: Poster

Imaging ultrasound effects on an ex vivo pancreas slice model

Andrew Chen, Aleksandar Jeremic, Vesna Zderic

The George Washington University, Washington, DC, USA

Background: The pancreas depends on calcium (Ca2+) to perform and regulate its normal functions such as secrete insulin. It was previously shown by our lab that ultrasound can be used to stimulate beta cells to release insulin. This study aims to use fluorescence microscopy to investigate the metabolic effects of ultrasound stimulation on pancreatic tissue to better understand the ultrasound effects and assess therapeutic potential for people with type 2 diabetes. The autofluorescence methods of imaging ultrasound effects on the pancreas presented here can lead to advances in understanding ultrasound effects on many types of endocrine tissue, a relatively unexplored field of ultrasound.

Materials and Methods: Acute rat pancreatic tissue slices are were for confocal autofluorescence imaging at 488 nm and 633 nm. Imaging at 488 nm was used to record the changes in levels of lipodamine dehydrogenase (Lip-DH), an indicator of cell metabolism. The redox state of Lip-DH has been shown to be in direct equilibrium with the redox state of nicotinamide adenine dinucleotide (NAD). Autofluorescence signal from the pancreas at 633 nm has been shown to highlight structures in the pancreas such as islets. Exposure parameters for the tissue slices are continuous ultrasound application at 1 W/cm2 and 0.5 W/cm2 at 800 kHz for 3 minutes as well as an 800 kHz 1 W/cm2 pulsed ultrasound application with a 0.5 Hz pulse repetition frequency and a 5% duty cycle. High glucose application and no ultrasound control experiments were also performed. We chose these ultrasound parameters as they were found to stimulate beta cells while retaining cell viability by previous studies in our laboratory. Fluorescence traces were extracted from areas of pancreatic islet and exocrine tissue from the time series of images. A difference in the normalized fluorescence trace before and after ultrasound treatment application was taken as the metric for response to the exposure parameters. Analysis was performed across tissue types (pancreatic islets and exocrine) for the same treatment groups via paired t-test and within tissue types across treatment groups by a one-way ANOVA.

Results: Our results are summarized in Table 1. A decrease in Lip-DH fluorescence indicates an increase in metabolic activity. Glucose application causes significantly larger increase in metabolic activity ($p < 0.05$) in the pancreatic islet ($-4.6 \pm 6.5\%$) compared to the exocrine tissue ($-1.6 \pm 5.5\%$) via paired t-test which is expected as the islet tissue is responsible for secreting insulin. The effect of our continuous ultrasound parameters produce a change in Lip-DH fluorescence that is much smaller in effect on average and with greater standard deviation indicating a much less consistent upregulation of metabolism with continuous compared to pulsed ultrasound (Table 1), though these differences were not significant with $p < 0.05$. In both pancreatic islet and exocrine tissue the change in 633 nm fluorescence of all ultrasound treatment groups was of significantly smaller magnitude when compared to control via one-way ANOVA ($p < 0.05$).

Conclusions: Our imaging of Lip-DH fluorescence shows increased metabolic activity in the pancreatic islet compared to exocrine tissue of glucose trials, as well as in pulsed ultrasound when compared to continuous ultrasound, indicating that the thermal effects may counteract the mechanical effects of ultrasound on pancreas metabolic activity.

		800 kHz 0.5 W/cm²	800 kHz 1 W/cm²	800 kHz 1 W/cm² Pulsed	Control	Glucose Application
488 nm	Islets	-1.3±10.7%	-2.3±11.5%	-4.3±3.5%	-8.4±23.8%	-4.6±6.5%
	Exocrine	-2.9±9.1%	-1.5±6.9%	-2.7±1.9%	-4.6±18.1%	-1.6±5.5%
633 nm	Islets	-3.3±7.3%	-4.1±5.7%	-1.4±1.4%	-13.5±7.8%	-5.3±5.2%
	Exocrine	-2.2±2.0%	-1.6±2.1%	-1.9±1.4%	-10.0±9.9%	-6.8±3.7%

Figure 1. The quantified change in fluorescence over the treatment period for all parameters, tissue types and color channels. Change is reported as a percent difference in the normalized signal.

P-PAC-3

Topic: Pancreatic Cancer
Presentation Type: Poster

The usefulness of high-intensity focused ultrasound (HIFU) therapy for unresectable pancreatic cancer

Atsushi Sofuni, Yasutsugu Asai, Takao Itoi

Tokyo Medical University, Tokyo, Japan

Background: High-intensity focused ultrasound (HIFU) is expected as new advanced therapy for unresectable pancreatic cancer (PC). We have evaluated the therapeutic effect of HIFU therapy in locally advanced and metastatic PC.

Materials and Methods: We treated PC patients by HIFU as optional local therapy as well as systemic chemo / chemo-radiotherapy, with whom an agreement was obtained in adequate IC, from the end of 2008 in our hospital. This study took approval of member of ethic society of our hospital. HIFU device used is FEP-BY02 (Yuande Bio-Medical Engineering Co.LTD., China). The subjects were 176 PC patients, i.e. 89 cases in stage III, 87 cases in stage IV.

Results: The effects of HIFU therapy were the following; the effectiveness of primary lesion was CR:0, PR:21, SD:106, PD:49 cases, primary disease control rate (DCR) more than SD was 72.2%. The therapy after HIFU treatment was operation in 8, chemotherapy in 143, immunotherapies in 4, and best supportive care (BSC) in 22 cases. MST after diagnosis in HIFU with chemotherapy and chemotherapy alone (100 patients in our hospital) was 772.3 vs 346.6 days, respectively ($p<0.05$). The mean duration to HIFU therapy from the diagnosis (including the pre-therapy period) was 391.5 ± 390.0 days (median: 288.5 days). MST after HIFU therapy was 379.8 days. Combination therapy of HIFU with chemotherapy was better result than common chemotherapy alone.

Conclusions: This study suggested that HIFU therapy has the potential of new method of combination therapy for PC.

P-PAC-4

Topic: Pancreatic Cancer
Presentation Type: Poster

Development of a high intensity focused ultrasound toroidal transducer for the treatment of pancreatic tumors under Doppler guidance: In vivo studies in a porcine model

Celia Cilleros[1], Aurelien Dupre[1], Yao Chen[2], Jeremy Vincenot[3], David Melodelima[1]

[1]LabTAU, Lyon, France
[2]Centre Leon Berard, Lyon, France
[3]EDAP-TMS, Vaulx-en-Velin, France

Background: Pancreatic cancer is the 7th most likely cause of cancer related deaths. Regardless of the treatment used, the survival rate after 5 years is lower than 6%. Ultrasound-guided high-intensity focused ultrasound (US-HIFU) has been shown to improve local control and alleviate pain. In a previous work we demonstrated the clinical utility of a toroidal HIFU transducer used during an open procedure for treating liver metastases. A new treatment strategy that uses this transducer intra-operatively under Doppler guidance for treating pancreatic tumors was developed. Here we report the results of a preclinical study evaluating, in an animal model, the feasibility and tolerance of an intraoperative HIFU treatment at the pancreas-mesenteric artery interface before application to patients.

Materials and Methods: The HIFU transducer has a toroidal shape with a radius of curvature of 70 mm focusing on a circle of 30 mm. The working frequency was 2.5 MHz. The diameter of the transducer was 70 mm. An ultrasound imaging probe working at 7.5 MHz was placed in the center of the HIFU transducer.

Seventeen animals were treated and followed from day 0 to day 15 days after the HIFU procedure. Ultrasound Doppler images were recorded for flow analyses before and after treatment. HIFU exposure lasted between 445 and 650 seconds using an acoustic power ranging from 80 W to 140 W. For each animal, the pancreas-mesenteric artery region was targeted to create homogeneous ablation around the artery while preserving its functionality.

Results: In total, 31 HIFU exposures were created. The average diameter of the pancreatic ablations was 33.1 ± 5.0 mm. The HIFU lesion encompassed all treated arteries. High decorrelation was observed in Doppler images at one extremity of the artery just after HIFU exposure and normal blood flow was observed 10 minutes after.

When using the highest acoustic energy an arterial spam occurred due to the nerve degeneration induced by HIFU with normal blood flow 10 minutes after. In that cases an average reduction of about 15% of the lumen of the artery was observed due to nerve degeneration.

Histological analyses confirmed the homogeneity of the coagulation necrosis that encompassed arteries in all cases.

Conclusions: An intraoperative HIFU treatment at the pancreas-mesenteric artery interface was shown to be safe and feasible using a toroidal HIFU transducer. Large and fast ablations were created while maintaining normal blood flow. The device was held by hand without resorting to mechanical scanning to treat the targeted region. Curative treatment rather than palliative approach may be conceivable using this device.

Acknowledgements: Canceropole Lyon Auvergne Rhone-Alpes (N° CVPPRCAN000165P) and SIRIC LyriCAN grant INCa_INSERM_DGOS_12563

P-PRO-1

Topic: Prostate
Presentation Type: Poster

MRI guided positioning device using focused ultrasound for treatment of prostate cancer

Marinos Giannakou[1], Theocharis Drakos[1], Nikolas Evripidou[2], George Menikou[3], Christakis Damianou[2]

[1]MEDSONIC LTD, Limassol, Cyprus
[2]Cyprus University of Technology, Limassol, Cyprus
[3]Nicosia General Hospital, Nicosia, Cyprus

Background: A magnetic resonance imaging (MRI)-positioning device with 2 computer-controlled axes (one linear and one angular) was developed. The positioning device holds a single element focused ultrasound (FUS) endorectal transducer. Four manually driven axes were also developed in order to properly place the transducer close to the rectum. The purpose of this positioning device is to ablate prostate cancer in humans in the future.

Materials and Methods: The positioning device includes MRI compatible piezoelectric motors, and optical encoders and ABS plastic. All the parts of the positioning device were developed using an industrial 3D printer.

Results: The MRI safety of the device was successfully evaluated in a GE 1.5 T MRI scanner. The positioning device has the ability to accurately move the transducer. The ability of the transducer to cause high temperatures was tested successfully in a water-agar phantom.

Conclusions: A reliable, simple, cost effective, portable positioning device has been developed which can be used in virtually any MRI scanner since it can be placed on the scanner's table. The proposed positioning device can be used in the future for clinical trials for prostate cancer treatment using FUS provided that it is evaluated extensively in animal models.

Acknowledgements: The project has been funded by the Research Promotion foundation of Cyprus under the project PROSTASONIC (ENTERPRISES/0918/0012).

P-STR-1

Topic: Stroke
Presentation Type: Poster

Intra-ventricular sonothrombolysis using MR-guided high intensity focused ultrasound (MRgHIFU) in in vivo porcine intra-ventricular hemorrhage (IVH) model: Safety and side-effect profile

Grace Lai[1], William Chu Kwan[2], Karolina Piorkowska[1], Matthias Wagner[1], Rishi Raghuram[2], Nicole Hon[1], Birgit Ertl-Wagner[1], Thomas Looi[1], Adam Waspe[1], James Drake[1]

[1]The Hospital for Sick Children, Toronto, ON, Canada
[2]University of Toronto, Toronto, ON, Canada

Background: High-grade intraventricular hemorrhage (IVH) is a complication affecting premature infants that can lead to life-time dependence on an implanted cerebrospinal fluid shunt and neurodevelopmental impairments. Our group has previously shown that clot lysis can be achieved using high-intensity focused ultrasound (HIFU) induced cavitation in an acute in vivo IVH porcine model, developing an incisionless therapy to break down clots without the risks associated with surgical endoscopic aspiration or intra-ventricular thrombolytic agents. In this abstract we present preliminary results from survival studies and describe the safety and side effect profile in developing methodology for delivering this novel treatment.

Materials and Methods: IVH was induced in one-week old piglets (n=4) through ultrasound-guided direct injection of 1.8-2.0 cc/kg of autologous blood into the lateral ventricle through a vertex craniotomy performed to simulate the neonatal "fontanelle" in humans. MRgHIFU sonothrombolysis was administered 24 hours after infusion using the Profound Sonalleve HIFU system on a Philips 3T MR scanner at an acoustic power of 400-500W, 10ms pulse duration, and 1Hz pulse repetition frequency. Treatment cells (2x8 mm) were planned to target clot in the lateral ventricles. Piglets were survived for 28 days with daily neurobehavioral observation, twice weekly head ultrasound for the first 14 days, and weekly MR imaging to assess brain damage and resultant ventriculomegaly.

Results: Two pigs survived to study completion with no neurologic deficits. Collateral brain damage was observed in 3 of 4 piglets. At 400W, far field effects caused damage when the nasal sinuses were centered within the ultrasound beam trajectory (Fig 1), but not when cavitation was stopped as soon as these effects were observed (Fig 2). Neither pig exhibited neurologic damage and both survived. In one case, head movement after the initial planning MRI resulted in inaccurate targeting that missed the blood clot with inadvertent sonication of brain (Fig 3) and early termination from symptomatic hydrocephalus. When treated at a higher power of 500W, near field effects known to occur with cavitation were observed (Fig 4). After the first instance, subsequent sonications also demonstrated near field effects, suggestive of shielding by the initial cavitation cloud. Post-mortem gross inspection immediately after treatment showed lack of clot lysis, further supporting prefocal shielding.

Conclusions: Both expected cavitation side effects and user error complications could occur in an in vivo setting. To minimize expected effects, air in the far field should be avoided and the focal point placed at the far side of the target. Development of passive cavitation detection can enable localization of cavitation activity for modulation of transducer output power to avoid over-treatment. Experimental errors can be avoided by repeating localizing scans and more secure immobilization. With appropriate precautions, HIFU lysis of intra-ventricular clot can be possible and safe. These results highlight adverse events and help improve our protocol for further investigation into the efficacy of MRgHIFU clot lysis.

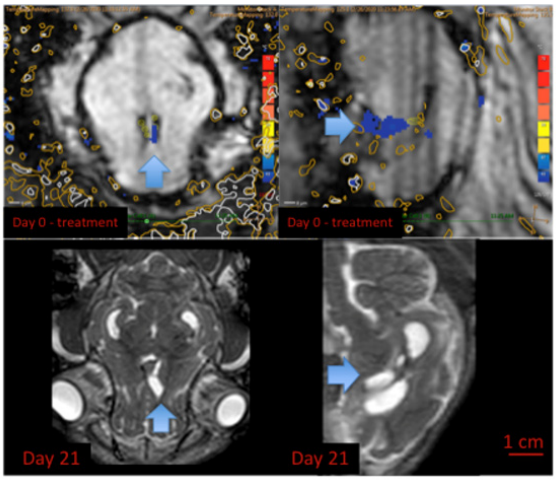

Figure 1. Arrows indicate regions of far field effects during treatment (top) and day 21 MRI showing orbitofrontal brain damage (bottom).

Acknowledgements:
Hydrocephalus Association, Pediatric Hydrocephalus Foundation.

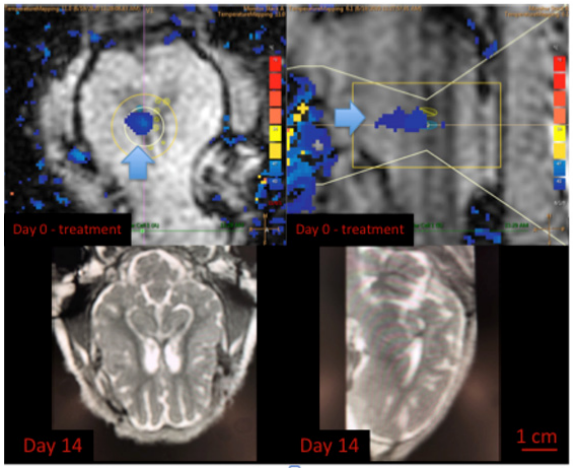

Figure 2. Arrows indicate far field effects with cavitation terminated early (top) and day 14 MR with no evidence of brain damage (bottom).

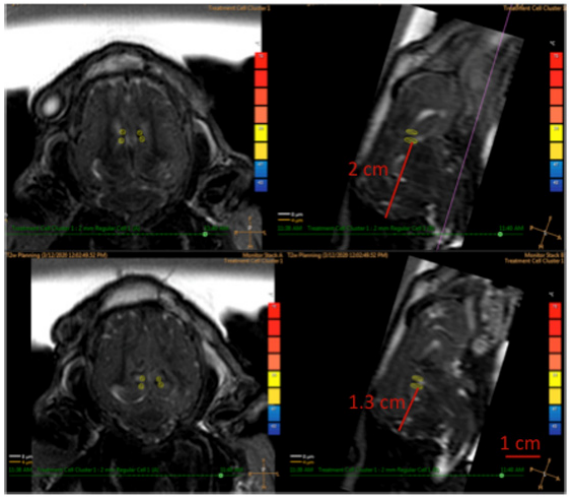

Figure 3. Movement between first (top) and repeat (bottom) localizing MR during HIFU treatment.

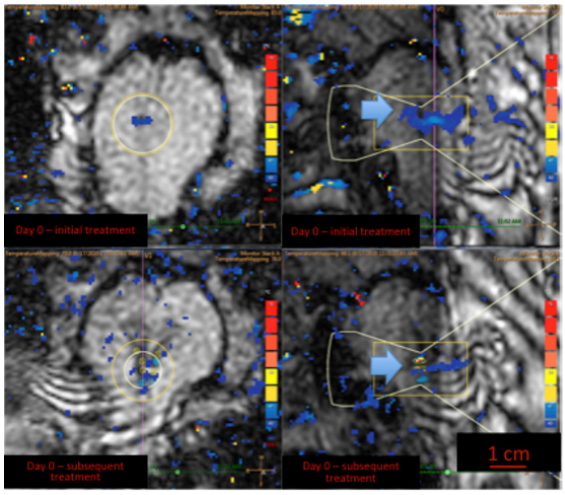

Figure 4. Arrows indicate near field effects on early (top) treatment cell and later (bottom) treatment cell.

P-TEC-1

Topic: Technical
Presentation Type: Poster

Feasibility of HIFU thermal monitoring using electrical impedance tomography (EIT)

Aharon Alfasi, Haim Azhari

Technion Institute of Technology, Haifa, Israel

Background: The aim of this study was to examine the feasibility of using Electrical Impedance Tomography (EIT) as a cost effective noninvasive tool for monitoring high intensity focused ultrasound (HIFU) treatment of the breast.

Materials and Methods: An EIT system comprising of 16 electrodes was built in our lab. The system produced images of the electrical conductivity in tissue samples. The system used the multi-frequency approach for scanning the samples. Ex-vivo tissue samples of chicken breast were scanned by the EIT system. A high intensity focused ultrasound (HIFU) assembly was used to insonify and heat the tissue. The EIT scanning plane was positioned at the HIFU focal distance (see Fig.1). EIT images of the mid-focal zone were acquired every 4 seconds, starting from the baseline "cold" state. A fiber optic thermocouple probe was inserted into the HIFU focal spot and was used to register the temperature as a function of time during the HIFU heating and the cooling processes.

Using post processing, the relative changes in the electrical conductivity resulting from the HIFU heating process were mapped. After completing the HIFU treatment, the tissue was cut along the imaged plane. A gross pathology picture depicting the ablated region was finally acquired to display the ablated region location and size and compared to EIT image.

Results: The results have shown that the change in electrical conductivity correlated well with the heating process. A region depicting significant changes was observed in the EIT maps after the heating was commenced. The location of the spot depicting the most prominent changes were located at the site of the HIFU focal zone. The size of this spot increased as the heating progressed. The maximal dimension of this spot was related to the heating duration. A typical EIT generated map along with a gross pathology picture are depicted in Fig.2.

Conclusions: EIT maps are sensitive to thermal changes in the tissue. The changes in the EIT image correlated with HIFU treatment duration. The EIT images can produce real-time monitoring of the heating process. In conclusion, EIT can potentially serve as a cost effective radiation free modality for non-invasive monitoring HIFU thermal treatment of the breast.

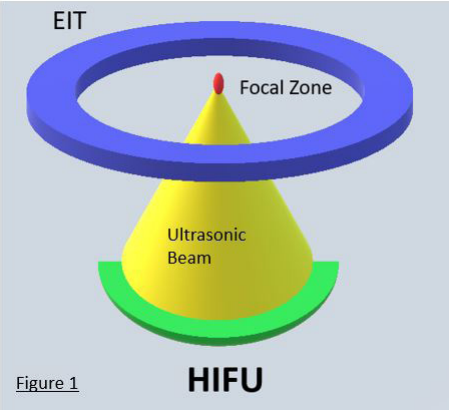

Figure 1: The EIT ring of electrodes was positioned at the plane containing the HIFU focal zone.

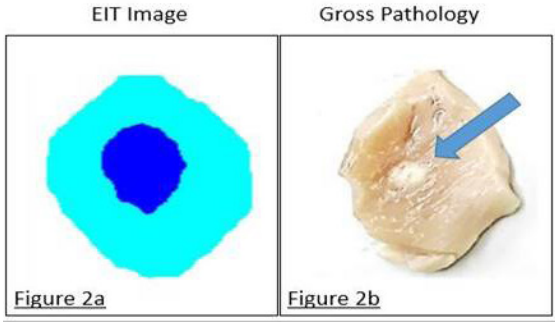

Figure 2. (left) An EIT image acquired at the end of the ablation procedure. (right) A gross pathology image of the treated tissue.

P-TEC-2

Topic: Technical
Presentation Type: Poster

Validation of raytracer approach for modelling temperature distribution under HIFU

Boris Breuer[1], Beatrice Lena[2], Peter Hilbers[1], Dragan Bosnacki[1], Huub ten Eikelder[1], Wilbert Bartels[2], Clemens Bos[2]

[1]Eindhoven University of Technology, Eindhoven, Netherlands
[2]UMC Utrecht, Utrecht, Netherlands

Background: The objective of this study is to experimentally validate the (Modena et al., 2018) raytracing approach for computing HIFU induced heat production and temperature profiles in fluids.

Materials and Methods: Computation of temperature profiles due to HIFU in a known environment consists of two phases:

1. computation of the heat production by the attenuation of ultrasound,

2. solving the bio-heat equation with the heat production as a source term.

To compute the heat production the elastodynamical wave equation must be solved. The numerical step (element) sizes must be small due to the wavelength, resulting in a high computational demand. We investigated whether a raytracing approach that incorporates interference between waves, may lead to sufficiently fast and precise alternatives to the more common acoustic wave equations solvers.

To validate the approach we conducted multiple sonication experiments on an agar silica gel-based Quality Assurance (QA) phantom at a power of 5, 10, 20 and 40 W. During sonication, the temperature is monitored using MR via the Proton Resonance Frequency Shift.

Results: Image 1 shows that the PRFS measured temperatures over time show good accordance with the simulated values at high power. Image 2 shows that also for a lower power and longer duration, the simulation and PRFS measurements coincide quite well.

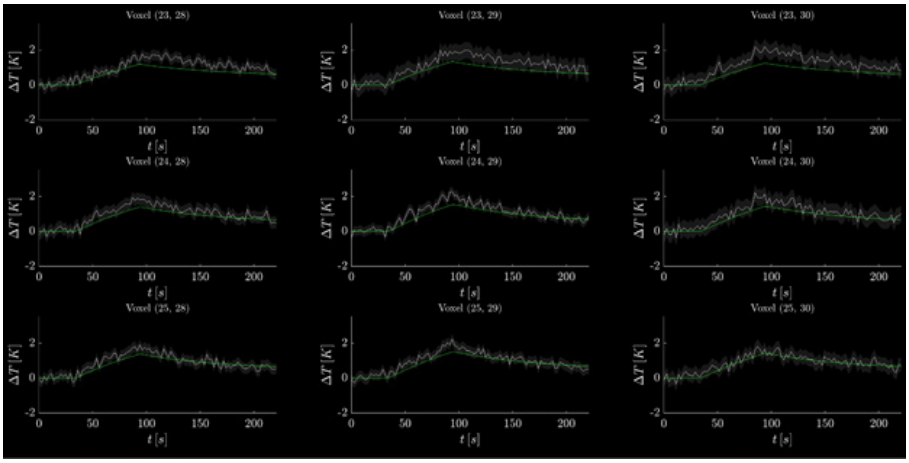

Figure 1. (top) QA (agar silica) phantom results near focus, experiment (PRFS) in white, simulation in green, 95 % confidence interval in gray. Settings: 40W, 2mm focus, 1.2MHz, sonication start at 20s, sonication en.

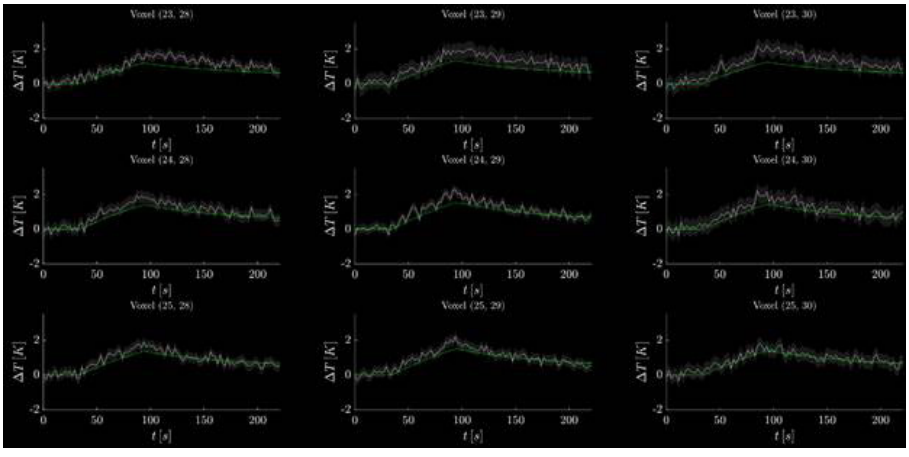

Figure 2. (bottom) QA (agar silica) phantom results near focus, experiment (PRFS) in white, simulation in green, 95 % confidence interval in gray. Settings: 20W, 2mm focus, 1.2MHz, sonication start at 20s, sonication end at 60s.

Conclusions: Because of the promising results of the initial validation study and the lower runtime of the model compared to other approaches combined with the accuracy which is on par with these approaches (Modena et al., 2018), effort is being made to further validate the model in a controlled fashion against solid materials.

After this validation step, the raytracing software will develop towards a planning tool to be used prior to MR-HIFU treatments.

Acknowledgements: Funded by STW/KWF.

P-TEC-3

Topic: Technical
Presentation Type: Poster

Pre-clinical MRI guided robotic device using focused ultrasound

Marinos Giannakou[1], Theocharis Drakos[1], Nikolas Evripidou[2], George Menikou[3], Antria Filippou[1], Christakis Damianou[1], George Evripidou[1]

[1]MEDSONIC LTD, Limassol, Cyprus
[2]Cyprus University of Technology, Limassol, Cyprus
[3]Nicosia General Hospital, Nicosia, Cyprus

Background: A magnetic resonance imaging (MRI)-robotic device with 4 computer-controlled axes (three linear and one angular) was developed. The positioning device holds a single element focused ultrasound (FUS) transducer. The purpose of this positioning device is to ablate small animals (mice, rats, cats, rabbits and small dogs) for preclinical research.

Materials and Methods: The robotic device includes MRI compatible piezoelectric motors, and optical encoders and ABS plastic. All the parts of the positioning device were developed using an industrial 3D printer. The diameter of the ultrasonic transducer can range from 20 to 60 mm. The transducer frequency was 2.6 MHz.

Results: The MRI safety of the device was successfully evaluated in a GE 1.5 T MRI scanner. The robotic device has the ability to accurately move the transducer. The ability of the transducer to cause high temperatures was tested successfully in a water-agar phantom.

Conclusions: A reliable, simple, cost effective, portable positioning device has been developed which can be used in virtually any MRI scanner since it can be placed on the scanner's table. The proposed positioning device can be used in the future for clinical trials for abdominal cancer treatment using FUS provided that it is evaluated extensively in animal models.

Acknowledgements: The project has been funded by the Research Promotion foundation of Cyprus under the project FUSROBOT (ENTERPRISES/0618/0016).

P-TEC-4

Topic: Technical
Presentation Type: Poster

OptimUS: A state-of-the-art computational suite for nonlinear therapeutic ultrasound modelling

Samuel Groth[1], Pierre Gelat[2], Seyyed Reza Haqshenas[2], Elwin van't Wout[3], Timo Betcke[2], Nader Saffari[2], Garth Wells[1]

[1]University of Cambridge, Cambridge, United Kingdom
[2]University College London, London, United Kingdom
[3]Pontifica Universidad Catolica de Chile, Santiago, Chile

Background: Treatment planning for therapeutic ultrasound based on numerical models still presents significant challenges. For realistic clinical scenarios, accurately simulating the nonlinear acoustic field using traditional solvers can be prohibitively expensive, requiring days to run on a computer cluster. The wider clinical translation and adoption of therapeutic ultrasound is dependent upon the ability to produce fast and accurate full wave patient specific simulations.

Materials and Methods: OptimUS is a fast and robust Python-scriptable computational suite, combining state-of-the-art finite element (FE) and integral equation (IE) techniques. The suite allows users to perform rapid and highly accurate full-wave FE simulations, implemented in the open-source FE library FEniCS-X. The FE implementation is scalable for large-scale parallel computations and can handle extremely heterogeneous domains in a straightforward manner. Alternatively, users may choose IE simulations, built on the boundary-element library BEMpp. IE simulations possess a significantly reduced computational burden when applied to domains with large regions of homogeneity (as often occur in ultrasound modelling in the abdomen), allowing them to be run on a single workstation. OptimUS therefore offers the flexibility for users to choose a method appropriate for their problem setting and available computing facilities.

Results: Linear and nonlinear ultrasonic fields are computed in realistic therapeutic ultrasound scenarios (see figures 1-2) and benchmarked against other solvers for both speed and accuracy. OptimUS can produce accurate results within a clinically relevant timeframe on a single workstation.

Conclusions: A range of cutting-edge finite element and integral equation formulations has been implemented and is available to download as an open-source Python library. It has been tested on clinically relevant scenarios. OptimUS represents a disruptive innovation in fast and accurate patient specific therapeutic ultrasound treatment planning.

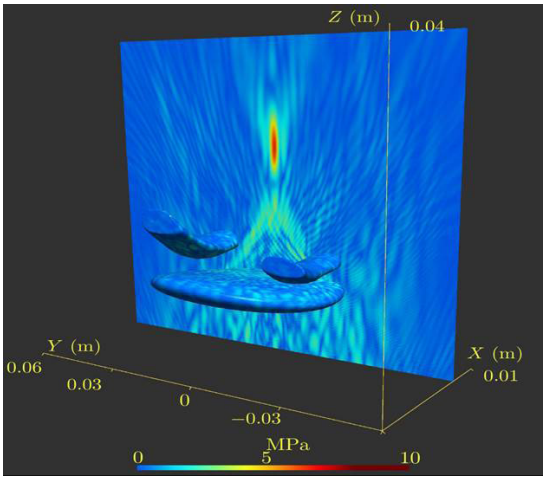

Figure 1. Absolute value of acoustic pressure generated by a 256-element HIFU array at 1MHz in an abdominal fat layer and ribs 10 and 11 using linear IE method.

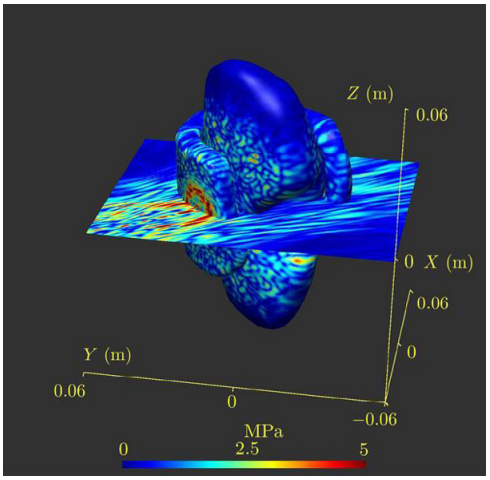

Figure 2. Absolute value of acoustic pressure generated by a 256-element HIFU array at 1MHz in a perinephric fat layer and the kidney using a linear IE method.

P-TEC-6

Topic: Technical
Presentation Type: Poster

Transient shear wave elastography using focused ultrasound excitations and sinusoidal magnetic resonance displacement encoding – a potential tool for MRgFUS treatment assessment

Lorne Hofstetter[1], Henrik Odéen[1], Bradley Bolster[2], Douglas Christensen[1], Allison Payne[1], Dennis Parker[1]

[1]University of Utah, Salt Lake City, UT, USA
[2]Siemens Medical Solutions, Salt Lake City, UT, USA

Background: A key mediator of cell death from ablative therapies is the denaturation of proteins, a process that is often marked by an alteration in tissue mechanical properties. Tissue stiffness mapping may be a useful tool to help predict the non-viable tumor volume following the ablation of cancerous tissues with MRI-guided focused ultrasound (MRgFUS). In this work we develop and evaluate a transient shear wave elastography approach that uses a sinusoidal displacement encoding strategy to record the displacement-time history of a transient propagating shear wave generated by the acoustic radiation force (ARF) from a focused ultrasound (FUS) transducer. This excitation and encoding strategy enabled the derivation of a simple analytic expression that can be used to generate shear wave speed maps. This approach may be particularly suited for treatment assessment of MRgFUS therapies since the same hardware used for therapy can also be used for elastography.

Materials and Methods: ARF impulses from a 256-element 950kHz FUS transducer were applied to a set of pre-selected positions. For each position a 3D segmented echo planar imaging (EPI) pulse sequence with sinusoidal-shaped motion encoding gradients (MEGs) was used to acquire the image volume twice for each excitation position. For the first acquisition, the start of the MEG waveform and ARF impulse occurred at the same time to acquire phase image phi_s. For the second acquisition, the ARF impulse was delayed by one quarter of the MEG period (T) in order to acquire phase image phi_c. These two differently encoded image volumes for each ARF position were acquired concurrently in an interleaved fashion. Shear wave speed maps (c_s) were computed for each excitation position using $c_s = 2\pi / (T * d/dr (angle (phi_c + i * phi_s)))$, where d/dr denotes the radial derivative in the imaging plane, angle() is the argument of the complex quantity and $i = sqrt(-1)$. Shear wave speed maps for each excitation position were combined using a pixel-wise median combination to generate a composite map. Measurement was performed in homogeneous and heterogeneous (inclusions, stiffer than the surrounding gelatin, ranging from 8.5 to 14mm in diameter) gelatin phantoms. In the homogenous phantom, a harmonic magnetic resonance elastography (MRE) measurement was performed using a prototype spin echo EPI MRE sequence with an external pneumatic driver to confirm the accuracy of the new approach.

Results: Shear wave speed images from measurements in the homogeneous phantom for six different ARF positions are depicted in Figure 1a-f and the composite shear wave speed map is shown in Figure 1g. The mean shear wave speed for the composite map shown in Figure 1g is 1.85 m/s and differed from all MRE measurements by no more than 14%. Figure 2 depicts the MRE measurement for six different harmonic excitation frequencies. For all MRE measurements the mean shear wave speed was between 1.62 and 1.69 m/s. MR phase images and individual shear wave speed maps from the inclusion phantom experiment are shown in Figure 3. Figure 3a and 3b depict the phi_s and phi_c images, respectively, for each ARF position and Figure 3c depicts the individual shear wave speed maps. The composite map of the measurements in Figure 3c is shown in Figure 4. Locations of the inclusions, depicted in the magnitude MR image (Figure 4a) are readily visible in the shear wave speed map (Figure 4b).

Conclusions: We have performed initial feasibility experiments to evaluate a novel magnetic resonance shear wave elastography technique that uses short ARF impulses from a FUS transducer and sinusoidal displacement encoding. This motion encoding strategy enables the use of an analytic expression to calculate the shear wave speed in heterogeneous and homogeneous viscoelastic mediums. Shear wave speed measurement was in close agreement with MRE. The shape, border, and location of inclusions 14 to 8.5mm in diameter could be identified in shear wave speed maps. While this approach shows promise, future work is needed to evaluate the ability of this method to measure changes in tissues stiffness following thermal ablation in ex vivo and in vivo models.

Acknowledgements: This work was supported by the NIH under Grants F30CA228363; R03EB023712; R01CA172787; R37CA224141; R01EB013433; S10OD018482; and the Mark H. Huntsman endowed chair.

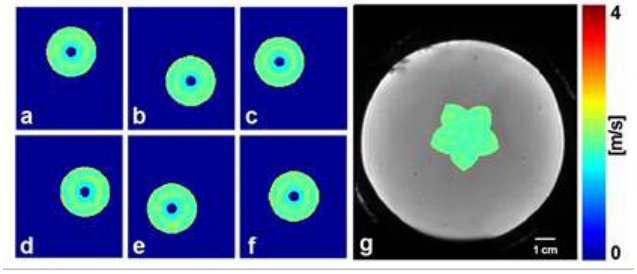

Figure 1. Shear wave speed measurements for each ARF excitation position in the homogeneous phantom are shown in (a-f) with composite map overlaid on magnitude image in (g).

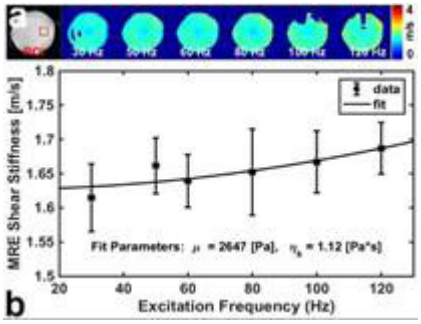

Figure 2. MRE maps for six different frequencies are shown in (a) with mean over 20x20 pixel ROI (red box) plotted in (b). Shear modulus (μ) and viscosity (η_s) were estimated using model fitting.

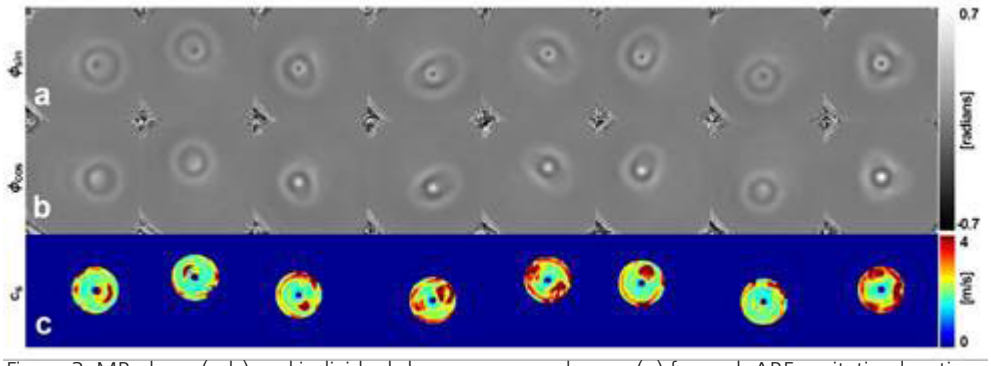

Figure 3. MR phase (a,b) and individual shear wave speed maps (c) for each ARF excitation location in the heterogeneous phantom with inclusions.

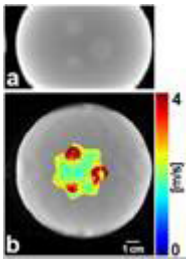

Figure 4. Reformatted gradient echo magnitude image of the heterogeneous phantom showing stiffer inclusions in (a) and composite shear wave speed map is shown in (b).

P-TEC-7

Topic: Technical
Presentation Type: Poster

Characterization of HIFU fields inside of a tissue-mimicking HIFU phantom

Sam Howard, Claudio Zanelli

Onda Corporation, Sunnyvale, CA, USA

Background: Development of a tissue-mimicking, transparent, scatterer-free gel phantom for HIFU has been previously described.[1] Up until now, this material has been used only as a thermal phantom, as it combines 0.6 dB/cm/MHz absorption with a thermal marker allowing easy visual detection wherever the temperature exceeds 65 °C.

Meanwhile, direct measurements of pressure are usually made in water. For piezoelectric hydrophones, damage or fouling is typically a concern for phantom usage. While reflectance-type fiber-optic hydrophones are easily refurbished by re-cleaving, and are widely used in water because their pressure range exceeds 400 Mpa, the optical scatterers in most phantoms represent an impediment for accurate measurement. As our phantom does not have scatterers, we decided to investigate its use with the fiber-optic hydrophone, in the hope of developing a technique which will be useful for treatment planning and quality assurance.

Materials and Methods: The phantom utilizes a polyacrylamide gel-matrix, doped with Bovine Serum Albumin (BSA) which provides the thermal marker, and proprietary additives for achieving the acoustic absorption without scatterers.[1]

The optical fiber probe (FO) consists of a 125 micron diameter glass fiber with 105 micron active diameter and is calibrated in water.[2] It was then inserted into a sample of the phantom through a cannula.

Sonication was provided by a 3.94 MHz F/1 nominally 19mm diameter HIFU source, driven in burst mode with 60 cycles to achieve its steady state response and with a 100 Hz pulse repetition rate to minimize the risk for cavitation and heating. The source was first characterized in water as a baseline. It was then acoustically coupled to the surface of the gel sample through a 5mm layer of water. The source transducer was then aligned in x-, y-and z-coordinates to peak the signal. The driving voltage was then gradually increased until cavitational instability in the hydrophone output was observed.

Results: Results at the maximum output power (an estimated pulse-average of 32W) are presented in Figs. (1-2) along with simulated results obtained using a Matlab-based tool[3] with a 15 mm effective diameter for the source. For the gel, the acoustic absorption velocity, and impedance measured in[1] were used, and the acoustic nonlinearity for water (B/A=5.2) was assumed.

Conclusions: We have demonstrated that the FO may be used with the scatterer-free phantom. Further refinements are planned to understand the differences with the model and place this measurement technique on a more rigorous footing:

A. Investigation of correction to the FO's water-based calibration by direct comparison to a needle hydrophone embedded in the gel. We expect that any correction factor to be generally applicable so this should only be necessary once
B. Measurement of the gel/s B/A ratio
C. Detailed raster scans of the source and improved source model for simulations
D. Rigorous evaluation of sources of measurement and modeling uncertainty

Figure 1.

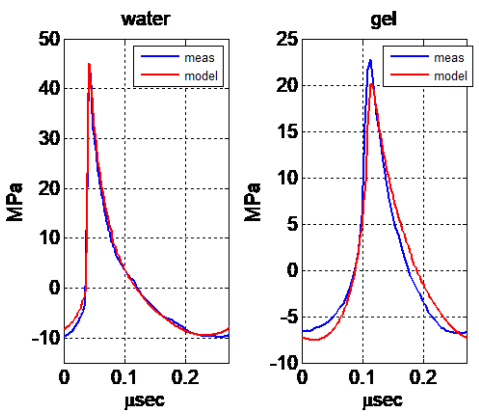

References:

1. S. Howard, J. Yuen, P. Wegner and C. Zanelli , "Characterization and FEA Simulation for a HIFU Phantom Material," IEEE Ultrasonics Symposium, 2003, pp. 1270-1273
2. S. Howard, C. Zanelli, "Validation of Reflectance-based Fiber-optic Hydrophones," International Congress of Acoustics, Aachen, Germany, 2019
3. HITU_simulator v2.0, retrieved November 9, 2020 at: https://www.fda.gov/about-fda/cdrh-offices/hitu-simulator

Figure 2.

	H_2O-meas	H_2O-model	Gel-meas	Gel-model
p^+ (MPa)	44.0	45.1	22.6	20.0
p^- (MPa)	-9.8	-9.9	-6.8	7.6
Intensity (W/cm^2)	9743	11000	4468	3575

P-TEC-8

Topic: Technical
Presentation Type: Poster

Young Investigator

Sonication strategies for delivery of volumetric ultrasound hyperthermia using the ExAblate body array

Kisoo Kim, Matthew Adams, Chris J Diederich, Eugene Ozhinsky

University of California, San Francisco, San Francisco, CA, USA

Background: Volumetric hyperthermia (HT) delivered with scanned focused ultrasound has potential to precisely enhance drug delivery or sensitize cancers to radiation and chemotherapy by elevating target tissue temperature to 40-43°C for 30-60 min. Clinically available MRgFUS systems are technically capable of delivering prolonged moderate heating required for HT deep within the body. ExAblate Body system (InSightec, Inc.) has FDA clearance for thermal ablation treatment of uterine fibroids and bone metastases. However, in order to perform volumetric HT with this system, advanced beamforming strategies should be developed, limited by the system constraints as designed for ablation, to accurately and conformally generate hyperthermia over large target regions. In this study, we investigated sector vortex beamforming methods as a sonication strategy for HT and developed an acoustic and biothermal simulation framework for rapid evaluation of the sector vortex approach.

Materials and Methods: The ExAblate Body system is comprised of an in-table sectored concentric-ring phased array operating at 1 MHz, with 208 elements and 12 cm diameter (Fig.1a). An acoustic and biothermal simulation framework was developed and used for the evaluation of a sector vortex method. In the simulation, the complex pressure distribution of each array element was calculated by the rectangular radiator method and summed at a common reference plane. The hybrid angular spectrum method was applied to calculate the 3D propagation and resultant acoustic intensity distribution within the absorbing tissue medium. For the biothermal simulation, a finite element method solver of Pennes Bioheat Equation (Comsol Multiphysics 5.5) was implemented to calculate steady-state temperature distributions resulting from the generated 3D acoustic intensity distributions, with maximum temperature set to 45°C as appropriate for hyperthermia treatments. To simulate hyperthermia on homogenous soft tissue, the parameters included attenuation = 6 Np/m, speed of sound = 1500 m/s, density = 1000 kg/m3, thermal conductivity = 0.5 W/m/K, specific heat = 3400 J/kg/K, perfusion = 3 kg/m3/s. We assessed focal size according to the number of vortex mode and the focal depth. Additionally, the experimental validation of a sector vortex method, axial and coronal views of a soft tissue-mimicking phantom were acquired with MR thermometry sequence at a 3T MR scanner.

Results: Simulations show that size of the focal region can be controlled by varying the sector vortex mode. General focal spot for the ablation (mode 0) has the smallest focal size (Fig.2, left, bottom), while the mode 4 provides the largest focal size (Fig.2, right, bottom). Volume above 41°C was found to be 4.90 – 34.55 cm3 with the vortex mode 4 across the focal depths (Fig.3). Approximately 22-40 times larger volume could be generated as compared to the vortex mode 0 standard for the array. Figure 4 shows axial and coronal views of soft tissue mimicking phantom. Large heating volume of the vortex mode 4 was clearly observed in MR thermometry. As a result, a single sonication with the vortex mode 1, 2, and 4 can be applied as an alternative to sequential mode zero multi-focus approach for large volume heating.

Conclusions: Acoustic and biothermal simulations, along with phantom studies with real-time MR thermometry, were used to evaluate a sector vortex method with four beam modes

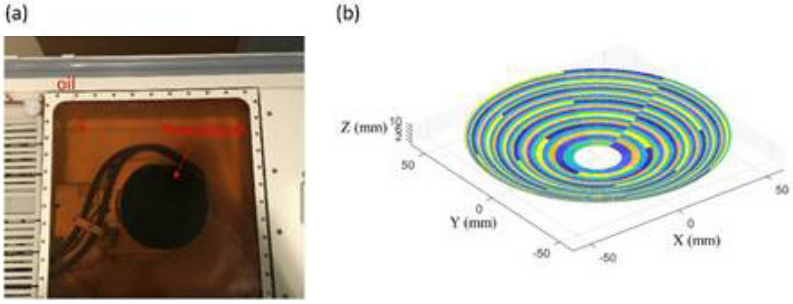

Figure 1. (a) Photo of the ExAblate body phased-array transducer. (b) Geometry of the sectored concentric-ring transducer array showing the constant surface area of each element.

as a sonication strategy for volumetric HT treatments. These vortex modes and focal depths can be controlled within the ExAblate Body System, thereby providing a method to control and increase hyperthermic volume with a single sonication pattern. Future efforts could include extending this approach to various phasing schemes combined with mechanically scanning to cover a larger volume.

Acknowledgements: NIH R21EB026018

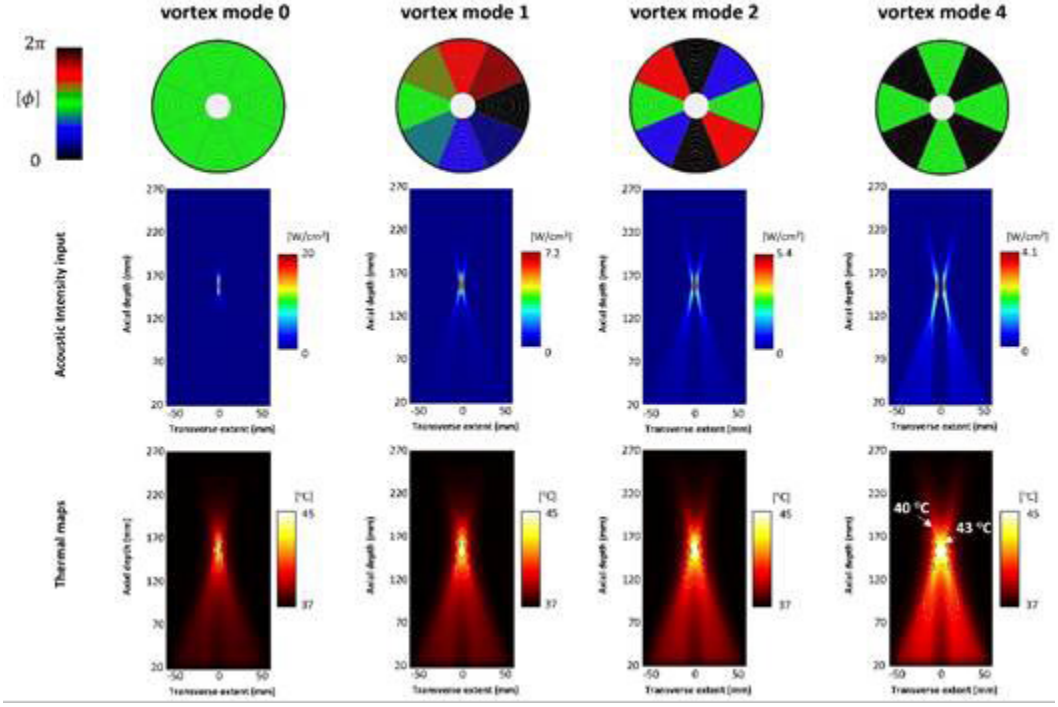

Figure 2. Top view (top row), acoustic intensity (middle row), and corresponding steady-state hyperthermia temperature distributions (bottom row) targeted at Z = 160 mm.

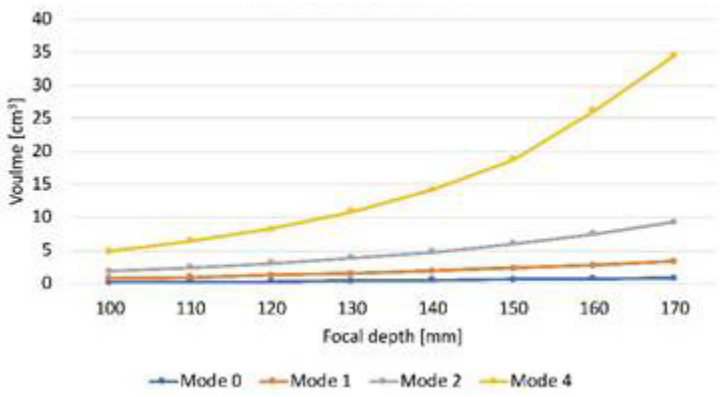

Figure 3. A focal spot volume over 41°C, heated by vortex mode 0, 1, 2, and 4 across the focal depths.

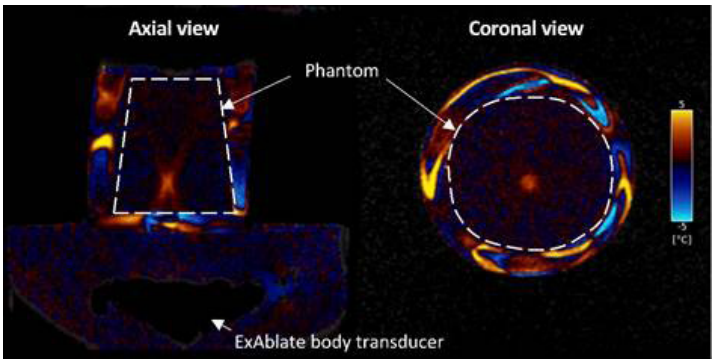

Figure 4. MR thermometry images of hyperthermia with the vortex mode 4. Axial and coronal views of soft tissue mimicking phantom were acquired with MR gradient echo sequence for MR thermometry.

P-TEC-9

Topic: Technical
Presentation Type: Poster

The use of graphic accelerators in modeling nonlinear ultrasound beams based on the Westervelt equation

Elena Konnova, Vera Khokhlova, Oleg Sapozhnikov, Petr Yuldashev

Lomonosov Moscow State University, Moscow, Russian Federation

Background: Development of high intensity focused ultrasound (HIFU) applications heavily relies on accurate prediction of ultrasound field parameters used for treatment planning. Several newer HIFU methods, such as histotripsy, effectively use nonlinear shock waves that form at the focus due to nonlinear propagation effects. The Westervelt equation is a commonly used model for simulating such nonlinear fields (Fig. 1). When three-dimensional beams are considered, simulations that include shocks take run times up to several days even using high performance servers with multicore CPUs. This precludes performing fast and efficient treatment planning. Computations can be accelerated using more parallelization on distributed cluster systems. However, availability of a cluster is not suitable for everyday practice. This problem can be mitigated by using graphics processors (GPU) that have up to several thousand mini cores and allow performing a wide range of mathematical operations.

Materials and Methods: In this project an algorithm to solve the Westervelt equation on a GPU was developed in order to achieve significant speed up over a CPU version. Conventional method of splitting the equation by physical factors was applied considering diffraction, nonlinear, and absorption effects separately at each propagation step. For diffraction operator, the angular spectrum approach, forward and reverse FFT using the cuFFT library, and propagator multiplication were implemented. For nonlinear operator, the solution was based on integrating the system of coupled differential equations for harmonics amplitudes by fourth-order Runge-Kutta method. Thermoviscous and tissue power law absorption effects were simulated using exact solution in the spectral domain. Both nonlinear and absorption operators were parallelized by space coordinates. For performance comparison, similar algorithm was also implemented on a multi-core CPU using OpenMP technology, the FFT was calculated based on the FFTW library. It was assumed that the algorithm implemented on the GPU would run several times faster than the algorithm for the CPU. Calculations were performed on a GPU of graphics card Nvidia GTX1070 with 8 GB of RAM and CPU Intel i7-4790K.

Results: In this work the results are presented for an example of modelling the field of a single focused transducer with a 1 MHz frequency. The amplitude distributions for the first 3 harmonics obtained in calculations at 8 CPU threads and GPU are presented in Fig. 2 in axial and focal planes of the transducer demonstrating the correct implementation of the algorithms. The speed of computing on the CPU increases proportionally to an increase in the number of threads. As expected, the 8-thread algorithm was faster than the 4-thread, but the rate of computing on GPU was much higher. The acceleration of calculations for 10 harmonics was obtained in the calculations on GPUs compared to CPU: 80 times (1 thread CPU), 20 times (4 threads) and 10 times (8 threads). When more harmonics were included, the acceleration gain increased proportionally to the number of harmonics (Fig. 3).

Figure 1. Schematic of the problem: simulation of nonlinear focused 3-D ultrasonic beams.

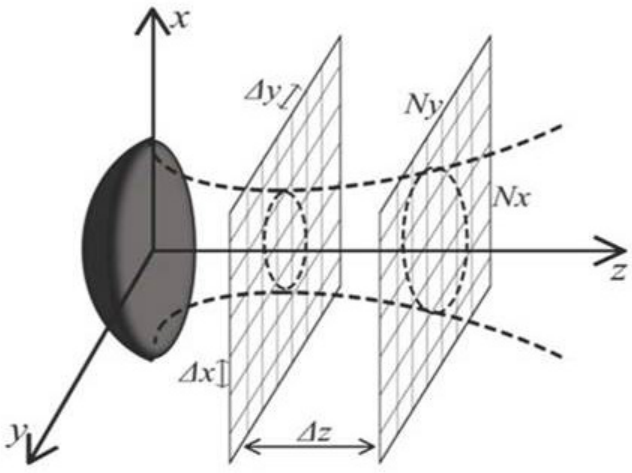

Conclusions: The C ++ programming language implements three algorithms for calculating high intensity focused ultrasound beams: single-thread for CPU, multi-threaded for CPU using OpenMP technology and algorithm for GPUsusing NVIDIA CUDA. It was shown that the use of graphic accelerators allows for about ten-fold acceleration of nonlinear 3D ultrasound beam simulation, for example from five hours to half an hour. This makes the implementation of numerical experiments feasible for practical implementation in HIFU applications using a personal computer.

Acknowledgements: This study was funded by RFBR 20-32-70142, the student stipend from "Basis" Foundation, and FUSF summer 2020 Internship Program.

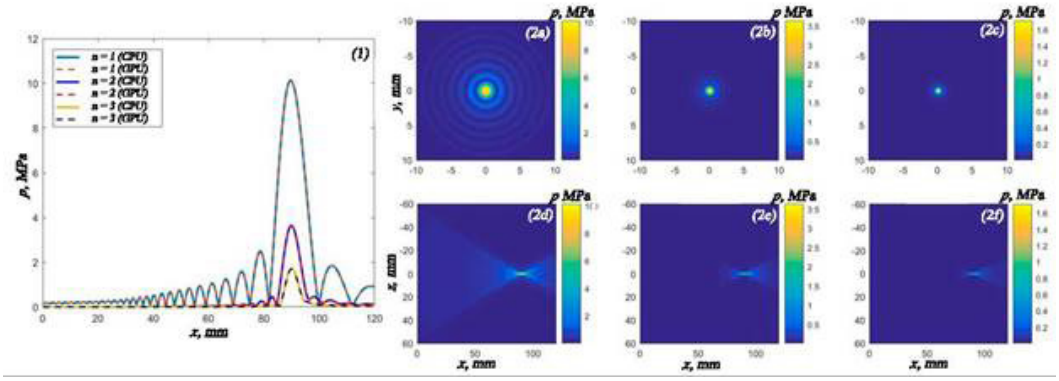

Figure 2. Amplitude distributions of the first three harmonics on the beam axis (1), in the axial (2a-2c) and in the focal (2d-2e) planes.

(1)

Matrix size $N_x * N_y$	Number of harmonic N_{max}	T, minutes			
		1 thread of the CPU	4 threads of the CPU	8 threads of the CPU	GPU (1920 threads)
2560*2560	10	1900	470 (4 times)	300 (6 times)	23 (80 times)
	50	43200	11520(4 times)	7800(6 times)	252(170 times)

(2)

Number of harmonic N_{max}		10	30	50	80	100
T, s	8 threads of the CPU	137	1100	3350	9850	16300
	GPU (1920 threads)	12,2	56	128	285	423
T_8/T_{GPU}		12	20	26	35	39

Figure 3. Comparison of the algorithm speed with various parallelization methods (1) and for 8 threads of GPU and CPU for a different number of harmonics included in simulations (2).

P-TEC-10

Topic: Technical
Presentation Type: Poster

Aberration effect induced by water coupling in therapeutic ultrasound

Varsha Kumar, Ellen Yeats, Timothy Hall, Zhen Xu

University of Michigan, Ann Arbor, MI, USA

Background: When a focused ultrasound beam propagates through heterogeneous media, sound travels at different speeds in different materials, and an aberration effect is observed which shifts and distorts the focus. In addition, the ultrasound pressure at the focus is reduced which has repercussions for histotripsy treatments. In therapeutic ultrasound, a water bath is typically used to couple ultrasound propagation from the transducer to the skin. Due to the difference in speed of sound between water and the skin, an aberration effect is induced, particularly for the large aperture, low f-number transducer arrays used in histotripsy, where the array elements at the outer rim sends sound waves through a very different water/tissue pathway compared to the inner transducer elements. This work investigates the focal position shift and pressure loss induced by the aberration from the water coupling bath in therapeutic ultrasound using a large aperture, low f-number transducer.

Materials and Methods: A simulation of a 500-kHz, 112-element array (f-number = 0.55) was used for the experiment. Glycerin solution containing 84.5% water and 15.5% glycerin yields the speed of sound in the skin/muscle (1560m/s) and was used to mimic soft tissue. A calibrated needle hydrophone was used to measure the pressure output. Glycerin solution contained in a cuboidal, acoustically transparent box was placed between the transducer and the hydrophone in a water tank, to mimic the situation of water-tissue coupling. The thickness of the glycerin box was varied in 25.4 mm increments from 0 mm to 50.8 mm to mimic different tissue path lengths. This experimental setup matched the computational conditions. The focal pressure and focal position were measured by experiments and compared to the simulation.

Results: K-wave simulations show that a focal shift of 4 mm and 6 mm for the glycerin box thickness of 25.4 mm and 50.8 mm, respectively. This focal position shift was due to (1) difference in the speed of sound between water and skin/muscle, and (2) the path-length: ultrasound pulses from the outer elements of the array propagated through a much longer distance in the media compared to the ultrasound path of the inner elements. The experiments yielded similar results, 4 mm and 6 mm for the glycerin box thickness of 25.4 mm and 50.8 mm, respectively, validating the k-wave simulation. The focal pressure loss was minimal, 4.6% for both glycerin box thickness of 25.4 mm and 50.8 mm.

Conclusions: These results show that the water coupling resulted in substantial focal shift due to the aberration effect using the low f-number histotripsy transducers. There was good agreement in ultrasound focal shifts between the experiment and the k-wave simulations. To correct the focal shift, the coupling medium may be changed from water to a solution that matches the speed of sound in tissue. Our next step will focus on investigating the aberration effects through multi-layer heterogeneous tissue.

P-TEC-11

Topic: Technical
Presentation Type: Poster

Interleaved water and fat MR thermometry for monitoring HIFU ablation of bone lesions

Beatrice Lena, Cyril Ferrer, Clemens Bos, Chrit T.W. Moonen, Wilbert Bartels

University Medical Center Utrecht, Utrecht, Netherlands

Background: MR guided Focused Ultrasound ablation is used for pain palliation in patients with bone metastases and for tumor control in osteoid-osteoma cases. MR Thermometry (MRT) is used to monitor heat delivery at the target, and to prevent damage to the surrounding tissues. Lesions in bone are often close to bone marrow and adipose tissue, e.g. subcutaneous fat, where conventional proton resonance frequency shift (PRFS)-based MRT does not work. Therefore, including a method for fat MRT would be of great interest. A promising approach is T1-based thermometry. Relatively fast T1 mapping can be performed using a 2D implementation of the Variable Flip Angle (VFA) method, which employs two RF-spoiled gradient echo (SPGR) scans acquired at different flip angles (FA), with a correction for the slice profile effect.[1–3] Here, we propose an interleaved method with PRFS-based MRT for water and 2D VFA-based MRT for fat. The technique was implemented and tested in an ex vivo experiment.

Materials and Methods: An interleaved scheme[4] was implemented on a clinical MR scanner to alternate one dynamic of a 2D PRF sequence with two dynamics of a 2D VFA sequence. In a pre-heating step, a set of reference PRFS phase maps and reference VFA scans was acquired. During heating and cooldown phases, the sequences were interleaved continuously. The PRFS scans provided temperature maps in water and the VFA magnitude images were used for MRT in fat (Figure 1). To determine which MRT method should be applied in each voxel, water and fat images were separated using the 3-point Dixon method from a pre-heating scan. From fat and water signal fraction maps, voxels with a fat fraction >70% were labelled as fat, voxels with a water fraction >70% were labelled as water.

The method was tested in an ex vivo pig leg experiment on a clinical 1.5T clinical MR-HIFU system (Philips Achieva + Sonalleve V2, Best, The Netherlands). Sonications were performed with an acoustic power of 40 W at 1.2 MHz, with intrinsic focus dimensions of 1 × 1 × 7 mm3. MR thermometry was performed during the whole experiment, consisting of three parts: 50s before heating, 60s of HIFU sonication and a cool-down period of 350 s (figure 2). Temperature change maps were computed every 6.3 s, i.e. after a cycle of 2 VFA scans and 1 PRFS scan.

Results: We were able to monitor temperature changes both in fat and in muscle, as shown in fig. 3, for one voxel in the muscle and one in bone marrow, close to the focus. Both curves reach a maximum at ~120 s from the start of the experiment. Different behavior is observed during the cooling: the fat returns to baseline temperature more rapidly than the muscle does. The high temperature peak in bone marrow probably occurs because bone cortex reaches a higher temperature than soft tissues and induces heating by conduction in its surrounding. In the cooldown, heat capacity differences play a key role, but the bone is able to maintain the temperature of tissues in its proximity by heat diffusion. Water and fat temperature change maps at the moment of highest temperature increase are presented in fig. 4. The combined water-fat temperature change map, fig 4c, shows, except of bone cortex, the continuous

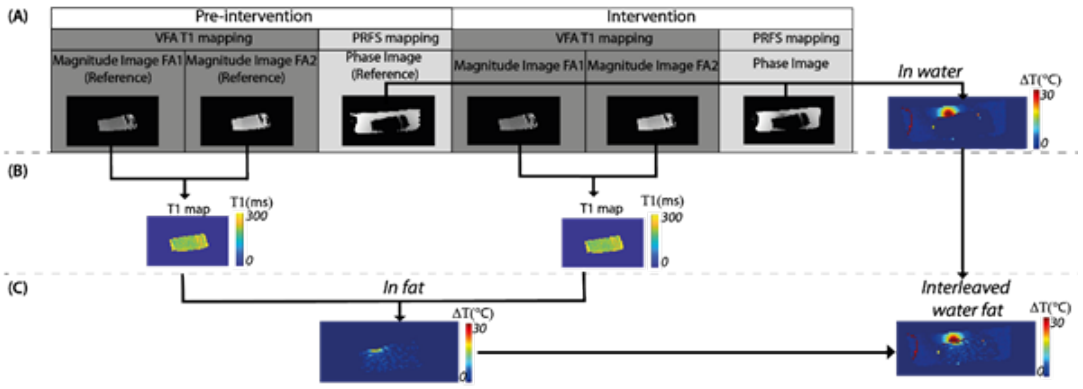

Figure 1. A, Scan images acquired from fat and water, with interleaved MRT and PRFS MRT calculation, B, 2D VFA T1 mapping, and C, the T1 MRT calculation and interleaved MRT map, overlapping PRF and T1 MRT maps.

spatial propagation of heating from the focus, through muscle, subcutaneous fat and bone marrow.

Conclusions: The use of interleaved 2D PRFS-VFA thermometry allows temperature mapping in water and fat. It allows to observe and study the different temperature behavior of muscle and adipose tissues, which are related to their respective acoustic and thermal properties, and their relative position to the heated cortical bone. Combining fat and water MRT gives a complete overview of the spatial heating distribution and could help in preventing damage to healthy fat tissue present in the target area. This approach may be of interest for other clinical applications involving mixed water and fat tissues, like HIFU procedures in the breast.

References:

1. *Med Phys* 44: 5930, 2017;
2. *MRM.* 45: 838, 2001;
3. *Proc. ISMRM* 4038, 2018;
4. *MRM.* 73: 692, 2015.

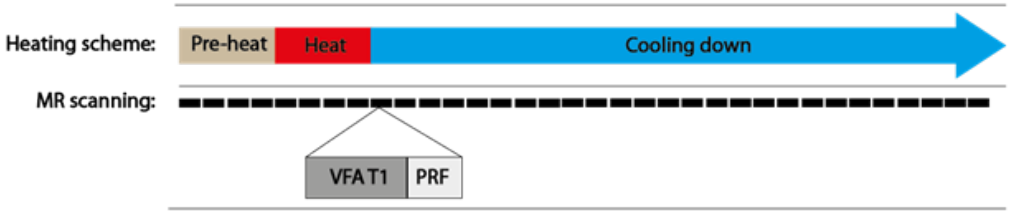

Figure 2. Schematic diagram over time of the HIFU experiment, consisting of pre-heating, heating and cool-down. MR scans were acquired for the whole experiment duration, as indicated.

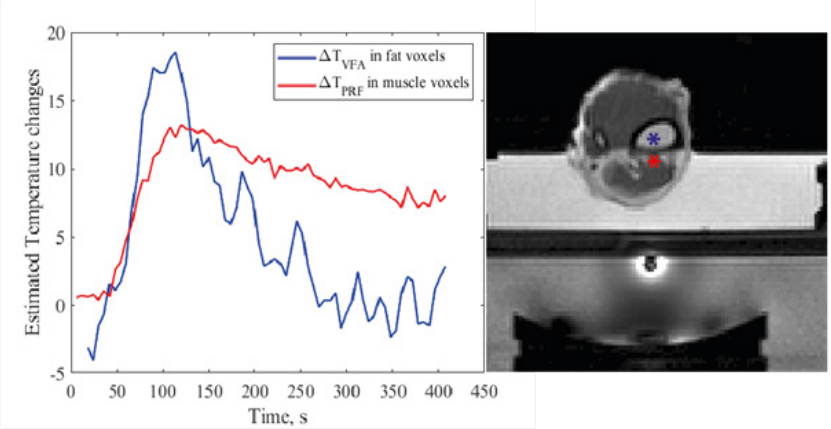

Figure 3. Temperature change (°C) vs time in a single muscle (red) and fat (blue) voxel: the red and the blue asterisks indicate the location of the voxels considered.

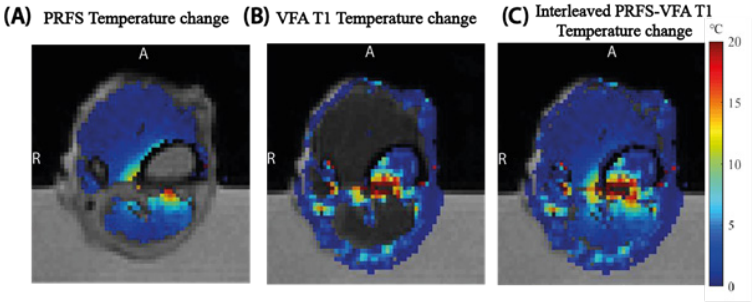

Figure 4. The temperature change map at the temperature peak from PRFS in water voxels (A.), from VFA T1 in fat voxels (B.) and from the interleaved thermometry (C.).

P-TEC-12

Topic: Technical
Presentation Type: Poster

Thermal dose optimization method for focused ultrasound treatment

Xilun Liu, Mohamed Almekkawy

The Pennsylvania State University, State College, PA, USA

Background: High intensity focused ultrasound (HIFU) is widely used as a technique that delivers the energy required to raise the tissue temperature to a cytotoxic level sufficiently fast such that heat can cause a coagulative necrosis. To maintain the temperature of the surrounding area at a physiological normal temperature and only target at tumorous area, the treatment should assure that the computed thermal dose is close enough to the desired one. This problem can be reduced by solving optimization problems subject to the Partial Differential Equation (PDE) constraints and other boundary conditions. The Skew Gradient Comparison (SGC) method, the conjugate gradient method (CGM) and adjoint method are previously used to solve this inverse problem. However, they are limited due to computational complexity. In this study, our proposed method is developed to significantly reduce the computational time by combining CGM, SGC and the adjoint method.

Materials and Methods: Our proposed method presents simple but effective modifications. The CGM in conjunction with the SGC and the adjoint method is analytically expressed and used to solve the PDE constrained optimization problem. The objective function can be reduced to the square difference between the actual thermal dose and the desired one. The minimization of the objective function is achieved through an iterative procedure. When a set of positions of foci are predetermined, the magnitudes of the focal point can be updated in each iteration and finally converge into an optimized solution.

Results: In our numerical simulations, different number of pairs of foci with predetermined locations which covered a targeted possible region of ablation are chosen as inputs. The results of the thermal dose distribution of using SGC is compared to our proposed method as shown in Fig.1: (a) Two pairs of foci are used to coagulate a region of [-2,2]\(mm\) and (b) three pairs of foci are used to coagulate a region of [-3,3]\(mm\). The dash line is the ideal thermal dose distribution, and the solid line and the dash-dotted line are the actual thermal dose distribution by using our proposed method and the SGC, respectively. Both optimization techniques can find an optimal thermal dose distribution. However, our proposed method is computationally more efficient than the SGC method.

Conclusions: This paper shows the application of SGC and CGM coupled with the adjoint problem to solve model-based optimization problem with PDE constrains. Our proposed method and SGC both can cover various computational region according to different locations and number of foci. However, we would like to highlight that our proposed method is at least 3 times faster than using the SGC. This proves that our proposed method can increase the efficiency without sacrificing the accuracy of the optimization method. This advantage can increase the feasibility and practicality of HIFU ablation, especially when the model is extended to 3D or real-time feedback and treatment are required.

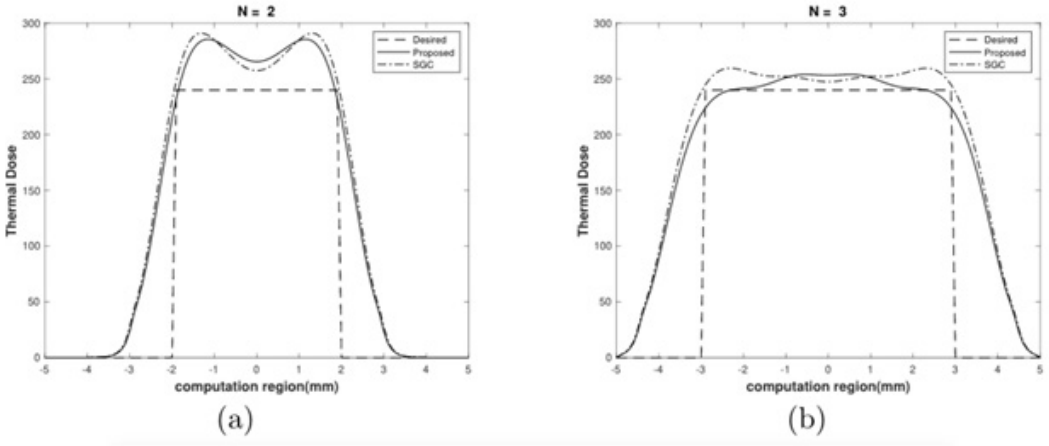

Figure 1. Thermal dose distribution when 2 and 3 pairs of foci approximated by Gaussian function with \(\sigma=0.52\) are used to treat a target region.

P-TEC-13

Topic: Technical
Presentation Type: Poster

Convective skin cooling device for MR-guided FUS treatments

Robb Merrill[1], Henrik Odéen[1], J. Rock Hadley[1], Pejman Ghanouni[2], Allison Payne[1]

[1]University of Utah, Salt Lake City, UT, USA
[2]Stanford University, Stanford, CA, USA

Background: MR-guided focused ultrasound (MRgFUS) ablation of large tumors routinely requires dozens to hundreds of individual sonications, repeatedly exposing the skin in the near- and far-field to low-level ultrasound intensities, causing accumulated heat to damage the skin. While body MRgFUS devices require a strict cooling period between successive ultrasound sonications, this incorporated safety metric is not only an inadequate guard against injury to the skin but also contributes to lengthened treatment times. Long treatment times and limited ability to treat superficial targets due to excessive skin damage remain major impediments to the adoption of MRgFUS for successful tumor treatment.

This study describes the development of a prototype device which (1) actively cools the skin during ultrasound sonications without compromising ablation effectiveness or introducing artifacts into MR temperature monitoring, (2) is conformable to a wide range of anatomy, and (3) is non-system specific.

Materials and Methods: The prototype skin cooling device consists of two 0.15mm-thick membranes welded to form a 21cm diameter circular pad. Baffles (same membrane material) were welded inside the pad to control flow for a convective cooling effect, with no baffles in the ultrasound beam path. Tubing ports were glued into opposite sides of the pad for input/output flow for distilled & degassed water coolant (Fig. 1) .

The coolant supply system consists of a peristaltic supply pump, pressure gauge, PID-controlled peristaltic return pump, and chiller unit. Dual-channel insulated tubing conveys chilled coolant from the supply system (MRI control room) through a waveguide to the cooling pad within the MRI scanner (Fig. 1).

System evaluation was performed using a preclinical MRgFUS system (Image Guided Therapy Inc.) on a 3T MRI scanner (PrismaFit Siemens). Non-ablation US through-transmission and pad conformability tests were performed using a phantom and normal human volunteer, respectively. Ablation tests were conducted under IACUC approval in an in vivo porcine model (N=2). Ablation was performed in the thigh muscle without active cooling as a control, and in the opposite thigh muscle with active cooling. Single point and volumetric ablation patterns, modeled after clinical protocols were evaluated at varied focal depths (0.1–5cm) and monitored with 3D MR temperature imaging. Ablation depth and skin damage were evaluated from MR temperature-based thermal dose measurements and gross pathology.

Figure 1. Skin cooling system components. (A) 3D CAD model of pad design (B) Welded pad filled with coolant (C) Support system in MRI control room (D) 3D CAD model of experiment setup (cooling pad = blue).

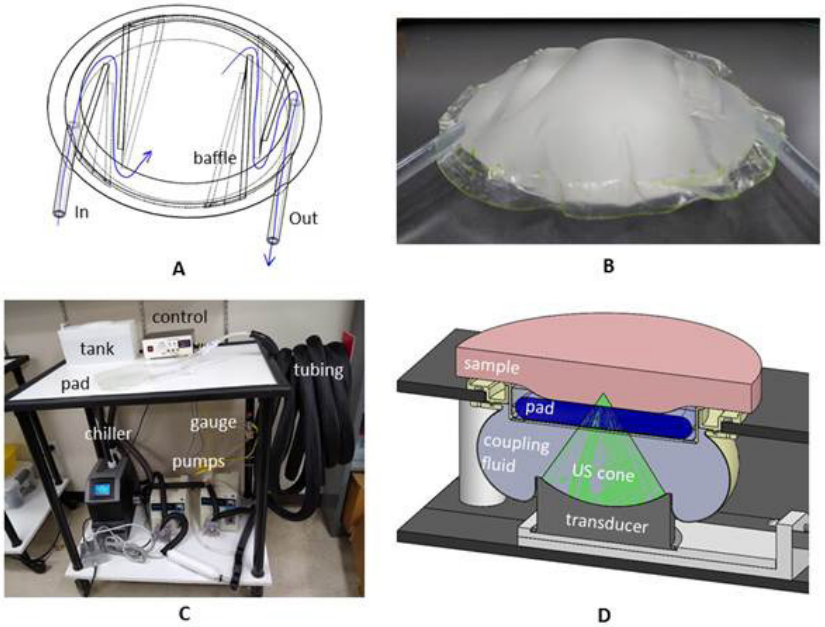

Results: Acoustic through-transmission testing of the pad showed 92% energy transmission through the pad into the sample. Phantom tests demonstrated no MR artifact and a temperature precision of 0.25 and 0.11°C during coolant flow- and no-flow conditions, respectively (Fig. 2). Conformability tests showed good acoustic coupling to a variety of human anatomy when the pad was at working pressure (Fig. 3). With the cooling pad in place, in vivo porcine model tests showed that superficial ablative procedures at 0.5 – 1 cm deep could be performed with little or no harm to the skin (Fig. 4). Indeed, red skin marks were observed on the control side (no cooling pad), while no markings were visible on the active cooling side (Fig. 5).

Conclusions: A conformable, convective skin-cooling device was developed that will enable safe, effective, and more rapid MRgFUS therapies. The device permits active cooling during ablation of both deep and

superficial targets. The device's ability to prevent skin burns during an ablation procedure was demonstrated in ex vivo tests as well as in vivo rabbit and porcine models. The developed, tested device described in this study will be used in human desmoid treatments at the conclusion of this project, having an immediate effect on MRgFUS treatments.

Acknowledgements: This work was supported by the Focused Ultrasound Foundation and NIH grant S10OD018482.

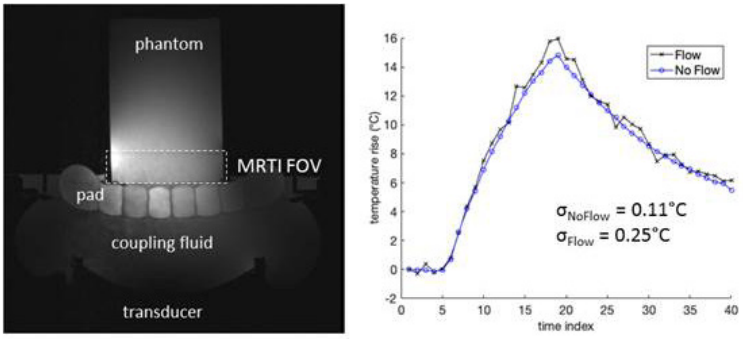

Figure 2. Comparison of flow vs. no flow conditions at 15°C coolant temp. and 630 mL/min flow rate. A volumetric sonication was performed in a gelatin phantom (5mm radius, 12 points, 200ms/point, 27W, 60 s).

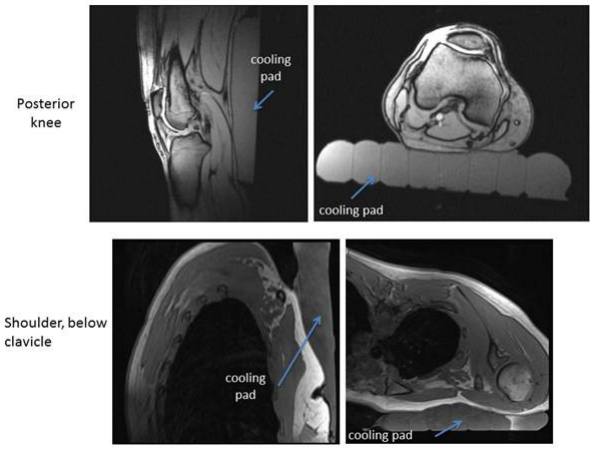

Figure 3. T1-weighted images showing good conformability and coupling to human anatomy at knee and shoulder. Early prototype pad was used in this study, which included baffles in center region.

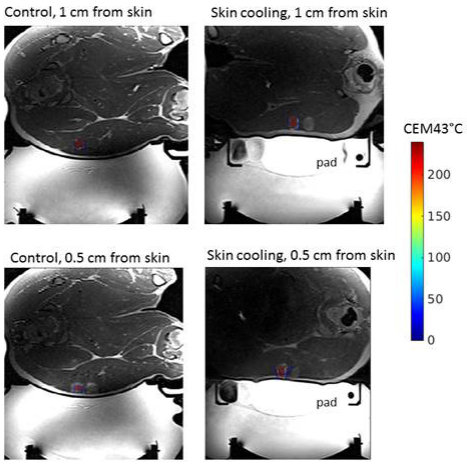

Figure 4. Ablation results, in vivo porcine studies. T2-weighted images (1.3mm isotropic, TR/TE: 2000/168ms) showing two target sites for each depth, and accumulated thermal dose in control and cooling setups.

P-TEC-15

Topic: Technical
Presentation Type: Poster

Agile, fully sampled modular 2D ultrasound arrays for HIFU

Paul Reynolds, Sean Taffler, Jerry Hopple, Stephen Barnes, Mike Sekins

Acoustiic Inc, Renton, WA, USA

Background: High Intensity Focused Ultrasound (HIFU) is a well known method for the ablation of tissue inside the body for applications such as cancer therapy. Traditionally, therapy systems consist of a focused bowl device with a single mechanical focal zone, or have limited ability to electronically adapt the focal zone using a small number of elements. If element count is significantly increased to allow for very improved and flexible focusing, traditional electronics cannot scale practically with number of elements needed. We present a HIFU array utilizing specialized electronics to enable fully sampled, high density element count (lambda/2 pitch), high power arrays for HIFU applications, in a modular and Magnetic Resonance (MR) imaging compatible construction.

Materials and Methods: An ideal HIFU system has high power output (>20W/cm2), sampled at half wavelength to avoid grating lobes, full element control for electronic steering, in a thermally efficient package. By adapting the microbeamforming technology typically restricted to high performance matrix imaging arrays, HIFU transducers have been built to meet these requirements. The ultrasound array is manufactured with piezoelectric materials suitable for high power drive, and impedance matched to human tissue. The tight element pitch ensures no grating lobes out to high steering angles (~45 degrees), and features element counts >1000 per module, requiring specialized emission plane electronics placed immediately next to the array, enabled with advanced interconnects. Attached electronics allow for rapid reprogramming of focal location, beam shape, and control of all critical functions. Efficient cooling mechanisms are implemented to maintain low temperature at the patient contact surface and to remove heat from the module. Careful construction methods ensure MR compatibility for a wide range of use cases.

Results: We present results from a >1,000 element, fully electronically controlled, lambda/2 spaced transducer module, operating in the 1 MHz range, capable of output up to 20W/cm2. Being modular form, this transducer can be a fully self-contained subunit of much larger configurable HIFU arrays, that will be MR compatible, and fully programmable. A range of results such as power output, steering, and lesion formation will be presented .

Conclusions: High density 2D ultrasound arrays are viable for HIFU therapy, meeting the requirements of a large number of applications that are otherwise limited due to lack of precision, speed, control or compactness. MR compatibility is possible and allows for combination with other imaging modalities or diagnostics/therapy.

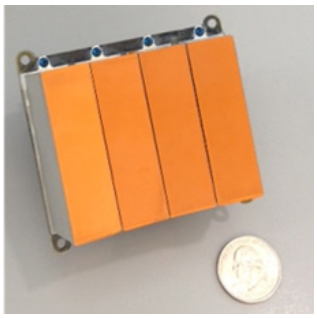

Figure 1. Mini modular HIFU therapy array

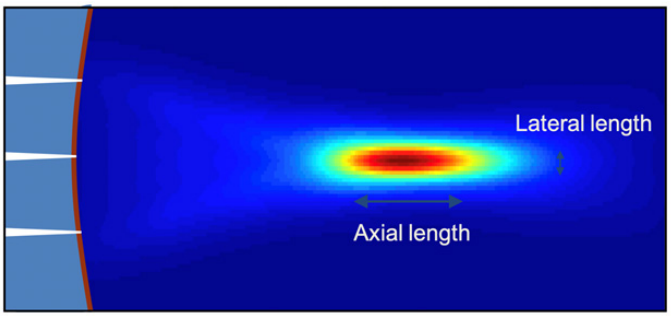

Figure 2. Axial focus simulation

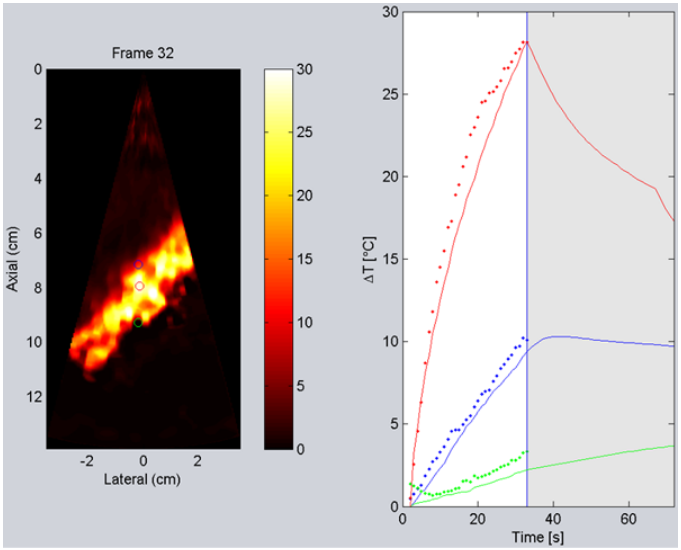

Figure 3. Temperature time plot sampled at different locations within the focal zone

P-TEC-16

Topic: Technical
Presentation Type: Poster

A high intensity focused ultrasound system for veterinary oncology patients

Kyriakos Spanoudes[1], Nikolas Evripidou[1], Marinos Giannakou[2], Theocharis Drakos[2], George Menikou[3], Christakis Damianou[1]

[1]Cyprus University of Technology, Limassol, Cyprus
[2]MEDSONIC LTD, Limassol, Cyprus
[3]Nicosia General Hospital, Nicosia, Cyprus

Background: MRgFUs technology is increasingly gaining interest for veterinary medicine applications. In our work, we are presenting a novel MRgFUS system for veterinary applications. The proposed system is fully compatible with any commercial 1.5T MRI due to its non-magnetic features and offers 4 degrees of freedom (X, Y, Z, Θ axes). A custom-made platform is designed to control the positioning device and the sonication parameters of the ultrasound system. The robotic device is compact and ergonomic. The device is carrying a single element transducer, that translates into a cost-effective solution for the veterinary market. In this in vivo feasibility study with rabbits the following aspects of the device were investigated: 1) Efficiency of coupling for a safe and efficient ablation, 2) Movement accuracy of the positioning device, 3) Animal placement during the procedure, 4) Efficiency of the transducer to create lesions (discrete & overlapping).

Materials and Methods: The positioning device was modelled using a CAD software and fabricated using fusion deposition modelling technology with Acrylonitrile Butadiene Styrene filament. It includes 4 computer-controlled axes (X, Y, Z and Θ). The moving plate of each axis is coupled to a threaded plastic screw attached directly to the shaft of a piezoelectric motor. The rotation of the shaft converts the angular motion to linear translation of the plate. The transducer's active element consisted of a P762-type piezoceramic crystal. Epoxy capable of withstanding temperatures up to 100 oC without losing its integrity was used as a backing material of the transducer element. The positioning device is controlled via an in-house developed user-friendly program developed in C #. The software holds the following functionalities: a) Communication with MRI, b) 2 axes movement either manually or automatically by specifying the algorithm, the step and the number of steps, c) MR thermometry, and d) ultrasound control (frequency, power, sonication time and cooling time). Ten locally bred rabbits were included in the study. A qualified veterinary surgeon was assigned to continuously monitor the vital signs of the animals throughout the experiment. Temperature maps were reconstructed in quasi real time after data processing. Image data were acquired in the coronal plane using Echo-planar Imaging single shot sequences for monitoring.

Results: Discrete and overlapping lesions were created with the device on the thigh of rabbits. Temperature maps reconstructed after data processing and which were obtained in the coronal plane. The temperature change recorded at 60 s was 17.06 oC (Fig. 2A). Figure 2B shows the temperature maps reconstructed after data processing and which were obtained in the sagittal plane. The temperature change recorded at 60 s was 39.59 oC.

Coronal MR images showing lesions with T2W-weighted fast spin echo sequence. A 3 X 3 grid pattern with 5 mm spacing and a cooling time of 140 s. between ablations was followed. The lesions appear in a plane perpendicular to the beam (Fig.3).

T2W-FRFSE image with fat suppression that were obtained after the completion of the ablation plan. Coronal (Fig 4A) and Axial (Fig 4B).

Conclusions: The system used in this experiment has shown to be capable of producing ablations in healthy tissue in vivo. Under MR guidance, the system can ablate tissues in depth with precision and efficiency. MRI enabled near real-time temperature monitoring of the treatment.

Acknowledgements: The project has been funded by the Cyprus Research and Innovation foundation under the project (FUSROBOT/0918/0016).

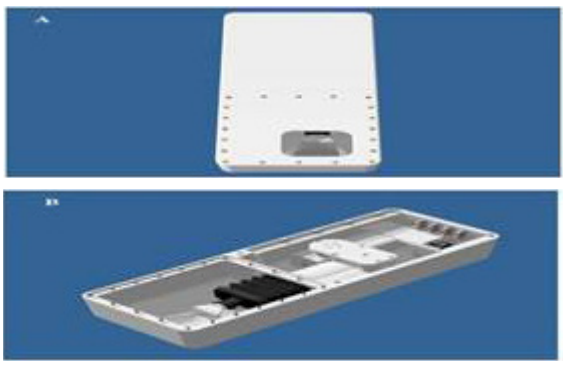

Figure 1. A: External CAD drawing of the robotic system. B: Internal CAD drawing of the robotic system.

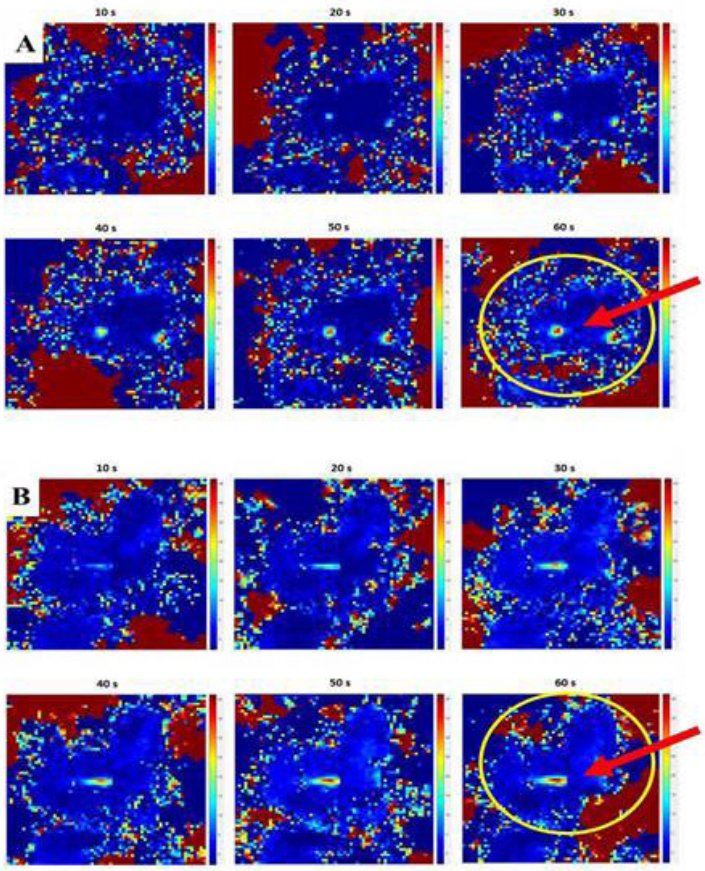

Figure 2. Temperature maps (coronal plane) recorded using single shot EPI sequence and the transducer (f=2.578 MHz, Acoustic Power= 27 W focal depth= 20 mm,) for sonication of 10 s, 20 s, 30 s, 40 s, 50 s and 6.

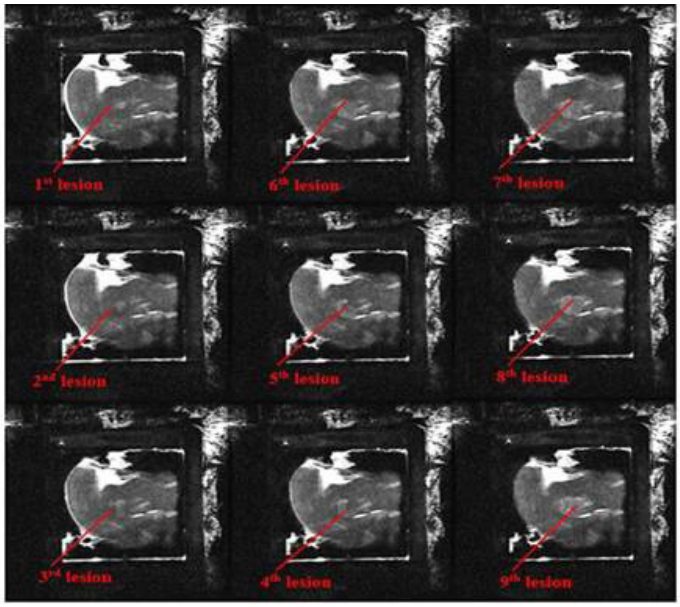

Figure 3. Coronal MR images showing lesions with T2W-weighted fast spin echo sequence was used with the following parameters: TR = 2500 ms, TE =60 ms, slice thickness=3 mm (gap 0.3 mm), matrix=256 X 256, FOV =1.

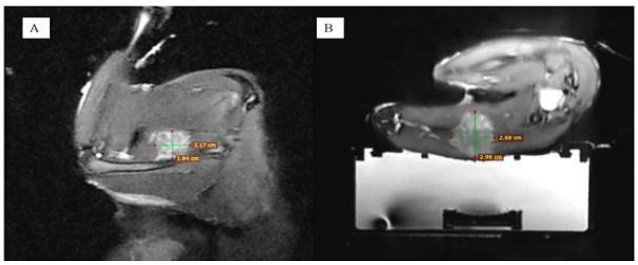

Figure 4. A: Coronal T2W-FRFSE image with fat suppression that was obtained after the completion of the ablation plan. B: Axial T2W-FRFSE axial image with fat suppression was acquired after the grid pattern in order to observe the ablated area.

P-TEC-17

Topic: Technical
Presentation Type: Poster

Learning multiparametric biomarkers for assessing MR-guided focused ultrasound treatments using vol-ume-conserving registration

Blake Zimmerman, Sara Johnson, Henrik Odéen, Jill Shea, Markus Foote, Nicole Winkler, Sarang Joshi, Allison Payne

University of Utah, Salt Lake City, UT, USA

Background: Noninvasive MR-guided focused ultrasound (MRg-FUS) treatments are promising alternatives to the surgical removal of malignant tumors. A significant challenge is assessing the viability of treated tissue during and immediately after MRgFUS procedures. Current clinical assessment uses the nonperfused

volume (NPV) biomarker immediately after treatment from contrast-enhanced MRI. The NPV has variable accuracy, and the use of contrast agent prevents continuing MRgFUS

treatment if tumor coverage is inadequate. Non-contrast, immediate MR biomarkers from multiparametric MR (MPMR) imaging have been investigated to assess MRgFUS immediately after treatment, including T2w images, MR temperature imaging (MRTI), and apparent diffusion coefficient (ADC) maps. This work presents a novel, noncontrast, learned multiparametric MR biomarker that can be used during treatment for intratreatment assessment, validated in a VX2 rabbit tumor model.

Materials and Methods: A rabbit animal model was used to generate a data set with and without contrast biomarkers to train and compare MPB-CNN against the clinical biomarker (NPV obtained immediately after treatment). New Zealand white rabbits (N=8, Charles River Laboratory) were injected with approximately 5 × 106 VX2 tumor cells in the belly of the quadriceps. Using a preclinical MRgFUS system (Image Guided Therapy, Inc., Pessac, France), ablation was performed on the tumor and surrounding muscle tissue with a 256-element phased-array transducer (Imasonic, Voray-sur-l'Ognon, France; 10-cm focal length, 14.4 x 9.8 cm aperture, f=940 kHz) inside a 3T MRI scanner (PrismaFIT Siemens, Erlangen, Germany). At 3-5 days post-treatment, the animal was anesthetized, and follow-up MR imaging was obtained. The MR sequences used during treatment/follow-up imaging and general setup are shown in Table 1 and Figure 1, respectively. A novel volume-conserving registration algorithm yielded a voxel-wise correlation between treatment and follow-up NPV, providing a rigorous validation of the biomarker. The follow-up NPV was semi-automatically segmented by an expert to provide a label of nonviable tissue. The MPB-CNN was trained using the registered follow-up NPV as a label and the following MPMR input images: (1) pre- and (2) post-ablation T2w images, (3) pre- and (4) post-ablation apparent diffusion coefficient (ADC) maps, (5) cumulative thermal dose (CTD) map, and (6) maximum temperature projection (MTP) map.

Figure 1.

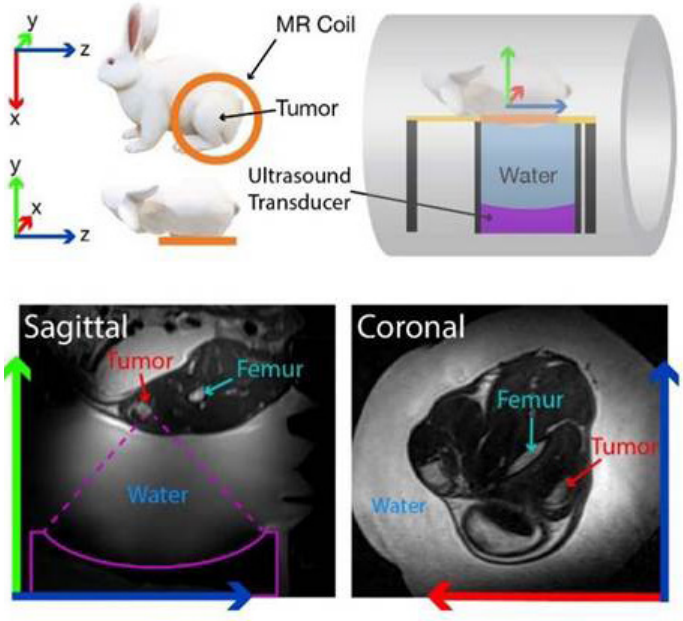

Results: The overall volume change of AVOCADO versus DRAMMS can be seen in Table 2. Not only does AVOCADO conserve volume throughout registration, but the target registration error is significantly less than DRAMMS (1.33 ± 0.16 mm vs 1.69 ± 0.64 mm, p=0.018). Figure 2 shows the improvement of the network output versus the immediate NPV measure used clinically. The DICE coefficient of the acute NPV prediction compared with the follow-up NPV was 0.53 ± 0.30 (mean ± standard deviation) whereas the DICE coefficient of the MPB-CNN prediction using noncontrast enhanced images compared with the follow-up NPV was 0.67 ± 0.20.

Conclusions: The presented comprehensive pipeline for volume-conserving registration generated a label of nonviable tissue and defined a non-contrast, multiparametric MR biomarker for treatment assessment using machine learning that outperforms clinical NPV assessment. Future work will include analyzing the MPB-CNN to determine the underlying intrinsic tissue properties that best predict tissue viability. This insight will allow the

design of a more targeted MR protocol and modify the network inputs to maximize the predictive power of the MPB-CNN. Although the presented registration has been applied to a specific animal model and data, the methods can be expanded to investigate and improve other minimally and noninvasive MR-guided treatments.

Acknowledgements: We would like to acknowledge Robb Merrill, Hailey McLean, and Elaine Hillas for their contributions. This work is supported by the National Institutes of Health [5R37CA224141, S10OD018482, 1R03EB026132]

Table 1.

Scan Type	Sequence	TR (ms)	TE (ms)	Flip Angle	Field of View (mm)	Pixel Bandwidth (Hz/Pixel)	Acquisition Resolution (mm)	Number Averages	Acquisition Time (mm:ss.ms)
MRTI	GRE-EPI (ETL=7)	25	11	14°	192×150×20	750	1.5×1.5×2.0	1	00:04.50
T1w*	VIBE	7.19	2.05	15°	256×192×52	250	1.0×1.0×1.0	1	1:03.00
T2w	SPACE	2000	300	120°	256×192×52	700	1.0×1.0×1.0	2	5:12.00
T1w**	VIBE	7.19	2.52	15°	256×192×56	250	0.5×0.5×1.0	3	6:19.00
Diffusion	SS-SE-EPI (ETL=92) (b=20,500)	7500	117	90°	160×116×20	1260	1.25×1.25×2.0	1	1:38.00

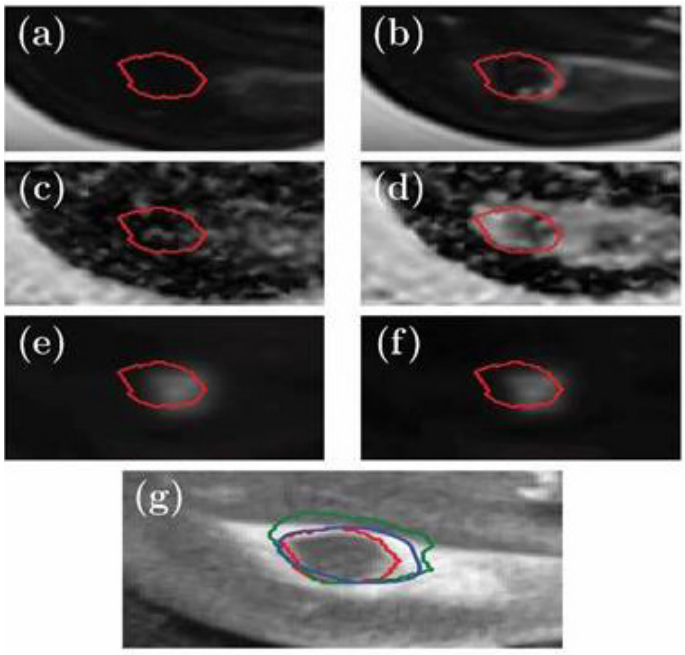

Figure 2.

Table 2.

	Original	DRAMMS		AVOCADO	
Subj.	Vol mm^3	Vol mm^3	%	Vol mm^3	%
1	1334.75	905.31	−32.17	1339.66	0.37
2	38.00	55.77	46.76	38.13	0.34
3	915.38	903.44	−1.30	911.82	−0.39
4	161.00	145.09	−9.88	161.57	0.36
5	20.38	12.61	−38.11	20.42	0.22
6	1949.15	1614.37	−17.18	1955.99	0.35
7	2628.12	3268.78	24.38	2629.99	0.07
8	3959.38	3878.74	−2.04	3966.28	0.17

P-WOM-1

Topic: Women's Health
Presentation Type: Poster

Evaluation of the learning curve observed during the implementation of the magnetic resonance image guided high intensity focused ultrasound treatment for uterine fibroids

Kimberley Anneveldt[1], Inez Verpalen[2], Joke Schutte[1], Jeroen Dijkstra[1], Miranda Van 't Veer - ten Kate[1], Rolf van den Hoed[1], Erwin de Boer[1], Ingrid Nijholt[1], Martijn Boomsma[1]

[1]Isala Hospital, Zwolle, Netherlands
[2]Amsterdam UMC, Amsterdam, Netherlands

Background: Although the Magnetic Resonance imaging guided High Intensity Focused Ultrasound (MR-HIFU) treatment for uterine fibroids has shown promising results, it is still not widely implemented in clinical practice. Implementation of new complex innovative therapies inherently comes with a learning curve. Previous studies reported a learning curve for the MR-HIFU treatment of uterine fibroids but did not define the learning curve in detail. The aim of this study was to analyze the learning curve observed while implementing MR-HIFU treatment of uterine fibroids to provide more insight in the number of treatments needed to reach clinical and technical relevant improvement of outcomes.

Materials and Methods: Women with uterine fibroids were counseled for MR-HIFU at the gynecologist outpatient clinic. After a screening-MRI, eligibility was determined by a multidisciplinary team consisting of radiologists and gynecologists. 76 MR-HIFU treatments were performed on the V1 Sonalleve (Profound Medical Inc.) system between June 2016 and January 2019. Clinical outcomes of the treatment were assessed by the Uterine Fibroid Symptoms – Quality of Life (UFS-QoL) questionnaire at baseline and 3, 6 and 12 months post-treatment. The % non-perfused volume (NPV%) was calculated directly after treatment using MRI-images. Treatment outcome is usually considered clinically relevant when the NPV% is >70% and/or a difference between baseline and follow-up of at last 10 points on the 0-100 scale of the UFS-QoL is found. In addition, treatment failures, adverse events and reinterventions were collected.

Results: 25%(19/76) of treatments were considered a failed treatment. Of these failed treatments, 68%(13/19) were a result of problems during treatment, which could be resolved while gaining more experience. 92%(12/13) of these problems occurred during the first 25 treatments, which we considered our learning curve. After the first 25 treatments, another type of failure appeared because when gaining experience, inclusion criteria were broadened. As a result of this overconfidence, additional failures appeared (6/19). The median NPV% of the first 25 treatments was 29,5%[range 0-99], the median NPV% of the subsequent treatments was 74,7%[0-120]. At 6 months both the decrease of symptoms and improvement of QoL were lower in the first 25 treatments compared to the subsequent 51 (Δ-16,6 vs. Δ-17,8 and Δ19,5 vs. Δ24,9). Three adverse events took place: 2 urinary tract infections and 1 third degree skin burn. The reintervention rate dropped after the learning curve from 52,0%(13/25) to 17,6%(9/51).

Conclusions: Clinically and technically successful MR-HIFU treatment of patients with uterine fibroids can be reached after approximately 25 treatments. Once competence is achieved, caution should be taken in order to prevent failures as a result of overconfidence.

Acknowledgements: This research was made possible with financial support from the Innovation and Science fund of Isala Hospital in Zwolle, the Netherlands. No author had any financial interest in the subject matter discussed in the abstract. No conflict of interest needs to be reported.

P-WOM-2

Topic: Women's Health
Presentation Type: Poster

MYCHOICE: The MYoma treatment Comparison study: High intensity image guided fOcused ultrasound versus standard (minimally) Invasive fibroid care – a (Cost) Effectiveness analysis: Rationale and design

Kimberley Anneveldt, Joke Schutte, Jeroen Dijkstra, Ingrid Nijholt, Martijn Boomsma

Isala Hospital, Zwolle, Netherlands

Background: Uterine fibroids appear in up to 70% of premenopausal women and can lead to symptoms of heavy bleeding, bulking and/or fertility problems. Both hysterectomy and myomectomy are surgical treatment options with a high risk of complications and long recovery times. Currently, uterine artery embolization (UAE) is the only reimbursed minimally invasive treatment option in the Netherlands. Magnetic Resonance image guided High Intensity Focused Ultrasound (MR-HIFU) is a safe, (cost)effective, non-invasive treatment option, which has a very short recovery time and less complications. However, a lack of comparative information on long-term (cost)effectiveness of the MR-HIFU treatment compared to the standard of care, keeps the MR-HIFU treatment from being reimbursed. In the MYCHOICE study we will determine the long-term (cost)effectiveness of MR-HIFU compared to standard (minimally) invasive fibroid care including UAE, myomectomy and hysterectomy.

Materials and Methods: The MYCHOICE study will be a national, multicenter, open randomized controlled trial with allocation in a 2:1 ratio to MR-HIFU or standard care. The non-inferiority margin is set to 15 points SSS reduction on the Uterine Fibroid Symptom - Quality of Life (UFS-QoL) questionnaire (range: 0-100). With an estimated drop-out of 20%, the sample size is 240 patients in 2:1 ratio for MR-HIFU (n=160) and standard care (n=80). Both an intention-to-treat and per protocol analysis will be performed. Follow-up will be 24 months. The study population consists in brief of women ≥18 years, premenopausal, diagnosed with symptomatic uterine fibroids in whom conservative treatment failed or is undesired and eligible for MR-HIFU. Exclusion criteria are MRI contra-indications, suspicion of malignancy, dominant adenomyosis, BMI ≥35kg/m2, currently pregnant or active wish to conceive (within 1 year) and not able or willing to sign informed consent. Primary outcomes of the study are quality of life at 24 months after treatment (measured by the UFS-QoL symptom severity score (SSS)) and costs consisting of direct health care costs, loss of productivity and patient costs.

Results: We expect to include the first patients in the autumn of 2020. Inclusion is expected to take 3,5 years followed by two years follow-up. Final results are therefore expected in 2026. Several centers, both academic and non-academic, will include patients. If randomized to MR-HIFU treatment, patients will be referred to the two MR-HIFU centers for uterine fibroids in the Netherlands.

Conclusions: By collecting data on the long-term (cost)effectiveness of the MR-HIFU treatment in comparison to the current standard of fibroid care, we will provide currently unavailable evidence about the proper place of MR-HIFU in the fibroid treatment spectrum. We expect our study to lead to reimbursement and implementation of the intervention in national uterine fibroid care guidelines, making the treatment available for all uterine fibroid patients.

Acknowledgements: The authors state that this work has not received any funding. None of the authors had financial interest or conflicts of interest in the subject matter discussed in the abstract. All authors state that this study complies with the Declaration of Helsinki

P-WOM-3

Topic: Women's Health
Presentation Type: Poster

Effects of T2* on accuracy of single reference variable flip angle T1 – mapping for MR thermometry

Michael Malmberg, Dennis Parker

University of Utah, Salt Lake City, UT, USA

Background: MR-guided focused ultrasound (MRgFUS) procedures for breast cancer need faster ways of accurately measuring temperature simultaneously in adipose tissue and glandular tissue. Since the proton resonance frequency shift (PRFS) method is not effective at measuring temperature change in fat, the T1-to-temperature relationship has been investigated due to its versatility across all tissue types. In 2019, a single reference (SR) method was published for the variable flip angle (VFA) method of T1-mapping, which method cut the necessary number of required dynamic acquisitions in half1. However, this SR-VFA method neglected changes in T2* with temperature1. This study eliminates that assumption and provides an understanding, through simulation, of the calculation bias produced by T2* changes with temperature. In addition, scanning parameters to minimize or eliminate this bias were determined to make the SR-VFA method a more viable choice towards fast T1 thermometry during MRgFUS procedures.

Materials and Methods: Monte Carlo simulations were performed 1000+ times on noisy data of a single simulated voxel to compare the VFA method with the SR-VFA method and the T2*-corrected version on accuracy and precision vs. the true T1 value. SNR was set at 100 relative to the Ernst angle signal for each TR/T1 baseline pair. Results were parameterized based on % change in T1 from baseline (0-200%), TE/T2*(0 - 0.5), TR/T1 baseline (0.01 - 3), and a temperature sensitivity ratio Z, defined as (% change in T2*) / (% change in T1) (0 - 1). Z was kept positive because in general T2 and T1 both increase with temperature. The bias and standard deviation of the 1000+ T1 estimates were calculated with sets of parameters in the above ranges. The bias value was found by taking the difference between the true T1 value and the mean of the noisy estimates.

For the flip angle sensitivity simulations, the reference and dynamic angles were varied from 0 to 90 at 0.5° increments. Angles that produced the minimum variance for a given parameter set were compared with the theoretical minimum obtained through the theory of propagation of errors. The "optimal" angles were defined as those that produced the minimum average variance over the 0-200% change in T1 for each parameter set. The T2* correction was simulated by fitting an a monoexponential curve to two noisy signals with the second TE/T2* = 1.

Results: Figure 1 shows a representative example of the effects of changes in T2* on the SR-VFA calculation. As T1 increases along the x-axis, T2* also increases according to the Z ratio. For this example, the bolded lines show equivalent data.

As shown in Figure 1, the SR-VFA calculation with T2* effects neglected produces a negative bias that increases in magnitude with larger changes in exp(-TE/T2*). This occurs both with increases in Z for a fixed TE/T2*baseline and with increases in TE/T2*baseline ¬for a fixed Z.

When the noisy T2* estimates were applied to the SR-VFA method's calculations on the bolded lines' data, the absolute bias dropped to less than 0.2% of the baseline T1, even exceeding the standard VFA method's accuracy. This is shown in Figure 2.

It was found that the "optimal" reference flip angle produces ~77% of the baseline TR/T1 Ernst angle signal, while the "optimal" dynamic angle produces 88-92% of the baseline TR/T1 Ernst angle signal.

Conclusions: It is shown that the SR-VFA method produces substantial calculation bias when T2* effects are neglected, which could lead to substantial temperature errors in T1 thermometry. Minimizing TE/T2* for the SR-VFA method is crucial to its accuracy. However, this bias can be removed by applying an estimate of the relative dynamic changes in T2*.

Though the SR-VFA method and PRFS thermometry require short and long TEs respectively, applying a T2* correction to the SR-VFA method can utilize both these needs via multi-echo acquisitions. Appropriately chosen TEs could allow both to be performed with reasonable speed and accuracy.

Future work will verify these relations in experiment, and TEs for optimizing speed and PRFS/T1 accuracy will be found.

Acknowledgements: Much thanks for our support in this work, specifically NIH Grant: NIHR01EB028316 with additional support from Insightec and Mark H. Hunstman Chair. We'd like to acknowledge Allison Payne, Viola Reike, and Henrik Odeen for their helpful conversations.

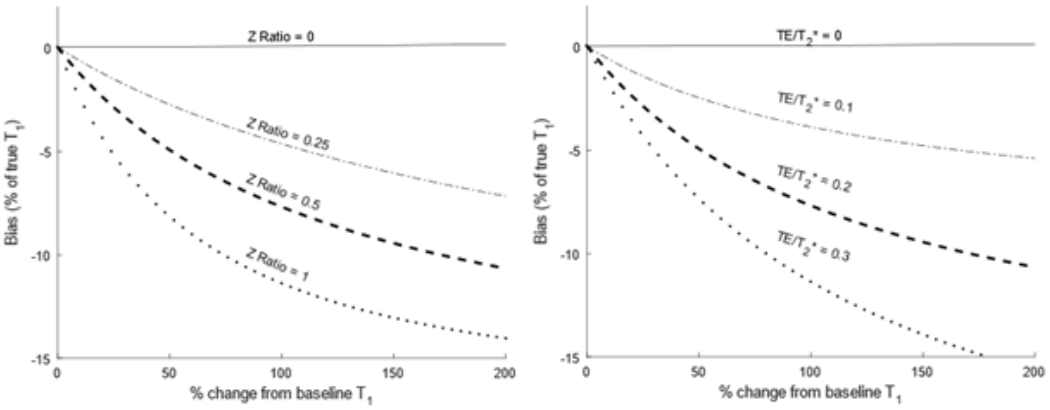

Figure 1:(left) – T1 calculation bias vs Z ratio, TE/T2* = 0.2;(right) – T1 calculation bias vs TE/T2*, Z ratio = 0.5; (both) – TR = 10 ms, T1 baseline = 350 ms, α = 6.4°, β = 21.2°. Bolded lines are equivalent.

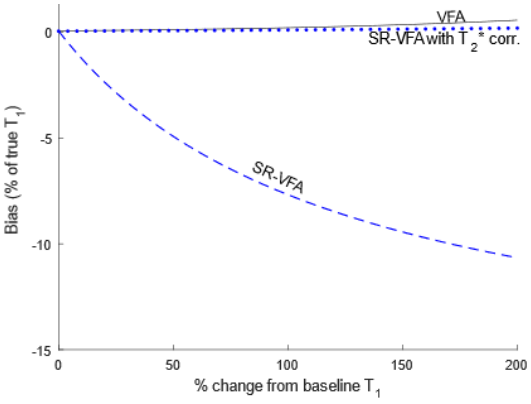

Figure 2: T1 calculation bias for VFA, SR-VFA, and T2*-corrected SR-VFA methods. TR = 10 ms, T1baseline = 350 ms, α = 6.4°, β = 21.2°, Z = 0.5, TE/T2* = 0.2. SR-VFA line = bolded lines in Figure 1.

Awards

Ferenc Jolesz Memorial Award

Nir Lipsman, MD, PhD, FRCSC

Nir Lipsman, MD, PhD, FRCSC

The Ferenc Jolesz Memorial Award was established in 2016 to honor the life of a true pioneer in focused ultrasound. The award has a two-fold purpose: to honor Ferenc's memory and to recognize and encourage this same innovative spirit in mid-career researchers and clinicians who continue to advance focused ultrasound.

We are honored to present the award to Nir Lipsman, MD, PhD, FRCSC.

Dr. Lipsman is currently the Director of Sunnybrook's Harquail Center for Neuromodulation, and the Clinical Director of Sunnybrook's Focused Ultrasound Centre of Excellence. He also serves as an Assistant Professor in the Department of Surgery at the University of Toronto.

Dr. Lipsman received his undergraduate degree from the University of Toronto. He went on to earn his medical degree from Queen's University and completed a neurosurgical residency and PhD at the University of Toronto. Over the last 10 years, Dr. Lipsman has pioneered several clinical applications of MR-guided focused ultrasound in novel indications, including essential tremor, Parkinson's disease, obsessive-compulsive disorder, and major depression. He has also initiated critical research investigating focused ultrasound's ability to temporarily open the blood-brain barrier in patients with a variety of debilitating diseases, including Alzheimer's disease, ALS, and primary and secondary brain tumors.

"It's an incredible honor to receive this award in Dr. Jolesz' name, a giant and pioneer in the focused ultrasound field," said Dr. Lipsman. "I share it with the amazing team at Sunnybrook and all our collaborators, without whom none of this exciting work would be possible."

The Ferenc Jolesz Memorial Award is supported by INSIGHTEC. Dr. Lipsman formally accepted the award, which includes a $5,000 cash prize, and presented his research at the 7th International Symposium on Focused Ultrasound during the awards ceremony on Wednesday, November 11, 2020.

The Ferenc Jolesz Memorial Award is sponsored by INSIGHTEC

In Memoriam — Ferenc Jolesz, MD

Ferenc Jolesz, MD

Ferenc Jolesz, MD, was a world-class visionary whose passion for pushing surgery into the 21st century led from developing image-guided minimally invasive therapy to pioneering focused ultrasound as a completely noninvasive approach. He passed away suddenly in December 2014.

Dr. Jolesz helped create the world's first MR-guided focused ultrasound system, and an early device was installed at Brigham and Women's Hospital. Research was conducted for several years under his guidance, eventually leading to the FDA approval of a system to treat uterine fibroids and establishing the technology's potential to noninvasively treat a range of serious medical conditions. Dr. Jolesz spent the last few years of his life championing the use of focused ultrasound for the brain, and was especially interested in exploring treatents for Alzheimer's disease.

2020 Visionary Award

Lawrence A. Crum, PhD

Lawrence A. Crum, PhD

Established in 2014, the Visionary Award is given every two years at our Symposium to recognize an individual who has created a larger vision for what the future of focused ultrasound may hold and whose effort, passion, and persistence have been crucial to advancing the field.

We are honored to present the award to Lawrence A. Crum, PhD.

Dr. Crum recently retired after a 25-year career in the field. Most recently he was Research Professor of Bioengineering and Electrical Engineering at the University of Washington (UW), Principal Physicist in UW's Applied Physics Laboratory, and Founder/Past Director of the Center for Industrial and Medical Ultrasound.

"Larry is one of the few true pioneers in the field of focused ultrasound," said Foundation Chairman Neal F. Kassell, MD. "From the beginning, he understood the technology's immense potential to help countless patients and led the field in both research and commercialization. We can all benefit from his insight on the opportunities that lie ahead."

A self-proclaimed "bubble expert," Dr. Crum received his doctoral degree in Physics from Ohio University and became interested in cavitation during his postdoctoral work at Harvard University. This interest collided with the field of focused ultrasound in 1994 when he was asked to consult on a new treatment for benign prostatic hyperplasia. That relationship led Dr. Crum to help establish the company that is now SonaCare Medical. Over the years, he co-founded three additional companies – Therus, Ekos, and Ultrasound Technologies – and the International Society for Therapeutic Ultrasound (ISTU).

He has held positions at Harvard University, the US Naval Academy, and the University of Mississippi, where he was F.A.P. Barnard Distinguished Professor of Physics and Director of the National Cancer Center for Physical Acoustics.

Dr. Crum has published more than 220 articles in professional journals (with a Google Scholar h-index of 84) and has been awarded 21 patents. He was recently awarded the Gold Medal of the Acoustical Society of America, its highest honor.

"The ultimate goal of most medical researchers is to participate in the development of a new technology that has a major impact on the health of our general society," said Dr. Crum. "I am confident that focused ultrasound will be one of those technologies."

During the awards ceremony on Wednesday, November 11, 2020, Dr. Crum gave a presentation on the path focused ultrasound has undergone from the Fry brothers to today and his vision for the technology's future.

Young Investigator Awards Program

The Focused Ultrasound Foundation established the Young Investigator Awards Program to encourage quality research by clinicians and scientists-in-training and to support their presentation of meritorious scientific papers at venues such as the 7th International Symposium on Focused Ultrasound.

Graduate students, research fellows, clinical fellows, and junior faculty members are eligible to apply for this early-career honor, which includes a $1,000 cash award. One of the 2020 Young Investigator Awards is sponsored by Bracco Suisse SA.

Nine Young Investigators are participating in the 7th International Symposium on Focused Ultrasound and being acknowledged with a special logo to call attention to their presentations on the virtual symposium platform. They recorded oral presentations and had an opportunity to participate in the question-and-answer sessions for the topical area of their research. To emphasize the significance of the Young Investigator Awards, the Foundation announced this year's award recipients in our monthly e-newsletter.

2020 Young Investigator Awards

CHP-1

Abstract: page 69

Abdul-Kareem Ahmed, MD

Awarded for: Bilateral magnetic resonance-guided focused ultrasound thalamotomy of the central lateral nucleus for medically-refractory neuropathic pain [CHP-1]

Abdul is a 3rd year neurosurgery resident at the University of Maryland. He studied neuroscience and philosophy at the University of Pittsburgh. He then earned his master's in science writing at MIT. Abdul completed medical school at Brown University where he was awarded the AANS Medical Student Research Fellowship. He was also awarded the ABTA Medical Student Research Fellowship for studying immune checkpoint blockade for gliobastoma. At the University of Maryland, he is invested in MRgFUS, studying methods to improve eligibility and outcomes in movement disorder patients with Dr. Howard Eisenberg, assisting in a trial to open the blood-brain barrier in glioma patients with Dr. Graeme Woodworth, and is working on a trial for treating neuropathic pain with Dr. Dheeraj Gandhi. Abdul hopes to one day bring focused ultrasound technology to his home state of Rhode Island.

IMM-1

Abstract: page 91

Harshini Ashar, MVSc

Awarded for: Immunological and therapeutic effects of focused ultrasound in canine cancer patients [IMM-1]

Harshini K Ashar is a PhD candidate under the mentorship of Dr. Ashish Ranjan in the Nanomedicine and Targeted Therapy Lab at Oklahoma State University. Her research is investigating the effects of focused ultrasound and nanoparticles on chemo-immunotherapy of chronic musculoskeletal infections and spontaneous canine cancers. She earned her bachelor's and master of veterinary science degrees from MAFSU, Maharashtra, India.

PSY-1

Abstract: page 184

Benjamin Davidson, MD

Magnetic Resonance Guided Focuses Ultrasound Capsulotomy for Psychiatric Disorders: Clinical Results and Neuroimaging Analysis [PSY-1]

Benjamin Davidson is a 4th year neurosurgery resident at the University of Toronto. He is in his final year of graduate studies, completing a PhD under the supervision of Dr Nir Lipsman and Dr Clement Hamani. His work focuses on developing novel neurosurgical treatments for treatment-resistant psychiatric disorders, and using neuroimaging tools to help predict and explain responses to psychiatric surgery.

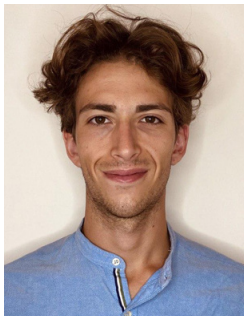

MSK-3

Abstract: page 284

Alessandro De Maio

Awarded for: MR-guided Focused Ultrasound versus External Radiation Therapy for the Treatment of Pain in Bone Metastases, a multicenter open-label phase-two clinical trial [MSK-3]

Alessandro De Maio is a student in his final year of Medical school, active in the field of imaging both diagnostic and interventional, at La Sapienza, University of Rome. He has been working with Dr. Alessandro Napoli and his team since 2017, where he had the opportunity to learn more about the Focused Ultrasound technologies as well as being involved in investigating clinical trials in bone metastases MRgFUS applications. Selected honors include Sapienza Excellence scholarship programs, research program fellowships with the University of Lund and University of Uppsala where he could work with experts in the field of Neuroimaging and MRI physics. Alessandro's main interests involve pursuing a career in science and radiology with enthusiasm on focused ultrasound therapies and emerging applications.

IMM-6

Abstract: page 96

Award sponsored by

BRACCO
LIFE FROM INSIDE

Avinash Eranki, PhD

Awarded for: Immune sensitization and therapeutic impact of boiling histotripsy in refractory murine neuroblastoma [IMM-6]

Avinash Eranki, is currently an Assistant Professor and Principal Investigator of Medical Ultrasound Research laboratory (MURL) within the Department of Biomedical Engineering at Indian Institute of Technology, Hyderabad, India. He has been working on therapeutic ultrasound for over 6 years, and medical ultrasound for over a decade. He worked with Prof. Chrit T. W. Moonen and Dr. Mario Ries at University Medical Center Utrecht, Netherlands, where he received his PhD. He also worked with Dr. Bradford J. Wood at the Clinical Center, National Institutes of Health, and the IGNITE group at Children's National Medical Center on developing novel therapeutic ultrasound techniques for solid tumor therapy in combination with immunotherapy, and chemotherapy. He is currently the Editorial Board Member of Ultrasound in Medicine and Biology journal, and serves as a reviewer for several other ultrasound, and imaging journals.

P-TEC-8

Abstract: page 336

Kisoo Kim

Awarded for: Sonication strategies for delivery of volumetric ultrasound hyperthermia using the ExAblate body array [P-TEC-8]

Kisoo Kim received his BS and MS degree in biomedical engineering at Kyung Hee University, Korea and earned his PhD at Strasbourg University, France in 2019. His dissertation work involved the development of quantitative MRI techniques (simultaneous MR elastography and MR thermometry) for the evaluation of MR-guided ultrasound thermal therapy. He currently works as a postdoctoral scholar under the mentorship of Drs. Chris Diederich and Eugene Ozhinsky at University of California, San Francisco. He is working to develop motion-robust, multi-slice, real-time MR thermometry for MR-guided ultrasound thermal therapy in abdominal organs such as pancreas, liver, and kidney. Additionally, he is working to develop a beamforming strategy for volumetric hyperthermia using the ExAblate body system. Kisoo pursues long-term research interest to develop all relevant MR/ultrasound techniques for MR-guided ultrasound thermal therapy and to achieve great growth in the field.

NMD-7

Abstract: page 160

Mehmet Ozdas, PhD

Awarded for: Non-invasive receptor-specific millimeter-precision manipulation of brain circuits by ultrasound-mediated aggregation and uncaging of drug carriers: In-vivo results [NMD-7]

Mehmet S. Ozdas received his MSc in Analogue and Digital Integrated Circuit Design from Imperial College London and his PhD from the Swiss Federal Institute of Technology Zurich (ETH Zurich) in 2019. During his PhD dissertation research at the Neurotechnology Laboratory of Prof. Mehmet Fatih Yanik, he worked on focused ultrasound and ultrasoundsensitive drug carriers to remotely concentrate drugs in the brain with millimeter resolution and orders of magnitude higher efficiency than systemic drug delivery. Mehmet S. Ozdas, Aagam S. Shah and Paul M. Johnson, and colleagues demonstrated that blood-brain barrier (BBB)-penetrant drugs can be focally delivered to specific brain regions without the need of BBB disruption, via a novel focused ultrasound sequence, ultrasound-sensitive drug carriers, and in-vivo electrophysiology.

Dr. Ozdas is currently a Postdoctoral Fellow in the Diffuse Midline Glioma (DMG) Research Center of the University Children's Hospital Zurich and the Neurotechnology Laboratory of ETH Zurich, where he is focused on developing novel tools for therapeutic interventions specifically for CNS disorders, including intractable childhood brain tumors. His research employs various methods including focused ultrasound, in-vivo electrophysiology, ultrasound-sensitive drug carriers and in-vivo micro-dialysis.

IMM-17

Abstract: page 111

Mohit Pratap Singh, DVM, PhD

Awarded for: Boiling histotripsy and CD40 activation re-sensitize the immunologically "cold" tumor to checkpoint blockade therapy [IMM-17]

Dr. Singh received his DVM from Madras Veterinary College, India and MS in Veterinary Surgery from GBPUAT, India. He earned a PhD at the College of Veterinary Medicine at the Oklahoma State University in 2015. During his doctoral studies in Dr. Ashish Ranjan's lab, he explored the role of combining focused ultrasound therapy with gene delivering nanoparticles and anti-CD40 agonistic antibody in improving tumor microenvironment of poorly immunogenic B16F10 murine melanoma. His interest lies in exploring novel ways of applying focused ultrasound therapy with various immune modulators such as nanomedicine and biologics and shaping the patient's immune system to fight cancer.

NDG-8

Abstract: page 150

Kristiana Xhima, PhD

Awarded for: Delivery of a selective TrkA agonist to the brain using transcranial focused ultrasound enhances cholinergic function and rescues cognition in a mouse model of Alzheimer's disease [NDG-8]

Kristiana Xhima is currently a postdoctoral fellow in Dr. Isabelle Aubert's lab at Sunnybrook Research Institute. She recently completed her PhD in Dr. Aubert's lab in the Department of Laboratory Medicine and Pathobiology and Collaborative Program in Neuroscience at the University of Toronto. Her research centers on focused ultrasound applications for neurodegenerative diseases, including ultrasound-mediated delivery of neurotrophic factors and gene therapies. Kristiana graduated from the University of Toronto with a BSc in pathobiology and neuroscience (with honours) in 2015.

Charles Steger Memorial Internship Program

Charles Steger, PhD

Claude Moore
CHARITABLE FOUNDATION

The Focused Ultrasound Foundation's Summer Internship Program was established in 2012 with the goal of giving accomplished high school, undergraduate, and graduate students the opportunity to collaborate with leaders in the field on a variety of projects that address preclinical, clinical, and business challenges.

In May 2018, the Foundation's internship program–which encompasses both local and global interns–was named in memory of Board of Directors member Charles Steger, PhD. The Foundation's summer technical internships are generously funded by the Claude Moore Charitable Foundation. The Claude Moore Summer Internship Program is part of the Charles Steger Focused Ultrasound Internship Program and is designed to foster interest in focused ultrasound technology among the next generation of researchers.

In the summer of 2019, the Foundation welcomed eight individuals from three countries who worked on both non-technical and technical projects.

In 2020, we accepted seven students and recent graduates to work remotely on a range of projects, including machine learning, Open Science policy, and treatment and technology research. Others worked with Foundation team members in the communications department and within the Foundation's FUS Partners program.

Despite not working in the office this summer, Foundation interns were still able to gain a thorough understanding of the technology and the Foundation. To supplement their experience, the Foundation's Director of Extramural Research, Matt Eames, PhD, coordinated a Zoom lecture series focusing on the different facets of focused ultrasound.

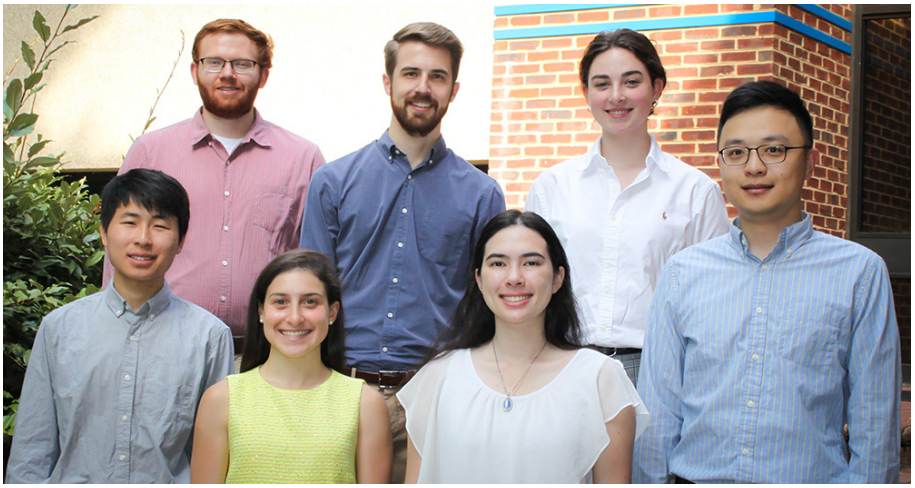

2019 Summer Interns

Back row, left to right: Sam Clinard, Nikolai Majorin, Juliette Strubel
Front row, left to right: Randy Wang, Isabella Small, Hannah DeVore, Zhihang Chen
Not pictured: Jackie Brenner, Kate Dieterle

2020 Summer Interns

Jon Carlini, Yisha He, Charlie Manning, John "Jack" Snell, Juliette Strubel, Annabel Taylor, Erin Wettstone

Because of the COVID-19 pandemic, it was not possible to take a group photo in 2020.

Global Internship Program

Hohyun (Henry) Lee

Receiving the highest peer-reviewed rating among submissions from the 2019 and 2020 FUSF Global Interns, Hohyun (Henry) Lee's abstract, entitled "A Benchtop Focused Ultrasound System for Drug Screening Investigations in Central Nervous System" earned him an award and an opportunity to present his work at the symposium.

The Focused Ultrasound Foundation offers an international internship opportunity for high school and university undergraduate students interested in the physical and life sciences. Interns supported through this program work in an established focused ultrasound laboratory under a researcher recognized in the field.

2019 Global Interns

Samuele Cabras
Instituto Besta
Mentor: Francesco Prada, MD

Jake Emrich
Vanderbilt University
Mentor: Charles Caskey, PhD

Arnav Garg
Albert Einstein College of Medicine
Mentor: Indranil Basu, PhD, MBA

Romik Ghosh
Ohio State University
Mentor: Vibhor Krishna, MD

Daniella Jimenez
Columbia University
Mentor: Elisa Konofagou, PhD

Camille Johnson
University of Chicago
Mentor: Kenneth Bader, PhD

Woongbin Kang
Jeju National University
Mentor: Dong-Guk Paeng, PhD

Chris Krasnichuk
University of Calgary
Mentor: Samuel Pichardo, PhD

Anna Kunturova
Moscow State University
Mentor: Vera Khokhlova, PhD

Varsha Kumar
University of Michigan
Mentor: Zhen Xu, PhD

Hohyun Lee
Georgia Tech
Mentor: Costas Arvanitis, PhD

Arjun Maystry
Albert Einstein College of Medicine
Mentor: Indranil Basu, PhD, MBA

Nathan Meulenbroek
University of Calgary
Mentor: Samuel Pichardo, PhD

Kaylee Meyers
Virginia Polytechnic Institute and State University
Mentor: Eli Vlaisavljevich, PhD

Andreas Mylonas
Cyprus University of Technology
Mentor: Christakis Damianou, MS, PhD

Anirudh Natarajan
Stanford University
Mentor: Raag Airan, MD, PhD

Polina Pestova
Moscow State University
Mentor: Oleg Sapozhnikov, PhD

Emma Slominski
University of Utah
Mentor: Henrik Odeen, PhD

Tayyaba Tahir
University of Calgary
Mentor: Laura Curiel, PhD

Karla Tapia
University of Utah
Mentor: Jan Kubanek, PhD

Sidney Trotter
University of Cincinnatti
Mentor: Kenneth Bader, PhD

2020 Global Interns

Daria Chupova
Moscow State University
Mentor: Vera Khokhlova, PhD

Ved Dattaray
Albert Einstein College of Medicine
Mentor: Indranil Basu, PhD, MBA

George Evripidou
Cyprus University of Technology
Mentor: Christakis Damianou, MS, PhD

Matteo Gionso
Istituto Neurologico Carlo Besta
Mentor: Francesco Prada, MD

Kethan Kommanapalli
University of Chicago
Mentor: Kenneth Bader, PhD

Elena Konnova
Moscow State University
Mentor: Oleg Sapozhnikov, PhD

Malia Sanghvi
SonaCare Medical
Mentor: Naren Sanghvi, PhD

Marie-Helene Tome
Albert Einstein College of Medicine
Mentor: Indranil Basu, PhD, MBA

Sponsors, Exhibitors, and Partner Organizaitons

Diamond Sponsor

INSIGHTEC

insightec.com

Advertisement: page 374

INSIGHTEC® is a global medical technology innovator transforming patient lives through incisionless brain surgery using focused ultrasound guided by MR imaging. The company's award-winning Exablate Neuro device is FDA-approved to treat medication-refractory Essential Tremor and Tremor-dominant Parkinson's Disease. Research for future applications in the neuroscience space is underway in partnership with leading academic and medical institutions. INSIGHTEC® is headquartered in Haifa, Israel, and Miami, Florida, with offices in Dallas, Shanghai and Tokyo.

Gold Sponsors

Electronics & Innovation, Ltd.

eandiltd.com

Advertisement: page 375

Electronics & Innovation Ltd, E&I, is a world leader in providing rugged and reliable Focused Ultrasound power products. We want to work with you from research to production, benchtop to module. In addition to our standard product lines, we offer custom modules and pallets – designed specifically to fulfill your OEM requirements. Operating globally and continuing to expand our technology, E&I is committed to providing RF power solutions of the highest quality, durability and ruggedness to the Focused Ultrasound Market.

PI (Physik Instrumente)

pi-usa.us

Advertisement: page 375

Making the impossible POSSIBLE – PI Ceramic focuses on custom piezo transducers and assemblies for therapeutic & focused ultrasound. Capabilities include miniature & complex PZT shapes such as hemispheres, customized composites and arrays, sub assembling expertise of gluing to substrates, custom electrode structuring, and specialty ultrasound transducers. 30+ Years' Experience.

Silver Sponsors

Bracco Suisse SA

bracco.com

BRACCO

LIFE FROM INSIDE

Bracco Imaging, part of the Bracco Group, is one of the world's leading companies in the diagnostic imaging business. Headquartered in Milan, Italy, it operates in more than 100 markets worldwide. Manufacturing activities are located in Italy, Switzerland, Japan, China, and Germany, while R&D activities are managed in three research centers located in Italy, Switzerland, and the U.S.

Daxsonics Ultrasound

daxsonics.com

DAXSONICS

ultrasound

Daxsonics Ultrasound provides engineering services for emerging ultrasound technologies. We work in at all stages of the life cycle providing a range of services including R&D, acoustic stack design, transducer design, electronics, software design, firmware design, and system integration. We can help overcome the barriers of developing novel ultrasound technology. We have experience designing and building high-frequency, miniaturized arrays, as well as complex, 1024-channel 2D arrays. Daxsonics is proud to be your ultrasound technology solution provider.

Shin Kong Group

shinkonggroup.com

新光人壽 慈善基金會
Shin Kong Life Foundation

The Shin Kong Wu Ho-Su Memorial Hospital contains 42 separate medical divisions, including: cardiology, thoracic surgery, nephrology, infectious diseases, gastroenterology, hematology / oncology, endocrinology / diabetes, allergy / immunology/ rheumatology, cardiac surgery, neurosurgery, plastic surgery, pediatric surgery, urology, general surgery, colorectal surgery, traumatology, neurology, orthopedics, family medicine, occupational medicine, obstetrics /gynecology, pediatrics, dermatology, psychiatry, otolaryngology, ophthalmology, anesthesiology, emergency medicine, rehabilitation, pathology, primary care, nuclear medicine, diagnostic radiology, tumor treatment, general dentistry, oral and maxillofacial surgery, prosthetic dentistry, endodontology, operative and cosmetic dentistry, periodontology, etc.

Society for Neuro-Oncology

soc-neuro-onc.org

The Society for Neuro-Oncology (SNO) is a multidisciplinary organization dedicated to promoting advances in neuro-oncology through research and education. SNO holds its Annual Meeting each year in November, and organizes additional stand-alone conferences on specific topics including pediatric neuro-oncology, metastatic disease and clinical trials. SNO publishes three peer-reviewed journals in partnership with Oxford University Press.

Sonic Concepts, Inc.

sonicconcepts.com

Sonic Concepts empowers our customers to reimagine ultrasound. We partner with research and biomedical organizations to develop premium ultrasound transducers and all-in-one turnkey systems for a range of applications, from neuromodulation to tissue ablation. We offer both MR-compatible and ultrasound-guided FUS transducer systems to provide accurate, real-time image guidance. Our specialty is delivering exceptional acoustic performance within budgetary constraints.

The IEEE Ultrasonics, Ferroelectrics, and Frequency Control Society (UFFC-S)

ieee-uffc.org

According to the UFFC-S Constitution, Article 3, Section 3.1, the field of interest of the UFFC-S shall include theory, technology, materials, and applications relating to:

- The generation, transmission, and detection of ultrasonic waves and related phenomena.
- Medical ultrasound and associated technologies.
- Ferroelectric, piezoelectric, and piezomagnetic materials.
- Frequency generation and control, timing, and time coordination and distribution.

This interest ranges from fundamental studies to the design and/or applications of devices, sensors, systems, and manufacturing technologies within the general scope defined above. Modification of the Field of Interest shall be in accordance with the procedures specified by the IEEE and amendments to this Constitution.

Verasonics, Inc.

verasoncis.com

Verasonics designs and markets the Vantage™ Ultrasound Research System which provides academic and commercial investigators with leading-edge solutions, including imaging and interventional ultrasound techniques, and focused ultrasound energy delivery. In collaboration with Sonic Concepts, Verasonics offers HIFUPlex transducers and the HIFUPLEX Plus, a full-turnkey research solution in ultrasound-guided focused ultrasound (USgFUS).

Exhibitors and Partner Organizations

AdvaMed

advamed.org

The Advanced Medical Technology Association (AdvaMed), is a trade association that leads the effort to advance medical technology in order to achieve healthier lives and healthier economies around the world. AdvaMed's membership has reached over 400 members and more than 80 employees with a global presence in countries including Europe, India, China, Brazil, and Japan. AdvaMed's member companies range from the largest to the smallest medical technology innovators and companies. The Association acts as the common voice for companies producing medical devices, diagnostic products and digital health technologies.

American Institute of Ultrasound in Medicine

aium.org

The American Institute of Ultrasound in Medicine is a multidisciplinary medical association of more than 9000 physicians, sonographers, scientists, students, and other health care providers. Established in the early 1950's, the AIUM is dedicated to advancing the safe and effective use of ultrasound in medicine through professional and public education, research, development of guidelines, and accreditation.

Breast Cancer Alliance

breastcanceralliance.org

The mission of Breast Cancer Alliance is to improve survival rates and quality of life for those impacted by breast cancer through better prevention, early detection, treatment and cure. To promote these goals, we invest in innovative research, breast surgery fellowships, regional education, dignified support and screening for the underserved.

Cancer Research Institute

www.cancerresearch.org

The Cancer Research Institute is motivated by a very simple but important scientific fact: the human body has the ability to defend itself from cancer. The mission is straightforward — save more lives with cancer immunotherapy. Our founding scientists believed that the key to long-term survival lay in learning how to manipulate the immune system to strengthen its defenses against cancer. We set out more than 60 years ago not only to prove this could be done, but also to do something with this knowledge that would truly help cancer patients. This work is now beginning to pay off: immunotherapies are transforming cancer treatment and bringing us closer to cures for all cancers.

Cooley

cooley.com

Cooley

Cooley's preeminence in life sciences goes back decades, beginning in the 1980s when the firm took public both Genentech and Amgen. Today, Cooley is trusted counsel to almost 1,800 public and private life sciences clients worldwide, including more than 50% of the NASDAQ Biotechnology Index.

U.S. Food and Drug Administration

fda.gov

FDA

CDRH Offices
fda.gov/about-fda/center-devices-and-radiological-health/cdrh-offices

Medical device submission package eCopy Program
CDRH-eCopyinfo@fda.hhs.gov
+1 240.402.3717

Focused Ultrasound Foundation (FUSF)

fusfoundation.org

Board of Directors: page 377
Research funding: page 378
8th International Symposium: Inside back cover

FOCUSED ULTRASOUND FOUNDATION

The Focused Ultrasound Foundation is a medical technology research, education, and advocacy organization dedicated to improving the lives of millions of people with serious medical disorders by accelerating the development and adoption of focused ultrasound. The Foundation works to clear the path to global adoption by organizing and funding research, fostering collaboration, building awareness at our various workshops and symposia, and cultivating the next generation through internships and fellowships.

FUS Partners

fusfoundation.org/the-foundation/programs/fus-partners

FUS Partners is a program of the Focused Ultrasound Foundation that serves as a galvanizing force in facilitating the rapid acceleration of commercialization of focused ultrasound technology, speeding the transition from laboratory research to widespread adoption and utilization of the technology.

The program systematizes, formalizes, and coordinates certain activities of the Foundation to address the critical unmet needs of members of the focused ultrasound community, including fostering relationships and developing critical resources with respect to regulatory and reimbursement; corporate financing; training and credentialing; employee recruiting; strategic partnerships and technology transfer; industry advocacy; and intellectual property.

Image Guided Therapy

imageguidedtherapy.com

Image Guided Therapy develops MR guided HIFU systems for preclinical research, based on phased array generators and transducer with up to 256 independent channels. IGT systems are used by renowned academic centers in diverse applications ranging from drug delivery to hyperthermia, ultrasound mediated blood-brain barrier opening, neurostimulation, and plain thermal ablation.

International Essential Tremor Foundation

essentialtremor.org

The mission of the International Essential Tremor Foundation is to provide hope to the essential tremor community worldwide through awareness, education, support and research.

Founded in 1988 as a 501(c)3 non-profit organization, the International Essential Tremor Foundation (IETF) is guided by an executive board of directors, a medical advisory board, and an executive director.

International Society for Therapeutic Ultrasound (ISTU)

istu.org

Advertisement: page 376

The International Society for Therapeutic Ultrasound (ISTU) is a nonprofit organization founded in 2001 to increase and diffuse knowledge of therapeutic ultrasound to the scientific and medical community, and to facilitate the translation of therapeutic ultrasound techniques into the clinical arena for the benefit of patients worldwide.

Korean Society for Therapeutic Ultrasound (KSTU)

kstu.or.kr

KSTU, the Korean Society for Therapeutic Ultrasound was founded in 2014. Since inception there has been rapid membership growth with approximately 100 attendees at our annual meetings. In 2018, KSTU began an official exchange program with Japanese Society for Therapeutic Ultrasound (JSTU) and Taiwan Association of Interventional and Therapeutic Ultrasound (TAITU) . We are looking to expand this program to other Asian societies for therapeutic ultrasound.

KSTU is honored to host the symposium of the International Society for Therapeutic Ultrasound (ISTU) at Gyeongju, Korea, June 6–9, 2021.

Medical Imaging & Technology Alliance

medicalimaging.org

The Medical Imaging & Technology Alliance is the collective voice of medical imaging equipment, radiopharmaceutical manufacturers and innovators. We represent companies whose sales comprise over 90 percent of the advanced imaging technologies global market. MITA's mission is to reduce regulatory barriers, establish standards and advocate for the medical imaging industry.

NaviFUS Corporation

navifus.com

NaviFUS Corporation is a medical device company pioneering Focused Ultrasound (FUS) therapies for Central Nervous System (CNS) diseases. Through the dedicated development of its NaviFUS System, including its implementation in clinical trials for brain cancer, Alzheimer's Disease, and Epilepsy, NaviFUS Corp. strives to drive innovative FUS research into clinical practice.

SonaCare Medical, LLC

sonacaremedical.com

SonaCare Medical is the worldwide leading innovator in minimally invasive ablation technology using high intensity focused ultrasound (HIFU). SonaCare Medical's prostate tissue ablation system, Sonablate®, incorporates MRI/US image fusion to provide a customized whole gland, hemi-gland, or focal prostate ablation.

SonoVol

sonovol.com

SonoVol offers a new twist on preclinical ultrasound with a robotic, AI driven approach. The instrument is completely automated; you no longer hold a probe in hand; scan three mice in minutes; obtain whole body data in 3D. HIFU/FUS & bioluminescence are integrated for anatomical, molecular and functional imaging.

***In vivo* imaging, made easy.**

Theraclion

theraclion.com

Theraclion has developed an innovative high-tech echotherapy solution using High Intensity Focused Ultrasound for the treatment of varicose veins, SONOVEIN®. The treatment solution, which obtained CE marking in April 2019, is based on the leading-edge echotherapy treatment expertise developed over years by Theraclion for non-invasive ablation of breast fibroadenomas and thyroid nodules using its ECHOPULSE® solution. Further improvements to the ECHOPULSE are the foundation for SONOVEIN® to provide the only non-invasive ablation therapy for varicose veins. This procedure allows for a treatment without a catheter, chemical injection, or incision. An operating room is not necessary and the treatment can be performed at a doctor's offices or in clinics, as well as in hospitals. Venous pathology is widespread worldwide and generates around 5 million treatment procedures per year, according to Millenium research Varicose Vein Device Market Study 2015. Theraclion's technological solutions are based on high-tech ultrasound medical imaging devices that are precise and easy to use for practitioners.

Located in Malakoff, near Paris, Theraclion brings together a team of 25 people, more than half of whom are dedicated to R&D and clinical trials.

INTERNATIONAL SOCIETY FOR THERAPEUTIC ULTRASOUND

The International Society for Therapeutic Ultrasound (ISTU) is a non-profit organization founded in 2001 to increase and diffuse knowledge of therapeutic ultrasound to the scientific and medical community, and to facilitate the translation of therapeutic ultrasound techniques into the clinical area for the benefit of patients worldwide.

We are committed to bringing knowledge of therapeutic ultrasound to scientific and medical communities around the world through our **Annual International Symposium for Therapeutic Ultrasound** and monthly **ISTU On-Air Webinar Series**.

ISTU 2023: Lyon, France on April 17 - 20, 2023

ON-AIR WEBINAR SERIES

2021 Webinar Series Schedule

Save the Dates!

January 21
February 25
March 25
April 29
May 27
June 24
July 22

Learn More at ISTU.org!

Thank you!

The Focused Ultrasound Foundation wishes to thank its exceptional Board of Directors and Council for their steadfast dedication to helping make focused ultrasound a clinical reality and improve the lives of millions of patients.

BOARD OF DIRECTORS

Scott Beardsley, PhD
Dean and Professor, Darden School of Business, University of Virginia
Former Global Leader, McKinsey & Company

Eugene V. Fife
Founding Principal, Vawter Capital
Former Chairman, Goldman Sachs International

John R. Grisham
Author

William A. Hawkins, III
Former Chairman & CEO, Medtronic

Daniel P. Jordan, PhD
President Emeritus, Thomas Jefferson Foundation, Inc.

Neal F. Kassell, MD
Chairman, Focused Ultrasound Foundation
Professor of Neurosurgery, University of Virginia

Syaru Shirley Lin, PhD
Compton Visiting Professor of World Politics,
Miller Center of Public Affairs, University of Virginia

Mike Lincoln
Global Business Department Chair, Cooley LLP

Michael Milken, MBA
Chairman, Milken Institute,
Co-founder, Milken Family Foundation

Edward D. Miller, MD
Former CEO, Johns Hopkins Medicine

Frederic H. Moll, MD
Co-founder, Intuitive Surgical
Chairman & CEO, Auris Health, Inc.

Charles W. "Wick" Moorman, IV
Former CEO, Amtrak
Former Chairman & CEO, Norfolk Southern

Stephen H. Rusckowski
President and CEO, Quest Diagnostics Inc.
Former CEO, Philips Healthcare

Gary Shapiro
CEO and President, Consumer Technology Association

Carl P. Zeithaml, PhD
Dean and F.S. Cornell Professor of Free Enterprise,
McIntire School of Commerce, University of Virginia

COUNCIL

Co-Chairs

Jane P. Batten

Charles H. Seilheimer, Jr.

John B. Adams, Jr.
Dorothy Batten
Ellen H. Block
Amanda Brown
Deborah Caldwell
Jessica Che-yi Chao
Thomas and Nancy Chewning
Norwood and Marguerite Davis
Peter Gabriel
David R. Goode
Rick Hamilton
Alice W. Handy
Diane Heller
William and Cecelia Howell
Kat Imhoff
Dean Kamen
Ann Kingston
Harry Lester
Jonna Hiestand Mendez
Paula F. Newcomb
Wyndham G. Robertson
Mary Lou Seilheimer
Alice H. Siegel
Allan C. Stam, PhD
Aaron Stern, MD, PhD
Howard and Fredericka Stevenson
Bernice Szeto
Andrew von Eschenbach, MD
Claude Wasserstein

FOCUSED ULTRASOUND FOUNDATION

www.fusfoundation.org

Funding Available for Focused Ultrasound Preclinical Research

Awards of approximately $100,000 for 1-year projects

The Foundation's **Preclinical Awards Program** supports technical and preclinical research to accelerate adoption of image-guided focused ultrasound.

For more information visit the **For Researchers** page at **fusfoundation.org** or contact **Matt Eames**, Director of Extramural Research, at meames@fusfoundation.org.

Research award recipient Seung-Schik Yoo, PhD, MBA

FOCUSED ULTRASOUND FOUNDATION

Funding Available for Focused Ultrasound Clinical Studies

The Foundation's **Clinical Awards Program** supports first-in-human and other innovative clinical trials involving the use of image-guided focused ultrasound to treat diseases.

Funding level determined on a case-by-case basis.

For more information visit the **For Researchers** page at **fusfoundation.org** or contact **Matt Eames**, Director of Extramural Research, at meames@fusfoundation.org.

FOCUSED ULTRASOUND FOUNDATION

Research award recipient Nir Lipsman, PhD

SAVE THE DATE

8th International Symposium on Focused Ultrasound

October 23-28, 2022

Bethesda North Marriott Hotel & Conference Center
Bethesda, MD, USA

Hybrid Format
In-Person & Virtual

Focused Ultrasound Foundation

FOCUSED
ULTRASOUND
FOUNDATION

Focused Ultrasound Foundation
1230 Cedars Court | Suite 206 | Charlottesville, VA, USA
+1 434.220.4993
www.fusfoundation.org